universiteit hasselt
KNOWLEDGE IN ACTION

2015 | Faculty of Sciences

DOCTORAL DISSERTATION

Thiazolo[5,4-*d*]thiazole-based semiconducting materials for organic photovoltaics

Doctoral dissertation submitted to obtain the degree of
Doctor of Science: Chemistry, to be defended by

Julija Kudrjasova

Promoter: Prof. Dr Wouter Maes
Co-promoters: Prof. Dr Dirk Vanderzande
Dr Laurence Lutsen

D/2015/2451/25

universiteit hasselt | imec
IMO - IMOMEC
INSTITUUT VOOR MATERIAALONDERZOEK

Chairman:	Prof. Dr. Marc Gyssens
Promoter:	Prof. Dr. Wouter Maes
Copromoters:	Prof. Dr. Dirk Vanderzande
	Dr. Laurence Lutsen, IMO-IMOMEC
Members of the jury:	Prof. Dr. Jean Manca, UHasselt
	Prof. Dr. Peter Adriaensens, UHasselt
	Prof. Dr. Wim Dehaen, Katholieke Universiteit Leuven
	Prof. Dr. Etienne Goovaerts, Universiteit Antwerpen

TABLE OF CONTENTS

Chapter 1

Introduction

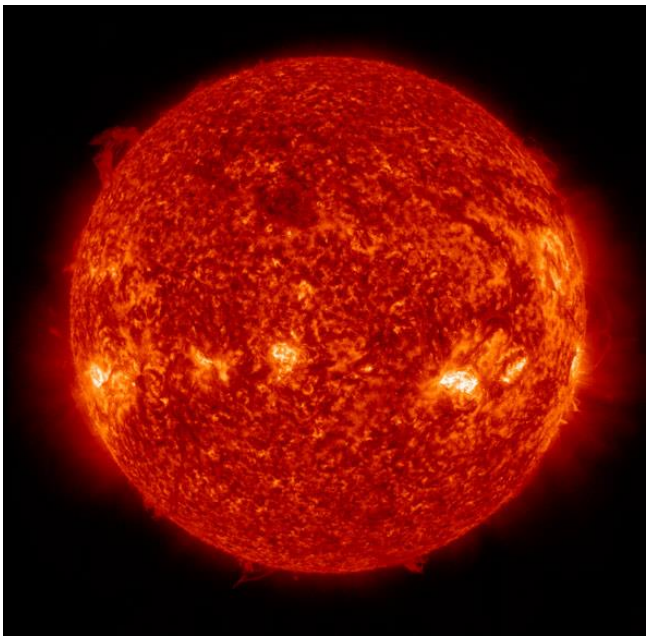

1.1. GENERAL INTRODUCTION

According to Prof. Richard Smalley, the Nobel Prize laureate in 1996, the main problem to solve in the world today is **energy**.[1] Due to the strong population growth and increasing industrialization, urbanization and modernization, the global electricity consumption is expected to continue to rise in the coming years. In 2013, the US Energy Information Administration has identified the current global primary energy demand to be 18.3 TW and it is projected to reach almost 27.4 TW by 2040.[2] It is also estimated that the global consumption of electrical energy will be doubled in the next 15−20 years.[3] To date, fossil fuels contribute to approximately 80% of our global primary energy needs. Reserves are decreasing rapidly and the projected depletion times for coal, natural gas and oil are estimated as 103, 33 and 31 years, respectively.[4] Furthermore, a rapid rise in global temperature has occurred due to the increasing concentration of greenhouse gases in the atmosphere, owing to the extensive fossil fuel usage. These issues demand for a rapid transition to **alternative, renewable, environmentally friendly and safe sources of energy**, which can be provided by wind power, solar energy, hydropower, bioenergy and geothermal energy.[5-8] Of these renewable energy sources, **solar energy** is most attractive as it is most abundant and virtually eternal. Considering that every hour the sun delivers more than enough energy to satisfy the global energy needs for an entire year, it is logical that more and more sunlight has been harvested worldwide over the last years. Figure 1 illustrates the solar energy growth in the U.S. since 2006 compared with alternative sustainable energy sources.[9]

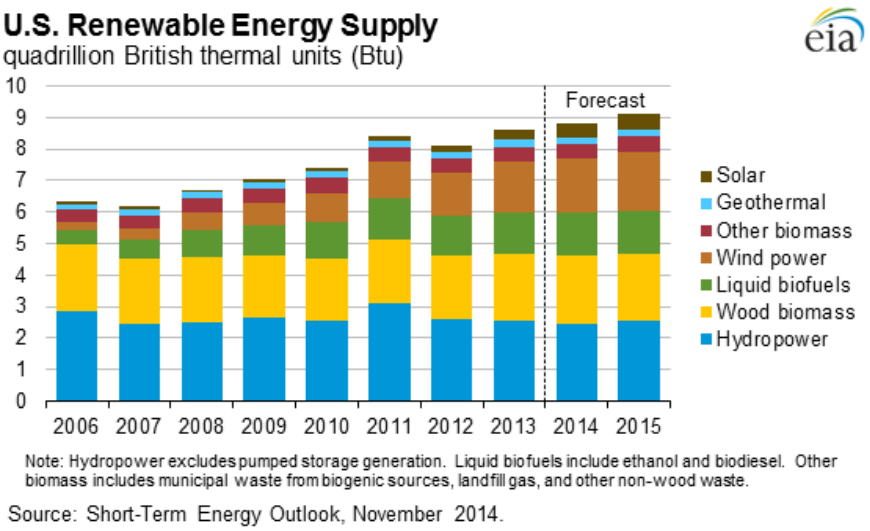

Figure 1. Distribution of renewable energy sources in the U.S. since 2006 (and a projection toward 2015).[9]

1.2. HISTORY OF ORGANIC PHOTOVOLTAICS

'Photo-voltaic' literally means '**light-electricity**', photo coming from the Greek word 'phos' for light and volt being derived from the name of Alessandro Volta, well known as the inventor of the first electrical battery in 1880. The working principle of solar cells based on the photovoltaic (PV) effect was discovered by the physicist Alexandre Becquerel in 1839 for electrolytic cells.[10] He showed that when silver chloride is placed in an acidic solution and exposed to sunlight, the platinum electrodes attached to it generate a photovoltage and photocurrent.

First reports on the electronic properties of organic materials date back to the start of the 20th century,[12-13] but the field of **organic photovoltaics** (**OPV**) only really took off in 1959, when Kallmann and Pope discovered the photovoltaic properties of anthracene, which, however, performed extremely poorly in solar cells.[14] A major breakthrough occurred following the polymerization of acetylene

in the 1970's, initially done by Shirakawa and co-workers using a Ziegler-Natta catalyst.[15] Despite its metallic appearance, the newly synthesized polyacetylene did not behave as a conductor. In 1977, Heeger and MacDiarmid discovered that oxidation with chlorine, bromine or iodine vapor resulted in polyacetylene films with a conductivity about 10^9 times larger.[16] For this discovery, the three scientists mentioned above were awarded with the Nobel Prize in Chemistry in 2000.

Another important milestone in the deployment of **organic semiconductors** in photovoltaics was reported by Tang in 1986.[17] His solar cell was based on a combination of a Cu-phthalocyanine (as electron donor material) and a perylene-3,4,9,10-tetracarboxy-bis(benzimidazole) (as electron acceptor material) in a **planar heterojunction** configuration, affording a power conversion efficiency (PCE) of 1%.

A next big step forward was not made until 1992, with the discovery of charge transfer from a **conjugated polymer** to buckminsterfullerene (C_{60}; Figure 2).[18] This discovery initiated a vast amount of research on **polymer:fullerene solar cells**. As standard C_{60}-fullerene has solubility issues, Hummelen and Wudl in 1995 synthesized a more soluble methanofullerene derivative, [6,6]-phenyl-C_{61}-butyric acid methyl ester or **$PC_{61}BM$** (Figure 2),[19] which is to date still one of the mostly applied electron acceptor materials in OPV devices, together with the analogous C_{70} derivative **$PC_{71}BM$** (Figure 2), with slightly advantageous absorption features.

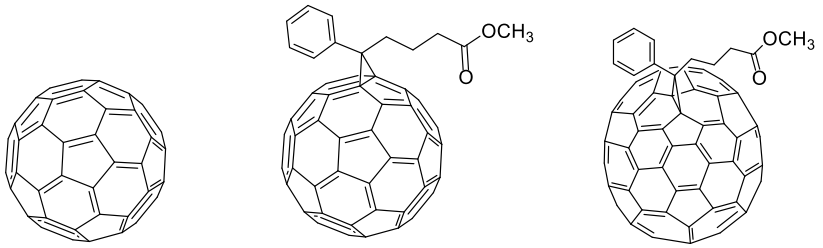

Figure 2. Chemical structures of buckminsterfullerene C_{60} and methanofullerenes $PC_{61}BM$ and $PC_{71}BM$.

The efficiency of organic solar cells having a bilayer of organic molecules remained quite low (<1%). This low performance originates from the fact that absorbed photons do not generate excitations that directly separate into free charges, but instead create tightly bound **excitons**, with a binding energy of about 0.4 eV. The generated excitons are not spontaneously separating in organic materials, but this only happens at the interface between donor and acceptor materials thanks to the difference in energy levels. Because the photoexcitation recombination lengths are typically around 10 nm in disordered organic materials, the length scale for self-assembly of the donor and acceptor materials must be of the order of 10–20 nm for efficient charge separation to occur.

In 1995, the **bulk heterojunction** (BHJ) concept was introduced by Heeger and co-workers to overcome the inherent limitations of bilayer devices.[20] The intermixed composite of organic donor and acceptor materials applied as the photoactive layer in BHJ OPV devices has a clear advantage in terms of a much larger interface area between the donor and acceptor components. A nanostructured film morphology is formed by spontaneous phase separation after deposition from a mixed solution of the two materials, which self-assemble to form bicontinuous interpenetrating networks intermixed at a length scale less than the

exciton diffusion length. To date, the BHJ structure is still the most successful OPV device architecture because exciton harvesting is nearly perfect. Record PCE's for BHJ devices have risen from 1% before 2000 to over 10% in 2014 (Figure 3),[21] partly as a consequence of the almost exponential increase of (academic) attention for the OPV field over the last decade (Figure 4). This huge interest can simply be understood considering the expected high potential of the technology.

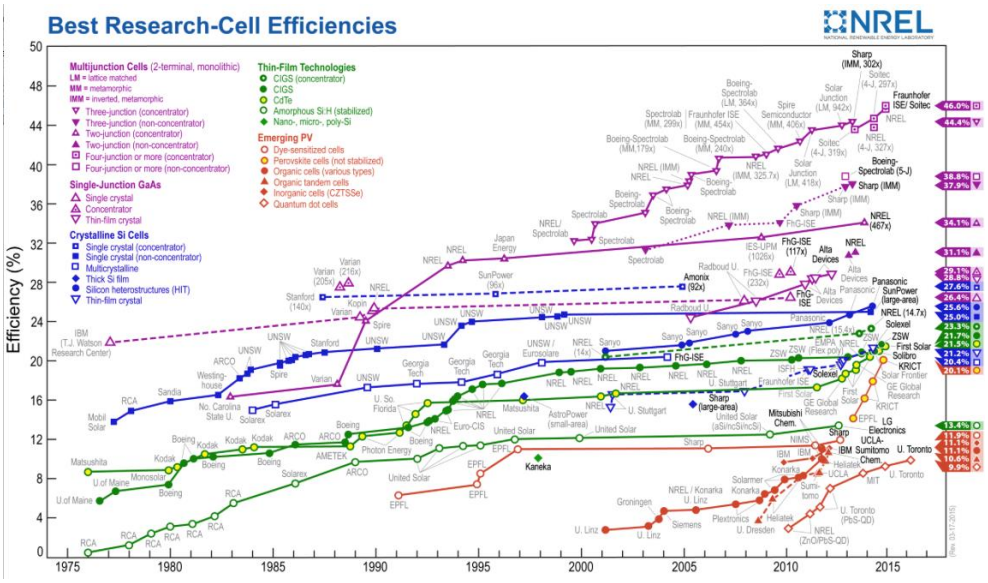

Figure 3. Evolution of the best (research) solar cell efficiencies over the last 40 years for different PV technologies (source: NREL, version date: 03-17-2015).[22]

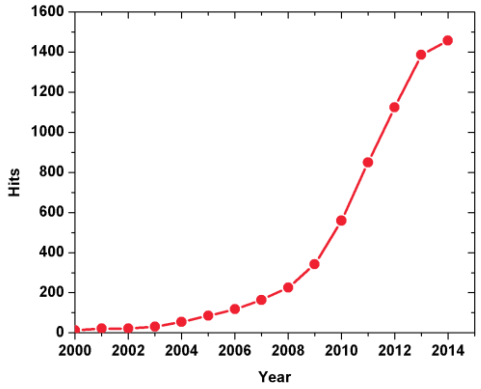

Figure 4. Web of Science hits for a search on topic = ''organic photovoltaic'' or ''organic solar cell'' (performed on 12-11-2014).

Some of the **main advantages** of organic solar cells – based on either vacuum or solution processed small molecules or conjugated polymers – are:

- Low cost of manufacturing by high-throughput roll-to-toll (R2R) printing or other low-temperature deposition techniques;
- Low energy cost of manufacturing;
- High structural versatility due to the powerful organic chemistry toolbox;
- Non-toxicity and low material consumption;
- Flexible, lightweight and robust solar panels.

1.3. OPERATIONAL ASPECTS OF ORGANIC SOLAR CELLS

In organic solar cells, organic materials are responsible for generating free charge carriers from sunlight. The operational mechanism of OPV's is illustrated in Figure 5 and can be summarized as follows:[23,24]

1. Light absorption: Upon the absorption of an incident photon of the appropriate energy, organic molecules will be excited from their ground state to

an excited state and an electron-hole pair is created. Right after its formation, the electron-hole pair will relax into a bound state, which is called an **exciton**. The binding energy of this organic exciton prevents charge separation in the absence of specific energy-favorable conditions, such as a D/A (donor/acceptor) interface and a strong electrical field. Excitons usually reside on one single molecule and can either recombine or randomly diffuse to a nearby molecule. This gives rise to the next step, exciton diffusion.

2. Exciton diffusion: In an organic layer (film) the excitons can move around via hopping among adjacent molecules. This exciton diffusion process is random in terms of direction. The presence of an electrical field will not help to orient the diffusion, because each exciton consists of one electron and one hole and therefore appears neutral. The exciton diffusion length, defined as the average distance an exciton can travel before its recombination, is relatively short for most organic materials, about 5−10 nm. If an exciton meets a D/A interface within its diffusion length, it will separate into an electron and hole.

3. Exciton dissociation: When an exciton created in the electron donor material diffuses to the D/A interface, it can transfer an electron to the adjacent electron acceptor molecule, leaving a hole behind. A minimum energy difference of ~0.3 eV is required to affect exciton splitting and charge dissociation. Exciton dissociation will generate an electron polaron in the lowest unoccupied molecular orbital (LUMO) of the acceptor molecule and a hole polaron in the highest occupied molecular orbital (HOMO) of the donor molecule. The electron and hole generated via exciton dissociation form a geminate electron-hole pair (GEHP), and they are still weakly bound depending on the initial separation distance.

4. Charge separation and collection: It is still possible for GEHP's to recombine due to Coulombic attraction, although the diffusion process will help the electron

and hole to further separate because of the D/A interface constraint. The direction and magnitude of the electrical field at the D/A interface is critical. If a strong electrical field, $\sim 10^6$ V/cm^2, is present and its direction helps the electron and hole to diffuse away from the interface, charge separation can be very efficient. Otherwise, the chance of GEHP recombination will be higher. After the electron and hole are completely separated, they can travel through the respective organic phases and they can be collected at the corresponding electrodes. The process is usually very efficient for typical operation conditions. The electron and hole can still potentially recombine during their travel in the organic layer, but this chance is generally small.

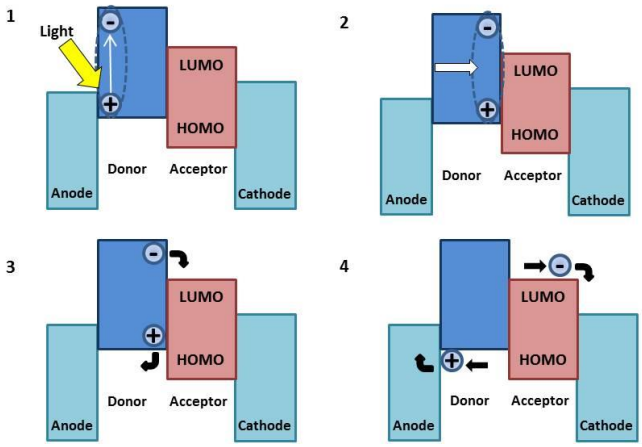

Figure 5. General mechanism of photoconversion in organic solar cells.

1.4. CONSTRUCTION AND PERFORMANCE FEATURES OF ORGANIC SOLAR CELLS

The most often used BHJ OPV device structure (Figure 6) consists of a glass substrate with on top of it a patterned and sputtered layer of indium tin oxide

(ITO), serving as a transparent highly conductive electrical contact. Next, a layer of poly(3,4-ethylenedioxythiophene):poly(styrenesulfonate) (PEDOT:PSS) is spin-coated on top to improve the contact properties, smoothen the irregular ITO surface and provide a good wettability for the active layer to be processed next. A solution containing the photoactive organic electron donor and acceptor materials, intermixed in a certain ratio, is used for casting of the composite BHJ active layer. To obtain a working device, a low work function cathode, often consisting of calcium and aluminum or silver, is finally deposited on top of the photoactive layer by thermal evaporation.

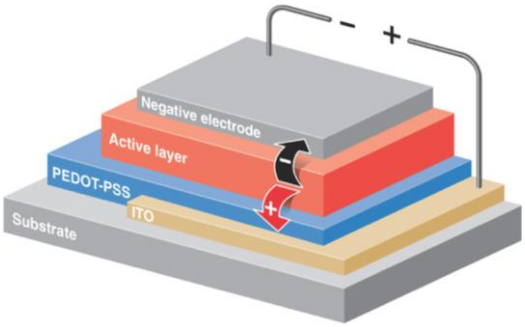

Figure 6. Standard organic solar cell stack.

Characterization of the solar cell performance is done by measuring the dependence of the current density (*J*) on the applied voltage (*V*) under standard AM 1.5G illumination conditions (Air Mass 1.5 Global spectrum on the ground when the sun is at 48.2° zenith angle with the average solar light intensity being 1000 W/m^2) (Figure 7).

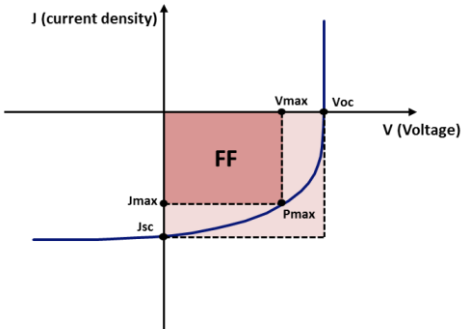

Figure 7. Current density-voltage curve of a solar cell under illumination with the most important parameters indicated.

There are three major device parameters which determine the final efficiency of the device (Figure 7):

a) the **short-circuit current density** (J_{sc})

The J_{sc} is the current that flows through the device when there is no external field applied. The charges are drifting because of the internal field. The J_{sc} is determined by the number of photons absorbed, the quantum efficiency for charge separation and the transport of the charge carriers through the materials. A broad absorption spectrum is advantageous, as one wants to harvest an as large as possible fraction of the photons emitted by the sun. The current is thus largely dependent on the bandgap of the organic material and the photoabsorption of the complete active layer, the intensity of the sunlight, the thickness of the active layer and the exciton/charge collection efficiency.

b) the **open-circuit voltage** (V_{oc})

The V_{oc} is the maximum voltage delivered by the solar cell. At this voltage, the current is zero. The V_{oc} is linearly related to the difference between the HOMO level of the electron donor material and the LUMO level of the electron acceptor material, and it does not depend much on the work functions of the electrodes.

c) the **fill factor** (FF)

The FF is the third key parameter in evaluating the performance of solar cells and it is determined as the maximum power P_{max} that the device can deliver divided by the product of the short-circuit current density and the open-circuit voltage:

$$\mathrm{FF} = \frac{\mathrm{Pmax}}{\mathrm{Voc\ Jsc}} = \frac{\mathrm{Vmax\ Jmax}}{\mathrm{Voc\ Jsc}}$$

It represents the ratio of the organic solar cell's actual maximal power output to the theoretical maximal power output. Due to physical limitations on the diode quality, the practical limit to the FF is lower than the ideal value of 1. The behavior of a real diode will deviate from the ideal, primarily because of recombination occurring at the junction of the D-A interface, which is distributed throughout the entire photoactive layer. For OPV's, fill factors are generally ranging from 0.3 to 0.7.

Finally, the **power conversion efficiency** of a solar cell is expressed as the maximum power deliverable by the device divided by the incident light power P_{in}, and thus can be calculated according to the following formula:

$$\mathrm{PCE} = \frac{\mathrm{Pmax}}{\mathrm{Pin}} = \frac{\mathrm{Voc\ Jsc\ FF}}{\mathrm{Pin}}$$

1.5. CONJUGATED ORGANIC MATERIALS

The primary goals in the development of effective electron donor and acceptor materials for organic solar cells are to design appropriate bandgaps and energy levels to maximally boost the J_{sc} and V_{oc}, to promote good charge carrier mobility along with good π–π stacking characteristics, and to develop stable materials, all while maintaining a reasonable solubility toward processability (printing) from solution. An immense progress in the aforementioned material properties

beneficial for BHJ polymer solar cells was realized over the last two decades. One of the first conjugated polymers applied in polymer solar cells is poly[2-methoxy-5-(2'-ethylhexyloxy)-*p*-phenylene vinylene] (**MEH-PPV**) (Figure 8), which was mixed with $PC_{61}BM$ by Yu *et al.* in 1995, affording an energy conversion efficiency at 430 nm of 2.9%.[20] This work opened up a new era of polymer photovoltaics based on a first generation of PPV-type conjugated polymers. After significant optimization, PCE's in the range of 3.0% were achieved for PPV-based OPV devices.[25] It quickly became clear that the relatively large bandgap (around 2.15 eV) of PPV-based materials, along with their moderate charge carrier mobilities, imposed significant limitations on the maximum achievable PCE's for devices made from these donor materials. As a result, the interest shifted toward a second generation of polymer donor materials, soluble poly(3-alkylthiophenes) (P3AT's), including the benchmark material **poly(3-hexylthiophene)** (**P3HT**) (Figure 8). P3HT with its relatively high hole mobility and broader spectral coverage (compared to PPV's) has become the workhorse donor material for polymer solar cells in the 2000's. Careful active layer morphology optimization has provided OPV devices with PCE's up to 5%.[26]

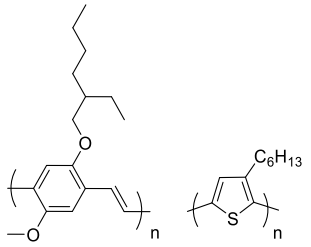

Figure 8. First and second generation conjugated polymers for polymer solar cells.

To address the still moderate light harvesting spectral width of polythiophenes, a third generation of conjugated polymers with bandgaps below 1.6 eV was developed, leading to polymer solar cells with efficiencies that nowadays surpass 10%.[21] Toward conjugated polymers and related small molecules with low bandgaps capable of absorbing photons up to the near-IR, two methods to decrease bond length alternation and improve electron delocalization are commonly used. The first approach involves alternating electron-rich and electron-poor (often heterocyclic) units along the molecular backbone in the so-called **donor-acceptor (D-A) approach**. This design strategy works through a 'push-pull' mechanism in which π electrons on the electron-rich donor building block are drawn toward the neighboring electron-deficient component, thereby increasing electron delocalization and inducing a higher contribution of the quinoid mesomeric structures ($D-A \longleftrightarrow D^{+}=A^{-}$). The second method for decreasing bond length alternation is similar to the mesomeric effect of the D-A approach and works by creating competing resonance structures that have a significant influence on the overall molecular backbone. With this so-called quinoidal effect, aromatic building blocks are designed to have increased quinoidal character, thereby increasing the overall electron delocalization along a conjugated material.

Polythiophene for example shows a dominant aromatic character because the thiophene ring structure is aromatic, whereas poly(isothianaphthene) (PITN) has been shown to have a dominant quinoidal charachter, because in the quinodal geometry the phenyl ring is aromatic (Figure 9).[27]

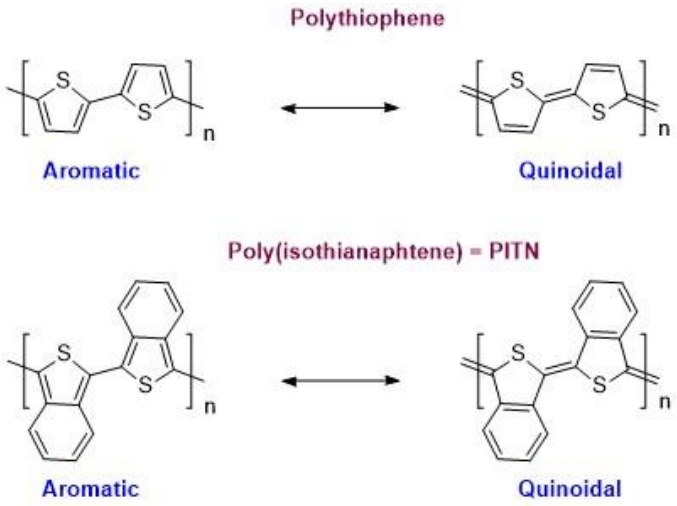

Figure 9. Aromatic and quinoidal resonance structures of polythiophene and PITN.

The decrease in material bandgap induced by the D-A approach or the quinoidal effect can be rationalized with molecular orbital theory. In the case of D-A hybridized materials, electron-rich substituents raise the energy levels of the donor unit, while electron-deficient functionalities lower the energy levels of the acceptor unit. The energy level mismatch between the donor and acceptor building blocks causes the molecular LUMO to resemble the (low-lying) acceptor LUMO and the molecular HOMO to resemble the (raised) donor HOMO (Figure 10a). The main advantage of this method is that one is able to fine-tune the energy levels of the final polymer by varying the strength of the donor and/or the acceptor, the HOMO level merely being determined by the donor and the LUMO by the acceptor.

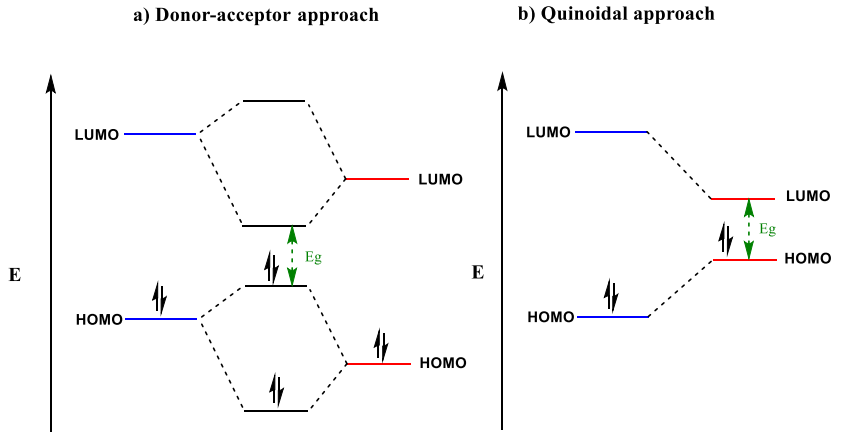

Figure 10. a) The electron-donating and withdrawing properties of donor and acceptor building blocks decrease the molecular bandgap through the D-A hybridization approach. b) The incorporation of significant quinoidal character into a molecular backbone energetically destabilizes a material and reduces its bandgap relative to aromatic materials.

The quinoidal effect decreases the molecular bandgap of standard aromatic materials by destabilizing its energy levels, as significant quinoidal character quite often decreases the aromatic stabilization energy (Figure 10b).

1.5.1. p-type materials

Numerous **p-type** (electron-donor) materials, conjugated polymers as well as small molecular compounds, have been developed for OPV applications in the past decade. Therefore, in this section, mainly those materials of relevance for the remaining part of this PhD thesis are discussed, together with the state-of-the-art materials providing highest solar cell efficiencies at this moment.

The top-performance polymer solar cells recently reported by the group of Yan *et al.* are based on three different D-A-D copolymers, combining thiophene donor units with either benzothiadiazole (**PffBT4T-2OD**, **PBTff4T-2OD**) or

naphtobisthiadiazole (**PNT4T-2OD**) (Figure 11), affording remarkable efficiencies up to 10.8% and astonishing fill factors up to 77%. It was elegantly demonstrated that the branching position and size of the alkyl size chains are critically important in enabling a well-controlled aggregation behavior, which resulted in a nearly ideal polymer:fullerene morphology.[21]

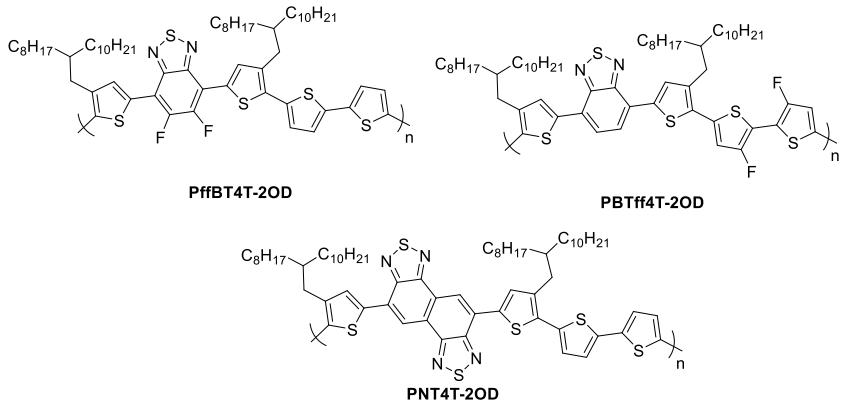

Figure 11. Today's state-of-the-art donor polymers for polymer solar cells.[21]

The plethora of D-A materials is generally realized based on a limited amount of key monomer units, among which the electron-deficient **thiazolo[5,4-*d*]thiazole** (TzTz) moiety. The fused TzTz biheterocycle has been introduced as an interesting candidate for integration in organic electronics due to its strong electron-withdrawing properties, high oxidative stability, planar and rigid structure and resulting strong tendency for π–π stacking. In combination with well-known electron-rich building blocks such as 4*H*-cyclopenta[2,1-*b*:3,4-*b*']dithiophene (CPDT), benzo[1,2-*b*:4,5-*b*']dithiophene (BDT) and N-acyl-substituted dithieno[3,2-*b*:2',3'-*d*]pyrrole (DTP), low bandgap copolymers (1.79, 1.73 and 1.81 eV, respectively) were synthesized, affording polymer solar cells with PCE's of 4.0% (**PCPDT-DTTzTz**),[28] 5.6% (**PDEHTzTz**)[29] and 3.3% (**PDTP-DTTzTz**),[30] respectively (Figure 12). The efficiency of the PCPDT-DTTzTz:$PC_{71}BM$

device later was on boosted to 5.4% by implementing an ionic polythiophene as charge transporting interlayer.[31]

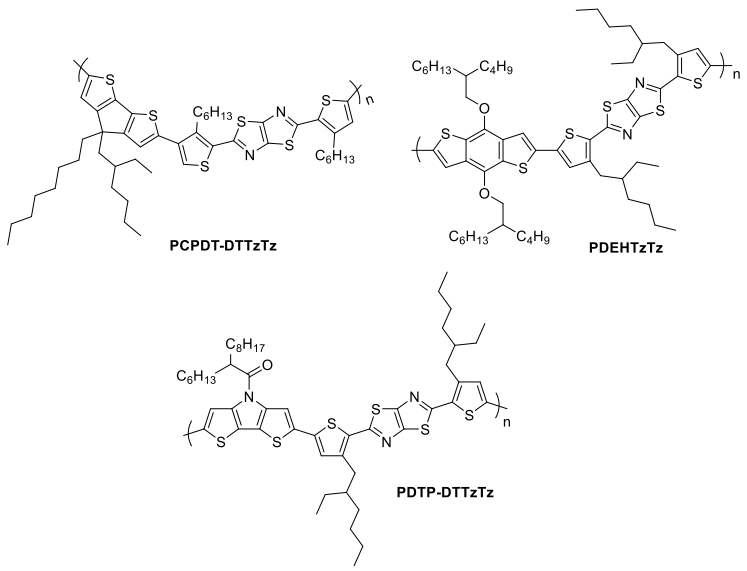

Figure 12. Low bandgap copolymers containing the TzTz acceptor moiety.

The group of Takimiya recently demonstrated that by fine-tuning the alkyl side chain composition of a rather simple thiophene-thiazolo[5,4-*d*]thiazole copolymer (Figure 13), the backbone orientation could be altered.[32] Higher solar cell efficiencies were obtained when the polymers showed well-ordered face-on orientation, affording higher out-of-plane mobilities (allowing the charge carriers to travel further through the bulk film), eventually contributing to higher FF's. An impressive PCE of 7.5% was achieved based on this copolymer.

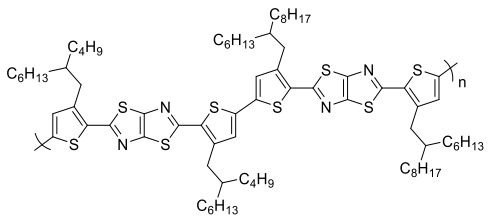

Figure 13. Takimiya's thiophene-TzTz copolymer.

As an alternative to low bandgap copolymers, **solution-processed conjugated small molecules** have attracted much attention in recent years as they have been shown to afford competitive solar cell performances.[33] Compared to their polymeric counterparts, small molecules have a higher structural precision and less batch to batch variations.[34] They have also been shown to attain higher hole mobilities than the corresponding polymer materials due to their enhanced stacking properties.[35] Additional advantages such as more reproducible fabrication protocols and a better understanding of structure–property relationships can be anticipated as well.

In 2013, Chen *et al.* reported the synthesis of a A-D-A small molecule comprising of a central BDT building block and ethylrhodanine acceptor units on both sides, linked by terthiophene spacers (**DR3TBDT2T**; Figure 14), affording small molecule solar cells with PCE's up to 8.0% (upon addition of 0.2 mg/mL of polydimethylsiloxane (PDMS) to the blend solution).[36] A year later, this result was further improved to 9.95% by substituting the BDT side chains with alkylthio moieties (**DR3TSBDT**; Figure 14).[37]

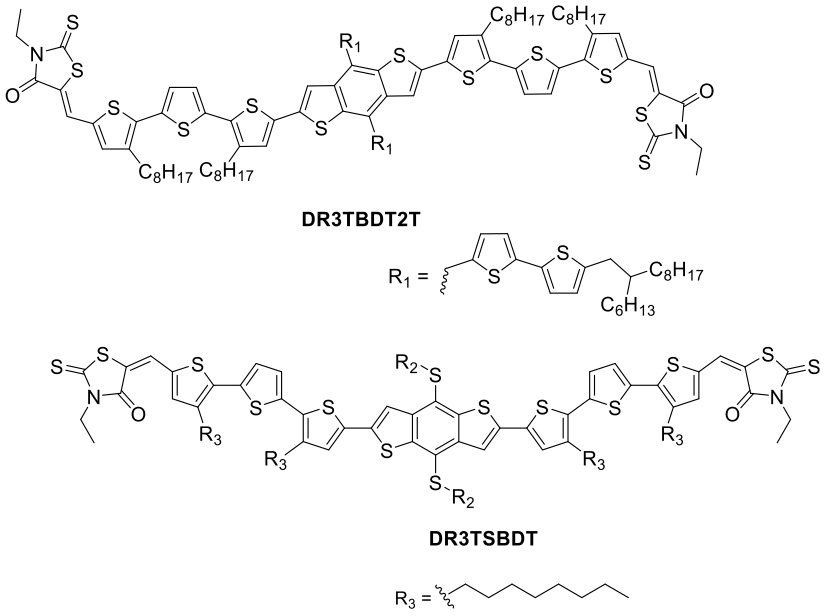

Figure 14. Benzodithiophene-based small molecules.[37,38]

In parallel to these studies on BDT-based small molecules, Bazan and co-workers also reported a series of benchmark small molecules. One of the highest performing molecular chromophores is based on a D-A-D-A-D architecture and is composed of fluorinated 2,1,3-benzothiadiazole as an acceptor unit, combined with bithiophene as the outer and dithieno[3,2-*b*:2',3'-*d*]silole (DTS) as the inner donor unit, affording **p-DTS(FBTTh$_2$)$_2$** (Figure 15). For this material, high hole mobilities up to 0.14 cm^2(Vs)$^{-1}$ have been obtained, originating from the highly crystalline nature of this small molecule. This resulted in a final solar cell performance of 8.0%, with a FF of 73%.[38]

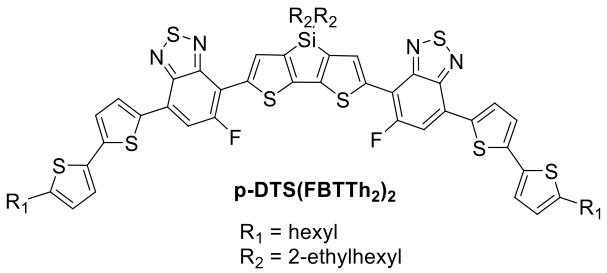

Figure 15. Bazan's dithienosilole-based small molecule for high performance organic solar cells.[38]

There are not so many examples of TzTz-based small molecules applied in organic solar cells. D-A-D type small molecules containing triphenylamine (TPA) donor groups coupled to a central dithienyl-TzTz unit were recently synthesized with either linear decyl or dodecyl side chains on the thiophene constituent by the groups of Lee and Zhan,[39,40] respectively (Figure 16). Both compounds gave a high V_{oc} of 0.92 eV when mixed with $PC_{71}BM$ and applied in standard BHJ organic solar cells, resulting in PCE's of 2.0 and 2.6%, respectively. For the dodecyl-substituted compound, thermal annealing at 110 °C for 10 minutes afforded a substantial improvement to an efficiency of 3.7%, mainly due to an increase of J_{sc} and FF.

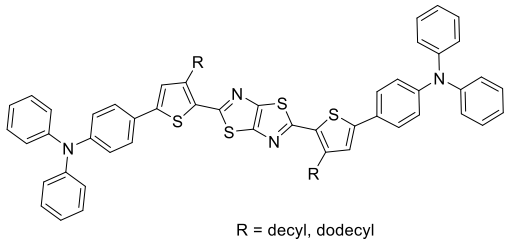

Figure 16. D-A-D type TzTz-containing small molecules for organic solar cells.[39,40]

This efficiency was further improved to 4.05% by adding additional thiophene units in the molecular backbone.[41] Increasing conjugation length resulted in a red-

shifted and enhanced absorption, a higher HOMO level, a down-shifted LUMO level and a reduced band gap.

Another enlarged D-A-D-A-D conjugated small molecule incorporating naphtho[1,2-*b*:5,6-*b*']dithiophene as a rigidly fused π-conjugated central donor, TzTz as an acceptor and TPA as a terminal auxiliary donor, with thiophene moieties linking the different components, was synthesized and characterized by the group of Lee *et al.* (Figure 17).[42] Photovoltaic devices with a small molecule:$PC_{71}BM$ active layer exhibited a maximum PCE of 1.4% (with a J_{sc}, V_{oc} and FF of 5.1 mA/cm^2, 0.75 V and 0.38, respectively).

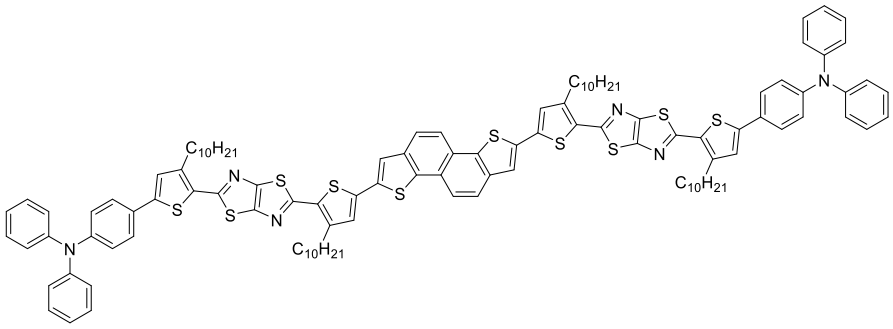

Figure 17. D-A-D-A-D type TzTz-containing small molecule for organic solar cells.[42]

1.5.2. n-type materials

Throughout the years, fullerene derivatives have remained the dominating class of electron acceptor materials for organic solar cells. Fullerenes have unique charge carrier capabilities and these have been exploited in well-optimized systems to obtain internal quantum efficiencies approaching 100% and FF's up to 80%.[43] However, despite numerous successes for laboratory scale devices, their relatively high cost is an important concern and fullerenes are far from ideal for production on an industrial scale.[44] They are expensive to synthesize, difficult to

modify chemically and rather unstable in air. As a consequence, the pursuit of high performance **non-fullerene acceptors** has drawn quite some attention. Both small molecules[45] and polymers[46] with high electron affinity have been investigated to find alternatives for $PC_{61}BM$ and $PC_{71}BM$. The replacement of fullerene acceptors by n-type organic molecules has a number of potential advantages, including a facile and cheap large-scale synthesis and purification and easy tailoring of the energy levels and bandgap toward smaller thermalization losses and a higher V_{oc}. Light harvesting can be enhanced through complementary absorption by the donor and acceptor components. Fullerene-free devices also offer more options for stabilization of the optimal active layer blend morphologies. One of the most successful recent examples of n-type small molecules based on perylenediimide (PDI) was demonstrated by the group of Yao *et al*.[47] They reported highly efficient polymer:small molecule fullerene-free OPV devices based on **PBDTTT-C-T** and 1,1′-bis(2-methoxyethoxy)-7,7′-(2,5-thienyl)-bis-PDI (**bis-PDI-T-EG**) (Figure 18). Upon using 1,8-diiodooctane (DIO) as a processing additive and annealing of the as-cast active film in an *ortho*-dichlorobenzene/DIO vapor, an average PCE of 6.0% was achieved. It was shown that tedious optimization of crucial parameters such as the additive content during film processing, the volume of the host solvent for solvent vapor annealing (SVA), the volume ratio of the additive versus the host solvent for SVA, and the time for SVA can significantly improve the PCE (in this case from 1.4 up to 6.0%).

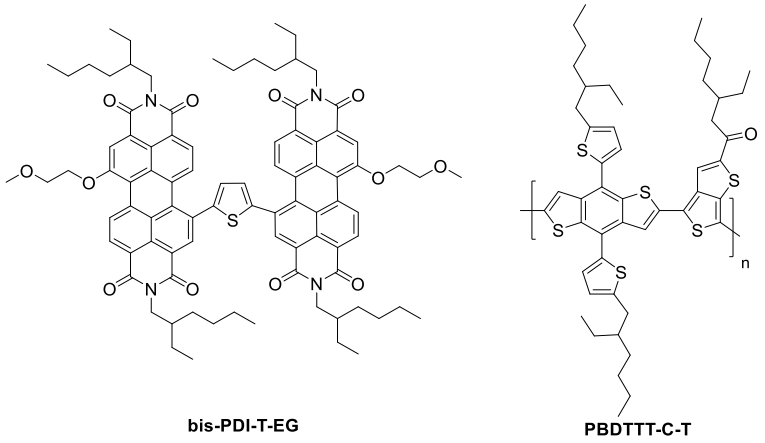

Figure 18. Bis-PDI-T-EG small molecule acceptor affording 6.0% efficiency combined with the PBDTTT-C-T donor polymer.[47]

TzTz-based small molecule materials were recently applied by our group as acceptor materials as well (Figure 19), in combination with MDMO-PPV as the electron donor polymer.[48] Although the PCE achieved was very poor (0.1%), high V_{oc} values were obtained and useful information on the charge transfer mechanism was gathered that may help in the future design of high performance fullerene-free devices.

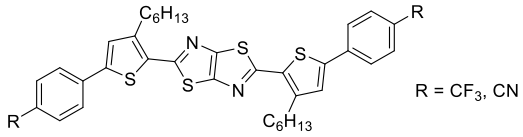

Figure 19. TzTz-based n-type small molecules.[48]

1.6. DIRECT ARYLATION

1.6.1. Introduction

For most small molecules and surely for the low bandgap conjugated polymers affording best results in organic solar cells, Suzuki or Stille cross-coupling

reactions are employed to create the required (het)aryl-(het)aryl connections. In parallel, **direct or C-H arylation reactions** have emerged as a viable alternative to traditional cross-coupling reactions, with a **number of advantages** such as higher yields, fewer synthetic operations, lower catalyst loadings and absence of organometallic intermediates (affording toxic stannyl side products in the Stille case), obviously rendering them attractive for the synthesis of semiconducting materials for organic electronics (Scheme 1).[49]

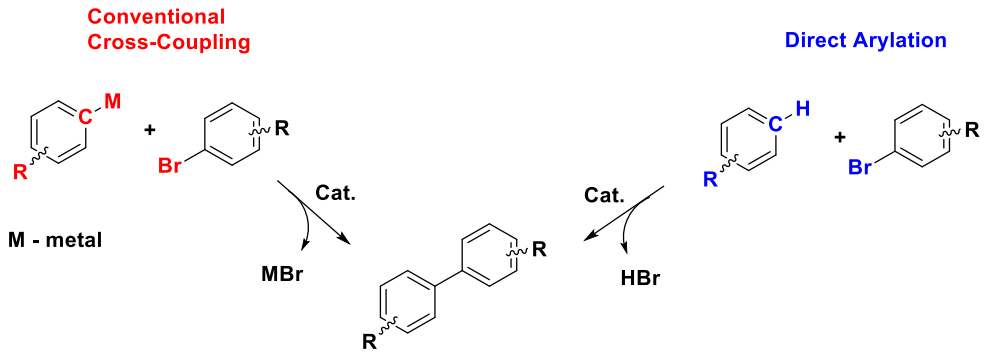

Scheme 20. Conventional cross-coupling vs direct arylation.

A couple of different mechanistic pathways have been proposed to explain direct arylations. After several years of research, the majority of the experiments support the concerted metalation-deprotonation (CMD) pathway. Scheme 2 shows the suggested mechanism.[50] A complexated palladium catalyst **I** first undergoes oxidative addition (1), affording a Pd intermediate **II**. Experimental and theoretical studies suggest that the pivalate anion then acts as a catalytic proton shuttle and this is the key component in the C-H bond cleavage step. Thus, in the proposed mechanism, proton abstraction from a C–H bond by the carboxylate ligand occurs, while a metal-carbon bond is being formed to create product **III** (2,3), the so-called CMD transition state. Afterwards, dissociation of the pivalate

anion occurs, giving intermediate **IV**. Finally, reductive elimination of Pd generates the cross-coupled product **V** and the Pd(0) species **I** is reformed (4).

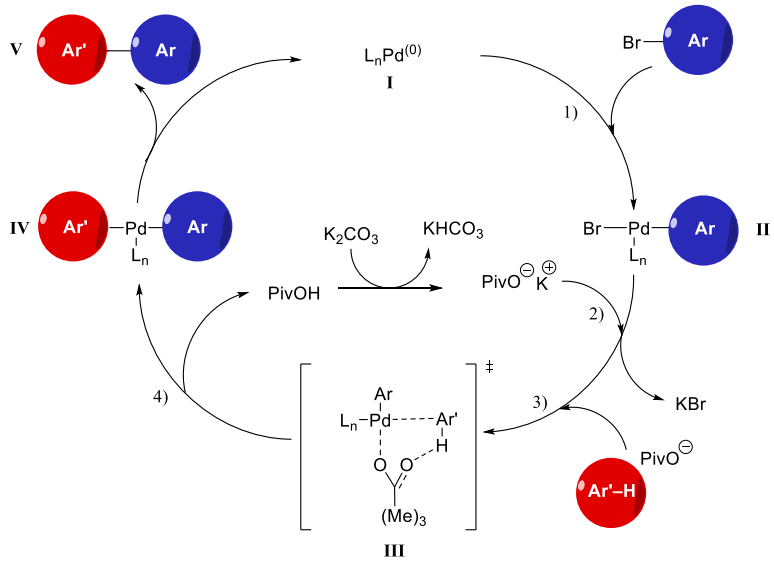

Scheme 21. Suggested mechanism for direct arylation reactions.

1.6.2. Direct arylation applied to small molecule semiconductors

Recently, C-H activation has been applied to a number of electron-poor building blocks relevant to optical and electronic materials, such as perylenediimide,[51] naphthalenediimide (NDI),[52] 3,6-dithiophen-2-yl-2,5-dihydro-1,4-diketopyrrolo[3,4-*c*]pyrrole (DPP),[50a,53] and benzothiadiazole.[50c] The group of Marder synthesized electron-rich and poor end-capped difluorobenzothiadiazole (DFBT) compounds via direct arylation in excellent yields up to 96%.[50c] Especially interesting are the DFBT molecules shown in Scheme 3, which potentially can be used as D-A-D' structures for organic solar cells. By adding just one equivalent of aryl bromide, the authors managed to synthesize monoarylated DFBT derivatives, which were then further directly arylated by other aryl bromides, as shown for the combination of 4-bromobenzaldehyde and 5-bromo-2-thiophenecarbaldehyde.

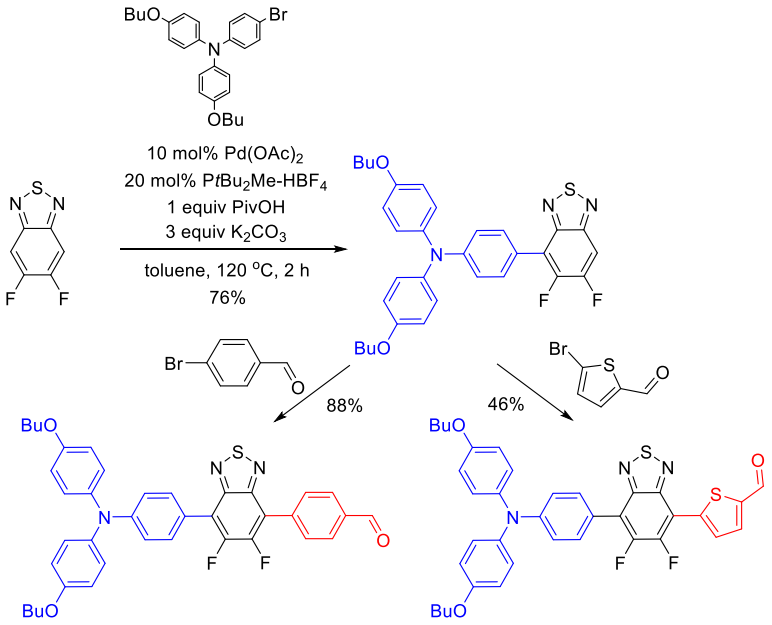

Scheme 22. Synthesis of asymmetrical DFBT-based triads.[50c]

Another recent paper reports a series of DPP-pyrene oligomers containing multiple DPP chromophores (Scheme 4).[50d] The materials were synthesized in noteworthy high yields by an effective direct arylation strategy and demonstrated fine organic field-effect transistor (OFET) and solar cell performances. Small molecule solar cells based on **SM1/2**:$PC_{71}BM$ blends afforded decent PCE's of 3.0 and 3.7%, respectively.

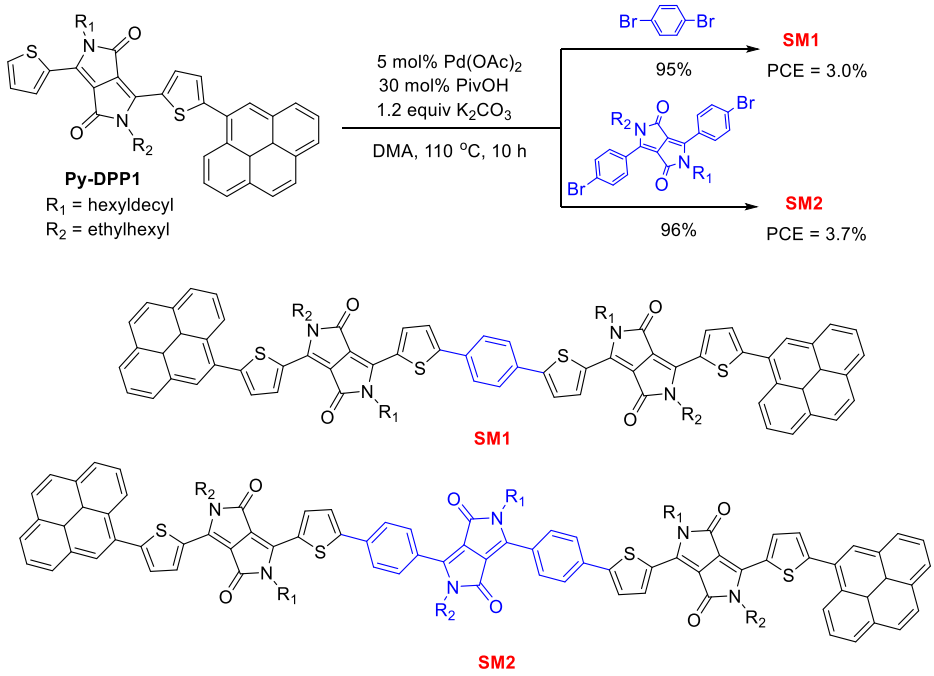

Scheme 23. Synthetic route toward DPP-pyrene small molecules **SM1** and **SM2**.[50d]

The examples mentioned above clearly show that the direct arylation strategy can be applied to the synthesis of a variety of novel symmetrical and asymmetrical conjugated materials. Nevertheless, some restrictions should be considered as well. Regioselective direct arylation is sometimes difficult to achieve because the (het)arene reagents often contain several nonequivalent C–H bonds that can react with the metal center at a similar rate if they are not protected or blocked. This selectivity problem usually furnishes undesired side products. The electronic properties of the substrate can control the position of C–H bond cleavage, but they can be difficult to abrogate and therefore this may limit the scope of substrates.

1.6.3. Direct polymerization

Direct arylation reactions have also been applied to the synthesis of various conjugated polymers, for example P3HT,[54] poly[(3,4-ethylenedioxythiophene-2,5-diyl)-(9,9-dioctylfluorene-2,7-diyl)] (**H-PEDOTF**),[55] poly[(9,9-dioctylfluorene-2,7-diyl)-(2,3,5,6-tetrafluoro-1,4-phenylene)] (**PDOF-TP**),[56] TPD-based polymers,[57] poly(4',4'-dialkyl-cyclopenta[2,1-*b*:3,4-*b*']dithiophene-alt-2,1,3-benzothiadiazole) (**PCPDTBT**) (Scheme 5),[58] and many others.[59]

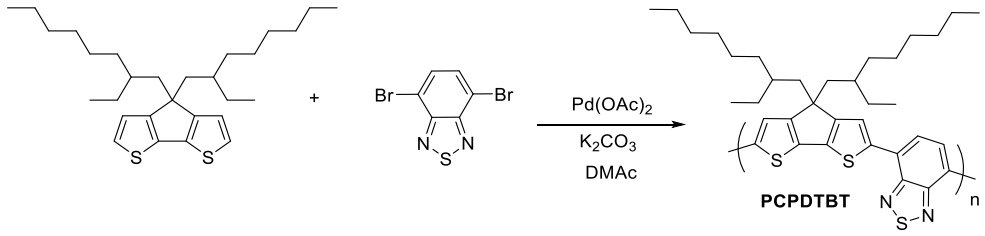

Scheme 24. PCPDTBT synthesis by direct polymerization.[58]

Direct polymerization reactions may provide high yields, low catalyst loadings, high molecular weights, and shortened reaction times toward the final products with an increased atom-economy. Nevertheless, it is not a fully optimized and established method for conjugated polymer synthesis yet and there is no standard procedure available to obtain conjugated polymers in high yields and with high molecular weights. Until now, different reaction conditions in terms of ligands, catalysts and additives have been used. In addition, the coupling of non-activated monomers can create misconnections of structural units and lead to branching of the polymer chains, if hydrogens on other reactive positions within the monomers are not protected.[60]

1.7. THESIS AIM AND OUTLINE

Over the past ten years, organic photovoltaics have made an impressive step forward. To date, OPV holds great potential as a renewable energy technology. The initial goal of the research described in this work was to develop a novel generation of n-type TzTz-based small molecule semiconductors as an alternative to the commonly used methanofullerene acceptors. Obviously, highly versatile and reproducible synthetic protocols, enabling fine-tuning of the material features, are desired toward rationalized material engineering. One of the possible synthetic protocols to develop TzTz-based semiconducting materials, with additional assets in terms of sustainability and synthetic complexity, is the direct arylation method, which was introduced at the start of the PhD project and then gradually implemented. During optimization of the direct arylation protocols, donor-type TzTz materials were synthesized as well, and as such the scope of the thesis was expanded to both p- and n-type materials. After successful synthesis, the most promising materials were evaluated in OPV devices.

After the general introduction (**Chapter 1**), the next chapters in this thesis deal with the experimental work conducted on different types of TzTz-based semiconductors for organic solar cell applications.

Chapter 2 focuses on the microwave-assisted synthesis of mono- and diarylated 2,5-dithienylthiazolo[5,4-*d*]thiazole derivatives via a direct arylation procedure. Implementing optimized reaction conditions, various (hetero)aryl bromides with different electron affinities are successfully reacted toward a variety of TzTz-based 'first generation' molecular chromophores with an extended conjugated backbone.

Furthermore, monoarylated precursors are further used for the synthesis of asymmetrically substituted push-pull-type 2,5-dithienylthiazolo[5,4-*d*]thiazoles.

Chapter 3 reports on the application of the TzTz materials prepared in Chapter 2 as solution-processable photon-harvesting materials for bulk heterojunction organic photovoltaics. From the synthesized series, a selection of symmetrical and asymmetrical small molecules is made based on their opto-electric properties and potential to be applied as p or n-type OPV materials. Power conversion efficiencies of 2.7 and 0.4% are achieved for TzTz small molecule donor and acceptor compounds, respectively.

In **Chapter 4** a series of three extended D'A'DADA'D'-type TzTz-based 'second generation' molecular chromophores is synthesized via a two-fold direct arylation protocol. The synthesized materials differ in their central acceptor moiety – bithiazole, quinoxaline or isoindigo – and are specifically designed to be applied as small molecule electron donor components in bulk heterojunction organic solar cells. Thermal and electro-optical material properties are studied by rapid heat-cool calorimetry, cyclic voltammetry and UV-Vis spectroscopy. An optimum solar cell efficiency of 4.86% is achieved, a record performance for TzTz-based small molecule compounds as well as small molecule materials prepared by C-H arylation.

Chapter 5 reports on the synthesis of two D–π-A-π–D-type small molecules based on a thiazolo[5,4-*d*]thiazole acceptor unit, electron-donating triphenylamine end groups and either a bithiazole or thienylenevinylene π–bridging moiety via a combination of traditional Stille cross-coupling and C-H arylation reactions. Whereas the first material is prepared in a straightforward manner, the second

(thienylenevinylene-based) molecule is obtained as a complicated and inseparable product mixture due to the lack of C-H regioselectivity. Preliminary solar cell measurements afford a moderate power conversion efficiency (0.6%).

The final experimental chapter (**Chapter 6**) deals with a somewhat different type of small molecule semiconducting materials. A series of fully conjugated quinoxaline-based oligophenylene macrocycles is synthesized by Ni^0-mediated Yamamoto-type diaryl homocoupling of (fluorinated) 2,3-bis(4'-bromophenyl)quinoxaline precursors. The cyclotrimers and cyclotetramers are fully characterized and structural confirmation is provided by X-ray crystallography.

In **Chapter 7** a general summary of the thesis is presented and an outlook is provided.

1.8. References

(1) Smalley, R. E. *MRS Bull.* **2005**, *30*, 412.

(2) US Energy Information Administration, International Energy Outlook 2013: http://www.eia.gov/oiaf/aeo/tablebrowser/ [accessed 24.10.13].

(3) Pavlović, T.M.; Radonjić, I.S.; Milosavljević, D.D.; Pantić, L. S. *Renew. Sustain. Energy Rev.* **2012**, *16*, 3891.

(4) Shafiee, S.; Topal, E. *Energy Policy* **2009**, *37*, 181.

(5) Yuan, J. S.; Tiller, K. H.; Al-Ahmad, H.; Stewart, N. R.; Stewart Jr, C. N. *Trends Plant Sci.* **2008**, *13*, 421.

(6) Chen, Z.; Blaabjerg, F. *Renew. Sustain. Energy Rev.* **2009**, *13*, 1288.

(7) Pazheri, F. R.; Othman, M. F.; Malik, N. H. *Renew. Sustain. Energy Rev.* **2014**, *31*, 835.

(8) Solangi, K. H.; Islam, M. R.; Saidur, R.; Rahim, N. A.; Fayaz, H. *Renew. Sustain. Energy Rev.* **2011**, *15*, 2149.

(9) http://www.eia.gov/forecasts/steo/pdf/steo_full.pdf

(10) Becquerel, A. E. *Compt. Rend. Acad. Sci.* **1839**, *9*, 561.

(11) Koenigsberger, J.; Schilling, K. *Ann. Phys.* **1910**, *337*, 179.

(12) Pochettino, A. *Accad. Licei Rend.* **1906**, *15*, 355.

(13) Volmer, M. *Ann. Phys.* **1913**, *345*, 775.

(14) Kallmann, H.; Pope, M. *J. Chem. Phys*. **1959**, *30*, 585.

(15) (a) Arlman, E. J.; Cossee, P. *J. Catal.* **1964**, *3*, 99; (b) Natta, G.; Danusso, F. Eds., Pergamon Press, *Stereoregular Polymers and Stereospecific Polymerizations*, **1967**.

(16) Chiang, C. K.; Fincher Jr, C. R.; Park, Y. W.; Heeger, A. J.; Shirakawa, H.; Louis, E. J.; Gau, S. C.; MacDiarmid. A. G. *Phys. Rev. Lett.* **1977**, *39*, 1098.

(17) Tang. C. W. *Appl. Phys. Lett*. **1986**, *48*, 183.

(18) Sariciftci, N. S.; Smilowitz, L.; Heeger, A. J.; Wudl, F. *Science* **1992**, *258*, 1474.

(19) Hummelen, J. C.; Knight, B. W.; LePeq, F.; Wudl, F.; Yao, J.; Wilkins, C. L. *J. Org. Chem*. **1995**, *60*, 532.

(20) Yu, G.; Gao, J.; Hummelen, J. C.; Wudl, F.; Heeger. A. J. *Science* **1995**, *270*, 1789.

(21) Liu, Y.; Zhao, J.; Li, Z.; Mu, C.; Ma, W.; Hu, H.; Jiang, K.; Lin, H.; Ade, H.; Yan, H. *Nat. Commun.* **2014**, *5*, 5293.

(22) http://www.nrel.gov/ncpv/index.html

(23) (a) Brabec, C. J. *Sol. Energy Mater. Sol. Cells* **2004**, *83*, 273; (b) Xue, J. *Polym. Rev.* **2010**, *50*, 411; (c) Deibel, C.; Dyakonov, V. *Rep. Prog. Phys.* **2010**, *73*, 096401; (d) Chidichimo, G.; Filippelli, L. *Int. J. Photoenergy* **2010**, 123534; (e) Nielsen, T. D.; Cruickshank, C.; Foged, S.; Thorsen, J.; Krebs, F. C. *Sol. Energy Mater. Sol. Cells* **2010**, *94*, 1553; (f) Helgesen, M.; Søndergaard, R.; Krebs, F. C. *J. Mater. Chem.* **2010**, *20*, 36; (g) Bundgaard, E.; Hagemann, O.; Manceau, M.; Jørgensen, M.; Krebs, F. C. *Macromolecules* **2010**, *43*, 8115; (h) Krebs, F. C. *Polymeric Solar Cells: Material, Design, Manufacture*; DEStech Publications, Inc., Lancaster, Pennsylvania, **2010**; (i) Arias, A. C.; MacKenzie, J. D.; McCulloch, I.; Rivnay, J.; Salleo, A. *Chem. Rev.* **2010**, *110*, 3; (j) Brabec, C. J.; Gowrisanker, S.; Halls, J. J. M.; Laird, D.; Jia, S.; Williams, S. P. *Adv. Mater.* **2010**, *22*, 3839; (k) Boudreault, P.-L. T.; Najari, A.; Leclerc, M. *Chem. Mater.* **2011**, *23*, 456; (l) Teichler, A.; Eckardt, R.; Hoeppener, S.; Friebe, C.; Perelaer, J.; Senes, A.; Morana, M.; Brabec, C.

J.; Schubert, U. S. *Adv. Energy Mater.* **2011**, *1*, 105; (m) Hübler, A.; Trnovec, B.; Zillger, T.; Ali, M.; Wetzold, N.; Mingebach, M.; Wagenpfahl, A.; Deibel, C.; Dyakonov, V. *Adv. Energy Mater.* **2011**, *1*, 1018.

(24) Kroon, R.; Lenes, M.; Hummelen, J. C.; Blom, P. W. M.; de Boer, B. *Polym. Rev.* **2008**, *48*, 531.

(25) (a) Brabec, C. J.; Shaheen, S. E.; Winder, C.; Sariciftci, N. S.; Denk, P. *Appl. Phys. Lett.* **2002**, *80*, 1288; (b) Wienk, M. M.; Kroon, J. M.; Verhees, W. J. H.; Knol, J.; Hummelen, J. C., Van Hal, P. A.; JanssenR. A. J. *Angew Chem. Int. Ed.* **2003**, *42*, 3371.

(26) (a) Huang, J.; Yao, Y.; Moriarty, T.; Emery, K.; Yang, Y. *Nat. Mater.* **2005**, *4*, 864; (b) Ma, W. L.; Yang, C. Y.; Gong, X.; Lee, K.; Heeger, A. J. *Adv. Funct. Mater.* **2005**, *15*, 1617.

(27) Hoogmartens, I.; Adriaensens, P.; Vanderzande, D.; Gelan, J; Quattrocchi, C.; Lazzaroni, R.; Brédas, J. L. *Macromolecules* **1992**, *26*, 7347.

(28) Van Mierloo, S.; Hadipour, A.; Spijkman, M.-J.; Van den Brande, N.; Ruttens, B.; Kesters, J.; D'Haen, J.; Van Assche, G.; de Leeuw, D. M.; Aernouts, T.; Manca, J.; Lutsen, L.; Vanderzande, D. J.; Maes, W. *Chem. Mater.* **2012**, *24*, 587.

(29) Subramaniyan, S.; Xin, H.; Kim, F. S.; Murari, N. M.; Courtright, B. A. E.; Jenekhe, S. A. *Macromolecules* **2014**, *47*, 4199.

(30) Vanormelingen, W.; Kesters, J.; Verstappen, P.; Drijkoningen, J.; Kudrjasova, J.; Koudjina, S.; Liégeois, V.; Champagne, B.; Manca, J.; Lutsen, L.; Vanderzande, D.; Maes, W. *J. Mater. Chem. A* **2014**, *2*, 7535.

(31) Kesters, J.; Ghoos, T.; Penxten, H.; Drijkoningen, J.; Vangerven, T.; Lyons, D. M.; Verreet, M.; Aernouts, T.; Lutsen, L.; Vanderzande, D.; Manca, J.; Maes, W. *Adv. Energy Mater*. **2013**, *9*, 1180.

(32) Osaka, I.; Saito, M.; Koganezawa, T.; Takimiya, K. *Adv. Mater.* **2014**, *26*, 331.

(33) (a) Mishra, A.; Bäuerle, P. *Angew. Chem. Int. Ed.* **2012**, *51*, 2020; (b) Lin, Y.; Li, Y.; Zhan, X. *Chem. Soc. Rev.* **2012**, *41*, 4245; (c) Chen, Y.; Wan, X.; Long, G. *Acc. Chem. Res.* **2014**, *46*, 2645.

(34) Walker, B.; Kim, C.; Nguyen, T. Q. *Chem. Mater.* **2011**, *23*, 470.

(35) Welch, G. C.; Perez, L. A.; Hoven, C. V.; Zhang, Y.; Dang, X. D.; Sharenko, A.; Toney, M. F.; Kramer, E. J.; Thuc-Quyen, N.; Bazan, G. C. *J. Mater. Chem.* **2011**, *21*, 12700.

(36) Zhou, J.; Zuo, Y.; Wan, X.; Long, G.; Zhang, Q.; Ni, W.; Liu, Y.; Li, Z.; He, G.; Li, C.; Kan, B.; Chen, Y. *J. Am. Chem. Soc.* **2013**, *135*, 8484.

(37) Kan, B.; Zhang, Q.; Li, M.; Wan, X.; Ni, W.; Long, G.; Wang, Y.; Yang, X.; Feng, H.; Chen, Y. *J. Am. Chem. Soc*. **2014**, *136*, 15529.

(38) Kyaw, A. K. K.; Wang, D. H.; Wynands, D.; Zhang, J.; Nguyen, T.-Q.; Bazan, G. C.; Heeger, A. J. *Nano Lett.* **2013**, *13*, 3796.

(39) Dutta, P.; Yang, W.; Eom, S. H.; Lee, S.-H. *Org. Electron.* **2012**, *13*, 273.

(40) Shi, Q.; Cheng, P.; Li, Y.; Zhan, X. *Adv. Energy Mater*. **2012**, *2*, 63.

(41) Cheng, P.; Shi, Q.; Lin, Y.; Li. Y.; Zhan, X. *Org. Electron.* **2013**, *14*, 599.

(42) Dutta, P.; Park, H.; Lee, W.-H.; Kang, I.-N.; Lee, S.-H. *Org. Electron.* **2012**, *13*, 3183.

(43) (a) Park, S. H.; Roy, A.; Beaupré, S.; Cho, S.; Coates, N.; Moon, J. S.; Moses, D.; Leclerc, M.; Lee, K.; Heeger, A. J. *Nat. Photonics* **2009**, *3*, 297; (b) Guo, X.; Zhou, N.; Lou, S. J.; Smith, J.; Tice, D. B.; Hennek, J. W.; Ortiz, R. P.; Navarrete, J. T. L.; Li, S.; Strzalka, J.; Chen, L. X.; Chang, R. P. H.; Facchetti, A.; Marks, T. J. *Nat. Photonics* **2013**, *7*, 825; (c) Savoie, B. M.;

Rao, A.; Bakulin, A. A.; Gelinas, S.; Movaghar, B.; Friend, R. H.; Marks, T. J.; Ratner, M. A. *J. Am. Chem. Soc.* **2014**, *136*, 2876.

(44) (a) Anctil, A.; Babbitt, C. W.; Raffaelle, R. P.; Landi, B. J. *Prog. Photovolt.: Res. Appl.* **2012**, *21*, 1541; (b) Lizin, S.; Van Passel, S.; De Schepper, E.; Maes, W.; Lutsen, L.; Manca, J.; Vanderzande, D. *Energy Environ. Sci.* **2013**, *6*, 3136.

(45) (a) Sonar, P.; Fong Lim, J. P.; Chan, K. L. *Energy Environ. Sci.* **2011**, *4*, 1558; (b) Anthony, J. E. *Chem. Mater.* **2011**, *23*, 583; (c) Lin, Y.; Li, Y.; Zhan, X. *Adv. Energy Mater.* **2013**, *3*, 724; (d) Eftaiha, A. F.; Sun, J.-P.; Hill, I. G.; Welch, G. C. *J. Mater. Chem. A* **2014**, *2*, 1201; (e) Lu, Z.; Jiang, B.; Zhang, X.; Tang, A.; Chen, L.; Zhan, C.; Yao, J. *Chem. Mater.* **2014**, *26*, 2907.

(46) (a) Facchetti, A. *Mater. Today* **2013**, *16*, 123; (b) Li, W.; Roelofs, W. S. C.; Turbiez, M.; Wienk, M. M.; Janssen, R. A. J. *Adv. Mater.* **2014**, *26*, 3304; (c) Zhou, Y.; Kurosawa, T.; Ma, W.; Guo, Y.; Fang, L.; Vandewal, K.; Diao, Y.; Wang, C.; Yan, Q.; Reinspach, J.; Mei, J.; Appleton, A. L.; Koleilat, G. I.; Gao, Y.; Mannsfeld, S. C. B.; Salleo, A.; Ade, H.; Zhao, D.; Bao, Z. *Adv. Mater.* **2014**, *26*, 3767; (d) Zhou, N.; Lin, H.; Lou, S. J.; Yu, X.; Guo, P.; Manley, E. F.; Loser, S.; Hartnett, P.; Huang, H.; Wasielewski, M. R.; Chen, L. X.; Chang, R. P. H.; Facchetti, A.; Marks, T. J. *Adv. Energy Mater.* **2014**, *4*, 1300785.

(47) Zhang, X.; Zhan, C.; Yao, J. *Chem. Mater.* **2015**, *27*, 166.

(48) Nevil, N.; Ling, Y.; Van Mierloo, S.; Kesters, J.; Piersimoni, F.; Adriaensens, P.; Lutsen, L.; Vanderzande, D.; Manca, J.; Maes, W.; Van Doorslaer, S.; Goovaerts, E. *Phys. Chem. Chem. Phys.* **2012**, *14*, 15774.

(49) (a) Schipper, D. J.; Fagnou, K. *Chem. Mater.* **2011**, *23*, 1594; (b) Zhang, J.; Kang, D.-Y.; Barlowa, S.; Marder, S. R. *J. Mater. Chem.* **2012**, *22*, 21392; (c) Zhang, J.; Chen, W.; Rojas, A. J.; Jucov, E. V.; Timofeeva, T. V.; Parker,

T. C.; Barlow, S.; Marder, S. R. *J. Am. Chem. Soc.* **2013**, *135*, 16376. (d) Liu, S.-Y.; Shi, M.; Huang, J.; Jin, Z.; Hu, X.; Pan, J.; Li, H.; Jen, A. K.-Y.; Chen, H.-Z. *ACS Appl. Mater. Interfaces* **2014**, *6* (9), 6765. (e) Liu, S.-T.; Shi, M.-M.; Huang, J.-C.; Jin, Z.-J.; Hu, H.-L.; Pan, Y.-J.; Li, H.-Y.; Jen, A. K.-Y; Chen, H.-Z. *J. Mater. Chem. A* **2013**, *1*, 2795.

(50) (a) Boutadla, Y.; Davies, D. L.; Macgregor, S. A.; Poblador-Bahamonde, A. I. *Dalton Trans.* **2009**, 5820. (b) Lapointe, D.; Fagnou, K. *Chem. Lett.* **2010**, *39*, 1118. (c) Ackermann, L. *Chem. Rev.* **2011**, *111*, 1315.

(51) (a) Battagliarin, G.; Li, C.; Enkelmann, V.; Müllen, K. *Org. Lett*. **2011**, *13*, 3012; (b) Teraoka, T.; Hiroto, S.; Shinokubo, H. *Org. Lett.* **2011**, *13*, 2532; (c) Zhang, J.; Singh, S.; Hwang, D. K.; Barlow, S.; Kippelen, B.; Marder, S. R. *J. Mater. Chem. C* **2013**, *1*, 5093.

(52) (a) Yue, W.; Lv, A.; Gao, J.; Jiang, W.; Hao, L.; Li, C.; Li, Y.; Polander, L. E.; Barlow, S.; Hu, W.; Di Motta, S.; Negri, F.; Marder, S. R.; Wang, Z. *J. Am. Chem. Soc.* **2012**, *134*, 5770; (b) Suraru, S.-L.; Zschieschang, U.; Klauk, H.; Würthner, F. *Chem. Commun.* **2011**, *47*, 11504.

(53) Liu, S.-Y.; Fu, W.-F.; Xu, J.-Q.; Fan, C.-C.; Jiang, H.; Shi, M.; Li, H.-Y.; Chen, J.-W.; Cao, Y.; Chen, H.-Z. *Nanotechnology* **2014**, *25*, 014006.

(54) (a) Wang, Q.; Takita, R.; Kikuzaki, Y.; Ozawa, F. *J. Am. Chem. Soc.* **2010**, *132*, 11420; (b) Lu, W.; Kuwabara, J.; Kanbara, T. *Macromolecules* **2011**, *44*, 1252.

(55) Choi, S. J.; Kuwabara, J.; Kanbara, T. *ACS Sustain. Chem. Eng.* **2013**, *1*, 878.

(56) Lu, W.; Kuwabara, J.; Iijima, T.; Higashimura, H.; Hayashi, H.; Kanbara, T. *Macromolecules* **2012**, *45*, 4128.

(57) Berrouard, P.; Najari, A.; Pron, A.; Gendron, D.; Morin, P.-O.; Pouliot, J-R.; Veilleux, J.; Leclerc, M. *Angew. Chem. Int. Ed.* **2012**, *51*, 2068.

(58) Kowalski, S.; Allard, S.; Scherf, U. *ACS Macro. Lett.* **2012**, *1*, 465.

(59) (a) Kuwabara, J.; Nohara, Y.; Jib Choi, S.; Fujinami, Y.; Lu, W.; Yoshimura, K.; Oguma, J.; Suenobu, K.; Kanbara, T. *Polym. Chem.* **2013**, *4*, 947; (b) Rudenko, A. E.; Wiley, C. A.; Stone, S. M.; Tannaci, J. F.; Thompson, B. C. *J. Polym. Sci., Part A: Polym. Chem.* **2012**, *50*, 3691.

(60) Hayashi, S.; Kojima, Y.; Koizumi, T. *Polym. Chem.* **2015**, *6*, 881.

Chapter 2

Direct arylation as a versatile tool toward thiazolo[5,4-*d*]thiazole-based semiconducting materials

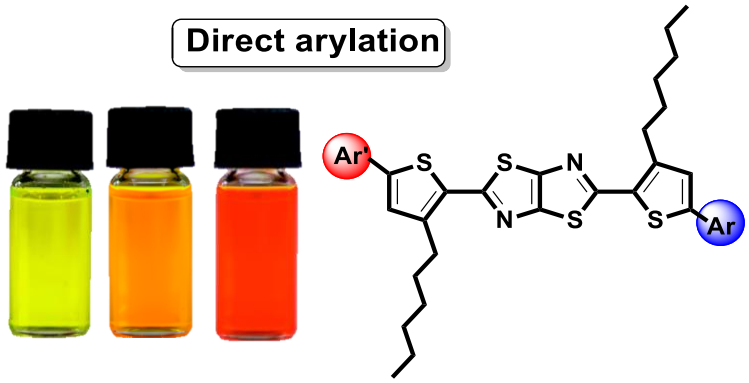

Kudrjasova, J.; Herckens, R.; Penxten, H.; Adriaensens, P.; Lutsen, L.; Vanderzande, D.; Maes, W. *Org. Biomol. Chem.* **2014**, *12*, 4663–4672.

(Article contribution: all synthesis and chemical analysis, main author)

ABSTRACT

A series of thiazolo[5,4-*d*]thiazole-based small molecule organic optoelectronic materials was synthesized via a straighforward microwave-activated Pd-catalyzed C-H arylation protocol. The procedure allows to obtain extended 2,5-dithienylthiazolo[5,4-*d*]thiazole chromophores with tailor-made energy levels and absorption patterns, depending on the introduced (het)aryl moieties and the molecular (a)symmetry, by shortened sequences without organometallic intermediates. The synthesized materials can be applied as either electron donor or electron acceptor light-harvesting materials in molecular bulk heterojunction organic solar cells.

2.1. INTRODUCTION

Optoelectronic devices based on organic semiconductors – organic solar cells, transistors, light-emitting diodes and related applications – are steadily entering the market as the organic components allow to develop very thin and flexible large area devices with tunable color and transparency at a low cost using solution-based deposition techniques such as roll-to-roll printing. The optoelectronic properties of the active materials can readily be optimized through versatile organic synthesis protocols. In the design of potent organic semiconductors, careful consideration of molecular properties such as oxidation potentials, electron affinities, light harvesting/emitting and/or charge transport features, solubility and intermolecular *π*-*π* interactions is of crucial importance. Oligothiophene structures have been shown to possess excellent semiconductor characteristics and a wide range of heterocycles has been introduced in thiophene-based *π*-conjugated small molecule materials to optimize particular properties.[1] Thiazolo[5,4-*d*]thiazole (TzTz) fused biheterocycles possess a number of features – a rigid planar structure, strong electron deficient character, high oxidative stability, and high charge mobility – that make them particularly attractive for organic electronics.[2-5] Nevertheless, their application has been limited, until recently, when the high potential of these molecules was more widely recognized, notably in the field of solution-processed organic photovoltaics (OPV).[6-8] Despite the strong rise in interest in these molecules, the synthetic chemistry behind the TzTz derivatives has only been developed to a minor extent, and there is certainly room for improvement and broadening of the material scope.[2]

In previous work, we have synthesized a number of 5'-aryl-substituted 2,5-bis(3'-hexylthiophen-2'-yl)thiazolo[5,4-*d*]thiazole derivatives via Suzuki and Stille cross-

coupling reactions and these expanded semiconductors were investigated as active materials for solution-processable organic field-effect transistors (OFET's).[9] On the other hand, it was shown that charge transfer (in the weak driving force limit) occurs in blends of dithienyl-TzTz's and MDMO-PPV (poly[2-methoxy-5-(3',7'-dimethyloctyloxy)-1,4-phenylene vinylene]) towards fullerene-free OPV devices with high open-circuit voltages (V_{oc}).[10] Fullerenes till now turn out to be the superior electron acceptors in organic solar cells. The promises of more generic and versatile low-cost non-fullerene small molecules as acceptors in bulk heterojunction (BHJ) organic solar cells have not been fulfilled so far, with maximum efficiencies approaching 4% (and routinely below 2%).[11] It has recently been calculated though that the cumulative energy demand (CED) required to produce BHJ OPV's, although on average 50% less than for conventional inorganic photovoltaics, is strongly affected by the presence of fullerenes, comprising 18–30% of the CED, despite being present in small quantities.[12] On the other hand, recent progress in the field of solution-processed molecular OPV, based on small molecule electron donor materials and fullerene acceptors, has afforded power conversion efficiencies in the same range as the best polymer BHJ OPV systems.[1b,13] In this line of thought, we now report on a series of TzTz-based small molecules, synthesized via microwave-activated direct arylation reactions, allowing to tune the energy levels and light absorption towards applications in OPV, either as small molecule electron donor materials or alternative electron acceptors.

2.2. RESULTS AND DISCUSSION

Direct arylation reactions, in which the Pd-catalyzed coupling occurs directly between an (hetero)aryl bromide and an (hetero)aryl compound with activated C-H groups, have a number of advantages over traditional cross-coupling techniques, i.e. fewer synthetic operations and potentially higher yields, lower catalyst loadings, and no need for (high purity) organometallic intermediates (resulting in toxic byproducts, *e.g.* trialkyltin compounds), rendering it an ideal strategy for the synthesis of advanced materials for organic electronics.[14] C-H arylation procedures are often conducted in combination with microwave activation to speed up the reactions. Direct arylation protocols have recently been employed for the synthesis of low bandgap small molecules[15] and polymer materials[16] for organic solar cells, but they haven't been applied on TzTz's so far.

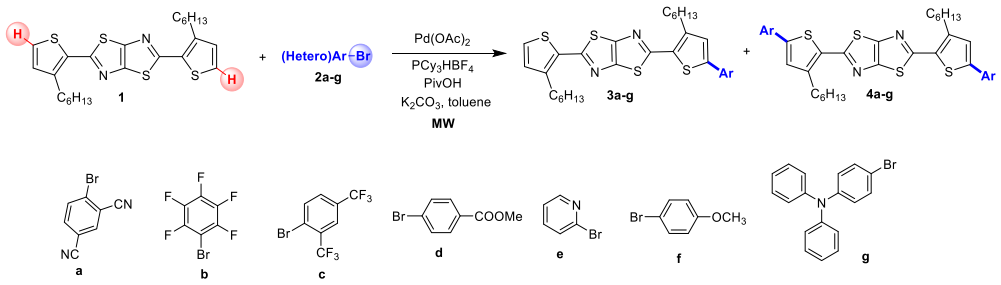

Scheme 1. Synthesis of 5'-mono- (**3a–g**) and diarylated (**4a–g**) 2,5-bis(3'-hexylthiophen-2'-yl)thiazolo[5,4-*d*]thiazole derivatives via C-H arylation.

In this work, we have used a C-H arylation strategy to synthesize a series of TzTz-based semiconductors with varying electron affinities to be applied in organic solar cells, with a particular emphasis on monosubstitution, enabling to obtain asymmetrical push-pull derivatives to broaden the absorption window.

As the activated C-H part we have chosen 2,5-bis(3'-hexylthiophen-2'-yl)thiazolo[5,4-*d*]thiazole (**1**) (Scheme 1), which was prepared in a

straightforward way (in 60% yield) via a condensation reaction at elevated temperature (130 °C) between dithiooxamide and 3-hexylthiophene-2-carbaldehyde in nitrobenzene, according to a modified literature procedure.[17] It's worth to mention that in this method only a stoichiometric amount of aldehyde (vs the 6 equiv used before[9,17]) has to be used. Dithienyl-TzTz **1** was then combined with different (hetero)aryl bromides **2a–g** (Scheme 1), chosen as such to generate a family of compounds with varying electron affinities. The reaction conditions ($PdOAc_2$, PCy_3HBF_4, pivalic acid, K_2CO_3, toluene, microwave heating)[14b] were first optimized for the combination of TzTz **1** and methyl 4-bromobenzoate (**2d**) (Table 1), in particular aiming at selective monoarylation as this provides an entry into unprecedented asymmetrically substituted TzTz materials. For that purpose, 1.1 equivalents **2d** were used and the reaction time was varied between 4 and 7 hours, whereas the reaction temperature was gradually increased from 100 to 180 °C. The highest yield was achieved at 180 °C (64% **3d**, 34% **4d**), although the selectivity was still modest. It should be mentioned here that the yield for the disubstituted product **4d** is based on the amount of TzTz **1** (a minority of 0.55 equiv with respect to **2d**) and might therefore look somewhat overestimated. In this respect, the isolated product amounts (as mentioned in the experimental section) might be more illustrative for the reaction selectivity (mono- vs disubstitution). At lower temperatures, quite some starting material (TzTz **1**) remained. Running the reaction at 100 °C for a longer time (7 h) did not significantly change the reaction outcome. Addition of an extra portion of fresh catalyst (2 mol%)[18] after 4 hours of reaction at 100 °C (and stirring for another 3 h at the same temperature) did not give any significant increase in the yield of **3d** and **4d** (49 and 7%, respectively) either.

Table 1. Optimization (of reaction time and temperature) for the direct arylation of TzTz **1** and methyl 4-bromobenzoate (**2d**) (1.1 equiv).

T (°C)	Time	**3d**	**4d**[a]
100	4h	43	8[b]
120	4h	41	30[b]
140	4h	57	33[b]
160	4h	60	33
180	4h	64	34
100	7h	46	4[b]

[a] Reaction yields might be somewhat misleading for the disubstituted product **4d** as they are based on the reaction partner in minority (TzTz **1**). [b] The remaining of the crude reaction mixture was mainly starting material (TzTz **1**).

The direct arylation of TzTz **1** was then extended to different types of aryl bromides **2a–g** using the same protocol (180 °C, 4 h) (Scheme 1, Table 2). The amount of (hetero)aryl bromide was adjusted for either mono- (1.1 equiv) or diarylation (2.1 equiv). Whenever separation and purification of the mono- and disubstituted compounds proved difficult, preparative size exclusion chromatography (SEC) was applied (see exp. section). In general, good overall yields were achieved, but selectivities were rather modest (with some notable exceptions, see Table 2). From the results obtained it is hard to detect clear trends in either yields or selectivities considering electronic substituent effects.

Table 2. Overview of the (isolated) yields and selectivities for the reactions between TzTz **1** and (hetero)aryl bromides **2a–g**.

(Hetero)Ar-Br	Yields			
	1.1 equiv		2.1 equiv	
2a–g	**3**	**4**[b]	**3**	**4**
a	49	44	34	52
b	35 49[a]	27 36[a]	30[a]	69[a]
c	33 58[a]	20 42[a]	27[a]	58[a]
d	64	34	6	92
e	69	27	34	50
f	28	70	32	64[b]
g	50	38	46	38[b]

[a] These reactions were run for 7 h (instead of the standard 4 h). [b] Reaction yields might be somewhat misleading for the disubstituted products as they are based on the reaction partner in minority (TzTz **1**).

All TzTz derivatives were completely characterized by ^{1}H and ^{13}C NMR and HRMS. UV-Vis absorption spectra of the functionalized TzTz molecules were collected to evaluate their light harvesting properties, and the corresponding data (λ_{max} and ε) are gathered in Table 3. The (normalized) absorption spectra of disubstituted TzTz's **4a–g** in chloroform solution are depicted in Fig. 1 (see Fig. S1 for the corresponding spectra of monosubstituted derivatives **3a–g**). All UV-Vis spectra display two distinct absorption bands in the UV (λ_{max} 250–320 nm) and visible region (λ_{max} 400–470 nm), attributed to the π–π* electronic transition and intramolecular charge transfer, respectively.[19] As expected, the difunctionalized

TzTz's show a more red-shifted (10–28 nm) absorption. In addition, they have broader absorption spectra and higher molar absorptivities. Optical HOMO-LUMO gaps were determined from the onset (λ_{onset}) of the absorption spectra in thin film. The optical HOMO-LUMO gaps are between 2.32 and 2.72 eV (Table 3), hence still rather high for OPV applications. The electron donating character of the triphenylamine substituent (**3g**/**4g**), together with the extended conjugation length, results in a broad and red-shifted absorption with the smallest optical HOMO-LUMO gaps. Basic electrochemical properties were investigated by cyclic voltammetry (CV) and the derived frontier orbital energy levels are depicted in Table 3. The presence of electron withdrawing substituents such as cyano, fluoro and trifluoromethyl groups endows the molecules with a deeper LUMO level (calculated from the HOMO level, as derived from the oxidation potential, and the optical HOMO-LUMO gap), rendering them possible candidates for n-type acceptor materials for organic solar cells. As known from former work,[9a] dithienyl-TzTz semiconducting molecules with electron accepting substituents can be combined with a donor polymer (in this case MDMO-PPV) to afford photoinduced charge transfer (CT) in the resulting blends. The CT efficiencies were shown to be strongly correlated with increasing acceptor strength. Some of the new compounds (**3a**/**4a**) have lower LUMO values as compared to the published TzTz materials, which could possibly improve the CT efficiency and the final solar cell performance (considering also other potential loss mechanisms and sufficient electron mobility), increasing the very low efficiency of 0.1% previously observed.[10] Fig. 2 gives an overview of the energy levels obtained for all materials, together with prototype electron donor polymers (MDMO-PPV and P3HT or poly(3-hexylthiophene)) and the most used acceptor PCBM ([6,6]-phenyl-C_{61}-butyric acid methyl ester). Whereas previously only MDMO-PPV could be applied as donor

material for the bis(4-cyanophenyl)-substituted dithienyl-TzTz acceptor (HOMO -5.76 eV, LUMO -3.25 eV), the LUMO levels of some of the novel materials (notably **4a**) are sufficiently low to enable combination with more effective low band gap polymers such as PCPDT-DTTzTz[7f] (poly{[4-(2'-ethylhexyl)-4-octyl-4*H*-cyclopenta[2,1-*b*:3,4-*b'*]dithiophene-2,6-diyl]-*alt*-[2,5-di(3'-hexylthiophen-2'-yl)thiazolo[5,4-*d*]thiazole-5',5''-diyl]}), also containing TzTz as the electron deficient part.

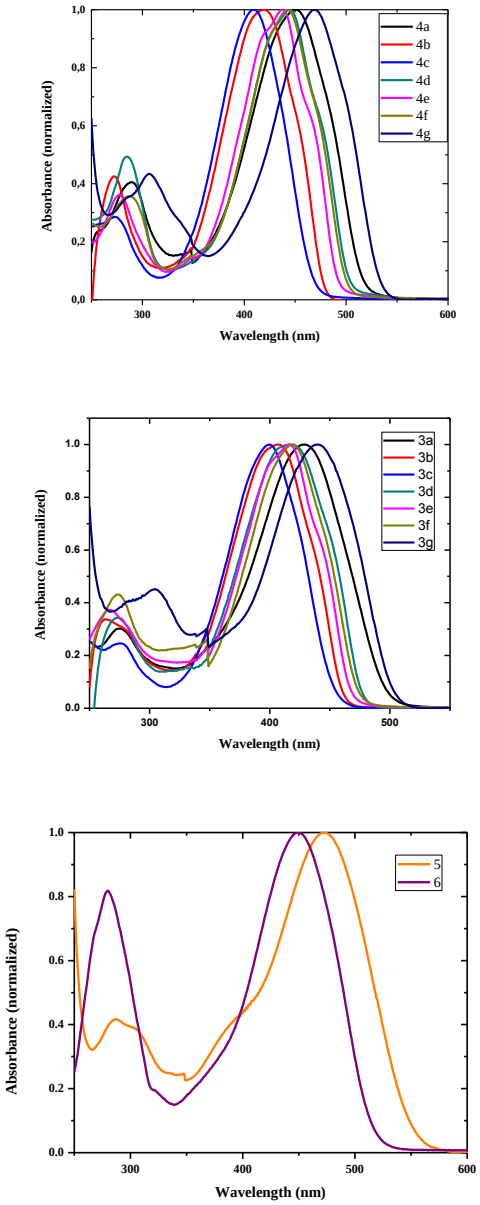

Fig. 1. Normalized UV-Vis absorption spectra of monofunctionalized TzTz's **3a–g** (top), difunctionalized TzTz's **4a–g** (middle)**,** and asymmetrical TzTz's **5** and **6** (bottom) in $CHCl_3$ solution.

Table 3. Optical and electrochemical properties of the synthesized TzTz's (and some reference materials).

TzTz	λ_{max} (nm)[b] (log ε)[c]	ΔE_{opt}[d]	E^{ox}_{onset} (V)	HOMO (eV)[g]	E^{red}_{onset} (V)	LUMO (eV)[i]	ΔE_{ec}[j]	$LUMO_{calc}$ (eV)[k]
3a	427 (4.54)	2.49	1.04[e]	-5.89	-1.46[e]	-3.38	2.50	-3.40
4a	451 (4.70)	2.40	1.06[e]	-5.91	-1.41[e]	-3.43	2.47	-3.51
3b	406 (4.55)	2.70	1.00[f]	-5.85	-1.79[f]	-3.05	2.80	-3.15
4b	421 (4.58)	2.59	1.04[f]	-5.88	-1.72[f]	-3.12	2.76	-3.29
3c	400 (4.60)	2.72	1.00[f]	-5.84	-1.75[h]	-3.10	2.75	-3.12
4c	410 (4.69)	2.66	1.03[e]	-5.87	-1.75[f]	-3.10	2.78	-3.21
3d	417 (4.40)	2.61	0.92[f]	-5.77	-1.78[e]	-3.06	2.71	-3.16
4d	445 (4.45)	2.46	0.88[e]	-5.73	-1.79[h]	-3.06	2.67	-3.27
3e	416 (4.58)	2.65	0.91[f]	-5.75	-1.76[f]	-3.09	2.66	-3.10
4e	440 (4.65)	2.51	0.85[e]	-5.70	-1.73[e]	-3.12	2.58	-3.19
3f	418 (4.65)	2.62	0.67[e]	-5.52	-1.91[e]	-2.94	2.58	-2.90
4f	442 (4.80)	2.47	0.77[e]	-5.62	-1.89[e]	-2.96	2.66	-3.15
3g	440 (4.70)	2.46	0.57[e]	-5.41	-1.89[e]	-2.96	2.45	-2.95
4g	469 (4.88)	2.32	0.53[e]	-5.38	-1.81[e]	-3.04	2.34	-3.06
5	473 (4.66)	2.26	0.56[e]	-5.41	-1.51[e]	-3.34	2.07	-3.15
6	449 (4.73)	2.40	0.56[e]	-5.40	-1.80[e]	-3.05	2.35	-3.00
PCBM	\	1.72	1.26	-6.12	-0.83	-4.03	2.09	-4.40
P3HT[a]	\	1.88	0.13	-5.10	-2.09	-2.87	2.22	-3.22
MDMO-PPV[a]	\	2.12	0.24	-5.21	-2.03	-2.93	2.28	-3.09

[a] CV data in film. [b] Measured in $CHCl_3$ solution. [c] Molar extinction coefficient ε, determined at λ_{max} in $CHCl_3$ solution. [d] Optical HOMO-LUMO gap, ΔE_{opt} = 1240/(λ_{onset}). [e] Reversible. [f] Quasi-reversible. [g] Determined from the oxidation onset. [h] Irreversible. [i] Determined from the reduction onset. [j] Electrochemical HOMO-LUMO gap. [k] $LUMO_{calc}$ = ΔE_{opt} + HOMO.

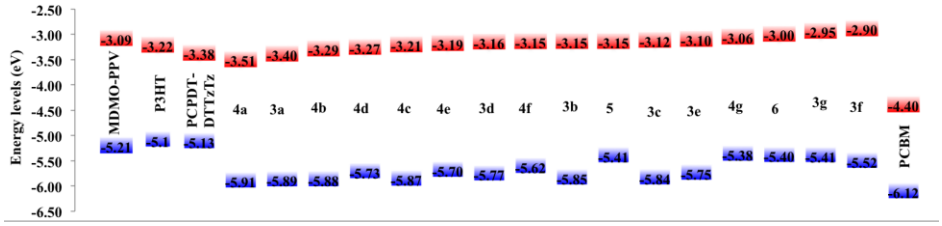

Fig. 2. HOMO-LUMO energy level diagram for the functionalized TzTz's.

A second particular goal was to prepare asymmetrical donor-TzTz-acceptor molecules with broadened absorption profiles by sequential direct coupling reactions, as these compounds are of high appeal as photoactive (electron donor) materials for OPV. The few literature examples of asymmetrically extended TzTz derivatives were prepared via traditional Suzuki cross-coupling reactions in moderate overall yields.[8e,20] Push-pull TzTz compounds **5** and **6** were synthesized from monoarylated derivatives **3g** and **3c** in 85 and 88% yield, respectively (Scheme 2). The UV-Vis absorption spectra of these materials (Fig. 1) indeed show extended absorption (up to λ_{max} 473 nm for **5**). Asymmetrical TzTz chromophore **5**, bearing triphenylamine and isophtalonitrile terminal units, has the highest HOMO/LUMO values among the series and shows potential as a small molecule electron donor compound, possibly even in combination with a more electron deficient TzTz material of the same family (Fig. 2).

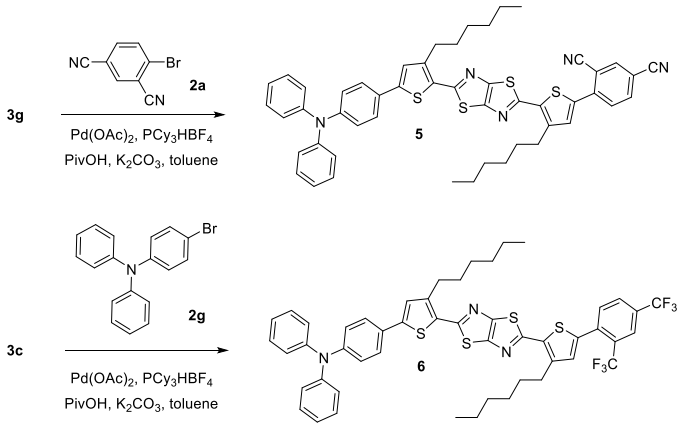

Scheme 2. Synthesis of asymmetrically substituted TzTz derivatives **5** and **6** via stepwise C-H arylation.

2.3. CONCLUSIONS

A facile and versatile microwave-assisted procedure was developed for the direct arylation of 2,5-dithienylthiazolo[5,4-*d*]thiazoles with various electron rich and poor (hetero)aryl bromides towards a variety of molecular chromophores with an extended conjugated backbone. Unsymmetrical derivatives were readily obtained by a sequential direct arylation approach. These materials are designed to be applied as solution-processable solar photon harvesting materials for bulk heterojunction organic photovoltaics, either as small molecule electron donor or acceptor constituents. Efforts in this direction are currently ongoing within our group. In a more general sense, the synthetic chemistry developed in this work can stimulate further progress on the development of controllable direct arylation protocols as powerful 'atom-economic' reactions towards advanced organic optoelectronic materials for printable electronics.

2.4. EXPERIMENTAL SECTION

General experimental methods

Unless stated otherwise, all reagents and chemicals were obtained from commercial sources and used without further purification. Toluene was dried using an MBraun solvent purification system (model MB-SPS 800) equipped with alumina drying columns. Microwave reactions were carried out in a CEM Discovery microwave at the given temperature by varying the irradiation power. A thick-walled pyrex reaction vessel (10 mL) with teflon septum was used for the microwave reactions. NMR chemical shifts (δ) were determined relative to the residual $CHCl_3$ absorption (7.26 ppm) or the ^{13}C resonance shift of $CDCl_3$ (77.16 ppm) or C_6D_5Cl (134.19 ppm). ^{13}C signals split up by *J*-coupling with ^{19}F are indicated by their chemical shifts. High resolution electrospray ionization mass spectrometry (ESI-MS) analysis of the samples was performed using an LTQ Orbitrap Velos Pro mass spectrometer (Thermo-Fischer Scientific) equipped with an atmospheric pressure ionization source operating in the nebulizer assisted electrospray mode. The instrument was calibrated in the *m/z* range 220**–**2000 using a standard solution containing caffeine, MRFA and Ultramark 1621. UV-Vis absorption spectra were recorded with an Agilent Cary 500 Scan UV-Vis-NIR spectrometer in a continuous run from 200 to 800 nm at a scan rate of 600 nm min^{-1}. Infrared spectra were collected with a resolution of 4 cm^{-1} (16 scans) using films drop-casted on a NaCl disk from $CHCl_3$ solution. Preparative size exclusion chromatography (SEC) was performed on JAIGEL 1H and 2H columns attached to an LC system equipped with a UV detector (path 0.5 mm) and a switch for recycling and collecting the eluent ($CHCl_3$: flow rate 3.5 mL min^{-1}, injection volume 2.5 mL). Electrochemical measurements were performed with an Eco Chemie

Autolab PGSTAT 30 potentiostat/galvanostat using a three-electrode microcell equipped with a Pt wire working electrode, a Pt wire counter electrode and a $Ag/AgNO_3$ reference electrode (Ag wire dipped in a solution of 0.01 M $AgNO_3$ and 0.1 M NBu_4PF_6 in anhydrous MeCN). Samples were prepared in anhydrous CH_2Cl_2 containing 0.1 M NBu_4PF_6, and ferrocene was used as an internal standard. The respective TzTz products were dissolved in the electrolyte solution, which was degassed with Ar prior to each measurement. To prevent air from entering the system, the experiments were carried out under a curtain of Ar. Cyclic voltammograms were recorded at a scan rate of 50 mV s^{-1}. The HOMO-LUMO energy levels of the products were determined using CV data and spectroscopic absorption data. For the conversion of V to eV, the onset potentials of the first oxidation/reduction peaks were used and referenced to ferrocene/ferrocenium, which has an ionization potential of -4.98 eV *vs.* vacuum. This correction factor is based on a value of 0.31 eV for Fc/Fc^+ *vs.* SCE[21a] and a value of 4.68 eV for SCE *vs.* vacuum[21b]: $E_{HOMO/LUMO}$ (eV) = -4.98 - $E_{onset\ ox/red}^{Ag/AgNO3}$ (V) + $E_{onset\ Fc/Fc+}^{Ag/AgNO3}$ (V). The HOMO energy levels of the TzTz products were determined from the CV data. The LUMO energy levels were either determined from the CV data or calculated as the difference between the HOMO values and the optical HOMO-LUMO gaps. To estimate the optical HOMO-LUMO gap, the wavelength at the intersection of the tangent line drawn at the low energy side of the (solution) absorption spectrum with the x-axis was used (E_g (eV) = 1240/(wavelength in nm)).

2,5-Bis(3'-hexylthiophen-2'-yl)thiazolo[5,4-*d*]thiazole (1). TzTz **1** was prepared by adding 3-hexylthiophene-2-carbaldehyde (1.96 g, 0.02 mol, 2 equiv) and dithiooxamide (2.39 g, 0.01 mol, 1 equiv) to nitrobenzene (20 mL) and heating the reaction mixture for 24 h at 130 °C under a nitrogen atmosphere.

Nitrobenzene was removed by vacuum distillation. The black solid residue was evaporated on silicagel and consequently purified via column chromatography (eluent hexanes/EtOAc 95/5). The tubes containing yellow/brown TLC spots (R_f 0.5) were evaporated. The product was then crystallized from a MeOH/EtOAc mixture (2/1) to afford TzTz **1** (1.40 g, 60%) as a yellow crystalline powder. Material identity and purity were checked via ^{1}H NMR and HRMS and were found to be identical to literature data.[9,17]

General procedure for the direct arylation reactions. 2,5-Bis(3'-hexylthiophen-2'-yl)thiazolo[5,4-*d*]thiazole (**1**) (119 mg, 0.25 mmol, 1 equiv), K_2CO_3 (52 mg, 0.375 mmol 1.5 equiv), $Pd(OAc)_2$ (1.1 mg, 5 µmol, 2 mol%), PCy_3HBF_4 (3.7 mg, 10.0 µmol, 4 mol%) and pivalic acid (7.7 mg, 0.075 mmol, 30 mol%) were weighed in air and placed in a microwave vial (10 mL) equipped with a magnetic stirring bar. The solid aryl bromides (**2a–g**) were added at this point (1.1 or 2.1 equiv). The vial was purged with Ar and dry toluene (1 mL; 0.25 M final concentration of TzTz **1**) was added. The liquid aryl bromides (**2a–g**) were added at this point (1.1 or 2.1 equiv). The reaction mixture was vigorously stirred under microwave irradiation at 180 °C for 4 h. The solution was then cooled down to room temperature and diluted with CH_2Cl_2 and H_2O. The aqueous phase was extracted with CH_2Cl_2. The organic fractions were combined and dried over $MgSO_4$, filtered, and evaporated under reduced pressure. The obtained product mixture was separated by column chromatography or preparative SEC to afford the pure mono- (**3a–g**) and disubstituted (**4a–g**) TzTz's.

4-{4-Hexyl-5-[5-(3-hexylthiophen-2-yl)thiazolo[5,4-*d*]thiazol-2-yl]thiophen-2-yl}isophthalonitrile (3a). 4-Bromoisophthalonitrile (**2a**) (57 mg, 0.275 mmol, 1.1 equiv); The mixture was purified by column chromatography (eluent gradient petroleum ether/$CHCl_3$ 4/1–1/1) to afford **3a** (74 mg, 49%) and

4a (41 mg, 44%); Red solid; Mp 110–111 °C; ^{1}H NMR (300 MHz, $CDCl_3$) δ 8.02 (d, J = 1.1 Hz, 1H), 7.86 (dd, J = 8.3, 1.1 Hz, 1H), 7.78 (d, J = 8.3 Hz, 1H), 7.73 (s, 1H), 7.37 (d, J = 5.1 Hz, 1H), 7.00 (d, J = 5.1 Hz, 1H), 3.09–2.89 (m, 4H), 1.87–1.64 (m, 4H), 1.55–1.41 (m, 4H), 1.40–1.26 (m, 8H), 0.99–0.83 (m, 6H); ^{13}C NMR (75 MHz, $CDCl_3$) δ 162.8, 159.7, 151.0, 150.4, 144.2, 143.8, 140.4, 138.1, 138.0, 136.0, 135.9, 132.7, 131.8, 131.1, 130.0, 128.0, 117.1, 116.7, 112.0, 110.7, 31.8, 31.7, 30.5, 30.4, 30.1, 30.0, 29.47, 29.45, 22.8 14.3; IR (NaCl) ν_{max} 2953/2928/2857 (saturated C-H), 2223 cm^{-1} (CN); HRMS (ESI) *m/z* calcd for $C_{32}H_{33}N_4S_4$ [M + H]$^+$ 601.1510; found 601.1564; UV-Vis ($CHCl_3$) λ_{max} (log ε) 427 nm (4.54).

4,4'-[Thiazolo[5,4-*d*]thiazole-2,5-diyl-bis(4-hexylthiophene-5,2-diyl)]diisophthalonitrile (4a). 4-Bromoisophthalonitrile (**2a**) (109 mg, 0.525 mmol, 2.1 equiv); The mixture was purified by column chromatography (eluent gradient petroleum ether/$CHCl_3$ 4/1–1/1) to afford **3a** and **4a** in 34% and 52% yield (96 and 52 mg), respectively; Red solid; Mp 285–286 °C; ^{1}H NMR (400 MHz, $CDCl_3$) δ 8.04 (d, J = 1.7 Hz, 2H), 7.88 (dd, J = 8.2, 1.7 Hz, 2H), 7.81 (d, J = 8.2 Hz, 2H), 7.74 (s, 2H), 3.06–2.98 (m, 4H), 1.85–1.72 (m, 4H), 1.55–1.44 (m, 4H), 1.42–1.31 (m, 8H), 0.91 (t, J = 6.8 Hz, 6H); ^{13}C NMR (100 MHz, $CDCl_3$) δ 160.8, 151.3, 144.7, 140.4, 138.5, 138.1, 136.1, 135.7, 132.8, 130.1, 117.0, 116.7, 112.2, 110.9, 31.8, 30.6, 30.0, 29.4, 22.8, 14.2; IR (NaCl) ν_{max} 2950/2927/2856 (saturated C-H), 2220 cm^{-1} (CN); HRMS (ESI) *m/z* calcd for $C_{40}H_{35}N_6S_4$ [M + H]$^+$ 727.1728; found 727.1773; UV-Vis ($CHCl_3$) λ_{max} (log ε) 451 nm (4.70).

2-[3-Hexyl-5-(perfluorophenyl)thiophen-2-yl]-5-(3-hexylthiophen-2-yl)thiazolo[5,4-*d*]thiazole (3b). 1-Bromo-2,3,4,5,6-pentafluorobenzene (**2b**) (33 µL, 0.275 mmol, 1.1 equiv); The reaction was run for 7 h; The mixture was purified by column chromatography (eluent gradient petroleum ether/$CHCl_3$ 9/1–

3/2). Since fine separation was not possible by column chromatography, the compounds were additionally purified by preparative SEC to afford **3b** and **4b** in 49 and 36% yield (78 and 36 mg), respectively; Yellow solid; Mp 84–85 °C; ^{1}H NMR (300 MHz, $CDCl_3$) δ 7.40 (s, 1H), 7.36 (d, J = 5.2 Hz, 1H), 6.98 (d, J = 5.2 Hz, 1H), 3.05–2.87 (m, 4H), 1.84–1.64 (m, 4H), 1.57–1.41 (m, 4H), 1.41–1.30 (m, 8H), 0.96–0.86 (m, 6H); ^{13}C NMR (75 MHz, $CDCl_3$) δ 162.3, 160.2, 150.7, 150.4, 144.3 (d, ^1J = 250 Hz), 143.6, 142.7, 140.3 (d, ^1J = 250 Hz), 138.2 (d, ^1J = 250 Hz), 134.4 (t, ^3J = 4.1 Hz), 133.7 (d, ^3J = 5.8 Hz), 131.8, 131.0, 127.8 (m), 127.7, 109.5 (dt, ^2J = 14.9 Hz; ^3J = 4.3 Hz), 31.8, 30.3, 30.0, 29.5, 22.8, 14.2; HRMS (ESI) *m/z* calcd for $C_{30}H_{30}F_5N_2S_4$ $[M + H]^+$ 641.1212; found 641.1212; UV-Vis ($CHCl_3$) λ_{max} (log ε) 406 nm (4.55).

2,5-Bis[3-hexyl-5-(perfluorophenyl)thiophen-2-yl]thiazolo[5,4-*d*]thiazole (4b). 1-Bromo-2,3,4,5,6-pentafluorobenzene (**2b**) (65 µL, 0.525 mmol, 2.1 equiv); The reaction was run for 7 h; The mixture was purified by column chromatography (eluent gradient petroleum ether/$CHCl_3$ 9/1–3/2). Since fine separation was not possible by column chromatography, the compounds were additionally purified by preparative SEC to afford **3b** and **4b** in 30 and 69% yield (49 and 140 mg), respectively; Yellow solid; Mp 158–159 °C; ^{1}H NMR (300 MHz, $CDCl_3$) δ 7.43 (s, 2H), 3.05–2.96 (m, 4H), 1.83–1.69 (m, 4H), 1.52–1.43 (m, 4H), 1.40–1.30 (m, 8H), 0.91 (t, J = 7.0 Hz, 6H); ^{13}C NMR (75 MHz, C_6D_5Cl) δ 160.8, 151.1, 145.9, 144.2 (d, ^1J = 250 Hz), 143.1, 140.1 (d, ^1J = 250 Hz), 138.0 (d, ^1J = 250 Hz), 134.6, 133.7, 109.6 (m), 31.8, 30.3, 30.0, 29.5, 22.8, 14.1; HRMS (ESI) *m/z* calcd for $C_{36}H_{29}F_{10}N_2S_4$ $[M + H]^+$ 807.1025; found 807.1054; UV-Vis ($CHCl_3$) λ_{max} (log ε) 421 nm (4.58).

2-{5-[2,4-Bis(trifluoromethyl)phenyl]-3-hexylthiophen-2-yl}-5-(3-hexylthiophen-2-yl)thiazolo[5,4-*d*]thiazole (3c). 1-Bromo-2,4-bis(trifluorome-

thyl)benzene (**2c**) (46 µL, 0.275 mmol, 1.1 equiv); The reaction was run for 7 h; The mixture was purified by column chromatography (eluent gradient petroleum ether/$CHCl_3$ 9/1–6/1). Since fine separation was not possible by column chromatography, the compounds were additionally purified by preparative SEC to afford **3c** and **4c** in 58 and 42% yield (99 and 47 mg), respectively; Yellow solid; Mp 77–78 °C; ^{1}H NMR (300 MHz, $CDCl_3$) δ 8.04 (s, 1H), 7.85 (d, J = 8.1 Hz, 1H), 7.71 (d, J = 8.1 Hz, 1H), 7.36 (d, J = 5.1 Hz, 1H), 7.07 (s, 1H), 6.99 (d, J = 5.1 Hz, 1H), 3.07–2.88 (m, 4H), 1.84–1.62 (m, 4H), 1.56–1.41 (m, 4H), 1.39–1.28 (m, 8H), 0.98–0.82 (m, 6H); ^{13}C NMR (75 MHz, $CDCl_3$) δ 162.2, 160.6, 150.5, 150.2, 143.5, 143.1, 139.3, 136.8, 133.9, 133.6, 132.3 (q, ^3J= 3 Hz), 131.9, 131.0 (q, ^2J = 34 Hz) 129.8 (q, ^2J = 32 Hz) 128.5 (q, ^3J = 3 Hz), 127.7, 125.2, 124.1, 123.4 (q, ^1J = 273 Hz), 123.3 (q, ^1J = 273 Hz), 31.8 (2C's), 30.4, 30.3, 30.1, 29.9, 29.5, 29.3, 22.8, 14.2 (Due to the poor compound solubility in $CDCl_3$, C_6D_5Cl was used for the ^{13}C NMR measurement. The solvent peaks obscure 4 signals between 133 and 124 ppm.); HRMS (ESI) *m/z* calcd for $C_{32}H_{33}F_6N_2S_4$ [M + H]$^+$ 686.3530; found 686.1429; UV-Vis ($CHCl_3$) λ_{max} (log ε) 400 nm (4.60).

2,5-Bis{5-[2,4-bis(trifluoromethyl)phenyl]-3-hexylthiophen-2-yl}thiazolo[5,4-*d*]thiazole (4c). 1-Bromo-2,4-bis(trifluoromethyl)benzene (**2c**) (89 µL, 0.525 mmol, 2.1 equiv); The reaction was run for 7 h; The mixture was purified by column chromatography (eluent gradient petroleum ether/$CHCl_3$ 9/1–6/1). Since fine separation was not possible by column chromatography, the compounds were additionally purified by preparative SEC to afford **3c** and **4c** in 27 and 58% yield (23 and 131 mg), respectively; Yellow solid; Mp 152–153 °C; ^{1}H NMR (400 MHz, $CDCl_3$) δ 8.05 (s, 2H), 7.86 (d, J = 8.1 Hz, 2H), 7.72 (d, J = 8.1 Hz, 2H), 7.08 (s, 2H), 3.04–2.93 (m, 4H), 1.82–1.70 (m, 4H), 1.53–1.42 (m, 4H), 1.38–1.31 (m, 8H), 0.91 (t, J = 7.0 Hz, 6H); ^{13}C NMR (75 MHz, $CDCl_3$) δ

161.1, 150.6, 143.3, 139.5, 136.8, 133.8, 133.6, 132.4 (q, ^{3}J = 3Hz), 130.9 (q, ^{2}J = 33 Hz), 129.9 (q, ^{2}J = 34 Hz), 128.6 (q, ^{3}J = 3 Hz), 124.1, 123.4 (q, ^{1}J = 273 Hz), 123.3 (q, ^{1}J = 273 Hz), 31.8, 30.4, 30.0, 29.3, 22.8, 14.2; HRMS (ESI) *m/z* calcd for $C_{40}H_{35}F_{12}N_2S_4$ $[M + H]^+$ 899.1413; found 899.1486; UV-Vis ($CHCl_3$) λ_{max} (log ε) 410 nm (4.69).

Methyl 4-{4-hexyl-5-[5-(3-hexylthiophen-2-yl)thiazolo[5,4-*d*]thiazol-2-yl]thiophen-2-yl}benzoate (3d). Methyl 4-bromobenzoate (**2d**) (59 mg, 0.275 mmol, 1.1 equiv); The mixture was purified by column chromatography (eluent gradient petroleum ether/$CHCl_3$ 12/1–10/1) to afford **3d** and **4d** in 64 and 34% yield (98 and 32 mg), respectively; Red solid; Mp 95–96 °C; ^{1}H NMR (300 MHz, $CDCl_3$) δ 8.05 (d, J = 8.2 Hz, 2H), 7.70 (d, J = 8.2 Hz, 2H), 7.36 (d, J = 5.1 Hz, 1H), 7.31 (s, 1H), 6.99 (d, J = 5.1 Hz, 1H), 3.92 (s, 3H), 3.04–2.90 (m, 4H), 1.84–1.65 (m, 4H), 1.54–1.41 (m, 4H), 1.40–1.23 (m, 8H), 0.98–0.83 (m, 6H); ^{13}C NMR (75 MHz, $CDCl_3$) δ 166.7, 162.0, 161.0, 150.4, 150.3, 144.3, 144.0, 143.4, 137.8, 132.6, 131.9, 131.0, 130.5, 129.6, 128.1, 127.6, 125.6, 52.4, 31.8 (2 C's), 30.6, 30.3, 30.1, 29.5, 22.8 14.3; IR (NaCl) ν_{max} 2956/2929/2857 (saturated C-H), 1719 cm^{-1} (COOMe); HRMS (ESI) *m/z* calcd for $C_{32}H_{37}N_2O_2S_4$ $[M + H]^+$ 609.1738; found 609.1730; UV-Vis ($CHCl_3$) λ_{max} (log ε) 417 nm (4.40).

Dimethyl 4,4'-[(thiazolo[5,4-*d*]thiazole-2,5-diyl)-bis(4-hexylthiophene-5,2-diyl)]dibenzoate (4d). Methyl 4-bromobenzoate (**2d**) (113 mg, 0.525 mmol, 2.1 equiv); The mixture was purified by column chromatography (eluent gradient petroleum ether/$CHCl_3$ 12/1–10/1) to afford **3d** and **4d** in 6 and 92% yield (9 and 178 mg), respectively; Red solid; Mp 211–213 °C; ^{1}H NMR (300 MHz, $CDCl_3$) δ 8.06 (d, J = 8.2 Hz, 4H), 7.70 (d, J = 8.2 Hz, 4H), 7.24 (s, 2H), 3.92 (s, 3H), 2.96–2.89 (m, 4H), 1.80–1.68 (m, 4H), 1.53–1.44 (m, 4H), 1.40–1.32 (m, 8H), 0.92 (t, J = 7.1 Hz, 6H); ^{13}C NMR (75 MHz, $CDCl_3$) δ 166.7, 161.1, 150.5,

144.3, 144.0, 137.7, 132.6, 130.5, 129.5, 128.0, 125.5, 52.4, 31.8, 30.6, 30.0, 29.6, 22.8, 14.3; IR (NaCl) ν_{max} 2950/2925/2853 (saturated C-H), 1718 cm^{-1} (COOMe); HRMS (ESI) *m/z* calcd for $C_{32}H_{37}N_2O_2S_4$ $[M + H]^+$ 743.2106; found 743.2067; UV-Vis ($CHCl_3$) λ_{max} (log ε) 445 nm (4.45).

2-[3-Hexyl-5-(pyridin-2-yl)thiophen-2-yl]-5-(3-hexylthiophen-2-yl)thiazolo[5,4-*d*]thiazole (3e). 2-Bromopyridine (**2e**) (26 µL, 0.275 mmol, 1.1 equiv); The mixture was purified by column chromatography (eluent gradient petroleum ether/$CHCl_3$ 10/1–7/1). Since fine separation was not possible by column chromatography, the compounds were additionally purified by preparative SEC to afford **3e** and **4e** in 69 and 27% yield (96 and 22 mg), respectively; Red solid; Mp 98–99 °C; ^{1}H NMR (300 MHz, $CDCl_3$) δ 8.59 (dd, *J* = 4.7, 0.8 Hz, 1H), 7.75–7.63 (m, 2H), 7.54 (s, 1H), 7.34 (d, *J* = 5.1 Hz, 1H), 7.23–7.15 (m, 1H), 6.98 (d, *J* = 5.1 Hz, 1H). 3.05–2.90 (m, 4H), 1.83–1.65 (m, 4H), 1.56–1.39 (m, 4H), 1.37–1.29 (m, 8H), 0.98–0.79 (m, 6H); ^{13}C NMR (75 MHz, $CDCl_3$) δ 161.9, 161.4, 151.6, 150.5, 150.3, 149.6, 144.8, 144.4, 143.3, 137.2, 133.5, 132.0, 130.9, 128.5, 127.5, 122.6, 119.3, 31.8 (2C's), 30.5, 30.3, 30.1, 30.0, 29.8, 29.5, 22.8, 14.3; HRMS (ESI) *m/z* calcd for $C_{34}H_{34}N_3S_4$ $[M + H]^+$ 552.1636; found 552.1635; UV-Vis ($CHCl_3$) λ_{max} (log ε) 416 nm (4.58).

2,5-Bis[3-hexyl-5-(pyridin-2-yl)thiophen-2-yl]thiazolo[5,4-*d*]thiazole (4e). 2-Bromopyridine (**2e**) (50 µL, 0.525 mmol, 2.1 equiv); The mixture was purified by column chromatography (eluent gradient petroleum ether/$CHCl_3$ 10/1–7/1). Since fine separation was not possible by column chromatography, the compounds were additionally purified by preparative SEC to afford **3e** and **4e** in 34 and 50% yield (47 and 78 mg), respectively; Red solid; Mp 168–169 °C; ^{1}H NMR (300 MHz, $CDCl_3$) δ 8.59 (d, *J* = 4.7 Hz, 2H), 7.80–7.60 (m, 4H), 7.50 (s, 2H), 7.21–7.15 (m, 2H), 3.08–2.87 (m, 4H), 1.85–1.61 (m, 4H), 1.57–1.40 (m,

4H), 1.40–1.29 (m, 8H), 0.98–0.85 (m, 6H); ^{13}C NMR (75 MHz, $CDCl_3$) δ 161.6, 151.8, 150.6, 149.9, 145.4, 144.4, 136.8, 133.3, 128.2, 122.6, 119.2, 31.8, 30.5, 30.0, 29.4, 22.8, 14.3; HRMS (ESI) *m/z* calcd for $C_{34}H_{37}N_4S_4$ $[M + H]^+$ 629.1901; found 629.1881; UV-Vis ($CHCl_3$) λ_{max} (log ε) 440 nm (4.65).

2-[3-Hexyl-5-(4-methoxyphenyl)thiophen-2-yl]-5-(3-hexylthiophen-2-yl)thiazolo[5,4-*d*]thiazole (3f). 1-Bromo-4-methoxybenzene (**2f**) (51 mg, 0.275 mmol, 1.1 equiv); The mixture was purified by column chromatography (eluent gradient petroleum ether/$CHCl_3$ 10/1–7/1). Since fine separation was not possible by column chromatography, the compounds were additionally purified by preparative SEC to afford **3f** and **4f** in 28 and 70% yield (41 and 60 mg), respectively; Orange solid; Mp 83–84 °C; ^{1}H NMR (300 MHz, $CDCl_3$) δ 7.56 (d, J = 8.7 Hz, 2H), 7.33 (d, J = 5.1 Hz, 1H), 7.08 (s, 1H), 6.97 (d, J = 5.1 Hz, 1H), 6.91 (d, J = 8.7 Hz, 2H), 3.85 (s, 3H), 3.01–2.86 (m, 4H), 1.81–1.61 (m, 4H), 1.53–1.25 (m, 8H), 0.96–0.81 (m, 6H); ^{13}C NMR (75 MHz, $CDCl_3$) δ 161.6, 161.4, 159.9, 150.2, 149.9, 145.7, 144.3, 143.1, 132.0, 130.9, 130.1, 127.4, 127.2, 126.4, 125.7, 114.5, 55.5, 31.8, 30.6, 30.3, 30.1, 30.0, 29.5, 22.8, 14.3; HRMS (ESI) *m/z* calcd for $C_{31}H_{37}N_2OS_4$ $[M + H]^+$ 581.1789; found 581.1765; UV-Vis ($CHCl_3$) λ_{max} (log ε) 418 nm (4.65).

2,5-Bis[3-hexyl-5-(4-methoxyphenyl)thiophen-2-yl]thiazolo[5,4-*d*]thiazole (4f). 1-Bromo-4-methoxybenzene (**2f**) (98 mg, 0.525 mmol, 2.1 equiv); The mixture was purified by column chromatography (eluent gradient petroleum ether/$CHCl_3$ 10/1–7/1). Since fine separation was not possible by column chromatography, the compounds were additionally purified by preparative SEC to afford **3f** and **4f** in 32 and 64% yield (55 and 93 mg), respectively; Red solid; Mp 166–167 °C; ^{1}H NMR (300 MHz, $CDCl_3$) δ 7.56 (d, J = 8.8 Hz, 4H), 7.08 (s, 2H), 6.92 (d, J = 8.8 Hz, 4H), 3.84 (s, 6H), 3.00–2.87 (m, 4H), 1.83–1.65 (m, 4H),

1.53–1.40 (m, 4H), 1.40–1.29 (m, 8H), 0.90 (t, *J* = 6.9 Hz, 6H); ^{13}C NMR (75 MHz, $CDCl_3$) *δ* 161.3, 159.9, 150.0, 145.6, 144.2, 130.2, 127.2, 126.4, 125.7, 114.5, 55.5, 31.8, 30.7, 30.0, 29.6, 22.8, 14.3; HRMS (ESI) *m/z* calcd for $C_{38}H_{43}N_2O_2S_4$ $[M + H]^+$ 687.2207; found 687.2187; UV-Vis ($CHCl_3$) λ_{max} (log *ε*) 442 nm (4.80).

4-{4-Hexyl-5-[5-(3-hexylthiophen-2-yl)thiazolo[5,4-*d*]thiazol-2-yl]thiophen-2-yl}-*N*,*N*-diphenylaniline (3g). 4-Bromo-*N*,*N*-diphenylaniline (**2f**) (89 mg, 0.275 mmol, 1.1 equiv); The mixture was purified by column chromatography (eluent gradient petroleum ether/$CHCl_3$ 10/1–7/1). Since fine separation was not possible by column chromatography, the compounds were additionally purified by preparative SEC to afford **3g** and **4g** in 50 and 38% yield (90 and 46 mg), respectively; Yellow viscous oil; ^{1}H NMR (400 MHz, $CDCl_3$) *δ* 7.50 (d, *J* = 8.7 Hz, 2H), 7.34 (d, *J* = 5.1 Hz, 1H), 7.32–7.26 (m, 4H), 7.17–7.04 (m, 9H), 6.98 (d, *J* = 5.1 Hz, 1H), 3.02–2.87 (m, 4H), 1.81–1.67 (m, 4H), 1.54–1.40 (m, 4H), 1.40–1.31 (m, 8H), 0.97–0.82 (m, 6H); ^{13}C NMR (75 MHz, $CDCl_3$) *δ* 161.6, 161.4, 150.2, 149.9, 148.2, 147.4, 145.7, 144.4, 143.2, 132.0, 130.9, 130.2, 129.5, 127.4, 127.2, 126.7, 125.8, 124.9, 123.6, 123.2, 31.8, 30.6, 30.3, 30.2, 30.0, 29.5 (2C's), 22.8, 14.3; HRMS (ESI) *m/z* calcd for $C_{42}H_{44}N_3S_4$ $[M + H]^+$ 718.2340; found 718.2375; UV-Vis ($CHCl_3$) λ_{max} (log *ε*) 440 nm (4.70).

4,4'-{5,5'-[Thiazolo[5,4-*d*]thiazole-2,5-diyl]-bis(4-hexylthiophene-5,2-diyl)}-bis(*N*,*N*-diphenylaniline) (4g). 4-Bromo-*N*,*N*-diphenylaniline (**2f**) (170 mg, 0.525 mmol, 2.1 equiv); The mixture was purified by column chromatography (eluent gradient petroleum ether/$CHCl_3$ 10/1–7/1). Since fine separation was not possible by column chromatography, the compounds were additionally purified by preparative SEC to afford **3g** and **4g** in 46 and 38% yield (83 and 91 mg), respectively; Red solid. Mp: 89–91 °C; ^{1}H NMR (300 MHz, $CDCl_3$) *δ* 7.50 (d, *J* =

8.6 Hz, 4H), 7.35–7.26 (m, 7H), 7.18–7.01 (m, 19H), 3.05–2.84 (m, 4H), 1.85–1.66 (m, 4H), 1.54–1.43 (m, 4H), 1.43–1.29 (m, 8H), 0.96–0.88 (m, 6H); ^{13}C NMR (75 MHz, $CDCl_3$) δ 161.3, 150.1, 148.2, 147.4, 145.6, 144.3, 130.3, 129.5, 127.3, 126.7, 125.8, 125.0, 123.6, 123.3, 31.8, 30.6, 30.0, 29.5, 22.8, 14.3; HRMS (ESI) *m/z* calcd for $C_{50}H_{57}N_4S_4$ $[M + H]^+$ 961.3466; found 961.3423; UV-Vis ($CHCl_3$) λ_{max} (log ε) 469 nm (4.88).

4-{5-[5-(5-(4-(*N*,*N*-diphenylamino)phenyl)-3-hexylthiophen-2-yl)thiazolo[5,4-*d*]thiazol-2-yl]-4-hexylthiophen-2-yl}isophthalonitrile (5). Triphenylamine monosubstituted TzTz **3g** (65 mg, 0.091 mmol, 1.0 equiv), 4-bromoisophthalonitrile (**2a**) (20.6 mg, 0.10 mmol, 1.1 equiv), K_2CO_3 (18.7 mg, 0.135 mmol, 1.5 equiv), $Pd(OAc)_2$ (0.6 mg, 2.7 µmol, 3 mol%), PCy_3HBF_4 (1.3 mg, 3.5 µmol, 4 mol%), pivalic acid (2.7 mg, 0.027 mmol, 30 mol%), toluene (0.4 mL); 180 °C for 4 h; Purification by column chromatography (eluent gradient petroleum ether/$CHCl_3$ 10/1–6/1). Since fine separation was not possible by column chromatography, the compounds were additionally purified by preparative SEC to afford TzTz **5** in 85% yield (64 mg); Red solid; Mp 172–173 °C; ^{1}H NMR (300 MHz, $CDCl_3$) δ 8.02 (d, J = 1.7 Hz, 1H), 7.86 (dd, J = 8.3, 1.7 Hz, 1H), 7.79 (d, J = 8.3 Hz, 1H), 7.74 (s, 1H), 7.53–7.45 (m, 2H), 7.33–7.26 (m, 4H), 7.17–7.03 (m, 9H), 3.06–2.88 (m, 4H), 1.85–1.65 (m, 4H), 1.56–1.42 (m, 4H), 1.42–1.28 (m, 8H), 1.00–0.81 (m, 6H); ^{13}C NMR (75 MHz, $CDCl_3$) δ 162.7, 159.3, 151.2, 150.2, 148.3, 147.4 (2C's), 146.3, 145.0, 144.1, 140.5, 138.1, 137.9, 136.1, 132.8, 130.0, 129.9, 129.6 , 127.0, 126.7, 125.9, 125.0, 123.7, 123.1, 117.1, 116.7, 112.0, 110.7, 31.8, 31.75, 30.7, 30.5, 30.0, 29.5 (2C's), 22.8, 14.3; IR (NaCl) ν_{max} 2955/2925/2855 (saturated C-H), 2232 cm^{-1} (CN); HRMS (ESI) *m/z* calcd for $C_{50}H_{46}N_5S_4$ $[M + H]^+$ 844.2558; found 844.2576; UV-Vis ($CHCl_3$) λ_{max} (log ε) 473 nm (4.66).

4-{5-[5-(5-(2,4-Bis(trifluoromethyl)phenyl)-3-hexylthiophen-2-yl)thiazolo[5,4-*d*]thiazol-2-yl]-4-hexylthiophen-2-yl}-*N*,*N*-diphenylaniline (6). Bis(trifluoromethyl)phenyl monosubstituted TzTz **3c** (100 mg, 0.146 mmol, 1.0 equiv), 4-bromo-*N*,*N*-diphenylaniline (**2g**) (51.9 mg, 0.160 mmol, 1.1 equiv), K_2CO_3 (30.2 mg, 0.218 mmol, 1.5 equiv), $Pd(OAc)_2$ (1 mg, 4.4 µmol, 3 mol%), PCy_3HBF_4 (1.3 mg, 3.5 µmol, 2.4 mol%), pivalic acid (4.5 mg, 0.044 mmol, 30 mol%), toluene (0.6 mL); 180 °C for 4 h; Purification by column chromatography (eluent gradient petroleum ether/$CHCl_3$ 10/1–6/1). Since fine separation was not possible by column chromatography, the compounds were additionally purified by preparative SEC to afford **6** in 88% yield (119 mg); Red solid; Mp 94–95 °C; ^{1}H NMR (300 MHz, $CDCl_3$) δ 8.05 (s, 1H), 7.85 (d, J = 8.2 Hz, 1H), 7.72 (d, J = 8.1 Hz, 1H), 7.50 (d, J = 8.7 Hz, 2H), 7.34–7.26 (m, 4H), 7.18–7.02 (m, 10H), 3.09–2.88 (m, 4H), 1.87–1.66 (m, 4H), 1.59–1.42 (m, 4H), 1.41–1.30 (m, 8H), 1.01–0.81 (m, 6H); ^{13}C NMR (75 MHz, $CDCl_3$) δ 162.7, 160.3, 150.6, 150.0, 148.3, 147.4, 146.0, 144.6, 143.0, 139.2, 136.9, 134.0, 133.6, 132.3 (m), 130.9 (q, ^2J = 33 Hz), 130.1, 129.8 (q, ^2J = 33 Hz), 129.5, 128.5 (m), 127.1, 126.7, 125.8, 125.0, 124.1, 123.6, 123.4 (q, ^1J = 273 Hz), 123.3 (q, ^1J = 273 Hz), 123.2, 31.8, 30.7, 30.4, 30.0 (2C's), 29.5, 29.3, 22.8, 14.2; HRMS (ESI) *m/z* calcd for $C_{50}H_{46}F_6N_3S_4$ $[M + H]^+$ 930.2479; found 930.2432; UV-Vis ($CHCl_3$) λ_{max} (log ε) 449 nm (4.73).

2.5. ACKNOWLEDGMENTS

The reported activity is supported by the Interuniversity Attraction Poles Programme (P7/05), initiated by the Belgian Science Policy Office, and the project ORGANEXT (EMR INT4-1.2-2009-04/054), selected in the frame of the operational program INTERREG IV-A Euregio Maas-Rijn. We also acknowledge Hercules for providing the funding for the LTQ Orbitrap Velos Pro mass spectrometer.

2.6. NOTES AND REFERENCES

1. (*a*) L. Zhang, C.-A. Di, G. Yu and Y. Liu, *J. Mater. Chem.*, 2010, **20**, 7059; (*b*) A. Mishra and. P. Bäuerle, *Angew. Chem. Int. Ed.*, 2012, **51**, 2020.
2. For a recent review on TzTz synthesis and applications: D. Bevk, L. Lutsen, D. Vanderzande and W. Maes, *RSC Adv.*, 2013, **3**, 11418.
3. (*a*) S. Ando, J.-I. Nishida, Y. Inoue, S. Tokito and Y. Yamashita, *J. Mater. Chem.*, 2004, **14**, 1787; (*b*) S. Ando, J.-I. Nishida, H. Tada, Y. Inoue, S. Tokito and Y. Yamashita, *J. Am. Chem. Soc.*, 2005, **127**, 5336; (*c*) S. Ando, D. Kumaki, J.-I. Nishida, H. Tada, Y. Inoue, S. Tokito and Y. Yamashita, *J. Mater. Chem.*, 2007, **17**, 553; (*d*) M. Mamada, J.-I. Nishida, D. Kumaki, S. Tokito and Y. Yamashita, *Chem. Mater.*, 2007, **19**, 5404; (*e*) Y. Fujisaki, M. Mamada, D. Kumaki, S. Tokito and Y. Yamashita, *Jpn. J. Appl. Phys.*, 2009, **48**, 111504.
4. Naraso and F. Wudl, *Macromolecules*, 2008, **41**, 3169.
5. (*a*) I. Osaka, G. Sauvé, R. Zhang, T. Kowalewski and R. D. McCullough, *Adv. Mater.*, 2007, **19**, 4160; (*b*) I. Osaka, R. Zhang, G. Sauvé, D.-M. Smilgies, T. Kowalewski and R. D. McCullough, *J. Am. Chem. Soc.*, 2009, **131**, 2521; (*c*)

I. Osaka, R. Zhang, J. Liu, D.-M. Smilgies, T. Kowalewski and R. D. McCullough, *Chem. Mater.*, 2010, **22**, 4191.

6. OPV reviews: (*a*) C. J. Brabec, S. Gowrisanker, J. J. M. Halls, D. Laird, S. Jia and S. P. Williams, *Adv. Mater.*, 2010, **22**, 3839; (*b*) J. Nelson, *Mater. Today*, 2011, **14**, 462; (*c*) P.-L. T. Boudreault, A. Najari and M. Leclerc, *Chem. Mater.*, 2011, **23**, 456; (*d*) L. J. A. Koster, S. E. Shaheen and J. C. Hummelen, *Adv. Energy Mater.*, 2012, **2**, 1246; (*e*) P. Kumar and S. Chand, *Prog. Photovoltaics Res. Appl.*, 2012, **20**, 377; (*f*) I. Gang, Z. Rui and Y. Yang, *Nat. Photonics*, 2012, **6**, 153; (*g*) M. Jørgensen, K. Norrman, S. A. Gevorgyan, T. Tromholt, B. Andreasen and F. C. Krebs, *Adv. Mater.*, 2012, **24**, 580; (*h*) K. Vandewal, S. Himmelberger and A. Salleo, *Macromolecules*, 2013, **46**, 6379; (*i*) S. B. Darling and F. You, *RSC Adv.*, 2013, **3**, 17633.
7. (*a*) T. W. Lee, N. S. Kang, J. W. Yu, M. H. Hoang, K. H. Kim, J.-L. Jin and D. H. Choi, *J. Polym. Sci., Part A: Polym. Chem.*, 2010, **48**, 5921; (*b*) S. Subramaniyan, H. Xin, F. Sunjoo Kim, S. Shoaee, J. R. Durrant and S. A. Jenekhe, *Adv. Energy Mater.*, 2011, **1**, 854; (*c*) M. Zhang, X. Guo, X. Wang, H. Wang and Y. Li, *Chem. Mater.*, 2011, **23**, 4264; (*d*) S. K. Lee, J. M. Cho, W. S. Shin, J.-C. Lee, W.-H. Lee, I.-N. Kang, H.-K. Shim and S.-J. Moon, *Chem. Commun.*, 2011, **47**, 1791; (*e*) I. Osaka, M. Saito, T. Koganezawa and K. Tamikiya, *Adv. Mater.*, 2012, **24**, 425; (*f*) S. Van Mierloo, J. Kesters, A. Hadipour, M.-J. Spijkman, N. Van den Brande, J. D'Haen, G. Van Assche, D. M. de Leeuw, T. Aernouts, J. Manca, L. Lutsen, D.Vanderzande and W. Maes, *Chem. Mater.*, 2012, **24**, 587; (*g*) J. Kesters, T. Ghoos, H. Penxten, J. Drijkoningen, T. Vangerven, D. M. Lyons, B. Verreet, T. Aernouts, L. Lutsen, D. Vanderzande, J. Manca and W. Maes, *Adv. Energy Mater.*, 2013, **3**, 1180; (*h*) S. Shoaee, S. Subramaniyan, H. Xin, C. Keiderling, P. S. Tuladhar, F.

Jamieson, S. A. Jenekhe and J. R. Durrant, *Adv. Funct. Mater.*, 2013, **23**, 3286; (*i*) I. Osaka, M. Saito, T. Koganezawa and K. Takimiya, *Adv. Mater.*, 2014, **26**, 331; (*j*) W. Vanormelingen, J. Kesters, P. Verstappen, J. Drijkoningen, J. Kudrjasova, S. Koudjina, V. Liégeois, B. Champagne, J. Manca, L. Lutsen, D. Vanderzande and W. Maes, *J. Mater. Chem. A*, 2014, **2**, 7535.

8. (*a*) Q. Shi, P. Cheng, Y. Li and X. Zhan, *Adv. Energy Mater*., 2012, **2**, 63; (*b*) P. Dutta, W. Yang, S. H. Eom and S.-H. Lee, *Org. Electron*., 2012, **13**, 273; (*c*) P. Dutta, H. Park, W.-H. Lee, I.-N. Kang and S.-H. Lee, *Org. Electron.*, 2012, **13**, 3183; (*d*) P. Cheng, Q. Shi, Y. Lin, Y. Li and X. Zhan, *Org. Electron.*, 2013, **14**, 599; (*e*) A. Dessì, B. G. Consiglio, M. Calamante and L. Zani, *Eur. J. Org. Chem.*, 2013, **10**, 1916.
9. (*a*) S. Van Mierloo, V. Liégeois, J. Kudrjasova, E. Botek, L. Lutsen, B. Champagne, D. Vanderzande, P. Adriaensens and W. Maes, *Magn. Reson. Chem.*, 2012, **50**, 379; (*b*) S. Van Mierloo, K. Vasseur, N. Van den Brande, A. E. Boyukbayram, B. Ruttens, S. D. Rodriguez, E. Botek, V. Liégeois, J. D'Haen, P. J. Adriaensens, P. Heremans, B. Champagne, G. Van Assche, L. Lutsen, D. J. Vanderzande and W. Maes, *ChemPlusChem*, 2012, **77**, 923.
10. (*a*) N. Nevil, Y. Ling, S. Van Mierloo, J. Kesters, F. Piersimoni, P. Adriaensens, L. Lutsen, D. Vanderzande, J. Manca, W. Maes, S. Van Doorslaer and E. Goovaerts, *Phys. Chem. Chem. Phys.*, 2012, **14**, 15774; (*b*) Y. Ling, S. Van Mierloo, A. Schnegg, P. J. Adriaensens, L. Lutsen, D. Vanderzande, W. Maes, E. Goovaerts and S. Van Doorslaer, *Phys. Chem. Chem. Phys.*, 2014, DOI: 10.1039/C3CP54635G.
11. (*a*) P. Sonar, J. P. Fong Lim and K. L. Chan, *Energy Environ. Sci.*, 2011, **4**, 1558; (*b*) J. E. Anthony, *Chem. Mater.*, 2011, **23**, 583; (*c*) Y. Lin, Y. Li and X. Zhan, *Adv. Energy Mater.*, 2013, **3**, 724; (*d*) A. F. Eftaiha, J.-P. Sun, I. G. Hill

and G. C. Welch, *J. Mater. Chem. A*, 2014, **2**, 1201; (*e*) Z. Lu, B. Jiang, X. Zhang, A. Tang, L. Chen, C. Zhan and J. Yao, *Chem. Mater.*, 2014, DOI: 10.1021/cm5006339.

12. (*a*) A. Anctil, C. W. Babbitt, R. P. Raffaelle and B. J. Landi, *Prog. Photovoltaics Res. Appl.*, 2013, **21**, 1541; (*b*) S. Lizin, S. Van Passel, E. De Schepper, W. Maes, L. Lutsen, J. Manca and D. Vanderzande, *Energy Environ. Sci.,* 2013, **6**, 3136.
13. (*a*) Y. Lin, Y. Li and X. Zhan, *Chem. Soc. Rev.*, 2012, **41**, 4245; (*b*) J. Zhou, Y. Zuo, X. Wan, G. Long, Q. Zhang, W. Ni, Y. Liu, Z. Li, G. He, C. Li, B. Kan, M. Li and Y. Chen, *J. Am. Chem. Soc.*, 2013, **135**, 8484; (*c*) A. K. K. Kyaw, D. H. Wang, D. Wynands, J. Zhang, T.-Q. Nguyen, G. C. Bazan and A. J. Heeger, *Nano Lett.*, 2013, **13**, 3796; (*d*) Y. Liu, Y. Yang, C-C. Chen, Q. Chen, L. Dou, Z. Hong, G. Li and Y. Yang, *Adv. Mater.*, 2013, **25**, 4657; (e) V. S. Gevaerts, E. M. Herzig, M. Kirkus, K. H. Hendriks, M. M. Wienk, J. Perlich, P. Müller-Buschbaum and R. A. J. Janssen, *Chem. Mater.*, 2014, **26**, 916.
14. (*a*) B. Liégault, D. Lapointe, L. Caron, A. Vlassova and K. Fagnou, *J. Org. Chem.*, 2009, **74**, 1826; (*b*) D. Schipper and K. Fagnou, *Chem. Mater.*, 2011, **23**, 1594; (*c*) M. Baghbanzadeh, C. Pilger and C. O. Kappe, *J. Org. Chem.*, 2011, **76**, 8138; (*d*) M. Durso, C. Bettini, A. Zanelli, M. Gazzano, M. G. Lobello, F. De Angelis, V. Biondo, D. Gentili, R. Capelli, M. Cavallini, S. Toffanin, M. Muccini and M. Melucci, *Org. Electron.*, 2013, **14**, 3089; (*e*) K. Okamato, J. Zhang, J. B. Housekeeper, S. R. Marder and C. K. Luscombe, *Macromolecules*, 2013, **46**, 8059.
15. (*a*) J. Zhang, D.-Y. Kang, S. Barlow and S. R. Marder, *J. Mater. Chem.*, 2012, **22**, 21392; (*b*) S.-Y. Liu, M.-M. Shi, J.-C. Huang, Z.- N. Jin, X.-L. Hu, J.-Y. Pan, H.-Y. Li, A. K. Y. Jen and H.-Z. Chen, *J. Mater. Chem. A*, 2013, **1**, 2795; (*c*) J.

Zhang, W. Chen, A. J. Rojas, E. V. Jucov, T. V. Timofeeva, T. C. Parker, S. Barlow and S. R. Marder, *J. Am. Chem. Soc.*, 2013, **135**, 16376.

16. (*a*) Y. Fujinami, J. Kuwabara, W. Lu, H. Hayashi and T. Kanbara, *ACS Macro Lett.*, 2012, **1**, 67; (*b*) S. Kowalski, S. Allard and U. Scherf, *ACS Macro Lett.*, 2012, **1**, 465; (*c*) L. Facchetti, A. Vaccaro and A. Marrocchi, *Angew. Chem. Int. Ed.*, 2012, **51**, 3520; (*d*) P. Berrouard, A. Najari, A. Pron, D. Gendron, P.-O. Morin, J.-R. Pouliot, J. Veilleux and M. Leclerc, *Angew. Chem. Int. Ed.*, 2012, **51**, 2068; (*e*) J. Jo, A. Pron, P. Berrouard, W. L. Leong, J. D. Yuen, J. S. Moon, M. Leclerc and A. J. Heeger, *Adv. Energy Mater.*, 2013, **2**, 1397.
17. (*a*) J. R. Johnson and R. Ketcham, *J. Am. Chem. Soc.*, 1960, **82**, 2719; (*b*) J. R. Johnson, D. H. Rotenberg and R. Ketcham, *J. Am. Chem. Soc.*, 1970, **92**, 4046; (*c*) R. C. Knighton, A. J. Hallett, B. M. Kariuki and S. J. A. Pope, *Tetrahedron Lett.*, 2010, **41**, 5419; (*d*) R. Ziessel, A. Nano, E. Heyer, T. Bura and P. Retailleau, *Chem. Eur. J.*, 2013, **19**, 2582; (*e*) A. Dessi, M. Calamante, A. Mordini, L. Zani, M. Taddei and G. Reginato, *RSC Adv.*, 2014, **4**, 1322.
18. Y. Kawamata, S. Tokuji, H. Yorimitsu and A. Osuka, *Angew. Chem. Int. Ed.*, 2011, **50**, 8867.
19. J. Song, F. Zhang, C. Li, W. Liu, B. Li, Y. Huang and Z. Bo, *J. Phys. Chem. C*, 2009, **113**, 13391.
20. L. Zani, G. Reginato, A. Mordini, M. Calamante and M. Bruzzi, *Tetrahedron Lett.*, 2013, **54**, 3944.
21. (*a*) J. Bard and L. R. Faulkner, *Electrochemical methods: fundamentals and applications*, 2nd Ed., 2001, Wiley; (*b*) S. Trasatti, *Pure Appl. Chem.*, 1986, **58**, 955.

Chapter 3

Organic solar cells based on symmetrical and asymmetrical extended dithienylthiazolo[5,4-*d*]thiazole donor and acceptor small molecules

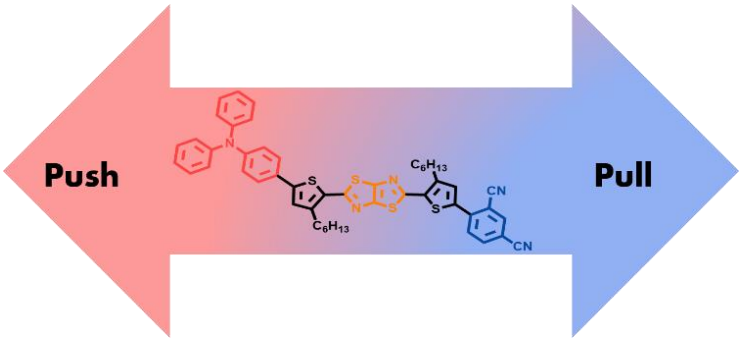

Julija Kudrjasova, Jurgen Kesters, Gaël H. L. Heintges, Ilaria Cardinaletti, Huguette Penxten, Jean Manca, Laurence Lutsen, Dirk Vanderzande and Wouter Maes, *to be submitted*.

(Article contribution: all synthesis and chemical analysis, main author)

ABSTRACT

A series of diaryl-substituted 2,5-dithienylthiazolo[5,4-*d*]thiazole molecular semiconductors prepared via a direct arylation approach is studied toward their application in organic photovoltaics. The opto-electrical and thermal material properties are carefully analyzed and depending on the observed frontier orbital energy levels the TzTz derivatives are implemented as either small molecule electron donor or acceptor materials. For the donor-type compounds, high-bandgap bulk heterojunction organic solar cells with high open-circuit voltages are realized, with a maximum power conversion efficiency of 2.7%. The most electron poor TzTz in the series can be used as an alternative to the commonly applied fullerene acceptors. In combination with P3HT as the electron donor component, a power conversion efficiency of 0.4% is achieved, mainly limited by the low short-circuit current.

3.1. INTRODUCTION

Organic photovoltaics (OPV) have attracted large attention as a sustainable energy-producing technology because of their of aesthetically and mechanically appealing features (flexibility, semitransparency, color modulation) combined with cost-effective large area production methods (roll-to-roll printing), rendering OPV particularly suitable for deployable photovoltaic items and building or textile integration.[1] Besides the established bulk heterojunction (BHJ) polymer solar cells,[2] solution-processed devices based on 'small' molecule semiconductor combinations have caught up fast in terms of power conversion efficiency (PCE) over the last couple of years.[3,4] Whereas (methano)fullerenes, notably $PC_{61}BM$ and $PC_{71}BM$, are generally applied as the n-type blend components in these devices,[5] a diversity of p-type molecular chromophores has been used. Compared to their polymer counterparts, small molecule or oligomeric structures are more easily purified, present smaller batch-to-batch variations, allow straightforward tuning of the frontier orbital energy levels and often show intrinsic higher mobilities and open-circuit voltages (V_{oc}).[3,4] On the downside, it has to be mentioned that small molecules are generally less forgiving with respect to minor impurities present. Similar structural push-pull motifs as commonly applied toward low bandgap donor-acceptor copolymers are also used for the small molecule analogues and small changes in the chemical structure can lead to strong variations in final solar cell performance, even more so than for conjugated polymers. Additional investigations of the structure-device relations are hence certainly still required to make further advances in the field.

The thiazolo[5,4-*d*]thiazole (TzTz) fused biheterocycle has been applied as an electron-deficient structural motif in multiple polymer and small molecule OPV

donor materials.[6–8] The strong electron-accepting character enhances intramolecular charge transfer and oxidative stability, whereas the rigid planar structure leads to efficient intermolecular *π*-*π* interactions and high charge carrier mobilities.[9] 2,5-Diaryl-substituted TzTz's can easily be synthesized starting from the corresponding arylcarbaldehydes and dithiooxamide,[6] and further extension of the conjugated system is usually achieved via Suzuki or Stille cross-coupling (polycondensation) reactions. We have previously prepared a number of 5'-aryl-substituted 2,5-bis(3'-hexylthiophen-2'-yl)thiazolo[5,4-*d*]thiazole derivatives and these expanded semiconductors were investigated as active materials for solution-processable organic field-effect transistors (FET's).[10] On the other hand, it was shown that charge transfer (in the weak driving force limit) occurs in blends of dithienyl-TzTz's and MDMO-PPV toward fullerene-free OPV devices with high V_{oc}.[11] More recently, a series of TzTz-based small molecule materials was synthesized via a straighforward microwave-activated Pd-catalyzed C-H arylation protocol.[12] The procedure allowed to obtain extended 2,5-dithienylthiazolo[5,4-*d*]thiazole chromophores with tailor-made energy levels and absorption patterns, depending on the introduced (het)aryl moieties and the molecular (a)symmetry, by shortened sequences without organometallic intermediates. In the present manuscript, we report on the solar cell results upon implementing these compounds as either electron donor or electron acceptor light-harvesting materials in molecular BHJ OPV devices.

3.2. RESULTS AND DISCUSSION

3.2.1. Material characterization

Controllable direct arylation protocols have recently emerged as powerful sustainable (atom-economic) reactions toward advanced organic semiconducting materials for printable electronics.[13] A facile and versatile microwave-assisted procedure for the direct arylation of 2,5-dithienylthiazolo[5,4-*d*]thiazoles with various (hetero)aryl bromides was recently developed in our group toward a variety of mono- and difunctionalized TzTz-based molecular chromophores with an extended conjugated backbone.[12] Asymmetrical derivatives were also readily obtained by a sequential C-H arylation approach. Among the synthesized materials, a few TzTz derivatives were selected to be investigated as solution-processable solar photon harvesting materials for BHJ organic solar cells, either as small molecule electron donor or acceptor constituents, depending on the electronic nature of the appended aryl moieties (Figure 1). TzTz **6** – with 2-ethylhexyl side chains on the bridging thiophene unit – was additionally synthesized, following the same direct arylation protocol (see experimental section),[12] as solubility issues were observed for the 3-hexylthiophene analogue **5**.

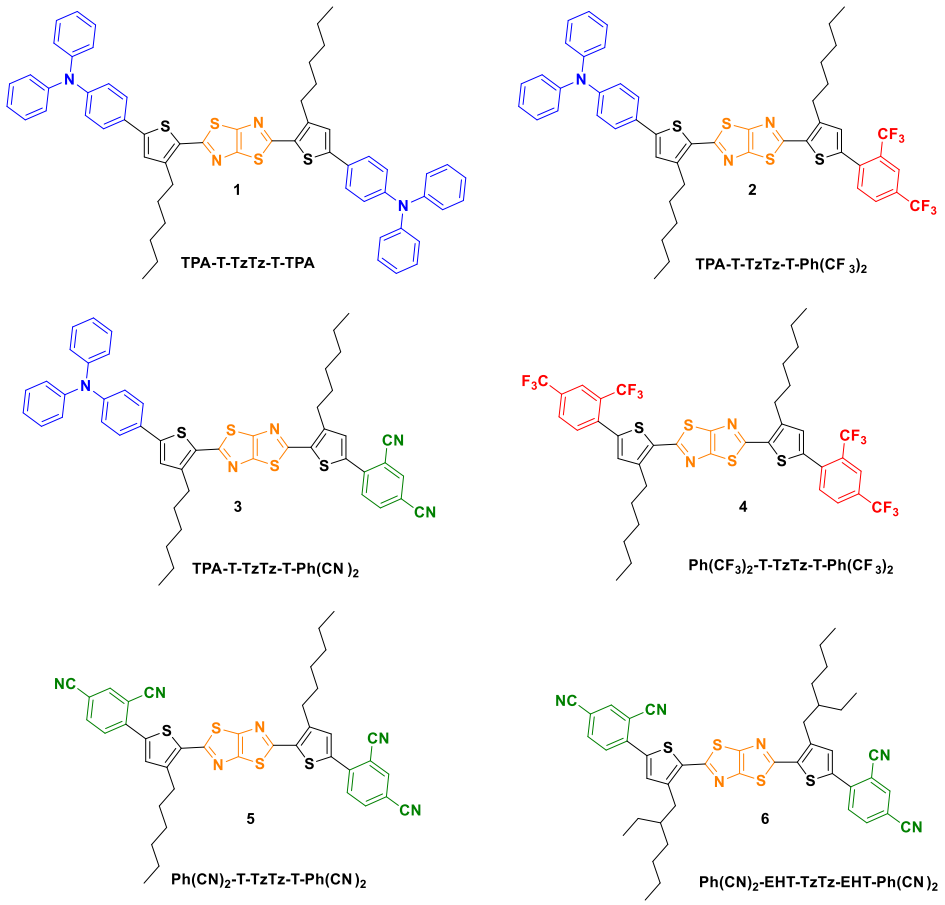

Figure 1: 2,5-Dithienyl-TzTz small molecules **1–6** analyzed in this study (TPA = triphenylamine, T = hexylthiophene, EH = 2-ethylhexyl).

The initial selection was made based on the absorption profiles of all dithienyl-TzTz materials and the estimated HOMO-LUMO energy levels as determined from cyclic voltammetry (CV).[12] All disubstituted molecules showed a broadened, red-shifted (10–28 nm) and stronger absorption (higher ε) as compared to the monofunctionalized derivatives. The (normalized) UV-Vis absorption spectra of the six selected molecules in chloroform are depicted in Figure 2 and the corresponding data (λ_{max} and ε) are gathered in Table 1. All UV-Vis spectra display two distinct absorption bands in the UV (λ_{max} = 250–320 nm) and visible region

(λ_{max} = 400–470 nm), attributed to the π–π* electronic transition and intramolecular charge transfer, respectively. Optical HOMO-LUMO gaps were determined from the onset (λ_{onset}) of the absorption spectra in solution and thin film (Table 1, Figure S3). The (film) optical HOMO-LUMO gaps are between 2.04 and 2.42 eV (Table 1), hence still rather high for OPV applications. The electron donating character of the triphenylamine (TPA) substituent, together with the extended conjugation length, results in a broad red-shifted absorption. The push-pull pattern created in the asymmetric derivatives **2** and **3** also results in red-shifted absorption profiles (up to λ_{max} = 473 nm for TzTz **3**). On the other hand, the symmetrical bis(trifluoromethyl)phenyl-substituted TzTz **4** shows the most blue-shifted absorption spectrum.

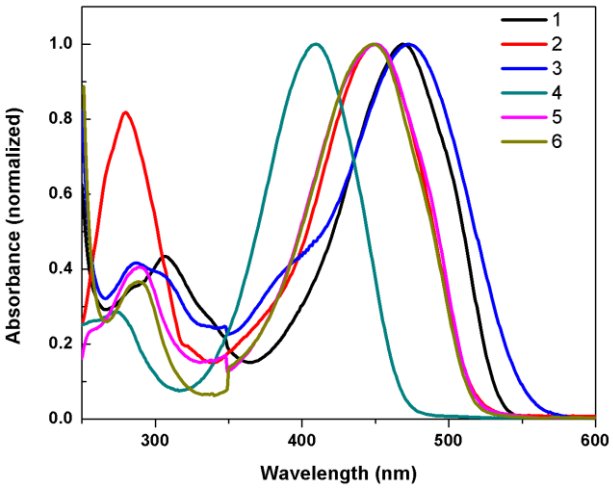

Figure 2: UV-Vis absorption spectra (normalized) of TzTz small molecules **1–6** in chloroform solution.

Basic electrochemical properties were investigated by CV and the data and derived frontier orbital energy levels are listed in Table 1. The more positive reduction potentials for TzTz's **3**, **5** and **6** point to a stronger electron acceptor character for

the compounds carrying bis(dicyanophenyl) moieties, rendering them possible candidates for n-type (non-fullerene) materials.[5,11] The ground state optical and electrochemical data were then treated based on the formalism developed by Veldman *et al.* (Table 1 and 2).[14] Effective thin-film optical HOMO and LUMO energies (*vs* vacuum), incorporating the intramolecular exciton binding energy in the solid state, were determined from the E_{ox}/E_{red} values related to the work function of the ferrocene/ferrocenium redox couple and the experimental difference between the electrochemical HOMO-LUMO gap in solution (E_{cv}^{sol}) and the optical HOMO-LUMO gap in thin film (E_g), assuming this difference can be equally divided over the HOMO and LUMO levels. From these optical HOMO/LUMO energies, the expected energy of the charge transfer state (E_{CT}) can also be estimated by an empirical rule based on the energy difference between the optical HOMO level of the electron donor component and the optical LUMO level of the electron acceptor component to be combined in a BHJ OPV device, corrected by a Coulomb term accounting for the higher energy of the intermolecular charge transfer (CT) exciton (vs intramolecular) due to the larger electron-hole separation distance. Additionally, the difference between the lowest optical HOMO-LUMO gap (among the donor and acceptor materials) and E_{CT} can be used as a criterion for successful photoinduced electron transfer. Applying these guidelines to the set of TzTz small molecule materials, it is clear that TzTz's **1**, **2** and **3** have most potential as electron donor compounds in combination with methanofullerenes. Maximum V_{oc} values around 1.0 V can be projected for these devices based on yet another empirical relation (Table 1). On the other hand, TzTz's **4**, **5** and **6** are less likely to give high-performance devices in combination with methanofullerenes, mostly due to the limited HOMO offset. Of the latter three, compounds **5** and **6** do show potential as fullerene replacements because

of the significantly lowered HOMO and LUMO values, pending a donor material with aligned energy levels (rule of thumb offset of ~0.35 eV required to ensure electron transfer[15]) can be found. TzTz **5** is barely applicable though because of its limited solubility in most standard processing solvents. Table 2 collects the electrochemical data of TzTz **6**, the previously investigated bis(4-cyanophenyl)-substituted TzTz analogue **7** (Figure S6),[11] and two prototype electron donor copolymers, MDMO-PPV and P3HT. Based on the standard (0.35 eV) offset and E_g^* – E_{CT} estimations, both MDMO-PPV and P3HT should be suitable donor polymers for TzTz **6**. Compared to TzTz **7**, the electron acceptor character obviously improved. Figure 3 provides a pictorial overview of the effective optical HOMO and LUMO energy levels obtained for all TzTz materials, together with the acceptor $PC_{71}BM$ and the prototype donor polymers MDMO-PPV and P3HT.

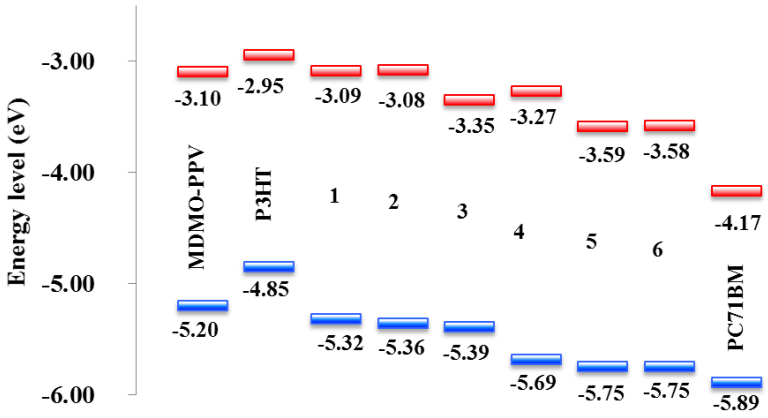

Figure 3: HOMO-LUMO energy level diagram for functionalized TzTz's **1–6** and some reference materials (E_{HOMO}^{opt} and E_{LUMO}^{opt} data from Table 1 and 2).

Table 1: Optical and electrochemical data for TzTz's **1–6** and $PC_{71}BM$, together with the derived optical HOMO-LUMO gaps, CT state energies (with $PC_{71}BM$ as the acceptor) and maximum V_{oc} values.

Cpd.	λ_{max} (nm)[a] (log ε)[b]	E_g^{sol} (eV)[c]	E_g (eV)[d]	E^{ox}_{onset} (V)	E^{red}_{onset} (V)	E_{cv} ^{sol} (eV) [e]	E_{HOMO}^{opt} (eV)[f]	E_{LUMO}^{opt} (eV)[g]	E_{CT} (eV)[h]	$E_g^* - E_{CT}$ (eV)[i]	eV_{oc} (eV)[j]
1	469 (4.88)	2.32	2.23	0.53	-1.81	2.34	-5.32	-3.09	1.44	0.28	0.97
2	449 (4.73)	2.40	2.30	0.55	-1.79	2.35	-5.36	-3.08	1.49	0.23	1.02
3	473 (4.66)	2.26	2.04	0.56	-1.51	2.07	-5.39	-3.35	1.51	0.21	1.04
4	410 (4.69)	2.66	2.42	1.03	-1.75	2.78	-5.69	-3.27	1.81	\	\
5	451 (4.70)	2.40	2.16	1.06	-1.41	2.47	-5.75	-3.59	1.87	\	\
6	448 (4.75)	2.42	2.17	1.06	-1.41	2.47	-5.75	-3.58	1.87	\	\
$PC_{71}BM$	372/461	2.05	1.72	1.21	-0.84	2.05	-5.89	-4.17	\	\	\

All CV measurements were done in CH_2Cl_2 solution. All voltammograms were reversible. [a] Measured in $CHCl_3$ solution. [b] Molar extinction coefficient ε, determined at λ_{max} in $CHCl_3$ solution. [c] Optical HOMO-LUMO gap in $CHCl_3$ solution, $E_g^{sol} = 1240/(\lambda_{onset})$. [d] Optical HOMO-LUMO gap in film, $E_g = 1240/(\lambda_{onset\ film})$. [e] Electrochemical HOMO-LUMO gap in solution (the difference between the oxidation and reduction onsets). [f] E_{HOMO}^{opt} (eV) = $-4.98 + 0.14^* - eE_{ox} + 1/2(E_{cv}^{sol} - E_g)$; * = Fc correction for CV measurement in CH_2Cl_2 solution. [g] E_{LUMO}^{opt} (eV) = $-4.98 + 0.14^* - eE_{red} - 1/2(E_{cv}^{sol} - E_g)$; * = Fc correction for CV measurement in CH_2Cl_2 solution. [h] $E_{CT} = |E_{HOMO}^{opt}(D) - E_{LUMO}^{opt}(A)| + 0.29$ eV with A = $PC_{71}BM$ (all values decrease by 0.03 eV for A = $PC_{61}BM$). [i] $E_g^* - E_{CT} \geq 0.08$ (± 0.02) is used as a general criterion for photoinduced electron transfer to occur, $E_g^* = \min[E_g(D), E_g(A)]$ with D = TzTz and A = $PC_{71}BM$. [j] $eV_{oc} = |E_{HOMO}^{opt}(D) - E_{LUMO}^{opt}(A)| - 0.18$ eV with A = $PC_{71}BM$ and e the elementary charge.

Table 2: Optical and electrochemical data for TzTz's **6** and **7**, P3HT and MDMO-PPV, together with the derived optical HOMO-LUMO (band)gaps, CT state energies (with the TzTz's as acceptors) and maximum V_{oc} values.

Cpd.	E_g^{sol} (eV)[d]	E_g (eV)[e]	E^{ox}_{onset} (V)	E^{red}_{onset} (V)	E_{cv}^{sol} (eV)[f]	E_{HOMO}^{opt} (eV)[g]	E_{LUMO}^{opt} (eV)[h]	E_{CT} (eV)[i]	$E_g^* - E_{CT}$ (eV)[j]	eV_{oc} (eV)[k]
6	2.42	2.17	1.06	-1.41	2.47	-5.75	-3.58	\	\	\
7	2.47	2.44	0.80	-1.56	2.37	-5.79	-3.35	\	\	\
P3HT[a]	2.24	1.90	0.13	-2.09	2.22	-4.93	-3.03	1.64 (1.87)	0.26	1.17
P3HT[b]	2.24	1.90	0.36	-2.06	2.42	-4.99	-2.91	1.70 (1.93)	0.20	1.23
MDMO-PPV[a]	2.24	2.06	0.24	-2.03	2.28	-5.09	-3.03	1.80 (2.03)	0.26	1.33
MDMO-PPV[b,c]	2.20	2.10	\	\	\	-5.20	-3.10	1.91 (2.14)	0.19	1.44

CV measurements for TzTz **6** were done in CH_2Cl_2 solution, whereas TzTz **7** was measured in MeCN solution. [a] CV data in film. [b] Measurements in *ortho*-dichlorobenzene solution. [c] Data taken from Veldman *et al.*[14]. [d] Optical HOMO-LUMO gap in solution, $E_g^{sol} = 1240/(\lambda_{onset})$. [e] Optical HOMO-LUMO gap in film, $E_g = 1240/(\lambda_{onset\ film})$. [f] Electrochemical HOMO-LUMO gap. [g] E_{HOMO}^{opt} (eV) = −4.98 − eE_{ox} + 1/2($E_{cv}^{sol} - E_g$) with an extra Fc correction depending on the solvent (0.14 for CH_2Cl_2, 0.03 for MeCN, 0.18 for *ortho*-dichlorobenzene). [h] E_{LUMO}^{opt} (eV) = −4.98 + 0.14 − eE_{red} − 1/2($E_{cv}^{sol} - E_g$) with an extra Fc correction depending on the solvent (0.14 for CH_2Cl_2, 0.03 for MeCN, 0.18 for *ortho*-dichlorobenzene). [i] $E_{CT} = |E_{HOMO}^{opt}(D) - E_{LUMO}^{opt}(A)| + 0.29$ eV with A = TzTz **6** (**7**). [j] $E_g^* - E_{CT} \geq 0.08$ (±0.02) is used as a general criterion for photoinduced electron transfer to occur, $E_g^* = \min[E_g(D), E_g(A)]$ with A = TzTz **6**. [k] $eV_{oc} = |E_{HOMO}^{opt}(D) - E_{LUMO}^{opt}(A)| - 0.18$ eV with A = TzTz **6**.

The thermal properties of the TzTz-based small molecules were investigated by rapid heat-cool calorimetry (RHC) (Figure S1, Table 3). RHC was chosen above regular differential scanning calorimetry (DSC) because of its increased sensitivity to thermal transitions as a result of the fast scanning rates and the low sample amounts required.[16] A clear difference in crystallization kinetics was observed between the mono- and disubstituted TzTz materials. The disubstituted derivatives generally show faster crystallization and higher melting points, whereas the monosubstituted compounds crystallize very slowly and are quenched easily. Even when cooled at 20 K/min, the monosubstituted materials remained amorphous in all cases. However, storage at room temperature seems to allow crystallization due to the low glass transition temperatures (T_g 's below room temperature) (Figure S1). Symmetrically extended TzTz's **4–6** show large melting enthalpies (ΔH_m), pointing to a high degree of crystallinity. On the other hand, no melting was observed for TPA-extended TzTz **1**, even when heated to 300 °C (no attempt at higher temperature was made to avoid degradation). As a reduced melting enthalpy and a lack of crystallization during storage (T_g slightly above room temperature) is also observed for the monosubstituted TPA analogue (Figure S1), TzTz **1** is probably amorphous, although melting at a temperature above 300 °C cannot be fully excluded. Asymmetrical TzTz's **4** and **5** do not show any sign of melting in the second heating, even when cooled slowly.

Table 3: Thermal properties of TzTz-based small molecules **1−6** (determined by RHC).[a]

TzTz	T_g (°C)	T_m (°C)	ΔH_m (J/g)
1	63.3	\[b]	\[b]
2	36.0	(85.2)[c]	(42.0)[c]
3	73.6	\[d]	\[d]
4	12.7	168.9	71.3
5	83.3	274.9	41.5
6[e]	\	5.8/231.4	6.6/61.6

[a] The second heating was chosen to avoid thermal history effects. Heating and cooling at 500 K/min. [b] No melting was seen, even when heated to 300 °C. [c] Melting was only observed during the first heating. [d] No crystallinity observed up to 250 °C, even when cooled slowly. [e] Heating at 500 K/min and cooling at 20 K/min.

3.2.2. TzTz donor small molecule solar cells

Based on the basic electrochemical screening (Table 1), TzTz small molecules **1−3** have the potential to give efficient BHJ organic solar cells in combination with fullerene-type acceptors. Due to the rather large HOMO-LUMO gap of the TzTz compounds, high-bandgap OPV devices with average (short-circuit current limited) PCE's can be expected.[8] To evaluate the performance of the donor-type TzTz small molecules in BHJ organic solar cells, the materials were used to fabricate standard architecture glass/ITO/PEDOT:PSS/photoactive layer/Ca/Al photovoltaic cells (Table 4). The processing conditions were optimized for symmetrical TzTz **1** (Table S1) and the optimum conditions were then also applied for asymmetric push-pull TzTz's **2** and **3**. The blend solutions, with *ortho*-dichlorobenzene (oDCB) as the processing solvent, were prepared in combination with $PC_{71}BM$ as the electron acceptor in a 1:3 (wt/wt%) ratio with a total concentration of 40 mg/mL. The small molecule solar cells with photoactive layer thicknesses of 50−60 nm afforded the best efficiencies, for which the

corresponding *J-V* curves are shown in Figure 4. All three small molecule solar cells exhibit high V_{oc}'s with values between 0.93 and 0.98 V, as predicted based on the opto-electric data (Table 1). The observed trend matches well with the predicted values. The final device efficiencies for TzTz's **1** and **3** are, however, limited by the rather low fill factors (FF's) and slightly lower than expected short-circuit current densities (J_{sc}'s), affording average PCE's of 2.29 and 2.32%, respectively (best devices 2.65 and 2.77%). The performance of TzTz **2** lags behind, mostly due an even lower FF (0.32) and a further reduced J_{sc}, resulting in an overall average PCE of 1.44% (best device 1.59%).

Table 4: Processing and output parameters of the standard architecture organic solar cells based on the small molecule TzTz donor materials blended with $PC_{71}BM$.

TzTz	D:A ratio	Solvent[a]	V_{oc} (V)	J_{sc} (mA/cm^2)	FF (%)	PCE[b] (%)
1	1:3	oDCB	0.93	5.99	43	2.44 (2.63)
2	1:3	oDCB	0.97	4.71	32	1.45 (1.59)
3	1:3	oDCB	0.98	6.45	40	2.51 (2.74)

[a] oDCB = *ortho*-dichlorobenzene, [b] Average values over at least 4 devices. The best device performance is shown in brackets.

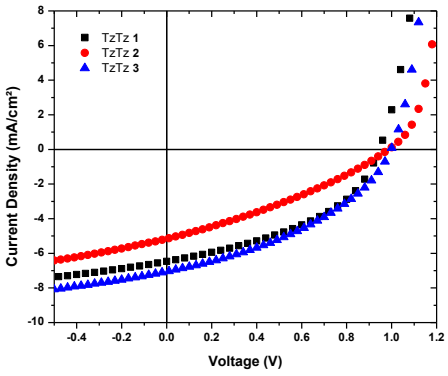

Figure 4: *J-V* characteristics of the best TzTz **1**–**3**:$PC_{71}BM$ solar cells.

Atomic force microscopy (AFM) measurements were performed to investigate if the fluctuations in device performance originate from topographical/morphological differences in the small molecule:fullerene films. Figure 5 clearly demonstrates a relatively intimate mixing of the small molecule and fullerene compounds and no distinct features can be detected for either of the TzTz-based blends.

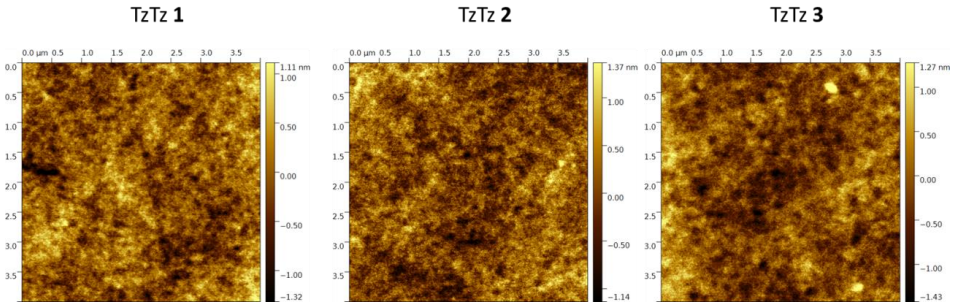

Figure 5: AFM (topography) images (4 x 4 μm) of the photoactive layers of the TzTz **1–3**:$PC_{71}BM$ solar cell devices.

Since the FF and, to a lesser extent, the J_{sc} are the parameters limiting photovoltaic efficiency, a possible correlation could be found with the occurrence of recombination processes or imbalanced charge carrier mobilities, especially taking into consideration the rather thin optimal photoactive layer thicknesses (50–60 nm).[17] To evaluate the charge transport, the hole mobility was assessed for the donor-type small molecule materials. Field-effect transistors (FET's) were prepared in the bottom gate bottom contacts configuration by depositing the TzTz materials from chloroform on a SiO_2 layer, thermally grown on highly n-doped Si. Gold source and drain contacts were pre-patterned on the substrate, on top of a Ti adhesion layer. The extracted hole mobilities from the saturation regime for TzTz's **1–3** were found to be 2.8×10^{-5}, 6.8×10^{-7} and 1.1×10^{-6} $cm^2(Vs)^{-1}$, respectively (Figure S2). In comparison to other commonly employed organic

semiconductors (e.g. P3HT with a value of 10^{-4} $cm^2(Vs)^{-1}$ [18]), these mobilities are (significantly) lower, possibly due to the amorphous nature of the TzTz small molecule donor materials. Nonetheless, the results correlate with the observed solar cell performances and the lower hole mobilities are in line with the low FF and J_{sc} values attained for each of the TzTz small molecule devices.

The external quantum efficiency (EQE) spectra for the best solar cell devices are depicted in Figure 6. The shape of the EQE profiles correlates well to the UV-Vis absorption spectra of the small molecules (Figure 2 and S3) and for all molecules a clear contribution of both the fullerene derivative and the donor material can be observed with maxima at ~350 and 500 nm, respectively. For the solar cell devices based on TzTz **1–3**, no major difference in shape can be observed, apart from a shift to higher/lower EQE values, correlating well with the differences in the measured J_{sc}'s.

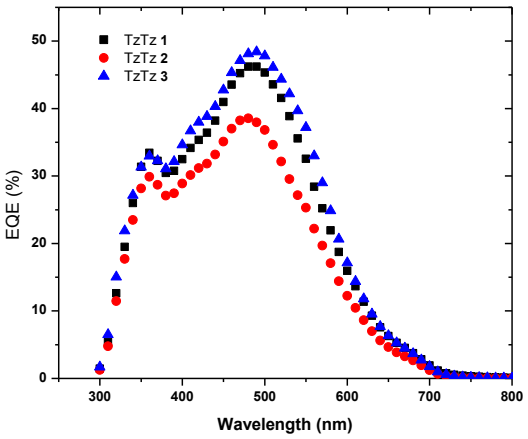

Figure 6: EQE spectra of the best TzTz **1–3**:$PC_{71}BM$ solar cells. The devices employed for the EQE measurements gave a J_{sc} of 6.2, 5.13 and 7.03 mA cm^{-2} for TzTz **1–3**, respectively, with J_{EQE}'s of 5.17, 4.19 and 5.51 mA cm^{-2}.

3.2.3. TzTz acceptor small molecule solar cells

As mentioned above and illustrated in Table 1 and 2, TzTz **6** shows more potential as a small molecule acceptor compound (rather than a donor) and could be combined with either P3HT or MDMO-PPV. Photovoltaic performance data for both photovoltaic blends are gathered in Table 5. A small optimization study was performed for the P3HT:TzTz **6** solar cells (Table S2). The optimal polymer:TzTz **6** blend solutions were prepared with chloroform as the processing solvent in a 2:1 or 1:1 ratio (wt/wt%) with a total concentration of 6 mg/mL. These low optimal concentrations already suggest an enlarged presence of charge traps in the films. The solar cells based on MDMO-PPV:TzTz **6** show a remarkably high V_{oc} of 1.20−1.25 V, but unfortunately the final performance is limited by the very low values for the J_{sc} and FF. On the contrary, photovoltaic devices based on P3HT:TzTz **6** exhibit a more modest V_{oc} of 0.85 V, but in combination with a J_{sc} and a FF of 0.88 mA/cm² and 0.47, respectively, a final average efficiency of 0.35% (best 0.41%) could be obtained.

Table 5: Processing and output parameters of the standard architecture organic solar cells based on MDMO-PPV:TzTz **6** and P3HT:TzTz **6**.

Donor	D:A ratio	Solvent[a]	V_{oc} (V)	J_{sc} (mA/cm^2)	FF (%)	PCE[b] (%)
MDMO-PPV	2:1	CF	1.21	0.11	27	0.04 (0.04)
MDMO-PPV	1:1	CF	1.24	0.08	26	0.03 (0.03)
P3HT	2:1	CF	0.85	0.88	47	0.35 (0.41)

[a] CF = chloroform, [b] Average values over at least 8 devices. The best device performance is shown in brackets.

To investigate whether the obtained lower values for J_{sc} and/or FF are of morphological origin, AFM measurements were performed (Figure 7). For the combination of MDMO-PPV and TzTz **6**, a homogeneous distribution of the donor

and acceptor compounds was obtained for both D:A ratios. On the other hand, the photoactive layers based on P3HT:TzTz **6** demonstrated the formation of crystalline structures, which is not really surprising considering the crystalline character of both components. The enhanced J_{sc} and FF in comparison to the MDMO-PPV:TzTz **6** combination can tentatively be ascribed to this improved crystallinity.

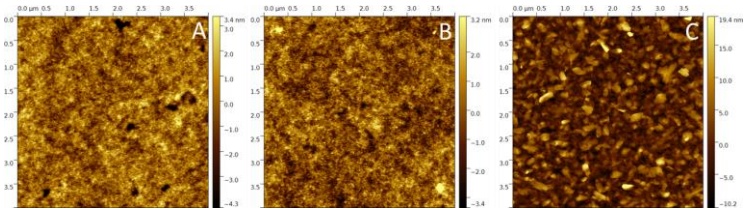

Figure 7: AFM (topography) images (4 x 4 μm) of the photoactive layers of A) MDMO-PPV:TzTz **6** (2:1), B) MDMO-PPV:TzTz **6** (1:1) and C) P3HT:TzTz **6** (2:1) solar cells.

3.3. CONCLUSIONS

In conclusion, a number of simple diaryl-extended 2,5-dithienylthiazolo[5,4-*d*]thiazole small molecules were selected for organic solar cell applications based on their opto-electrical characteristics. Depending on the appended substituents, the materials could be applied as either electron donor or acceptor constituents in bulk heterojunction organic photovoltaic devices. For the (high-bandgap) TzTz electron donor compounds, high open-circuit voltages are obtained, with a maximum power conversion efficiency of 2.7%. On the other hand, an efficiency of 0.4% was achieved for the most electron poor TzTz in combination with P3HT. For both device layouts, the performance is mainly limited by the short-circuit current. Current efforts are oriented toward improved understanding of the limiting factors, for example by investigation of the charge transfer state and

polaron formation, and the synthesis of a second generation of TzTz chromophores with broadened absorption profiles.

3.4. EXPERIMENTAL SECTION

3.4.1. Materials and methods

Unless stated otherwise, all reagents and chemicals were obtained from commercial sources and used without further purification. Solvents were dried by a solvent purification system (MBraun, MB-SPS-800) equipped with alumina columns. 2,5-Bis[3'-(2''-ethyl)hexylthiophen-2'-yl]thiazolo[5,4-*d*]thiazole was prepared according to a literature procedure.[19] Microwave reactions were carried out in a CEM Discovery microwave at the given temperature by varying the irradiation power and using a thick-walled pyrex reaction vessel (10 mL) with teflon septum.

NMR chemical shifts (δ, in ppm) were determined relative to the residual $CHCl_3$ (7.26 ppm) absorption or the ^{13}C resonance shift of $CDCl_3$ (77.16 ppm). MALDI-TOF mass spectra were recorded on a Bruker Daltonics Ultraflex II Tof/Tof. 1 µL of the matrix solution (16 mg mL^{-1} DTCB (*trans*-2-[3-(4-*tert*-butylphenyl)-2-methyl-2-propenylidene]malononitrile) in $CHCl_3$) was spotted onto an MTP Anchorchip 600/384 MALDI plate. The spot was allowed to dry and 1 µL of the analyte solution (0.5 mg mL^{-1} in $CHCl_3$) was spotted on top of the matrix. Rapid heat-cool calorimetry (RHC) experiments were performed on a prototype RHC of TA Instruments, equipped with liquid nitrogen cooling and specifically designed for operation at high scanning rates.[16] RHC measurements were performed at 500 K min^{-1} in aluminum crucibles, using helium (6 mL min^{-1}) as a purge gas. UV-Vis absorption spectra were recorded with an Agilent Cary 500 Scan UV-Vis-NIR

spectrometer in a continuous run from 200 to 800 nm at a scan rate of 600 nm min^{-1}. The thin films for the solid-state UV-Vis measurements were prepared by drop casting chloroform solutions of the TzTz compounds. Electrochemical measurements were performed with an Eco Chemie Autolab PGSTAT 30 potentiostat/galvanostat using a three-electrode microcell equipped with a Pt wire working electrode, a Pt wire counter electrode and a $Ag/AgNO_3$ reference electrode (Ag wire dipped in a solution of 0.01 M $AgNO_3$ and 0.1 M NBu_4PF_6 in anhydrous MeCN). Samples were prepared in anhydrous CH_2Cl_2 containing 0.1 M NBu_4PF_6, and ferrocene was used as an internal standard. The respective TzTz products were dissolved in the electrolyte solution, which was degassed with Ar prior to each measurement. To prevent air from entering the system, the experiments were carried out under a curtain of Ar. Cyclic voltammograms were recorded at a scan rate of 50 mV s^{-1}. The HOMO-LUMO energy levels of the products were determined using CV data and spectroscopic absorption data. For the conversion of V to eV, the onset potentials of the first oxidation/reduction peaks were used and referenced to ferrocene/ferrocenium, which has an ionization potential of -4.98 eV *vs.* vacuum. This correction factor is based on a value of 0.31 eV for Fc/Fc^+ *vs.* SCE[20a] and a value of 4.68 eV for SCE *vs.* vacuum[20b]: $E_{HOMO/LUMO}$ (eV) = -4.98 - $E_{onset\ ox/red}^{Ag/AgNO3}$ (V) + $E_{onset\ Fc/Fc+}^{\ Ag/AgNO3}$ (V). The HOMO energy levels of the TzTz products were determined from the CV data. The LUMO energy levels were either determined from the CV data or calculated as the difference between the HOMO values and the optical HOMO-LUMO gaps. The accuracy of measuring redox potentials by CV is about 0.01−0.02 V. Reproducibility can be less because the potentials do depend on concentration and temperature.[14] To estimate the optical HOMO-LUMO gaps, the wavelength at the intersection of the tangent line

drawn at the low energy side of the solution/film absorption spectrum with the x-axis was used (E_g (eV) = 1240/(wavelength in nm)).

4,4'-{Thiazolo[5,4-d]thiazole-2,5-diyl-bis[4-(2-ethyl)hexylthiophene-5,2-diyl)}diisophthalo-nitrile (6). 2,5-Bis[3′-(2′′-ethyl)hexylthiophen-2′-yl]thiazolo[5,4-*d*]thiazole (100 mg, 0.188 mmol, 1 equiv), K_2CO_3 (39 mg, 0.283 mmol 1.5 equiv), $Pd(OAc)_2$ (1.0 mg, 5 µmol, 2 mol%), PCy_3HBF_4 (2.7 mg, 7.5 µmol, 4 mol%) and pivalic acid (5.7 mg, 0.057 mmol, 30 mol%) were weighed in air and placed in a microwave vial (10 mL) equipped with a magnetic stirring bar. 4-Bromoisophthalonitrile (82 mg, 0.396 mmol, 2.1 equiv) was added. The vial was purged with Ar and dry toluene (1 mL) was added. The reaction mixture was vigorously stirred under microwave irradiation at 180 °C for 4 h. The solution was then cooled down to room temperature and diluted with CH_2Cl_2 and H_2O. The aqueous phase was extracted with CH_2Cl_2. The organic fractions were combined and dried over $MgSO_4$, filtered, and evaporated under reduced pressure. The obtained product mixture was separated by column chromatography (eluent gradient petroleum ether/$CHCl_3$ 4/1–1/1) to afford the pure mono- (15 mg, 11%) and disubstituted (128 mg, 87%; red solid) TzTz's. ^{1}H NMR (400 MHz, $CDCl_3$) δ 8.04 (dd, J = 1.7, 0.6 Hz, 2H), 7.88 (dd, J = 8.3, 1.7 Hz, 2H), 7.81 (dd, J = 8.3, 0.6 Hz, 2H), 7.70 (s, 2H), 2.97 (d, J = 7.3 Hz, 4H), 1.91–1.75 (m, 2H), 1.52–1.37 (m, 8H), 1.36–1.20 (m, 8H), 0.98–0.85 (m, 12H); ^{13}C NMR (75 MHz, $CDCl_3$) δ 160.9, 151.1, 144.0, 140.4, 138.2, 138.1, 136.1, 133.5, 130.1, 117.0, 116.6, 112.2, 110.9, 39.9, 34.9, 32.7, 28.8, 25.8, 23.2, 14.3, 10.7; UV-Vis ($CHCl_3$) λ_{max} (log ε) 448 nm (4.75)

3.4.2. Solar cell and FET preparation and characterization

Solar cells in standard architecture were prepared with a layout glass/ITO/PEDOT:PSS/TzTz:$PC_{71}BM$/Ca/Al. Substrates with pre-patterned ITO on glass were purchased from Kintec (100 nm, 20 Ohm/sq) and cleaned through sonication in soap, deionized water, acetone and isopropyl alcohol before proceeding with the spin-coating of PEDOT:PSS (Heraeus Clevios AI 4083). Substrates were subsequently brought inside a N_2 filled glovebox and annealed during 10 min at 130 °C to remove residual humidity. All subsequent steps of processing and characterization were conducted in inert atmosphere. For the small molecule donor TzTz's, the active layer blends were spin-casted on the PEDOT:PSS layer using a 1:3 ratio (wt/wt%) TzTz:$PC_{71}BM$ in *ortho*-dichlorobenzene solution with a total concentration of 40 mg/mL. For the best small molecule acceptor devices, blend solutions were prepared with MDMO-PPV or P3HT as the donor polymer and TzTz **6** as the electron acceptor in a 2:1 ratio (wt/wt%) in chloroform and an optimal total concentration of 6 mg/mL Finally, the Ca and Al top electrodes were deposited by vacuum deposition aiming at thicknesses of 30 and 80 nm, respectively, resulting in an active device area of 0.03 cm^2 through the use of shadow masks. Electrical characterization was carried out under illumination from a Newport class A solar simulator (model 91195A), calibrated with a silicon solar cell to give an AM 1.5G spectrum. EQE measurements were performed with a Newport Apex illuminator (100 W Xenon lamp, 6257) as light source, a Newport Cornerstone 130 monochromator and a Stanford SR830 lock-in amplifier for the current measurements. A silicon-calibrated FDS-100 photodiode was employed as a reference cell. Peak Force Tapping AFM images were acquired with a Bruker Multimode 8 AFM, employing ScanAsyst. The silicon nitride tip had a spring constant of 0.4 N m^{-1}. FET's were

prepared by spin-coating solutions of TzTz's **1–3** in chloroform, with a concentration of 16 mg/mL, on 200 nm of thermally grown SiO_2. The gate contact consisted of highly n-doped Si. Source and drain electrodes were pre-patterned, comprising of a stack of Ti/Au (10/100 nm). FET substrates were acquired from Philips. The channel length was 10 µm. Two Keithley 2400 source meters were used to measure the I_{DS} and correct it for leakage through the gate electrode. All FET preparations and characterizations were carried out in a N_2 filled glove box.

3.5. ACKNOWLEDGEMENTS

This work was supported by the project ORGANEXT (EMR INT4-1.2-2009-04/054), selected in the frame of the operational program INTERREG IV-A Euregio Maas-Rijn, and the IAP 7/05 project FS2 (Functional Supramolecular Systems), granted by the Science Policy Office of the Belgian Federal Government (BELSPO). We are also grateful for financial support by the Research Programme of the Research Foundation – Flanders (FWO) (projects G.0415.14N, G.0B67.15N and M.ERA-NET project RADESOL). P. Verstappen and G. Heintges acknowledge the Agency for Innovation by Science and Technology in Flanders (IWT) for their PhD grants. Hasselt University, IMO-IMOMEC and TUEindhoven are partners within the Solliance network, the strategic alliance for research and development in the field of thin-film PV energy in the Eindhoven-Leuven-Aachen region.

3.6. REFERENCES

[1] Recent OPV reviews: (*a*) M. Jørgensen, K. Norrman, S. A. Gevorgyan, T. Tromholt, B. Andreasen and F. C. Krebs, *Adv. Mater.*, 2012, **24**, 580; (*b*) H. Zhou, L. Yang and W. You, *Macromolecules*, 2012, **45**, 607; (*c*) Y. Li, *Acc. Chem. Res.*, 2012, **45**, 723; (*d*) Y. Su, S. Lan and K. Wei, *Mater. Today*, 2012, **15**, 554; (*e*) R. Søndergaard, M. Hösel, D. Angmo, T. T. Larsen-Olsen and F. C. Krebs, *Mater. Today*, 2012, **15**, 36; (*f*) R. A. J. Janssen and J. Nelson, *Adv. Mater.*, 2013, **25**, 1847; (*g*) S. Lizin, S. Van Passel, E. De Schepper, W. Maes, L. Lutsen, J. Manca and D. Vanderzande, *Energy Environ. Sci.*, 2013, **6**, 3136; (*h*) T. Xu and L. Yu, *Mater. Today*, 2014, **17**, 11.

[2] (*a*) Z. He, C. Zhong, S. Su, M. Xu, H. Wu and Y. Cao, *Nat. Photonics*, 2012, **6**, 591; (*b*) C. Cabanetos, A. El Labban, J. A. Bartelt, J. D. Douglas, W. M. Mateker,

J. M. Fréchet, M. D. McGehee and P. M. Beaujuge, *J. Am. Chem. Soc.*, 2013, **135**, 4556; (*c*) K. H. Hendriks, G. H. L. Heintges, V. S. Gevaerts, M. M. Wienk and R. A. J. Janssen, *Angew. Chem. Int. Ed.*, 2013, **52**, 8341; (*d*) L. Dou, C.-C. Chen, K. Yoshimura, K. Ohya, W.-H. Chang, J. Gao, Y. Liu, E. Richard and Y. Yang, *Macromolecules*, 2013, **46**, 3384; (*e*) I. Osaka, T. Kakara, N. Takemura, T. Koganezawa and K. Takimiya, *J. Am. Chem. Soc.*, 2013, **135**, 8834; (*f*) Y. Deng, J. Liu, J. Wang, L. Liu, W. Li, H. Tian, X. Zhang, Z. Xie, Y. Geng and F. Wang, *Adv. Mater.*, 2014, **26**, 471; (*g*) M. Zhang, X. Guo, S. Zhang and J. Hou, *Adv. Mater.*, 2014, **26**, 1118; (*h*) L. Ye, S. Zhang, W. Zhao, H. Yao and J. Hou, *Chem. Mater.*, 2014, **26**, 3603; (*i*) Y. Liu, J. Zhao, Z. Li, C. Mu, W. Ma, H. Hu, K. Jiang, H. Lin, H. Ade and H. Yan, *Nat. Commun.*, 2014, **5**, 5293.

[3] Reviews on BHJ small molecule organic solar cells: (*a*) A. Mishra and P. Bäuerle, *Angew. Chem. Int. Ed.*, 2012, **51**, 2020; (*b*) Y. Lin, Y. Li and X. Zhan, *Chem. Soc. Rev.*, 2012, **41**, 4245; (*c*) Y. Chen, X. Wan and G. Long, *Acc. Chem. Res.*, 2013, **46**, 2645; (*d*) J. Roncali, P. Leriche and P. Blanchard, *Adv. Mater.*, 2014, **26**, 3821.

[4] (*a*) Y. Liu, C.-C. Chen, Z. Hong, J. Gao, Y. M. Yang, H. Zhou, L. Dou, G. Li and Y. Yang, *Scientific Reports*, 2013, **3**, 3356; (*b*) A. K. K. Kyaw, D. H. Wang, V. Gupta, J. Zhang, S. Chand, G. C. Bazan and A. J. Heeger, *Adv. Mater.*, 2013, **25**, 2397; (*c*) A. K. K. Kyaw, D. H. Wang, D. Wynands, J. Zhang, T.-Q. Nguyen, G. C. Bazan and A. J. Heeger, *Nano Lett.*, 2013, **13**, 3796; (*d*) J. Zhou, Y. Zuo, X. Wan, G. Long, Q. Zhang, W. Ni, Y. Liu, Z. Li, G. He, C. Li, B. Kan, M. Li and Y. Chen, *J. Am. Chem. Soc.*, 2013, **135**, 8484; (*e*) Y. Liu, Y. Yang, C-C. Chen, Q. Chen, L. Dou, Z. Hong, G. Li and Y. Yang, *Adv. Mater.*, 2013, **25**, 4657; (*f*) V. S. Gevaerts, E. M. Herzig, M. Kirkus, K. H. Hendriks, M. M. Wienk, J. Perlich, P. Müller-Buschbaum and R. A. J. Janssen, *Chem. Mater.*, 2014, **26**, 916; (*g*) D. Liu, M.

Xiao, Z. Du, Y. Yan, L. Han, V. A. L. Roy, M. Sun, W. Zhu, C. S. Lee and R. Yang, *J. Mater. Chem. C*, 2014, **2**, 7523; (*h*) B. Kan, Q. Zhang, M. Li, X. Wan, W. Ni, G. Long, Y. Wang, X. Yang, H. Feng and Y. Chen, *J. Am. Chem. Soc.*, 2014, **136**, 15529; (*i*) J. Min, Y. N. Luponosov, A. Gerl, M. S. Polinskaya, S. M. Peregudova, P. V. Dmitryakov, A. V. Bakirov, M. A. Shcherbina, S. N. Chvalun, S. Grigorian, N. Kaush-Busies, S. A. Ponomarenko, T. Ameri and C. J. Brabec, *Adv. Energy Mater.*, 2014, **5**, 1301234; (*j*) M. Jung, Y. Yoon, J. H. Park, W. Cha, A. Kim, J. Kang, S. Gautam, D. Seo, J. H. Cho, H. Kim, J. Y. Choi, K. H. Chae, K. Kwak, H. J. Son, M. J. Ko, H. Kim, D.-K. Lee, J. Y. Kim, D. H. Choi and B. Kim, *ACS Nano*, 2014, **8**, 5988; (*k*) H. Qin, L. Li, F. Guo, S. Su, J. Peng, Y. Cao and X. Peng, *Energy Environ. Sci.*, 2014, **7**, 1397; (*l*) B. Kan, Q. Zhang, F. Liu, X. Wan, Y. Wang, W. Ni, G. Long, X. Yang, H. Feng, Y. Zuo, M. Zhang, F. Huang, Y. Cao, T. P. Russell and Y. Chen, *J. Am. Chem. Soc.*, 2015, **137**, DOI: 10.1021/jacs.5b00305.

[5] (*a*) A. Facchetti, *Mater Today*, 2013, **16**, 123; (*b*) Y. Lin and X. Zhan, *Mater. Horiz.*, 2014, **1**, 470; (*c*) A. F. Eftaiha, J.-P. Sun, I. G. Hill and G. C. Welch, *J. Mater. Chem. A*, 2014, **2**, 120.

[6] D. Bevk, L. Marin, L. Lutsen, D. Vanderzande and W. Maes, *RSC Adv.*, 2013, **3**, 11418.

[7] TzTz-based donor polymers: (*a*) T. W. Lee, N. S. Kang, J. W. Yu, M. H. Hoang, K. H. Kim, J.-L. Jin and D. H. Choi, *J. Polym. Sci., Part A: Polym. Chem.*, 2010, **48**, 5921; (*b*) S. Subramaniyan, H. Xin, F. Sunjoo Kim, S. Shoaee, J. R. Durrant and S. A. Jenekhe, *Adv. Energy Mater.*, 2011, **1**, 854; (*c*) M. Zhang, X. Guo, X. Wang, H. Wang and Y. Li, *Chem. Mater.*, 2011, **23**, 4264; (*d*) S. K. Lee, J. M. Cho, W. S. Shin, J.-C. Lee, W.-H. Lee, I.-N. Kang, H.-K. Shim and S.-J. Moon, *Chem. Commun.*, 2011, **47**, 1791; (*e*) I. Osaka, M. Saito, T. Koganezawa and K. Tamikiya, *Adv. Mater.*, 2012, **24**, 425; (*f*) S. Van Mierloo, J. Kesters, A. Hadipour,

M.-J. Spijkman, N. Van den Brande, J. D'Haen, G. Van Assche, D. M. de Leeuw, T. Aernouts, J. Manca, L. Lutsen, D.Vanderzande and W. Maes, *Chem. Mater.*, 2012, **24**, 587; (*g*) J. Kesters, T. Ghoos, H. Penxten, J. Drijkoningen, T. Vangerven, D. M. Lyons, B. Verreet, T. Aernouts, L. Lutsen, D. Vanderzande, J. Manca and W. Maes, *Adv. Energy Mater.*, 2013, **3**, 1180; (*h*) S. Shoaee, S. Subramaniyan, H. Xin, C. Keiderling, P. S. Tuladhar, F. Jamieson, S. A. Jenekhe and J. R. Durrant, *Adv. Funct. Mater.*, 2013, **23**, 3286; (*i*) I. Osaka, M. Saito, T. Koganezawa and K. Takimiya, *Adv. Mater.*, 2014, **26**, 331; (*j*) S. Subramaniyan, H. Xin, F. Sunjoo Kim, N. M. Murari, B. A. E. Courtright and S. A. Jenekhe, *Macromolecules*, 2014, **47**, 4199; (*k*) E. Bundgaard, F. Livi, O. Hagemann, J. E. Carlé, M. Helgesen, I. M. Heckler, N. K. Zawacka, D. Angmo, T. T. Larsen-Olsen, G. A. dos Reis Benatto, B. Roth, M. V. Madsen, M. R. Andersson, M. Jørgensen, R. R. Søndergaard and F. C. Krebs, *Adv. Energy Mater.*, 2015, 1402186; (*l*) M. Helgesen, J. E. Carlé, G. A. dos Reis Benatto, R. R. Søndergaard, M. Jørgensen, E. Bundgaard and F. C. Krebs, *Adv. Energy Mater.*, 2015, 1401996.

[8] TzTz-based small molecule donor compounds: (*a*) Q. Shi, P. Cheng, Y. Li and X. Zhan, *Adv. Energy Mater*., 2012, **2**, 63; (*b*) P. Dutta, W. Yang, S. H. Eom and S.-H. Lee, *Org. Electron*., 2012, **13**, 273; (*c*) P. Dutta, H. Park, W-H. Lee, I-N. Kang and S-H. Lee, *Org. Electron.*, 2012, **13**, 3183; (*d*) P. Cheng, Q. Shi, Y. Lin, Y. Li and X. Zhan, *Org. Electron.*, 2013, **14**, 599; (*e*) A. Dessì, B. G. Consiglio, M. Calamante and L. Zani, *Eur. J. Org. Chem.*, 2013, **10**, 1916; (*f*) L. Zani, G. Reginato, A. Mordini, M. Calamante and M. Bruzzi, *Tetrahedron Lett.*, 2013, **54**, 3944; (*g*) M. Nazim, S. Ameen, M. Shaheer Akhtar, Y.-S. Lee and H.-S. Shin, *Chem. Phys. Lett.*, 2013, **574**, 89; (*h*) W. Zhang, Q. Feng, Z.-S. Wang and G. Zhou, *Chem. Asian J.*, 2013, **8**, 939; (*i*) R. Ziessel, A. Nano, E. Heyer, T. Bura and P. Retailleau, *Chem. Eur. J.*, 2013, **19**, 2582; (*j*) Y. Chen, Z. Du, W. Chen, S. Wen,

L. Sun, Q. Liu, M. Sun and R. Yang, *New J. Chem.*, 2014, **38**, 1559; (*k*) A. Fitri, A. T. Benjelloun, M. Benzakour, M. Mcharfi, M. Hamidi and M. Bouachrine, *Spectrochim. Acta Part A: Molecular and Biomolecular Spectroscopy*, 2014, **132**, 232.

[9] (*a*) S. Ando, J.-i. Nishida, Y. Inoue, S. Tokito and Y. Yamashita, *J. Mater. Chem.*, 2004, **14**, 1787; (*b*) S. Ando, J.-i. Nishida, H. Tada, Y. Inoue, S. Tokito and Y. Yamashita, *J. Am. Chem. Soc.*, 2005, **127**, 5336; (*c*) M. Mamada, J.-i. Nishida, D. Kumaki, S. Tokito and Y. Yamashita, *Chem. Mater.*, 2007, **19**, 5404.

[10] (*a*) S. Van Mierloo, V. Liégeois, J. Kudrjasova, E. Botek, L. Lutsen, B. Champagne, D. Vanderzande, P. Adriaensens and W. Maes, *Magn. Reson. Chem.*, 2012, **50**, 379; (*b*) S. Van Mierloo, K. Vasseur, N. Van den Brande, A. E. Boyukbayram, B. Ruttens, S. Rodriguez, E. Botek, V. Liégeois, J. D'Haen, P. J. Adriaensens, P. Heremans, B. Champagne, G. Van Assche, L. Lutsen, D. J. Vanderzande and W. Maes, *ChemPlusChem*, 2012, **77**, 923.

[11] (*a*) N. Nevil, Y. Ling, S. Van Mierloo, J. Kesters, F. Piersimoni, P. Adriaensens, L. Lutsen, D. Vanderzande, J. Manca, W. Maes, S. Van Doorslaer and E. Goovaerts, *Phys. Chem. Chem. Phys.*, 2012, **14**, 15774; (*b*) Y. Ling, S. Van Mierloo, A. Schnegg, M. Fehr, P. Adriaensens, L. Lutsen, D. Vanderzande, W. Maes, E. Goovaerts and S. Van Doorslaer, *Phys. Chem. Chem. Phys.*, 2014, **16**, 10032.

[12] J. Kudrjasova, R. Herckens, H. Penxten, P. Adriaensens, L. Lutsen, D. Vanderzande and W. Maes, *Org. Biomol. Chem.*, 2014, **12**, 4663.

[13] (*a*) J. Zhang, D.-Y. Kang, S. Barlow and S. R. Marder, *J. Mater. Chem.*, 2012, **22**, 21392; (*b*) S.-Y. Liu, M.-M. Shi, J.-C. Huang, Z.- N. Jin, X.-L. Hu, J.-Y. Pan, H.-Y. Li, A. K. Y. Jen and H.-Z. Chen, *J. Mater. Chem. A*, 2013, **1**, 2795; (*c*) J. Zhang, W. Chen, A. J. Rojas, E. V. Jucov, T. V. Timofeeva, T. C. Parker, S. Barlow and S. R. Marder, *J. Am. Chem. Soc.*, 2013, **135**, 16376; (*d*) K. Okamoto, J.

Zhang, J. B. Housekeeper, S. R. Marder and C. K. Luscombe, *Macromolecules*, 2013, **46**, 8059; (*e*) R. Matsidik, J. Martin, S. Schmidt, J. Obermayer, F. Lombeck, F. Nübling, H. Komber, D. Fazzi and M. Sommer, *J. Org. Chem.*, 2015, **80**, 980; (*f*) S. M. McAfee, J. M. Topple, A.-J. Payne, J.-P. Sun, I. G. Hill and G. C. Welch, *ChemPhysChem*, 2015, DOI: 10.1002/cphc.201402662.

[14] D. Veldman, S. C. J. Meskers and R. A. J. Janssen, *Adv. Funct. Mater.*, 2009, **19**, 1939.

[15] M. C. Scharber, D. Mühlbacher, M. Koppe, P. Denk, C. Waldauf, A. J. Heeger and C. J. Brabec, *Adv. Mater.*, 2006, **18**, 789.

[16] (*a*) R. L. Danley, P. A. Caulfield and S. R. Aubuchon, *Am. Lab.*, 2008, **40**, 9; (*b*) T. Ghoos, N. Van den Brande, M. Defour, J. Brassinne, C.-A. Fustin, J.-F. Gohy, S. Hoeppener, U. S. Schubert, W. Vanormelingen, L. Lutsen, D. J. Vanderzande, B. Van Mele and W. Maes, *Eur. Polym. J.*, 2014, **53**, 206.

[17] L. J. A. Koster, V. D. Mihailetchi and P. W. M. Blom, *Appl. Phys. Lett.*, 2006, **88**, 052104.

[18] J.-C. Bolsée and J. Manca, *Synthetic Met.*, 2011, **161**, 789.

[19] R. C. Knighton, A. J. Hallett, B. M. Kariuki and S. J. A. Pope, *Tetrahedron Lett.*, 2010, **41**, 5419.

[20] (*a*) J. Bard and L. R. Faulkner, *Electrochemical methods: fundamentals and applications*, 2nd Ed., 2001, Wiley; (*b*) S. Trasatti, *Pure Appl. Chem.*, 1986, **58**, 95.

3.7. SUPPLEMENTARY INFORMATION

3.7.1. RHC spectra of mono- and disubstituted TzTz molecular chromophores

Figure S1: RHC profiles for a series of mono- and disubstituted TzTz molecular chromophores (heating and cooling at 500 K/min).

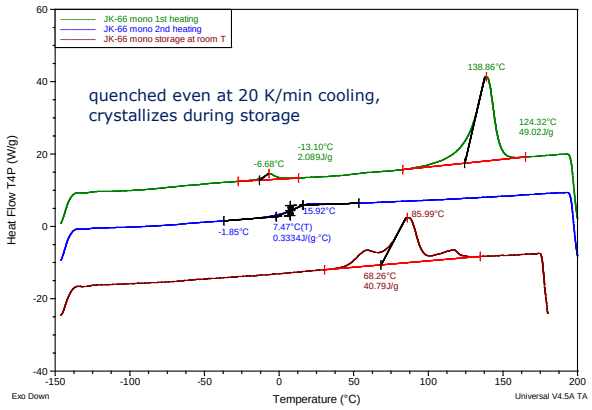

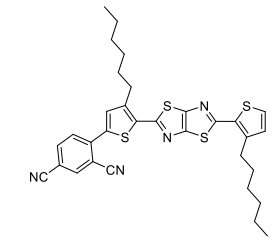

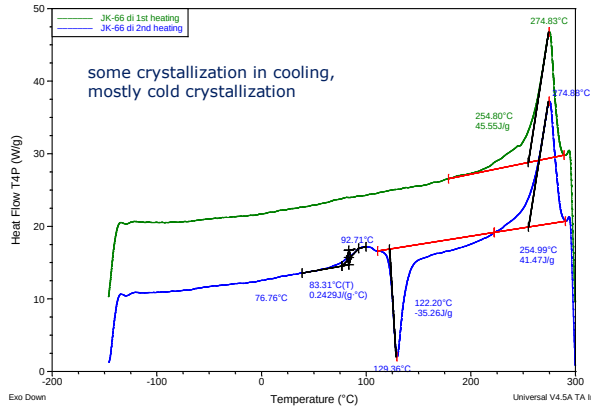

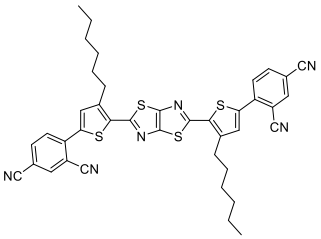

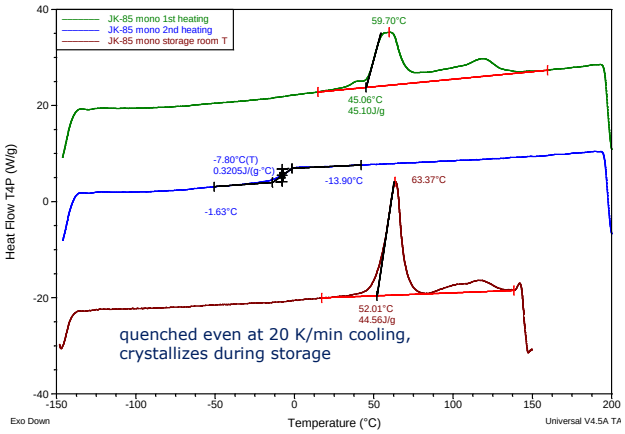
JK-85 mono 1st heating
JK-85 mono 2nd heating
JK-85 mono storage room T
59.70°C
45.06°C
45.10J/g
-7.80°C(T)
0.3205J/(g·°C)
-13.90°C
-1.63°C
63.37°C
52.01°C
44.56J/g
quenched even at 20 K/min cooling,
crystallizes during storage
Heat Flow T4P (W/g)
Temperature (°C)
Exo Down
Universal V4.5A TA

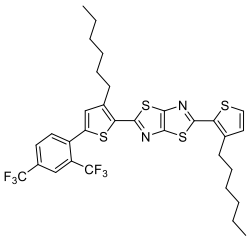

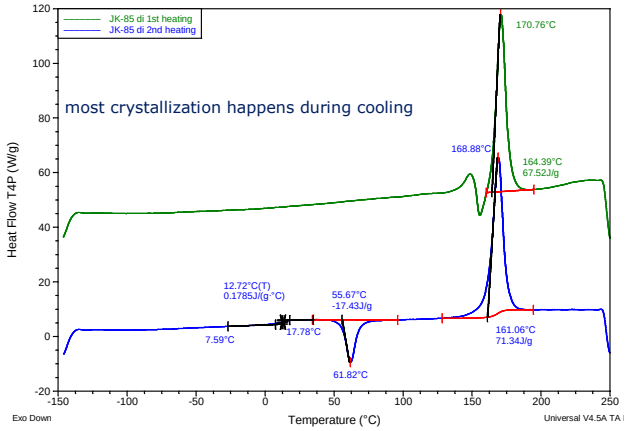
JK-85 di 1st heating
JK-85 di 2nd heating
170.76°C
most crystallization happens during cooling
168.88°C
164.39°C
67.52J/g
12.72°C(T)
0.1785J/(g·°C)
55.67°C
-17.43J/g
7.59°C
17.78°C
161.06°C
71.34J/g
61.82°C
Heat Flow T4P (W/g)
Temperature (°C)
Exo Down
Universal V4.5A TA

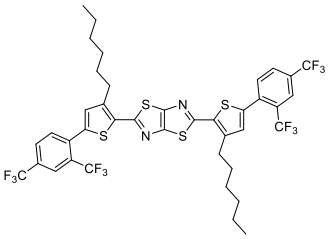

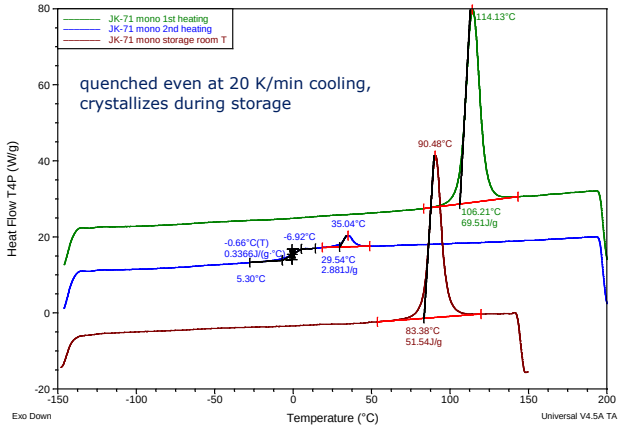
JK-71 mono 1st heating
JK-71 mono 2nd heating
JK-71 mono storage room T
114.13°C
quenched even at 20 K/min cooling,
crystallizes during storage
90.48°C
106.21°C
69.51J/g
35.04°C
-0.66°C(T)
0.3366J/(g·°C)
-6.92°C
29.54°C
2.881J/g
5.30°C
83.38°C
51.54J/g
Heat Flow T4P (W/g)
Temperature (°C)
Exo Down
Universal V4.5A TA

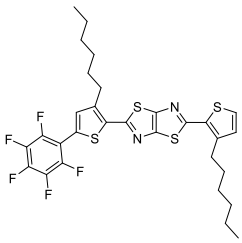

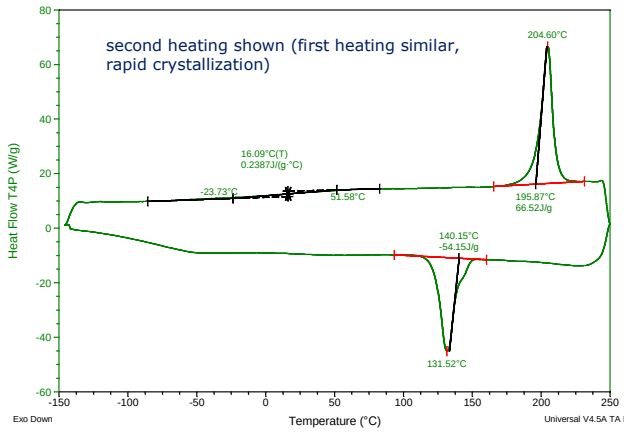
second heating shown (first heating similar, rapid crystallization)
204.60°C
16.09°C(T)
0.2387J/(g·°C)
-23.73°C
51.58°C
195.87°C
66.52J/g
140.15°C
-54.15J/g
131.52°C
Heat Flow T4P (W/g)
Temperature (°C)
Exo Down
Universal V4.5A TA

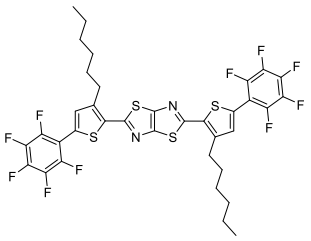

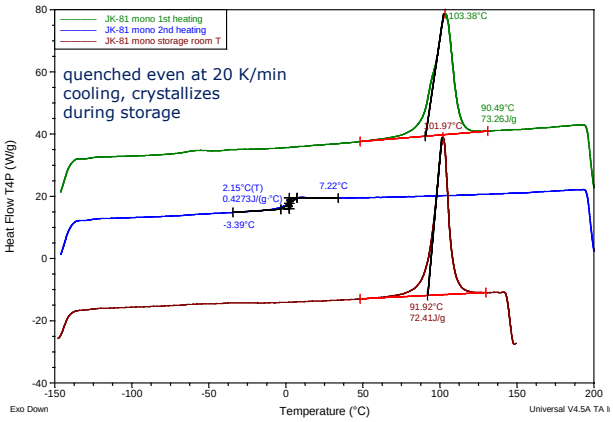
JK-81 mono 1st heating
JK-81 mono 2nd heating
JK-81 mono storage room T
quenched even at 20 K/min cooling, crystallizes during storage
103.38°C
90.49°C
73.26J/g
101.97°C
2.15°C(T)
0.4273J/(g·°C)
7.22°C
-3.39°C
91.92°C
72.41J/g
Heat Flow T4P (W/g)
Temperature (°C)
Exo Down
Universal V4.5A TA

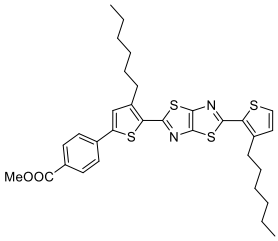
MeOOC

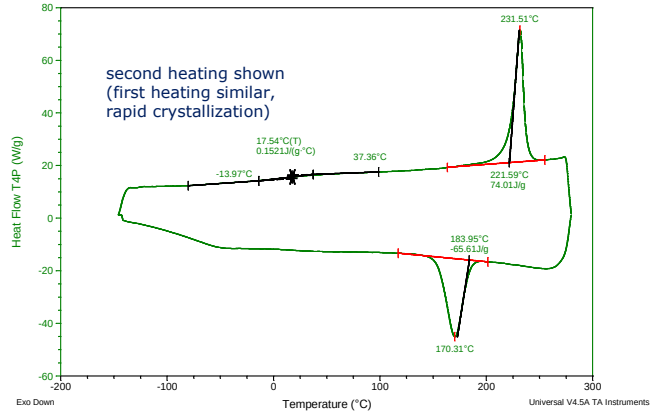
second heating shown (first heating similar, rapid crystallization)
231.51°C
17.54°C(T)
0.1521J/(g·°C)
37.36°C
-13.97°C
221.59°C
74.01J/g
183.95°C
-65.61J/g
170.31°C
Heat Flow T4P (W/g)
Temperature (°C)
Exo Down
Universal V4.5A TA Instruments

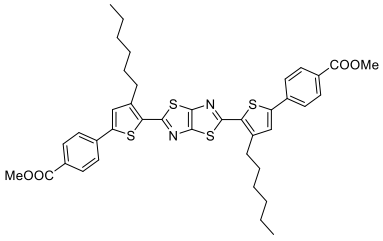
COOMe
MeOOC

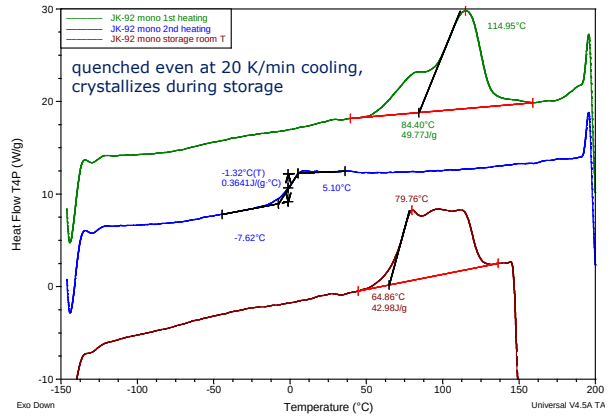
JK-92 mono 1st heating
JK-92 mono 2nd heating
JK-92 mono storage room T
quenched even at 20 K/min cooling,
crystallizes during storage
114.95°C
84.40°C
49.77J/g
-1.32°C(T)
0.3641J/(g·°C)
5.10°C
-7.62°C
79.76°C
64.86°C
42.98J/g
Heat Flow T4P (W/g)
Temperature (°C)
Exo Down
Universal V4.5A TA

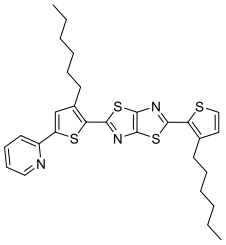

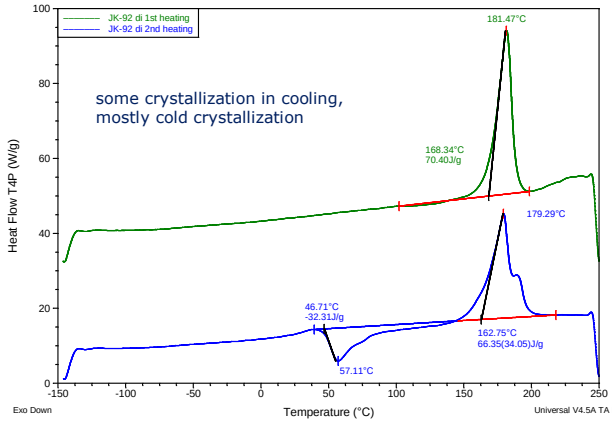
JK-92 di 1st heating
JK-92 di 2nd heating
some crystallization in cooling,
mostly cold crystallization
181.47°C
168.34°C
70.40J/g
179.29°C
46.71°C
-32.31J/g
162.75°C
66.35(34.05)J/g
57.11°C
Heat Flow T4P (W/g)
Temperature (°C)
Exo Down
Universal V4.5A TA

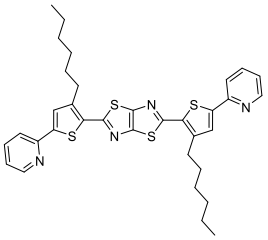

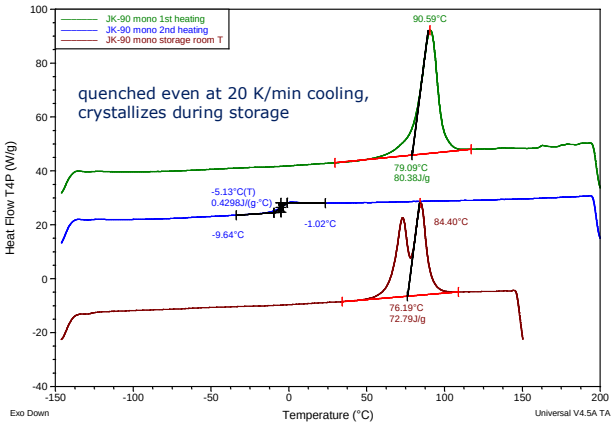
JK-90 mono 1st heating
JK-90 mono 2nd heating
JK-90 mono storage room T
quenched even at 20 K/min cooling,
crystallizes during storage
90.59°C
79.09°C
80.38J/g
-5.13°C(T)
0.4298J/(g·°C)
-1.02°C
-9.64°C
84.40°C
76.19°C
72.79J/g
Heat Flow T4P (W/g)
Temperature (°C)
Exo Down
Universal V4.5A TA

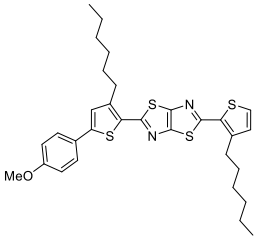
MeO

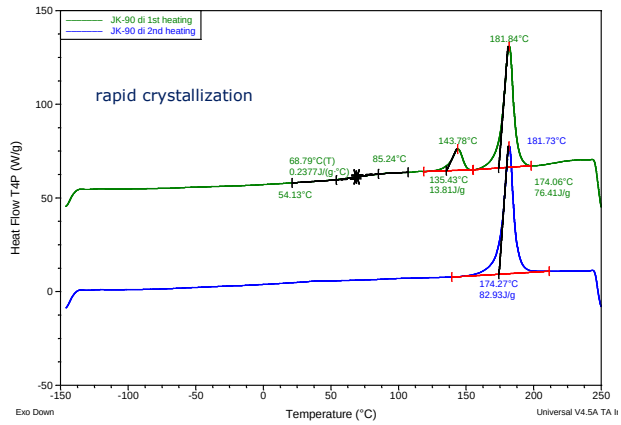
JK-90 di 1st heating
JK-90 di 2nd heating
rapid crystallization
181.84°C
143.78°C
181.73°C
68.79°C(T)
0.2377J/(g·°C)
85.24°C
54.13°C
135.43°C
13.81J/g
174.06°C
76.41J/g
174.27°C
82.93J/g
Heat Flow T4P (W/g)
Temperature (°C)
Exo Down
Universal V4.5A TA

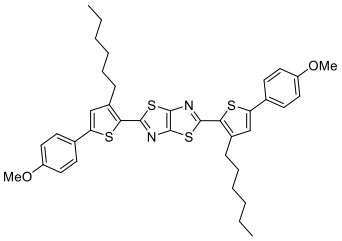
OMe
MeO

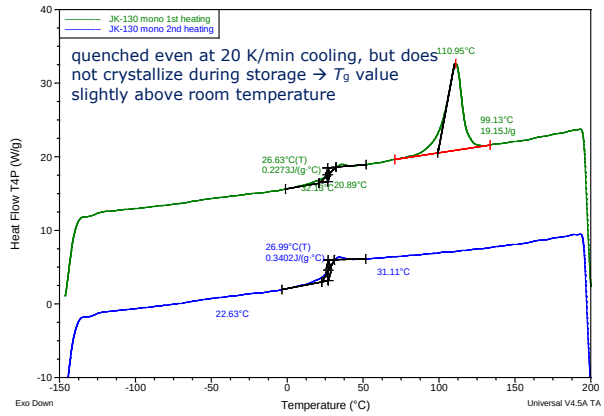
JK-130 mono 1st heating
JK-130 mono 2nd heating
quenched even at 20 K/min cooling, but does not crystallize during storage → T_g value slightly above room temperature
110.95°C
99.13°C
19.15J/g
26.63°C(T)
0.2273J/(g·°C)
20.89°C
26.99°C(T)
0.3402J/(g·°C)
31.11°C
22.63°C
Heat Flow T4P (W/g)
Temperature (°C)
Exo Down
Universal V4.5A TA

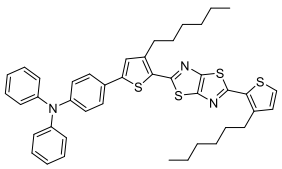

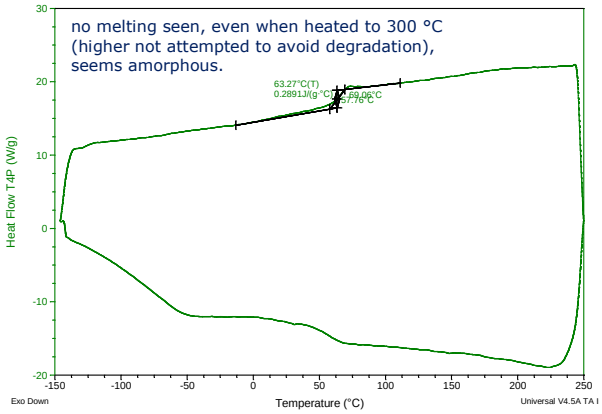
no melting seen, even when heated to 300 °C (higher not attempted to avoid degradation), seems amorphous.
63.27°C(T)
0.2891J/(g·°C)
Heat Flow T4P (W/g)
Temperature (°C)
Exo Down
Universal V4.5A TA

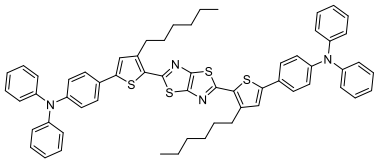

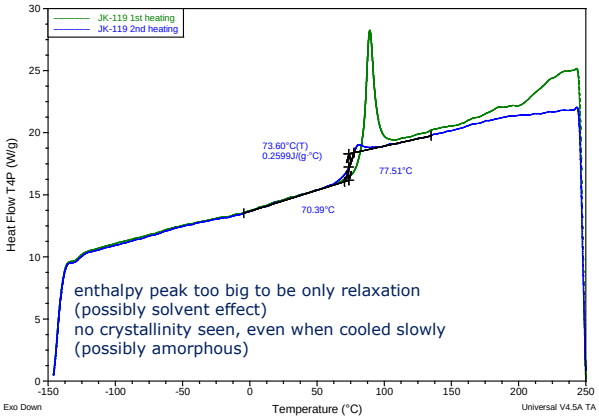
JK-119 1st heating
JK-119 2nd heating
73.60°C(T)
0.2599J/(g·°C)
77.51°C
70.39°C
enthalpy peak too big to be only relaxation
(possibly solvent effect)
no crystallinity seen, even when cooled slowly
(possibly amorphous)
Heat Flow T4P (W/g)
Temperature (°C)
Exo Down
Universal V4.5A TA

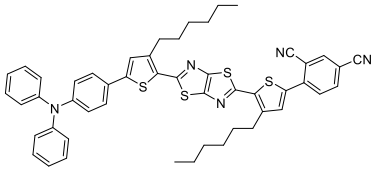
NC
CN
N
S
S
N
S
S
N

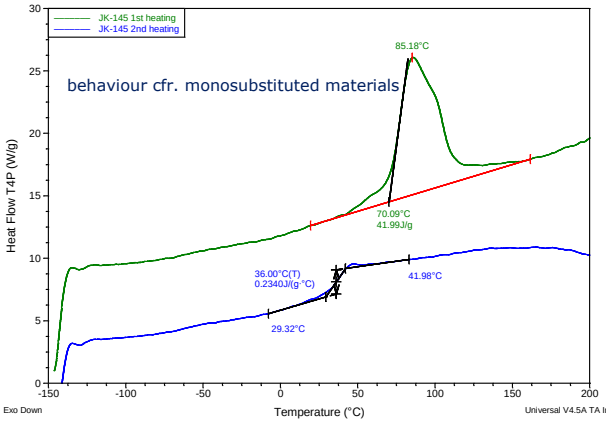
JK-145 1st heating
JK-145 2nd heating
85.18°C
behaviour cfr. monosubstituted materials
70.09°C
41.99J/g
36.00°C(T)
0.2340J/(g·°C)
41.98°C
29.32°C
Heat Flow T4P (W/g)
Temperature (°C)
Exo Down
Universal V4.5A TA

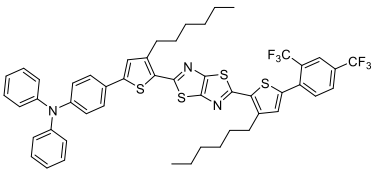
F3C
CF3
N
S
S
N
S
S
N

3.7.2. Overview of the solar cell optimization studies

Table S1: Optimization of the solar cell devices based on **TPA-T-TzTz-T-TPA (1)** and $PC_{71}BM$.

D:A ratio	Solvent[a]	V_{oc} (V)	J_{sc} (mA/cm^2)	FF	PCE[b] (%)
1:3	CF	0.90	5.50	0.32	1.59 (1.79)
1:3	CF + 10% oDCB	0.87	2.89	0.24	0.60 (0.69)
1:3	CF + 2% DIO	0.81	1.62	0.27	0.35 (0.39)
1:2	oDCB	0.93	5.16	0.42	1.98 (2.04)
1:3	oDCB	0.93	5.99	0.43	2.44 (2.63)
1:4	oDCB	0.90	6.43	0.39	2.21 (2.41)
1:3	oDCB + 1% CN	0.93	5.81	0.43	2.32 (2.65)
1:3	oDCB + 1% DIO	0.88	5.39	0.41	1.94 (2.06)
1:3	CB	0.94	5.30	0.41	2.04 (2.09)
1:3	CB + 1% CN	0.81	3.92	0.38	1.21 (1.33)
1:3	CB + 1% DIO	0.79	1.60	0.85	1.07 (1.27)

[a] CF = chloroform, oDCB = *ortho*-dichlorobenzene, DIO = 1,8-diiodooctane, CN = 1-chloronaphthalene, CB = chlorobenzene. [b] Average values over at least 4 devices. The best device performance is shown in brackets.

Table S2: Optimization of the solar cell devices based on P3HT and TzTz **6**.

D:A ratio	Solvent[a]	Total concentration (mg/mL)	V_{oc} (V)	J_{sc} (mA/cm²)	FF	PCE[b] (%)
1:1	CB	30	0.91	0.12	0.27	0.03 (0.03)
1:1	oDCB	34	0.90	0.20	0.29	0.05 (0.05)
1:2	CF	15	0.97	0.20	0.23	0.05 (0.05)
1:1	CF	20	0.95	0.09	0.27	0.02 (0.03)
1:1	CF	10	0.83	0.31	0.29	0.07 (0.08)
2:1	CF	15	0.77	0.39	0.31	0.09 (0.10)
2:1	CF	6	0.85	0.88	0.47	0.35 (0.41)
2:1	CF + 0.4% DIO	15	0.80	0.29	0.27	0.06 (0.06)
2:1	CF + 1% DIO	15	0.77	0.36	0.30	0.08 (0.09)

[a] CB = chlorobenzene, oDCB = *ortho*-dichlorobenzene, CF = chloroform, DIO = 1,8-diiodooctane, [b] Average values over at least 4 devices. The best device performance is shown in brackets.

3.7.3. FET mobility measurements

Figure S2: FET output (left column) and transfer characteristics (right column) of devices made from small molecules TzTz's **1**, **2**, and **3** (a, b, and c, respectively). The red lines represent the fits used to extract the mobility in the saturation regime, at V_{DS} = -40 V.

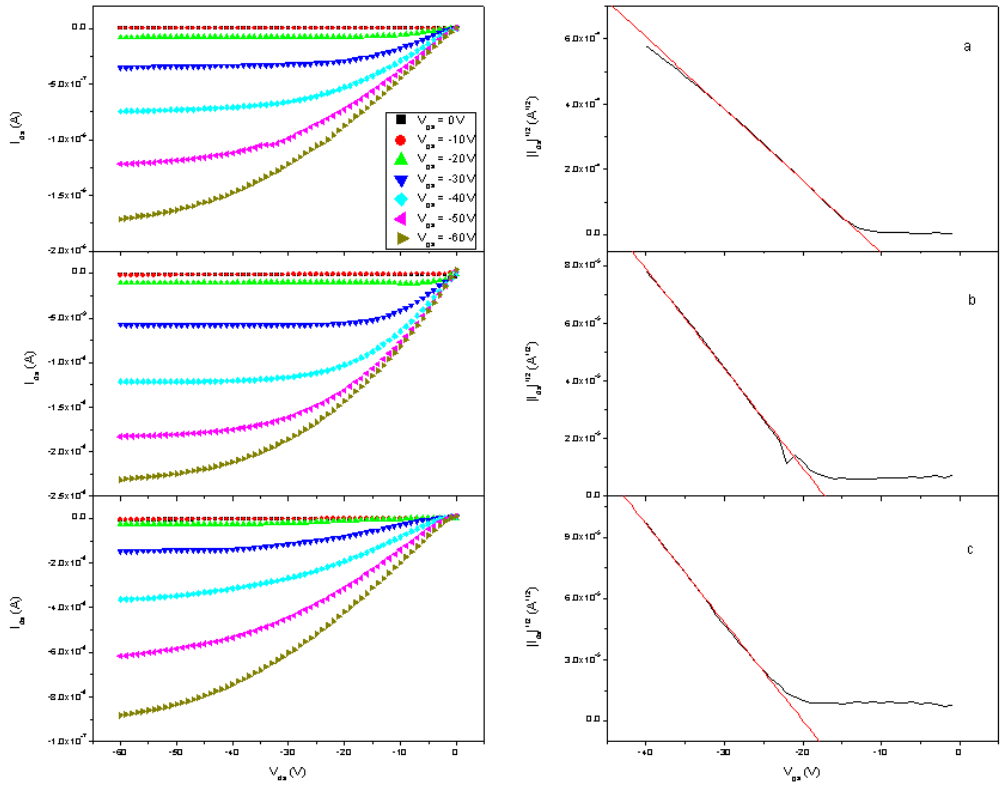

3.7.4. UV-Vis absorption spectra of TzTz's 1–6 in thin film

Figure S3: UV-Vis absorption spectra (normalized) of TzTz small molecules **1–6** in thin film (drop-casted from dichoromethane).

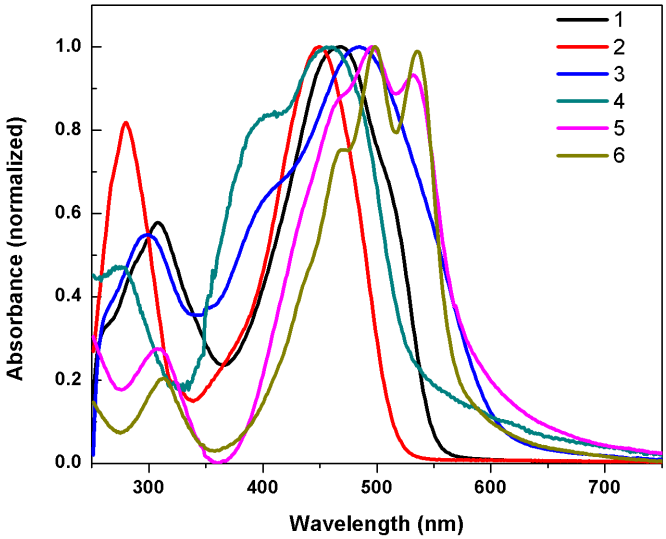

3.7.5. $^{1}H\backslash^{13}C$ NMR spectra of TzTz 6

Figure S4: ^{1}H NMR spectrum ($CDCl_3$, 400 MHz) of TzTz **6**.

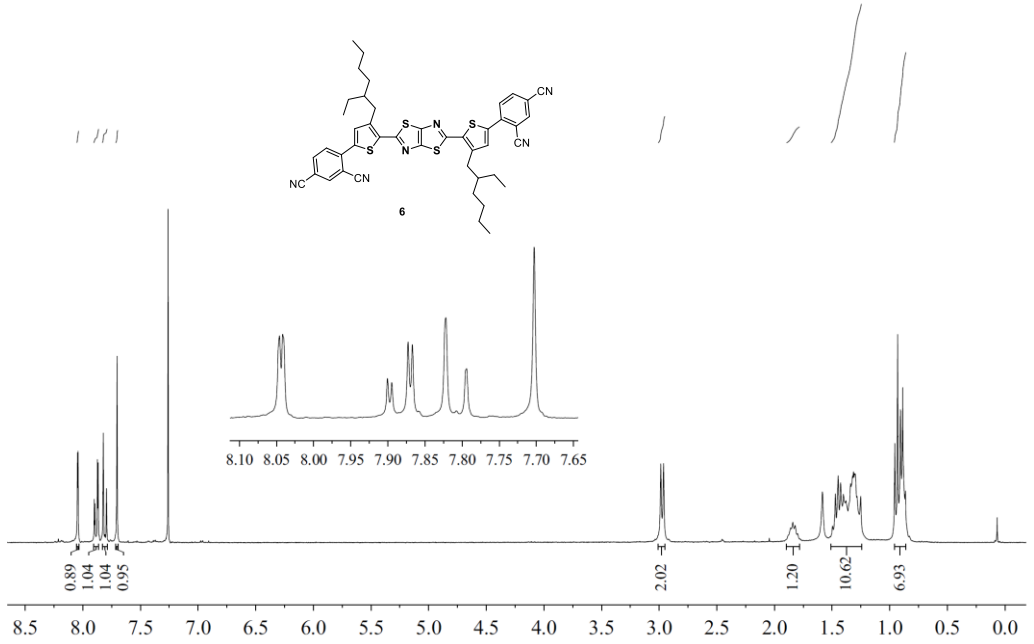

Figure S5: ^{13}C NMR spectrum ($CDCl_3$, 75 MHz) of TzTz **6**.

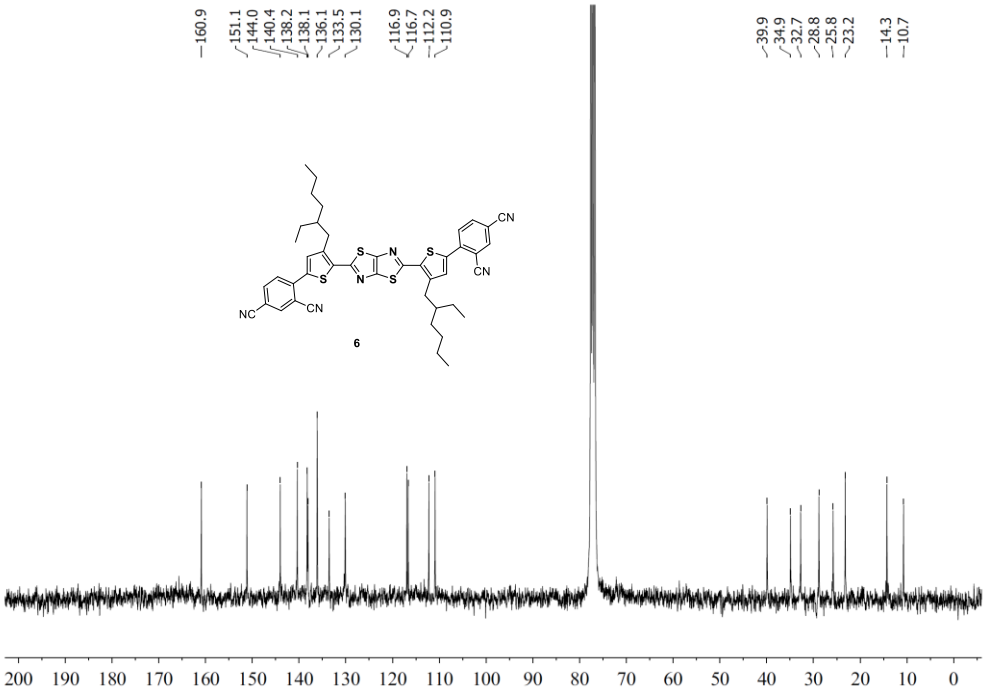

3.7.6. Chemical structure of TzTz 7

Figure S6: Chemical structure of the previously investigated bis(4-cyanophenyl)-substituted 2,5-dithienyl-TzTz (electron acceptor compound).

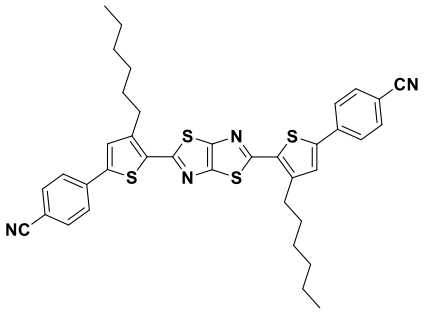

Chapter 4

A direct arylation approach toward efficient small molecule organic solar cells

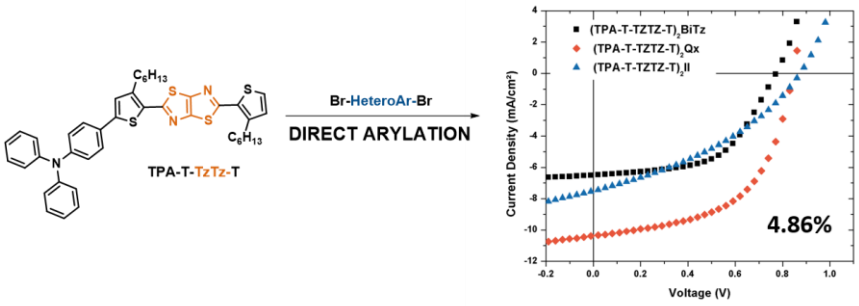

Julija Kudrjasova, Jurgen Kesters, Pieter Verstappen, Jeroen Brebels, Tim Vangerven, Jeroen Drijkoningen, Jean Manca, Laurence Lutsen, Dirk Vanderzande, Wouter Maes, *to be submitted*.

(Article contribution: all synthesis and chemical analysis, main author)

ABSTRACT

A small series of three extended thiazolo[5,4-*d*]thiazole (TzTz) based molecular chromophores is synthesized via a two-fold C-H arylation protocol. The D'A'DADA'D'-type structures differ in the central acceptor moiety – bithiazole (BiTz), quinoxaline (Qx) or isoindigo (II) – and are specifically designed to be applied as small molecule electron donor components in bulk heterojunction organic solar cells. Best results are achieved for the TPA-T-TzTz-Qx-T-TzTz-T-TPA material, providing a power conversion efficiency of 4.86% when blended with $PC_{71}BM$ in the photoactive layer, a record performance for both TzTz-based small molecules and molecular chromophores prepared via a direct arylation approach. The lack of regioselectivity of the applied C-H arylation protocol, limiting product yields, is illustrated by side product analysis via MALDI.

4.1. INTRODUCTION

Solution-processed bulk heterojunction organic solar cells (BHJ OSC's) containing light-harvesting and charge transporting conjugated polymers or analogous small molecule chromophores have attracted large attention from both academia and industry over the last few years because of their appealing aesthetical (color, semitransparency), mechanical (flexibility, light-weight), conditional (low light, temperature) and cost features (large area production via simple printing processes).[1] Very recently, small molecule organic solar cells (SMOSC's) have surpassed the 10% power conversion efficiency (PCE) treshold value, becoming a viable alternative to their polymeric counterparts.[2] In comparison to semiconducting polymers, 'small' molecules possess some specific desirable features such as less batch-to-batch variability due to their well-defined structure, more reproducible synthetic protocols, easier purification, and a more straightforward understanding of molecular structure-performance relationships.[3] Additionally, small molecules more readily allow tuning of the optoelectronic properties through straightforward synthesis procedures and they can exhibit fairly high charge carrier mobilities.[4] The current generation polymer and small molecule electron donor materials usually apply the alternating donor-acceptor (D-A) (or push-pull) strategy, allowing for a lowering of the HOMO-LUMO gap and a better overlap with the solar spectrum through the induced intramolecular charge transfer. More advanced molecular scaffolds with D-A-D, A-D-A, D-A-A, and even more extended D-A architectures are acquiring increased attention to optimize photon collection and charge carrier transport.[5] The more efficient organic semiconductors currently reported for SMOSC's contain, among others, electron deficient (A) moieties such as benzothiadiazole,[4a,6] squaraine,[7] or

diketopyrrolopyrrole.[7a,8] Alternatively, thiazolo[5,4-*d*]thiazole (TzTz) has also emerged as a powerful electron withdrawing building block showing particular advantages such as easy synthetic access, a planar and rigid structure with strong π–π stacking tendency, promoting mobility, and oxidative stability.[9] Due to these favorable features, TzTz based polymer[10] and small molecule[11] materials have successfully been applied in BHJ organic photovoltaics. In 2012, Lee *et al.* reported on a D-A-D-A-D conjugated small molecule consisting of naphtho[1,2-*b*:5,6-*b*']dithiophene as a rigidly fused π-conjugated central donor unit and a thienyl-TzTz flanked by triphenylamine (TPA) as the terminal conjugated segment, providing SMOSC's with a PCE of 1.4%. The somewhat lower than expected performance could be attributed to the medium sized HOMO-LUMO gap (2.0 eV) and a relatively low hole mobility, possibly due to the reduced planarity of the small molecule induced by the presence of the 3-decylthiophene π-bridging unit.[11c] More encouraging results were obtained for the combination of 2,5-dithienyl-TzTz's (T-TzTz-T) with TPA terminal units in a simple D-A-D built-up, granting PCE's up to 3.7%.[11d] Through the incorporation of two additional thiophene units, thereby extending the conjugation length, Zhan *et al.* were able to attain a record 'TzTz' SMOSC efficiency of 4.0%.[11d]

Conventionally, small molecule semiconductors are synthesized employing standard transition metal catalyzed cross-coupling reactions for (het)aryl-(het)aryl connections, such as Suzuki-Miyaura and Stille reactions, requiring the preparation of organoboron or organotin precursors. Direct (hetero)arylation of activated C-H moieties has recently emerged as a viable alternative, with particular advantages in terms of (atom) efficiency, sustainability and functional group compatibility, and it has been applied for SMOSC materials with reasonable success.[12] In previous work, we have demonstrated a facile direct arylation

strategy for the synthesis of a series of diaryl-substituted T-TzTz-T small molecule semiconductors with varying electron affinities, particularly emphasizing on monosubstitution toward asymmetric push-pull structures.[13] Unfortunately, this first generation C-H arylation TzTz chromophores showed a relatively narrow absorption window and SMOSC efficiencies remained below 3%. Prompted by these initial results, more complex structures were pursued, but still avoiding traditional cross-coupling protocols. In the present contribution, we report on the combination of the asymmetric TPA-T-TzTz-T precursor with three different brominated central acceptor derivatives – a bithiazole (BiTz), diphenylquinoxaline (Qx) and isoindigo (II) (Scheme 1), varying the electron affinity, solubility and stacking features – by direct arylation and their incorporation in SMOSC's, providing (best) PCE's up to 4.86%.

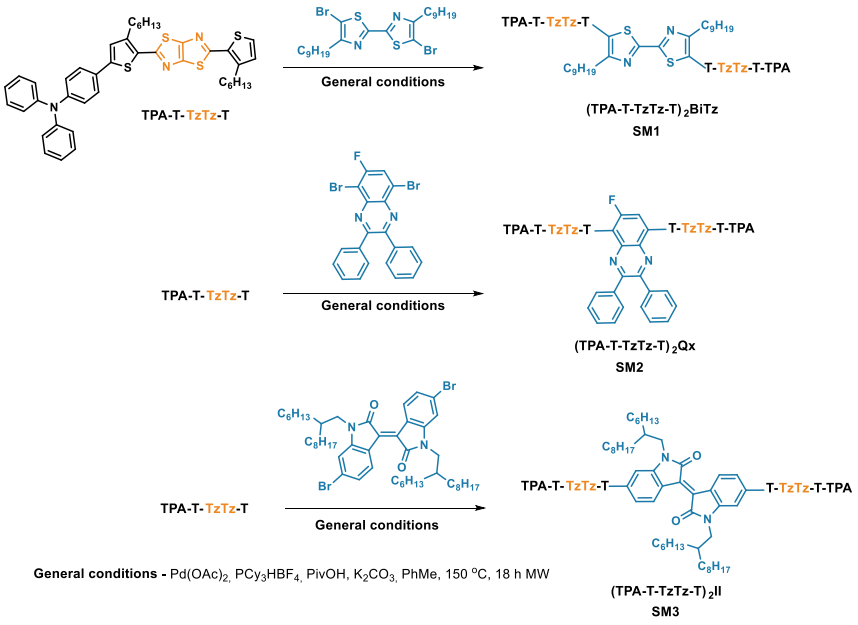

Scheme 1. Combination of the TPA-T-TzTz-T precursor with three different acceptor cores via direct heteroarylation.

4.2. RESULTS AND DISCUSSION

4.2.1. Synthesis and characterization

The three novel small molecules were synthesized according to a general direct arylation procedure, as outlined in Scheme 1. Similar conditions as previously optimized to construct the monoarylated TPA-T-TzTz-T starting material were employed.[13] The central units consisting of bithiazole,[14] isoindigo,[15] and quinoxaline[16] derivatives were prepared according to literature procedures. The final C-H heteroarylation reaction produced the target small molecules **(TPA-T-TzTz-T)$_2$BiTz** (**SM1**), **(TPA-T-TzTz-T)$_2$Qx** (**SM2**) and **(TPA-T-TzTz-T)$_2$II** (**SM3**) in modest yields (~30%). These reduced reaction yields can be mainly attributed to the formation of (multiple) side products, for example induced by the reactive C-H bond on the 3-position of the thiophene units. By analyzing the filtrate after precipitation of **SM2** by MALDI-TOF MS, two major side products could be identified, corresponding to **SM2** with extra TPA-T-TzTz-T or TPA-T-TzTz-T-Qx units (Figure S3), clearly illustrating the regioselectivity issues that can result from direct arylation protocols.

Except for **SM2**, all small molecules showed good solubility in common organic solvents (such as chloroform). Since material purity is of major importance for the fabrication of optoelectronic devices, all small molecules were carefully purified by standard column chromatography (on silica). **SM1** and **SM3** were additionally purified by recycling preparative size exclusion chromatography (prep-SEC). Due to its limited solubility in chloroform, **SM2** was instead precipitated twice in ethyl acetate.

UV-Vis absorption spectra in solution and thin film for all three compounds are shown in Figure 1 and HOMO-LUMO gap and λ_{max} data are gathered Table 1. In

solution, **SM1** shows a maximum absorption at 492 nm. A slightly red shifted absorption maximum (~15 nm) can be observed when moving from solution to the solid state and a shoulder appears at 581 nm, suggesting intermolecular interactions and aggregation in the film. Upon altering the central unit to the stronger Qx acceptor in **SM2**, the absorption spectra are considerably broader with two distinct maxima located at 437 and 527 nm for the solution spectrum. **SM3** displayed the broadest absorption spectra, covering almost the entire spectrum from 350 up to 750 nm with maxima positioned at 449 and 598 nm (in solution), and the smallest optical HOMO-LUMO gap (1.74 eV in film). The HOMO and LUMO frontier energy levels of the small molecules were estimated via cyclic voltammetry (CV) from the onset of the oxidation and reduction peaks, respectively (Table 1). The HOMO energy levels are nearly invariant (within 0.05 eV). Since the LUMO's are generally mostly localized on the acceptor parts, a decreasing trend is expected when increasing the electron withdrawing nature of the acceptor building block, which is indeed illustrated in the present series. The narrowest electrochemical HOMO-LUMO gap (1.45 eV) was obtained for the small molecule bearing the strongest acceptor unit (II), in accordance to the optical data. The low LUMO value for **SM3** actually allows it to be used as an electron acceptor molecule as well, replacing the commonly used methanofullerenes.[17]

Table 1. Optical and electrochemical properties of the small molecule series.

SM	λ_{max}[a] (nm) (log ε) solution	λ_{max} (nm) film	E_g^{OPb} (eV)	E^{ox}_{onset} (V)	HOMO (eV)	E^{red}_{onset} (V)	LUMO (eV)	E_g^{ECc} (eV)
SM1	492 (4.704)	507	2.17	0.47	-5.33	-1.59	-3.26	2.07
SM2	437 (4.78)/527 (4.79)	450/564	1.97	0.43	-5.33	-1.54	-3.36	1.97
SM3	449 (5.02)/598 (4.99)	452/578	1.74	0.52	-5.38	-0.93	-3.93	1.45

[a] In chloroform. [b] Optical HOMO-LUMO gap, determined from the onset of the solid-state UV-Vis spectrum. [c] Electrochemical HOMO-LUMO gap.

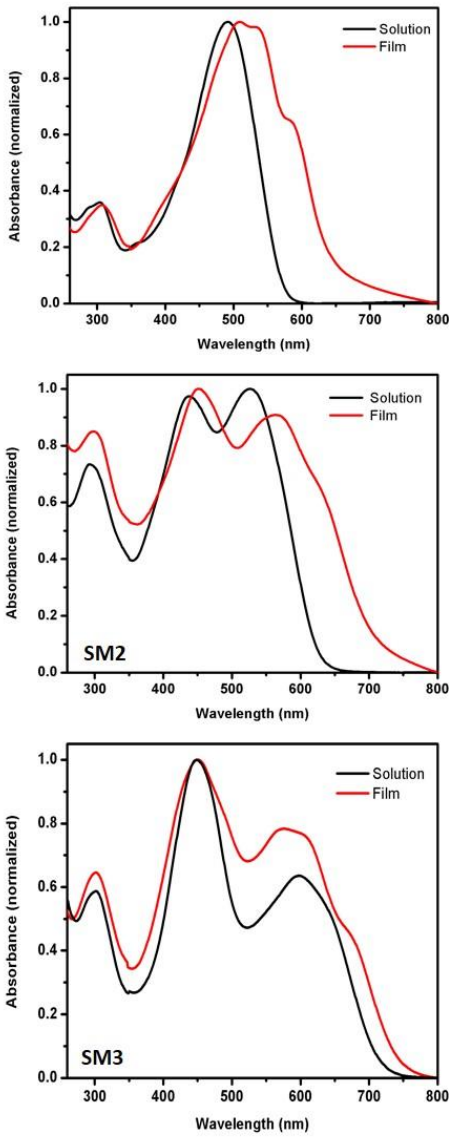

Figure 1. Normalized UV-Vis absorption spectra in solution ($CHCl_3$) and thin film for **SM1–3**.

The thermal properties of the three small molecules were investigated by rapid heat-cool calorimetry (RHC) measurements (Figure 2, Table 2). RHC was chosen above regular differential scanning calorimetry (DSC) because of its increased

sensitivity to thermal transitions as a result of the fast scanning rates and the low sample amounts required.[18] The obtained results clearly demonstrate a strong impact on the glass transition temperature (T_g), the melting temperature (T_m) and the melting enthalpy (ΔH_m) upon alteration the central acceptor unit. **SM1** displays two melting temperatures (172/244.5 °C), as well as the highest ΔH_m (30.9 J g^{-1}) in the series, indicating a high crystalline character. **SM2** appears to be significantly less crystalline (ΔH_m = 4.1 J g^{-1}, T_m = 214.1 °C) and a pronounced T_g (112.6 °C) becomes visible. Finally, **SM3** falls somewhat in between, with a T_m of 234.3 °C and a ΔH_m of 21.5 J g^{-1}.

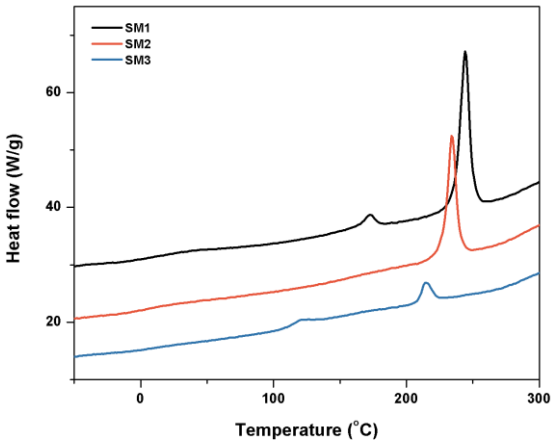

Figure 2. RHC profiles of **SM1**−**3** (second heating curves, curves shifted vertically for clarity).

4.2.2. Photovoltaic properties

Thin film BHJ OSC's with the traditional architecture glass/ITO/PEDOT:PSS/**SM1**−**3**:$PC_{71}BM$/Ca/Al were fabricated and tested under AM1.5G solar illumination to evaluate the photovoltaic features of the synthesized small molecules. Optimal devices were procured from chloroform (CF) based

blends in combination with $PC_{71}BM$ as the electron acceptor in a 1:1 (wt/wt%) ratio (optimization tests in Table S1−3). Solar cells produced with **SM2** demonstrated highest photovoltaic performance, yielding an open-circuit voltage (V_{oc}) of 0.86 V in combination with a short-circuit current density (J_{sc}) of 9.78 mA cm^{-2} and a fill factor (FF) of 0.50, with an average PCE of 4.11% (best device 4.86%) (Table 2, Figure 3). The performance of **SM1** and **SM3** was found to be somewhat worse, with average PCE's of 1.77 and 2.11%, respectively, when using chloroform as a processing solvent. Upon addition of 1-chloronaphthalene (CN) as a processing additive, the average PCE of the **SM1** device could be enhanced up to 2.50%, mainly attributable to an enhancement in J_{sc} and FF (Table 2, Figure 3). Unfortunately, a similar approach did not result in a further performance enhancements for **SM2** and **SM3**.

Table 2. Photovoltaic output parameters for the (optimized) **SM1**−**3**:$PC_{71}BM$ (1:1) SMOSC's.[a]

Small molecule	Processing solvent[b]	V_{OC} (V)	J_{SC} (mA cm^{-2})	FF	Average η (%)[c]	Best η (%)
SM1	CF	0.75	5.80	0.41	1.77	1.96
SM1	CF + 1% CN	0.76	6.14	0.54	2.50	2.78
SM2	CF	0.83	9.78	0.50	4.11	4.86
SM2	CF + 1% CN	0.86	7.81	0.40	2.68	2.84
SM3	CF	0.86	7.04	0.35	2.11	2.42
SM3	CF + 1% CN	0.85	6.41	0.32	1.73	1.83

[a] Device structure glass/ITO/PEDOT:PSS/**SM1−3**:$PC_{71}BM$/Ca/Al. The active layer thicknesses for the optimized devices were ~120−150 nm. [b] Total concentration of 4 mg mL^{-1} in chloroform (CF). [c] Averages taken over 4−8 devices.

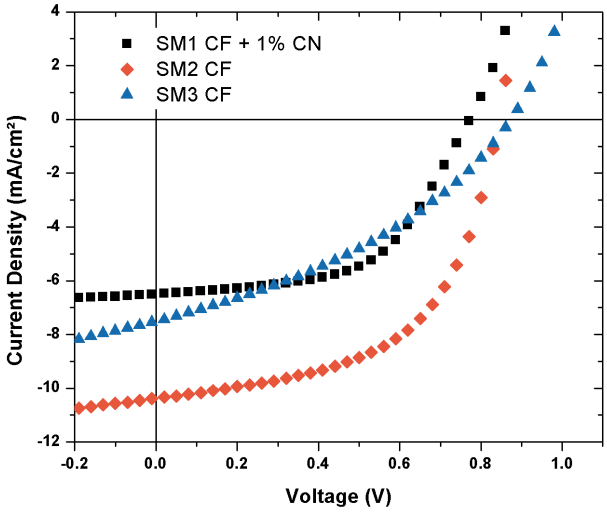

Figure 3. *J-V* curves under illumination for the best solar cell devices based on **SM1**−**3**.

The external quantum efficiency (EQE) spectra reflect the difference in performance for the three small molecule:$PC_{71}BM$ OSC's (Figure 4) and follow the trend observed in the absorption spectra. The **SM2**:$PC_{71}BM$ device shows a maximum EQE of ~65%. The current densities extracted from the EQE measurements performed on the best devices correlate well with the measured J_{sc} values, in accordance with standard measurement deviations (J_{EQE} vs J_{sc}: 7.08 vs 7.19, 10.16 vs 10.39 and 5.95 vs 5.60 mA cm^{-2} for **SM1** in CF+1% CN and **SM2-3** in CF, respectively).

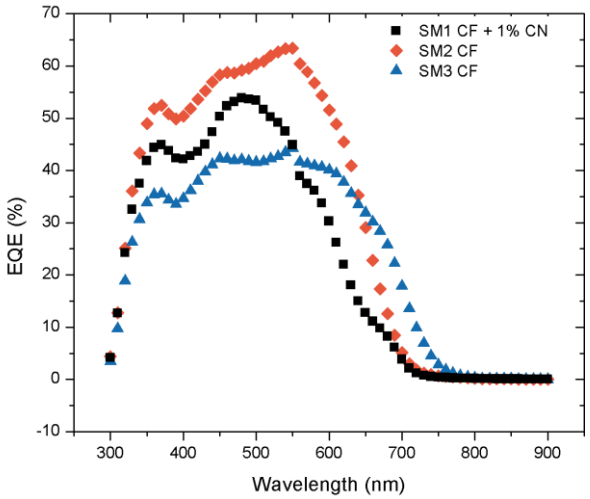

Figure 4. EQE spectra for the top performing solar cell devices comprising **SM1**–**3**.

Atomic force microscopy (AFM) measurements were performed to investigate the film topographies and to portray the influence of the processing additive. As illustrated in Figure 5, upon addition of CN to the **SM1**:$PC_{71}BM$ blend solution, a significant alteration of the topography/morphology becomes apparent, with clear formation of specific needle-shaped structures, apparently responsible for an increase in J_{sc} and FF. The addition of the processing additive to the **SM2**-based SMOSC resulted in a noticeable decrease in performance (the average PCE drops from 4.11 to 2.68%), possibly induced by a too finely intermixed blend morphology. For **SM3**, CN did not have a large impact on either the layer topography or solar cell performance.

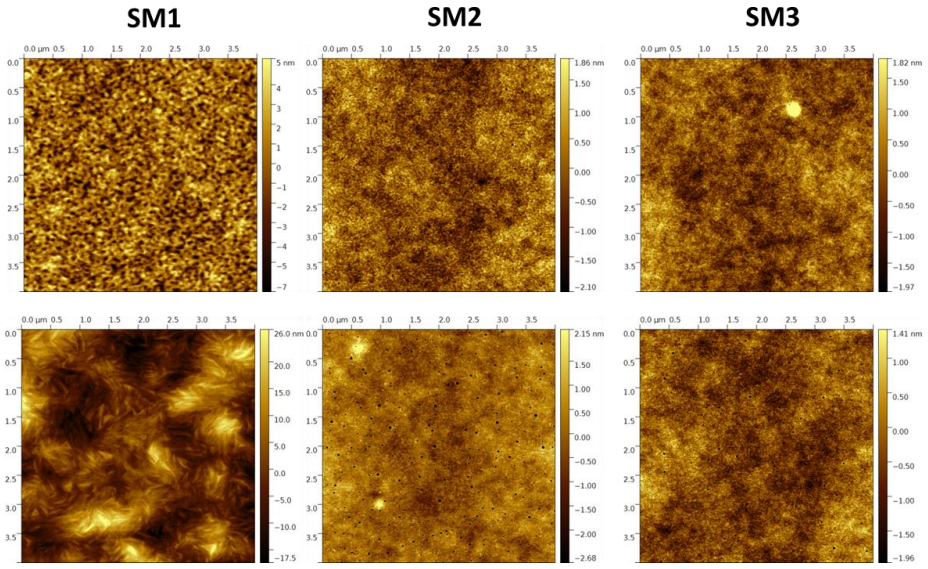

Figure 5. AFM (topography) images (4 x 4 μm) of the photoactive layers of the **SM1**−**3**:$PC_{71}BM$ solar cells prepared without (upper row) and with (bottom row) CN (1%) as a processing additive.

In a final stage, photo-induced charge extraction by linearly increasing voltage (photo-CELIV) measurements were performed on the SMOSC's to investigate the charge transport features. Unfortunately, even with layer thicknesses above 300 nm, no interpretable signal could be obtained for the **SM1** device, and only preliminary data could be acquired for the **SM2** and **SM3** devices. The charge carrier mobility was found to be ~2 x 10^{-4} and ~6 x 10^{-5} cm^2 V^{-1} s^{-1} (Figure S5) for the **SM2** and **SM3** devices, respectively, correlating with the observed J_{sc} trend. The low charge carrier mobility might explain the modest performance for the SMOSC based on **SM3**, even though the absorption features are most favorable.

4.3. CONCLUSIONS

In summary, three π-expanded D'A'DADA'D'-type molecular chromophores were synthesized via a two-fold C-H arylation approach to be applied as electron donor compounds for organic photovoltaics. The physicochemical and optoelectronic material characteristics were investigated and a power conversion efficiency of 4.86% was achieved for the TPA-T-TzTz-T-Qx-T-TzTz-T-TPA small molecule, a record performance for molecular chromophores prepared via direct arylation. Despite the success of the approach in affording small molecule donor materials for efficient OPV devices, we should not ignore for the current limitations of the C-H heteroarylation protocols. If one desires to employ sustainable direct arylations procedures toward advanced organic semiconductors, further efforts should certainly be devoted to optimization of the C-H regioselectivity to increase reaction yields and simplify compound purification.

4.4. ACKNOWLEDGEMENTS

This work was supported by the project ORGANEXT (EMR INT4-1.2-2009-04/054), selected in the frame of the operational program INTERREG IV-A Euregio Maas-Rijn, and the IAP 7/05 project FS2 (Functional Supramolecular Systems), granted by the Science Policy Office of the Belgian Federal Government (BELSPO). We are also grateful for financial support by the Research Programme of the Research Foundation – Flanders (FWO) (projects G.0415.14N, G.0B67.15N and M.ERA-NET project RADESOL). P. Verstappen, J. Brebels and T. Vangerven acknowledge the Agency for Innovation by Science and Technology in Flanders (IWT) for their PhD grants. Hasselt University, IMO-IMOMEC and TUEindhoven are partners within the

Solliance network, the strategic alliance for research and development in the field of thin-film PV energy in the Eindhoven-Leuven-Aachen region.

4.5. REFERENCES

(1) Recent reviews on organic solar cells: (*a*) Jørgensen, M.; Norrman, K.; Gevorgyan, S. A.; Tromholt, T.; Andreasen, B.; Krebs, F. C. *Adv. Mater.*, **2012**, *24*, 580; (*b*) Zhou, H.; Yang, L.; You, W. *Macromolecules*, **2012**, *45*, 607; (*c*) Li, Y. *Acc. Chem. Res.*, **2012**, *45*, 723; (*d*) Su, Y.; Lan, S.; Wei, K. *Mater. Today*, **2012**, *15*, 554; (*e*) Søndergaard, R.; Hösel, M.; Angmo, D.; Larsen-Olsen T. T.; Krebs, F. C. *Mater. Today*, **2012**, *15*, 36; (*f*) Janssen, R. A. J.; Nelson, J. *Adv. Mater.*, **2013**, *25*, 1847; (*g*) Lizin, S.; Van Passel, S.; De Schepper, E.; Maes, W.; Lutsen, L.; Manca J.; Vanderzande, D. *Energy Environ. Sci.*, **2013**, *6*, 3136; (*h*) Xu, T.; Yu, L. *Mater. Today*, **2014**, *17*, 11.

(2) Kan, B.; Li, M.; Zhang, Q.; Liu, F.; Wan, X.; Wang, Y.; Ni, W.; Long, G.; Yang, X.; Feng, H.; Zuo, Y.; Zhang, M.; Huang, F.; Cao, Y.; Russell, T. P.; Chen, Y. *J. Am. Chem. Soc.*, **2015**, *137*, 3886.

(3) (*a*) Mishra, A.; Bäuerle, P. *Angew. Chem. Int. Ed.*, **2012**, *51*, 2020; (*b*) Y. Lin, Y. Li, X. Zhan, *Chem. Soc. Rev.* **2012**, *41*, 4245; (*c*) Chen, Y.; Wan, X.; Long, G. *Acc. Chem. Res.*, **2013**, *46*, 2645; (*d*) Roncali, J.; Leriche, P., Blanchard, P. *Adv. Mater.*, **2014**, *26*, 3821.

(4) (*a*) Walker, B.; Kim, C.; Nguyen, T.-Q. *Chem. Mater.*, **2011**, *23*, 470; (*b*) Uy, R. L.; Price, S. C.; You, W. *Macromol. Rapid Commun.*, **2012**, *33*, 1162; (*c*) Jeffries-EL, M.; Kobilka, B. M.; Hale, B. J. *Macromolecules*, **2014**, *47*, 7253; (*d*) Coughlin, J. E.; Henson, Z. B.; Welch, G. C.; Bazan, G. C. *Acc. Chem. Res.*, **2014**, *47*, 257.

(5) (*a*) Sun, Y.; Welch, G. C.; Leong, W. L.; Takacs, C. J.; Bazan, G. C.; Heeger, A. J. *Nat. Mater.*, **2011**, *11*, 44; (*b*) Zhou, J.; Wan, X.; Liu, Y.; Zuo, Y.; Li, Z.; He, G.; Long, G.; Ni, W.; Li, W.; Su, X.; Chen, Y. *J. Am. Chem. Soc*., **2012**, *134*, 16345; (*c*) Zhou, J.; Zuo, Y.; Wan, X.; Long, G.; Zhang, Q.; Ni, W.; Liu, W.; Li, Z.; He, G.; Li, C.; Kan, B.; Li, M.; Chen, Y. *J. Am. Chem. Soc*., **2013**, *135*, 8484; (*d*) Chen, Y.; Wan, X.; Long, G. *Acc. Chem. Res.*, **2013**, *46*, 2645.

(6) (*a*) Roncali, J. *Acc. Chem. Res.*, **2009,** *42*, 1719; (*b*) Hains, A.; Liang, Z.; Woodhouse, M.; Gregg, B. *Chem. Rev.*, **2010** *110*, 6689; (c) Li, Y.; Guo, Q.; Li, Z.; Pei, J.; Tian, W. *Energy Environ. Sci*., **2010**, *3,* 1427.

(7) (*a*) Walker, B.; Tamayo, A.; Dang, X.; Zalar, P.; Seo, J.; Garcia, A.; Tantiwiwat, M.; Nguyen, T.-Q. *Adv. Funct. Mater.*, **2009**, *19*, 3063; (*b*) Shang, H.; Fan, H.; Liu, Y.; Hu, W.; Li, Y.; Zhan, X. *Adv. Mater.*, **2011**, *23*, 1554.

(8) (*a*) Tamayo, A. B.; Dang, X. D.; Walker, B.; Seo, J.; Kent, T.; Nguyen, T. Q. *Appl. Phys. Lett.*, **2009**, *94*, 103301; (*b*) Pan, J.; Zuo, L.; Hu, X.; Fu, W.; Chen, M.; Fu, L.; Gu, X.; Shi, H.; Shi, M.; Li, H.; Chen, H.-Z. *ACS Appl. Mater. Interfaces*, **2013**, 5, 972; (*c*) Liu, J.; Sun, Y.; Moonsin, P.; Kuik, M.; Proctor, C. M.; Lin, J.; Hsu, B. B.; Promarak, V.; Heeger, A. J.; Nguyen, T. Q. *Adv. Mater.*, **2013**, *25*, 5898; (*d*) Gevaerts, V. S.; Herzig, E. M.; Kirkus, M.; Hendriks, K. H.; Wienk, M. M.; Perlich, J.; Müller-Buschbaum, P.; Janssen, R. A. J. *Chem. Mater.* **2014**, *26*, 916; (*e*) Huang, J.; Wang, X.; Zhang, X.; Niu, Z.; Lu, Z.; Jiang, B.; Sun, Y.; Zhan, C.; Yao, J. *ACS Appl. Mater. Interfaces*, **2014**, *6*, 3853.

(9) For a recent review on TzTz synthesis and applications: Bevk, D.; Lutsen, L.; Vanderzande, D.; Maes, W. *RSC Adv.*, **2013**, *3*, 11418.

(10) (*a*) Van Mierloo, S.; Kesters, J.; Hadipour, A.; Spijkman, M.-J.; Van den Brande, N.; D'Haen, J.; Van Assche, G.; de Leeuw, D. M.; Aernouts, T.; Manca, J.; Lutsen, L.; Vanderzande, D.; Maes, W. *Chem. Mater.*, **2012**, *24*, 587; (*b*)

Osaka, I.; Saito, M.; Koganezawa, T.; Takimiya, K. *Adv. Mater.*, **2014**, *26*, 331; (*c*) Subramaniyan, S.; Xin, H.; Sunjoo Kim, F.; Murari, N. M.; Courtright, B. A. E.; Jenekhe, S. A. *Macromolecules*, **2014**, *47*, 4199; (*d*) Bundgaard, E.; Livi, F.; Hagemann, O.; Carlé, J. E.; Helgesen, M.; Heckler, I. M.; Zawacka, N. K.; Angmo, D.; Larsen-Olsen, T. T.; dos Reis Benatto, G. A.; Roth, B.; Madsen, M. V.; Andersson, M. R.; Jørgensen, M.; Søndergaard, R. R.; Krebs, F. C. *Adv. Energy Mater.*, **2015**, 1402186.

(11) (*a*) Shi, Q.; Cheng, P.; Li, Y.; Zhan, X. *Adv. Energy Mater.*, **2012**, *2*, 63; (*b*) Dutta, P.; Yang, W.; Eom, S.H.; Lee, S.-H. *Org. Electron.*, **2012**, *13*, 273; (*c*) Dutta, P.; Park, H.; Lee, W.-H.; Kang, I.-N.; Lee, S.-H. *Org. Electron.*, **2012**, *13*, 3183; (*d*) Cheng, P.; Shi, Q.; Lin, Y.; Li. Y.; Zhan, X. *Org. Electron.*, **2013**, *14*, 599; (*e*) Chen, Y.; Du, Z.; Chen, W.; Wen, S.; Sun, L.; Liu, Q.; Sun, M.; Yang, R. *New J. Chem.*, **2014**, *38*, 1559.

(12) (*a*) Zhang, J.; Kang, D.-Y.; Barlow, S.; Marder, S. R. *J. Mater. Chem.*, **2012**, *22*, 21392; (*b*) Liu, S.-Y.; Shi, M.-M.; Huang, J.-C.; Jin, Z.- N.; Hu, X.-L.; Pan, J.-Y.; Li, H.-Y.; Jen, A. K. Y.; Chen, H.-Z. *J. Mater. Chem. A*, **2013**, *1*, 2795; (*c*) Zhang, J.; Chen, W.; Rojas, A. J.; Jucov, E. V.; Timofeeva, T. V.; Parker, T. C.; Barlow, S.; Marder, S. R. *J. Am. Chem. Soc.*, **2013**, *135*, 16376; (*d*) Okamoto, K.; Zhang, J.; Housekeeper, J. B.; Marder S. R.; Luscombe, C. K. *Macromolecules,* **2013**, *46*, 8059; (*e*) Matsidik, R.; Martin, J.; Schmidt, S.; Obermayer, J.; Lombeck, F.; Nübling, F.; Komber, H.; Fazzi, D.; Sommer, M. *J. Org. Chem.*, **2015**, *80*, 980; (*f*) McAfee, S. M.; Topple, J. M.; Payne, A.-J.; Sun, J.-P.; Hill, I. G.; Welch, G. C. *ChemPhysChem*, **2015**, DOI: 10.1002/cphc.201402662.

(13) Kudrjasova, J.; Herckens, R.; Penxten, H.; Adriaensens, P.; Lutsen, L.; Vanderzande, D.; Maes, W. *Org. Biomol. Chem.*, **2014**, *12*, 4663.

(14) Wong, W.-Y; Wang, X.-Z.; He, Z.; Chan, K.-K.; Djurišić A. B.; Cheung, K.-Y.; Yip, C.-T.; Ng, A. M.-C.; Xi, Y.-Y.; Mak, C. S.-K.; Chan, W.-K. *J. Am. Chem. Soc.*, **2007**, *129*, 14372.

(15) Wang, W.; Ma, Z.; Zhang, Z.; Vandewal, K.; Henriksson, P.; Inganäs, O.; Zhang, F.; Andersson, M. R. *J. Am. Chem. Soc.*, **2011**, *133*, 14244.

(16) Verstappen, P.; Kesters, J.; Vanormelingen, W.; Heintges, G. H. L.; Drijkoningen, J.; Vangerven, T.; Marin, L.; Koudjina, S.; Champagne, B.; Manca, J.; Lutsen, L.; Vanderzande, D.; Maes, W. *J. Mater. Chem. A*, **2015**, *3*, 2960.

(17) (*a*) Nevil, N.; Ling, Y.; Van Mierloo, S.; Kesters, J.; Piersimoni, F.; Adriaensens, P.; Lutsen, L.; Vanderzande, D.; Manca, J.; Maes, W.; Van Doorslaer, S.; Goovaerts, E. *Phys. Chem. Chem. Phys.*, **2012**, *14*, 15774; (*b*) Lin, Y.; Zhan, X.; *Mater. Horiz.*, **2014**, *1*, 470; (*c*) Eftaiha, A. F. ; Sun, J.-P.; Hill, I. G.; Welch, G. C. *J. Mater. Chem. A*, **2014**, *2*, 120.

(18) (*a*) Danley, R. L.; Caulfield, P. A.; Aubuchon, S. R. *Am. Lab.*, **2008**, *40*, 9; (*b*) Ghoos, T.; Van den Brande, N.; Defour, M.; Brassinne, J.; Fustin, C.-A.; Gohy, J.-F.; Hoeppener, S.; Schubert, U. S.; Vanormelingen, W.; Lutsen, L.; Vanderzande, D. J.; Van Mele, B.; Maes, W. *Eur. Polym. J.*, **2014**, *53*, 206.

4.6. SUPPORTING INFORMATION

4.6.1. General experimental methods

4.6.1.1. Synthesis and characterization

Unless stated otherwise, all reagents and chemicals were obtained from commercial sources and used without further purification. 5,5'-Dibromo-4,4'-dinonyl-2,2'-bithiazole,[1] 5,8-dibromo-6-fluoro-2,3-diphenylquinoxaline[2] and (*E*)-6,6'-dibromo-1,1'-bis(2-hexyldecyl)-[3,3'-biindolinylidene]-2,2'-dione[3] were synthesized according to procedures reported in the literature. Toluene was dried using an MBraun solvent purification system (model MB-SPS 800) equipped with alumina drying columns. Microwave reactions were carried out in a CEM Discovery microwave at the given temperature by varying the irradiation power. A thick-wall pyrex reaction vessel (10 mL) with teflon septum was used for the microwave reactions. Preparative size exclusion chromatography (prep-SEC) was performed on JAIGEL 1*H* and 2*H* columns attached to an LC system equipped with a UV detector (path 0.5 mm) and a switch for recycling and collecting the eluent ($CHCl_3$: flow rate 3.5 mL min^{-1}, injection volume 2.5 mL).

NMR chemical shifts (δ) were determined relative to the residual $CHCl_3$ absorption (7.26 ppm) or the ^{13}C resonance shift of $CDCl_3$ (77.16 ppm). MALDI-TOF mass spectra were recorded on a Bruker Daltonics Ultraflex II Tof/Tof. 1 µL of the matrix solution (4 mg mL^{-1} DTCB (*trans*-2-[3-(4-*tert*-butylphenyl)-2-methyl-2-propenylidene]malononitrile) in $CHCl_3$) was spotted onto an MTP Anchorchip 600/384 MALDI plate. The spot was allowed to dry and 1 µL of the analyte solution (0.5 mg mL^{-1} in $CHCl_3$) was spotted on top of the matrix. Reported masses originate from the 100% intensity peaks of the isotopic distributions. Rapid heat-cool calorimetry (RHC) experiments were performed on a prototype RHC of TA

Instruments, equipped with liquid nitrogen cooling and specifically designed for operation at high scanning rates.[4] RHC measurements were performed at 500 K min^{-1} (after cooling at 20 K min^{-1}; the second heating was chosen to avoid thermal history effects) in aluminum crucibles, using helium (6 mL min^{-1}) as a purge gas. UV-Vis absorption spectra were recorded with an Agilent Cary 500 Scan UV-Vis-NIR spectrometer in a continuous run from 200 to 800 nm at a scan rate of 600 nm min^{-1}. The thin films for the solid-state UV-Vis measurements were prepared by drop casting chloroform solutions of **SM1–3**. Electrochemical measurements were performed with an Eco Chemie Autolab PGSTAT 30 potentiostat/galvanostat using a three-electrode microcell equipped with a Pt wire working electrode, a Pt wire counter electrode and a $Ag/AgNO_3$ reference electrode (Ag wire dipped in a solution of 0.01 M $AgNO_3$ and 0.1 M NBu_4PF_6 in anhydrous MeCN). Samples were prepared in anhydrous CH_2Cl_2 containing 0.1 M NBu_4PF_6, and ferrocene was used as an internal standard. The respective TzTz products were dissolved in the electrolyte solution, which was degassed with Ar prior to each measurement. To prevent air from entering the system, the experiments were carried out under a curtain of Ar. Cyclic voltammograms were recorded at a scan rate of 50 mV s^{-1}. The HOMO-LUMO energy levels of the products were determined using CV data and spectroscopic absorption data. For the conversion of V to eV, the onset potentials of the first oxidation/reduction peaks were used and referenced to ferrocene/ferrocenium, which has an ionization potential of -4.98 eV *vs.* vacuum. This correction factor is based on a value of 0.31 eV for Fc/Fc^+ *vs.* SCE[5a] and a value of 4.68 eV for SCE *vs.* vacuum[5b]: $E_{HOMO/LUMO}$ (eV) = -4.98 - $E_{onset\ ox/red}^{Ag/AgNO3}$ (V) + $E_{onset\ Fc/Fc+}^{\ Ag/AgNO3}$ (V). The HOMO energy levels of the TzTz products were determined from the CV data. The LUMO energy levels were either determined from the CV data or calculated as the difference between the HOMO values and

the optical HOMO-LUMO gaps. The accuracy of measuring redox potentials by CV is about 0.01−0.02 V. Reproducibility can be less because the potentials do depend on concentration and temperature.[6] To estimate the optical HOMO-LUMO gaps, the wavelength at the intersection of the tangent line drawn at the low energy side of the (solution/film) absorption spectrum with the x-axis was used (E_g (eV) = 1240/(wavelength in nm)).

(TPA-T-TzTz-T)$_2$BiTz (SM1). 4-(4-Hexyl-5-(5-(3-hexylthiophen-2-yl)thiazolo[5,4-*d*]thiazol-2-yl)thiophen-2-yl)-*N*,*N*-diphenylaniline (**TPA-T-TzTz-T**) (100 mg, 0.14 mmol, 2 equiv), K_2CO_3 (28.9 mg, 0.209 mmol, 3 equiv), $Pd(OAc)_2$ (0.6 mg, 2.8 µmol, 4 mol%), PCy_3HBF_4 (2.0 mg, 5.6 µmol, 8 mol%), pivalic acid (4.3 mg, 0.075 mmol, 60 mol%) and 5,5'-dibromo-4,4'-dinonyl-2,2'-bithiazole (40.3 mg, 0.07 mmol, 1 equiv) were weighed in air and placed in a microwave vial (10 mL) equipped with a magnetic stirring bar. The vial was purged with Ar and dry toluene (2 mL) was added. The reaction mixture was vigorously stirred under microwave irradiation at 150 °C for 18 h. The solution was then cooled down to room temperature and diluted with CH_2Cl_2 and H_2O. The aqueous phase was extracted with CH_2Cl_2. The organic fractions were combined and dried over $MgSO_4$, filtered, and evaporated under reduced pressure. The obtained product mixture was separated by column chromatography on silica gel using a mixture of CH_2Cl_2 and petroleum ether (2/3) as the eluent. Product containing fractions (with minor impurities) were collected and the small molecule was additionally purified by recycling prep-SEC to afford **SM1** as a pure dark red solid (42 mg, 33%). ^{1}H NMR (400 MHz, $CDCl_3$) δ = 7.44 (d, J = 8.6 Hz, 4H), 7.30–7.27 (m, 6H), 7.25–7.24 (m, 2H), 7.14–6.97 (m, 20H), 2.98 (t, J = 7.8 Hz, 4H), 2.95–2.84 (m, 8H), 1.85 (p, J = 7.6 Hz, 4H), 1.82–1.66 (m, 8H), 1.54–1.42 (m, 12H), 1.43–1.22 (m, 36H), 0.97–0.84 (m, 18H); ^{13}C NMR (75 MHz, $CDCl_3$) δ = 161.6,

160.1, 157.4, 155.3, 150.4, 150.1, 148.1, 147.4, 145.7, 144.3, 143.1, 134.5, 132.6, 130.5, 130.2, 129.5, 127.9, 127.2, 126.6, 125.7, 125.0, 123.6, 123.1, 32.1, 31.9, 31.0, 30.8, 30.5, 29.8, 29.6, 29.3, 22.8, 14.3; MS (MALDI-TOF) calcd. for $C_{108}H_{122}N_8S_{10}$ *m/z* = 1851.7 ($[M]^+$), found *m/z* = 1853.0; UV-Vis ($CHCl_3$) λ_{max} (log ε) = 492 nm (4.704).

(TPA-T-TzTz-T)$_2$Qx (SM2). 4-(4-Hexyl-5-(5-(3-hexylthiophen-2-yl)thiazolo[5,4-*d*]thiazol-2-yl)thiophen-2-yl)-*N*,*N*-diphenylaniline (**TPA-T-TzTz-T**) (100 mg, 0.14 mmol, 2 equiv), K_2CO_3 (28.9 mg, 0.209 mmol, 3 equiv), $Pd(OAc)_2$ (0.6 mg, 2.8 µmol, 4 mol%), PCy_3HBF_4 (2.0 mg, 5.6 µmol, 8 mol%), pivalic acid (4.3 mg, 0.075 mmol, 60 mol%) and 5,8-dibromo-6-fluoro-2,3-diphenylquinoxaline (31.9 mg, 0.07 mmol, 1 equiv) were weighed in air and placed in a microwave vial (10 mL) equipped with a magnetic stirring bar. The vial was purged with Ar and dry toluene (2 mL) was added. The reaction mixture was vigorously stirred under microwave irradiation at 150 °C for 18 h. The solution was then cooled down to room temperature and diluted with CH_2Cl_2 and H_2O. The aqueous phase was extracted with CH_2Cl_2. The organic fractions were combined and dried over $MgSO_4$, filtered, and evaporated under reduced pressure. The obtained product mixture was separated by column chromatography on silica gel using a mixture of $CHCl_3$ and petroleum ether (1/1) as the eluent to afford **SM2**. Minor impurities were removed by precipitating the small molecule (twice) from EtOAc. The pure product was obtained as a dark purple solid (35 mg, 29%). Due to its limited solubility in $CHCl_3$, the product could not be further purified by recycling prep-SEC. ^{1}H NMR (300 MHz, $CDCl_3$) δ = 7.78–7.58 (m, 5H), 7.52–7.34 (m, 12H), 7.33–7.26 (m, 6H), 7.25–7.21 (m, 2H), 7.17–6.83 (m, 18H), 3.07–2.52 (m, 8H), 1.80–1.62 (m, 8H), 1.53–1.28 (m, 24H), 1.02–0.86 (m, 12H); MS (MALDI-TOF) calcd. for $C_{104}H_{95}FN_8S_8$ *m/z* = 1731.5 ($[M]^+$), found *m/z* = 1731.5;

UV-Vis ($CHCl_3$) λ_{max} (log ε) = 527 (4.79), 437 nm (4.78). Due to the compound's limited solubility, ^{13}C NMR data were not gathered.

(TPA-T-TzTz-T)$_2$II (SM3). 4-(4-Hexyl-5-(5-(3-hexylthiophen-2-yl)thiazolo[5,4-*d*]thiazol-2-yl)thiophen-2-yl)-*N*,*N*-diphenylaniline (**TPA-T-TzTz-T**) (100 mg, 0.14 mmol, 2 equiv), K_2CO_3 (28.9 mg, 0.209 mmol, 3 equiv), $Pd(OAc)_2$ (0.6 mg, 2.8 µmol, 4 mol%), PCy_3HBF_4 (2.0 mg, 5.6 µmol, 8 mol%), pivalic acid (4.3 mg, 0.075 mmol, 60 mol%) and 6,6'-dibromo-1,1'-bis(2-hexyldecyl)-[3,3'-biindolinylidene]-2,2'-dione (49.5 mg, 0.07 mmol, 1 equiv) were weighed in air and placed in a microwave vial (10 mL) equipped with a magnetic stirring bar. The vial was purged with Ar and dry toluene (2 mL) was added. The reaction mixture was vigorously stirred under microwave irradiation at 150 °C for 18 h. The solution was then cooled down to room temperature and diluted with CH_2Cl_2 and H_2O. The aqueous phase was extracted with CH_2Cl_2. The organic fractions were combined and dried over $MgSO_4$, filtered, and evaporated under reduced pressure. The obtained product mixture was separated by column chromatography on silica gel using a mixture of CH_2Cl_2 and petroleum ether (1/2). Product containing fractions (with minor impurities) were collected and the small molecule was additionally purified by recycling prep-SEC to afford **SM3** as a dark black solid (47 mg, 32%). ^1H NMR (300 MHz,) δ = 9.10 (d, J = 8.5 Hz, 2H), 7.43 (d, J = 8.7 Hz, 4H), 7.32–7.27 (m, 6H), 7.25–7.24 (m, 2H), 7.22–6.97 (m, 22H), 6.81 (s, 2H), 3.76–3.62 (m, 4H), 2.98–2.78 (m, 8H), 1.92 (s, 2H), 1.81–1.65 (m, 8H), 1.44–1.12 (m, 70H), 1.02–0.90 (m, 12H), 0.89–0.78 (m, 12H); ^{13}C NMR (75 MHz, CD_2Cl_2) δ = 168.9, 161.5, 160.7, 150.8, 148.5, 148.0, 146.0, 145.7, 145.0, 144.6, 144.2, 136.1, 132.9, 131.5, 131.2, 131.1, 130.1, 127.7, 127.4, 127.0, 126.0, 125.7, 124.2, 123.4, 122.2, 118.5, 104.5, 45.1, 37.5, 32.8, 32.6, 31.5, 31.1, 30.8, 30.6, 30.4, 30.3, 27.6, 23.7, 23.6, 14.8.; MS (MALDI-TOF) calcd. for

$C_{132}H_{156}N_8O_2S_8$ *m/z* = 2142.0 ([M]$^+$), found *m/z* = 2142.5; UV-Vis ($CHCl_3$) λ_{max} (log ε) = 598 (4.99), 449 nm (5.02).

4.6.1.2. Photovoltaic device fabrication and characterization

Bulk heterojunction organic solar cells were fabricated using the traditional device architecture glass/ITO/PEDOT:PSS/photoactive layer/Ca/Al. Prior to processing, the pre-patterned indium tin oxide (ITO, Kintec, 100 nm, 20 Ohm/sq) coated glass substrates were thoroughly cleaned using soap, demineralized water, acetone, isopropanol and a UV/O_3 treatment. PEDOT:PSS [poly(3,4-ethylenedioxythiophene):poly(styrenesulfonic acid), Heraeus Clevios] was deposited by spin-coating, aiming at a layer thickness of ~30 nm. Afterwards, processing was continued under nitrogen atmosphere in a glove box (<1 ppm O_2/H_2O), starting off with an annealing step at 130 °C for 15 min to remove any residual water. Subsequently, all active layer small molecule:$PC_{71}BM$ ([6,6]-phenyl-C_{71}-butyric acid methyl ester; Solenne) blend solutions were spin-coated with optimal layer thicknesses of ~120−150 nm, as confirmed by profilometry (DEKTAK). Optimal device performance was procured for the solar cells processed from chloroform-based blends with a small molecule concentration of 4 mg mL^{-1}. In a final step, devices with an active device area of 3 mm^2 were obtained by evaporation of Ca and Al as top electrodes with thicknesses of 30 and 80 nm, respectively. The *I-V* characteristics of the resulting photovoltaic devices were evaluated under AM1.5G solar illumination (100 mW cm^{-2}) using a Newport class A solar simulator (model 91195A), calibrated with a silicon solar cell. EQE measurements were performed with a Newport Apex illuminator (100 W Xenon lamp, 6257) as a light source, a Newport Cornerstone 130° monochromator and a Stanford SR530 lock-in amplifier for the current measurements. A silicon

FDS100-CAL photodiode was employed as a reference cell. For atomic force microscopy (AFM) imaging, a Bruker Multimode 8 AFM was used in PeakForce tapping mode, employing ScanAsyst. The images were produced with a silicon tip on a nitride lever with a spring constant of 4 N m^{-1}. Photo-induced charge extraction by linearly increasing voltage (Photo-CELIV) signals were registered on complete photovoltaic devices utilizing a pulsed laser (Continuum minilite II, 532nm), a Tektronix TDS 620B oscilloscope and a Tektronix AFG3101 function generator. The samples were placed in a sample holder filled with nitrogen to avoid exposure to ambient air.

4.6.2. MALDI-TOF mass spectra of small molecules SM1–3

(TPA-T-TzTz-T)$_2$BiTz (**SM1**)

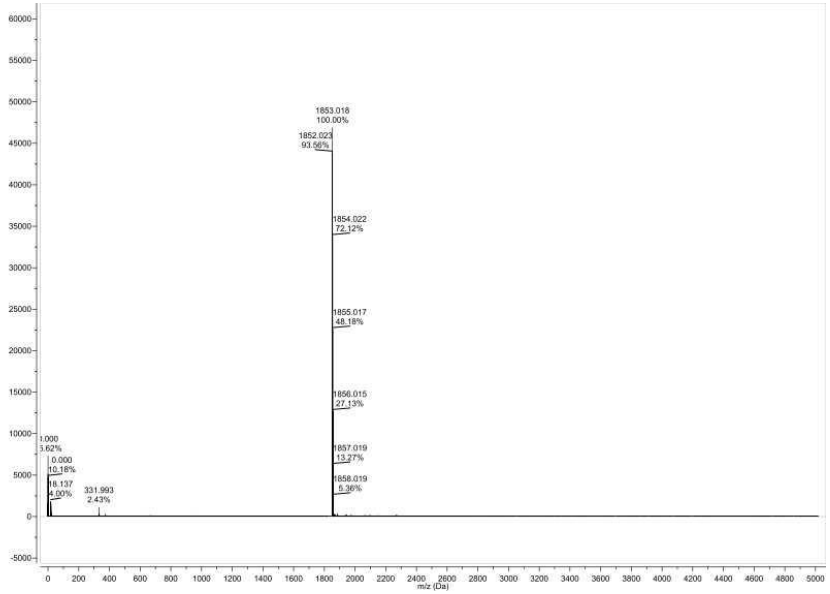

Figure S1. MALDI-TOF mass spectrum of **SM1**.

(TPA-T-TzTz-T)$_2$Qx (**SM2**)

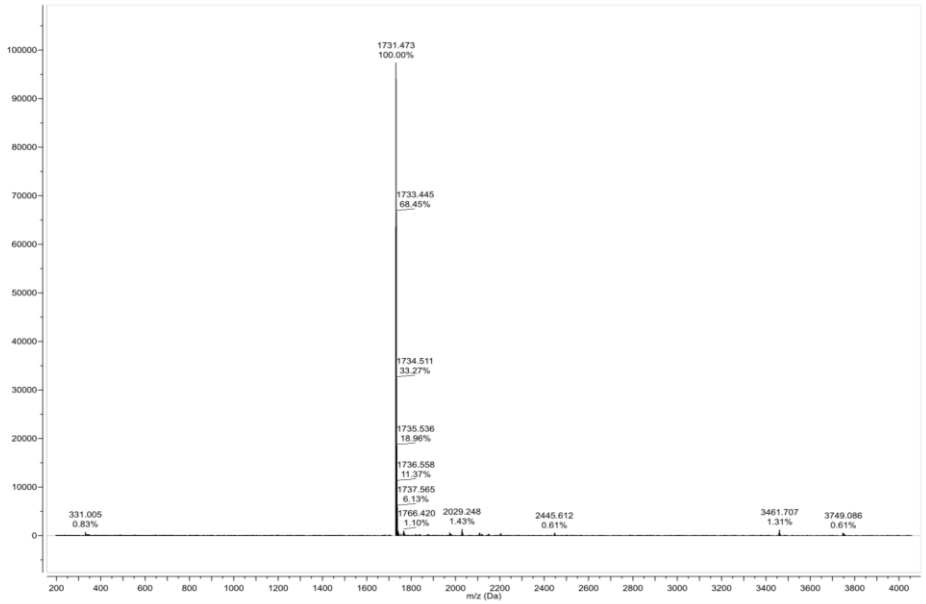

Figure S2. MALDI-TOF mass spectrum of **SM2**.

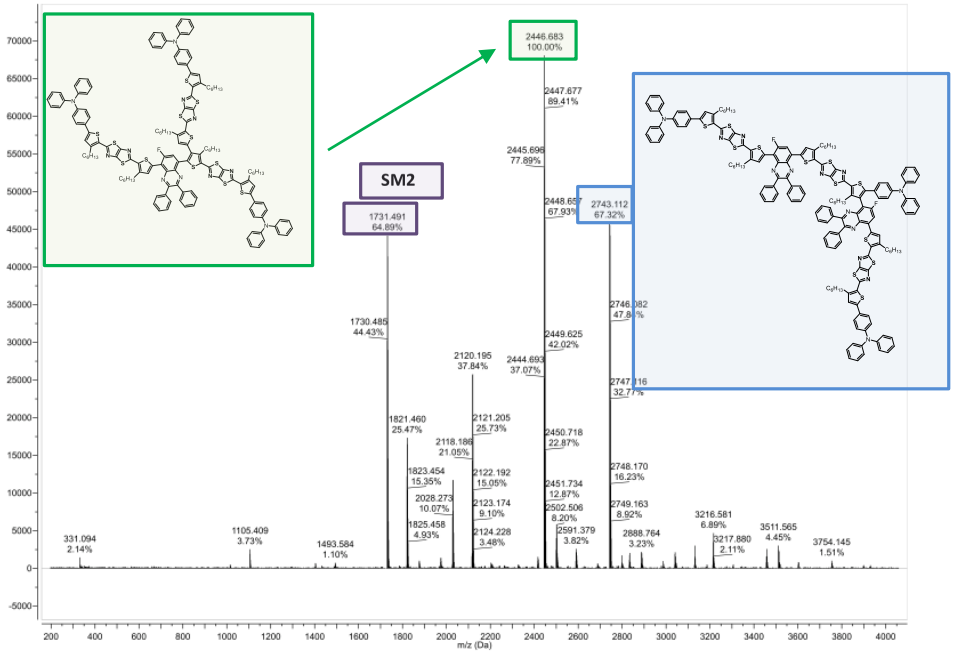

Figure S3. MALDI-TOF mass spectrum of the filtrate after precipitation of **SM2** (the exact position of the extra substituent remains unknown).

(TPA-T-TzTz-T)$_2$II (**SM3**)

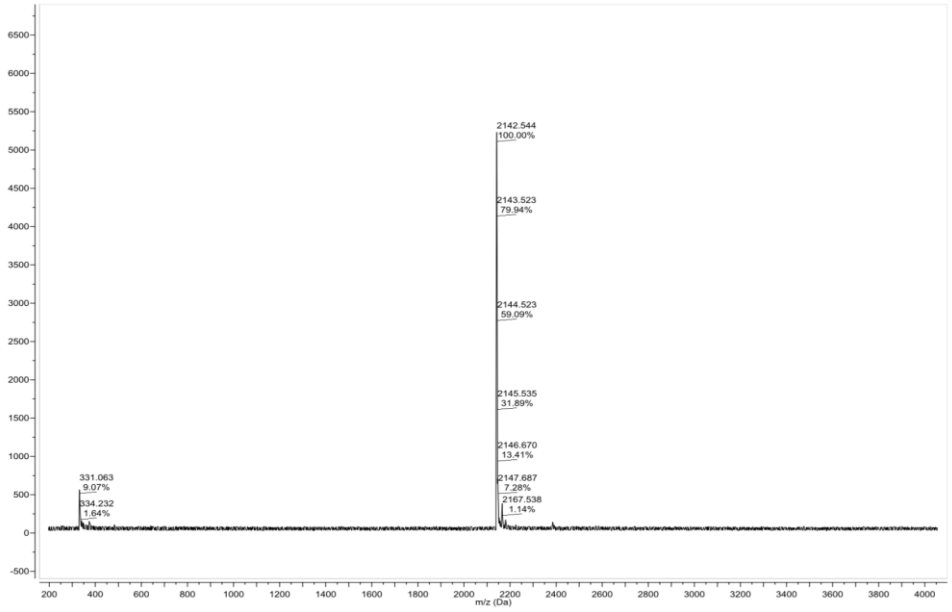

Figure S4. MALDI-TOF mass spectrum of **SM3**.

4.6.3. Optimization of the SM1−3:$PC_{71}BM$ organic solar cell performances

Table S1. Optimization of the solar cell devices based on **SM1**.

Processing solvent[a]	**SM1**:$PC_{71}BM$	Total concentration (mg mL^{-1})	V_{OC} (V)	J_{SC} (mA cm^{-2})	FF	Average η (%)[b]	Best η (%)
CF	2:1	15	0.80	3.60	0.60	1.74	1.78
CF	1:1	16	0.75	5.80	0.41	1.77	1.96
CF	1:3	16	0.70	3.31	0.28	0.66	0.93
CF + 1% CN	1:1	16	0.76	6.14	0.54	2.50	2.78
CF + 3% CN	1:1	16	0.79	3.44	0.50	1.35	1.41

[a] CF = chloroform, CN = 1-chloronaphthalene. [b] Average values over at least 4 devices.

Table S2. Optimization of the solar cell devices based on **SM2**.

Processing solvent[a]	**SM2**:$PC_{71}BM$	Total concentration (mg mL^{-1})	V_{OC} (V)	J_{SC} (mA cm^{-2})	FF	Average η (%)[b]	Best η (%)
CF	2:1	15	0.89	6.95	0.43	2.66	2.77
CF	1:1	16	0.83	9.78	0.50	4.11	4.86
CF	1:3	16	0.79	7.12	0.34	1.93	1.92
CF + 1% CN	1:1	16	0.85	7.91	0.39	2.63	2.89
CF + 3% CN	1:1	16	0.84	6.89	0.42	2.43	2.72
CB	1.1	32	0.81	6.60	0.35	1.86	1.99

[a] CF = chloroform, CN = 1-chloronaphthalene, CB = chlorobenzene. [b] Average values over at least 4 devices.

Table S3. Optimization of the solar cell devices based on **SM3**.

Processing solvent[a]	**SM3**:$PC_{71}BM$	Total concentration (mg mL^{-1})	V_{OC} (V)	J_{SC} (mA cm^{-2})	FF	Average η (%)[b]	Best η (%)
CF[c]	1:1	16	0.86	7.04	0.35	2.11	2.42
CF + 1% CN[c]	1:1	16	0.85	6.41	0.32	1.73	1.83
CF + 3% CN[c]	1:1	16	0.61	3.68	0.30	0.70	1.07

[a] CF = chloroform, CN = 1-chloronaphthalene. [b] Average values over at least 4 devices.

4.6.4. Photo-CELIV

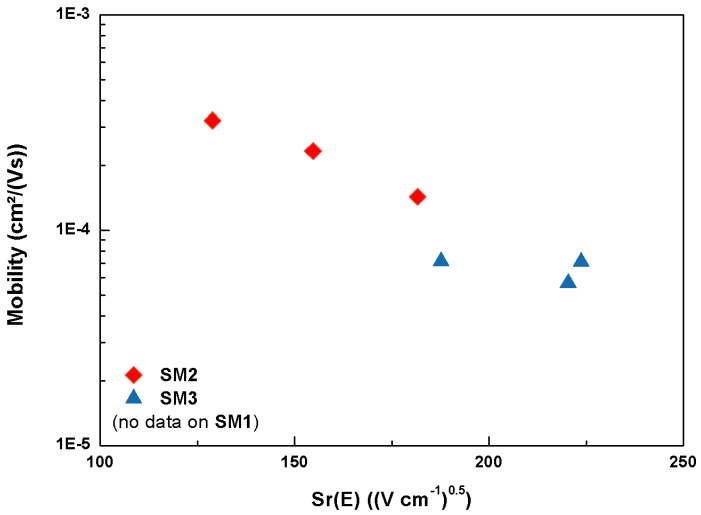

Figure S5. Data obtained from photo-CELIV measurements on organic solar cell devices based on **SM2–3** with photoactive layer thicknesses of > 300 nm (no data could be acquired for **SM1**).

4.6.5. References

(1) Wong, W.-Y; Wang, X.-Z.; He, Z.; Chan, K.-K.; Djurišić A. B.; Cheung, K.-Y.; Yip, C.-T.; Ng, A. M.-C.; Xi, Y.-Y.; Mak, C. S.-K.; Chan, W.-K. *J. Am. Chem. Soc.*, **2007**, *129*, 14372.

(2) Verstappen, P.; Kesters, J.; Vanormelingen, W.; Heintges, G. H. L.; Drijkoningen, J.; Vangerven, T.; Marin, L.; Koudjina, S.; Champagne, B.; Manca, J.; Lutsen, L.; Vanderzande, D.; Maes, W. *J. Mater. Chem. A*, **2015**, *3*, 2960.

(3) Wang, W.; Ma, Z.; Zhang, Z.; Vandewal, K.; Henriksson, P.; Inganäs, O.; Zhang, F.; Andersson, M. R. *J. Am. Chem. Soc.*, **2011**, *133*, 14244.

(4) (*a*) Danley, R. L.; Caulfield, P. A.; Aubuchon, S. R. *Am. Lab.*, **2008**, *40*, 9; (*b*) Ghoos, T.; Van den Brande, N.; Defour, M.; Brassinne, J.; Fustin, C.-A.; Gohy, J.-F.; Hoeppener, S.; Schubert, U. S.; Vanormelingen, W.; Lutsen, L.; Vanderzande, D. J.; Van Mele, B.; Maes, W. *Eur. Polym. J.*, **2014**, *53*, 206.

(5) (*a*) Bard, J.; Faulkner, L. R. *Electrochemical methods: fundamentals and applications*, 2nd Ed., **2001**, Wiley; (*b*) Trasatti, S. *Pure Appl. Chem.*, **1986**, *58*, 95.

(6) Veldman, D.; Meskers, S. C. J.; Janssen, R. A. J. *Adv. Funct. Mater.* **2009**, *19*, 1939.

Chapter 5

A combined Stille-direct arylation approach toward D–π-A-π–D-type small molecules for organic photovoltaics

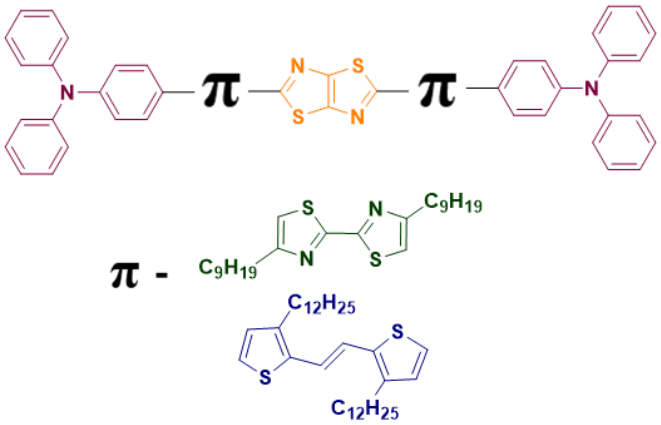

Julija Kudrjasova, Jurgen Kesters, Pieter Verstappen, Laurence Lutsen, Dirk Vanderzande, Wouter Maes

(Contribution: all synthesis and chemical analysis, main author)

ABSTRACT

Two D–π-A-π–D-type molecular chromophores based on a thiazolo[5,4-*d*]thiazole (TzTz) acceptor core, electron donating triphenylamine (TPA) end groups and either a bithiazole (BiTz) or thienylenevinylene (TV) π–bridging moiety are designed and synthesized via a combination of traditional Stille cross-coupling and C-H arylation reactions toward small molecule organic solar cell applications. The outcome of the final direct arylation reaction is highly dependent on the applied π–bridge as complications arise when the number of activated C-H groups increases. Non-optimized solar cell devices based on a TPA-BiTz-TzTz-BiTz-TPA:$PC_{71}BM$ blend afford a power conversion efficiency of 0.6%.

5.1. INTRODUCTION

In the past few years, so-called 'small molecules' have attracted considerable interest for bulk heterojunction (BHJ) organic photovoltaics (OPV) due to their well-defined molecular structure, easier purification and scale-up, and lower batch-to-batch variations as compared to the traditionally applied (low bandgap) conjugated polymers.[1] From the perspective of molecular design of small molecule electron donor materials (commonly combined with methanofullerenes in BHJ OPV devices), good solubility, a narrow HOMO-LUMO gap with broad UV-VIS-NIR absorption, a relatively low HOMO energy level and high hole mobility are key requirements toward high photovoltaic performance. The recent impressive improvement in power conversion efficiency (PCE) of small molecule organic solar cells (to over 10%) has been achieved by implementing the push-pull or donor-acceptor (D-A) strategy to enhance light absorption and carefully adjusting structural parameters (e.g. solubilizing side chain tuning).[2] In addition to the electron rich (donor) and electron poor (acceptor) (heteroaromatic) subunits, π-bridging moieties are often applied to tailor the physicochemical material properties, significantly affecting the push-pull communication and thereby the intramolecular charge transfer efficiency.

Thiazolo[5,4-*d*]thiazole (TzTz) has recently emerged as a promising acceptor moiety for both low bandgap copolymers and related molecular chromophores because the fused biheterocycle possesses a number of favorable properties, *i.e.* electron deficiency, strong light absorption, photochemical and thermal stability, high stacking tendency, good to excellent charge carrier mobility and easy synthesis from corresponding (het)aryl carbaldehydes.[3–5] In previous work, we have prepared extended TzTz-based semiconductors toward organic solar cell and

field-effect transistor applications employing classical Suzuki cross-coupling reactions.[6] In contrast to all previous efforts, a simple and effective direct arylation strategy was recently developed as well to afford both symmetrically and asymmetrically disubstituted 2,5-dithienyl-TzTz derivatives.[7] In the present work, we report on novel D–π-A-π–D molecules with TzTz as acceptor unit, triphenylamine (TPA) as donor unit and two different π-bridging entities, thienylenevinylene (TV) and bithiazole (BiTz). The planar electron rich TV building block is designed to provide extended π-conjugation via a vinylene spacer between the thiophene units.[8] On the other hand, the electron deficient bithiazole is known to provide strong interchain interactions, leading to higher crystallinity and improved mobility.[9]

5.2. RESULTS AND DISCUSSION

The synthetic route toward the envisaged small molecules **SM1** and **SM2** is outlined in Scheme 1. The required precursors 2,5-dibromothiazolo[5,4-*d*]thiazole (**5**),[10] 4,4'-dinonyl-2,2'-bithiazole (**6**),[11] and (*E*)-2,2'-(1,2-ethenediyl)-3,3'-didodecylbisthiophene (**8**)[12] were prepared according to literature procedures. Compounds **6** and **8** were then mono-stannylated. Stille cross-coupling between dibromo-TzTz **5** and stannylated derivatives **7** and **9** afforded small molecules **10** and **11** in good yields (76 and 70%, respectively), especially considering the mono-stannyl derivatives were not purified in advance. The targeted small molecules **SM1** (TPA-BiTz-TzTz-BiTz-TPA) and **SM2** (TPA-TV-TzTz-TV-TPA) were then obtained via direct arylation with 4-bromo-*N*,*N*-diphenylaniline (2.1 equiv). After purification by standard column chromatography (silica), **SM1** was obtained as a pure orange crystalline solid, as confirmed by NMR and MALDI-TOF MS (see

SI). On the other hand, major side products were still observed for **SM2**. MALDI analysis showed the presence of additional mono-, tri- and even tetra-arylated compounds (see SI) and the complicated mixture was proven very hard to separate in its constituents, even when employing multiple (recycling) preparative size exclusion chromatography (prep-SEC) runs. The difference between the two C-H hetarylation reactions is striking and clearly indicates the limitations of the direct arylation approach. Whereas the reaction on bithiazole precursor **10**, with only two reactive C-H moieties, happens smoothly and the desired product is achieved in quite pure state already before column chromatographic purification, the same reaction on thienylenevinylene precursor **11**, with up to 6 possibly reactive thienyl positions, gives rise to a complicated product mixture.

The thermal properties of **SM1** were investigated by rapid heat-cool calorimetry (RHC) (Figure S1, Table 1). **SM1** displays a melting temperature of 219.4 °C, as well as a large melting enthalpy (ΔH_m = 56.0 J g^{-1}), indicating a highly crystalline character. UV-Vis absorption spectra of **SM1** in solution and thin film are depicted in Fig. 1. In $CHCl_3$ solution, maximum absorption is observed at 478 nm (molar absorptivity of 8.70 $\times 10^4$ L mol^{-1} cm^{-1}). In thin film, the absorption spectrum is red-shifted by 11 nm and a shoulder appears at ~538 nm, suggesting intermolecular interactions and aggregation in the solid state. The optical HOMO-LUMO gap estimated from the absorption edge of the thin film spectrum is 2.28 eV, which is rather high for OPV applications. The HOMO and LUMO frontier energy levels of **SM1** were estimated via cyclic voltammetry (CV) from the onset of the oxidation and reduction peaks, respectively (Table 1). The electron withdrawing bithiazole and TzTz moieties endow the molecule with a rather deep LUMO (-3.40 eV), enabling the small molecule to be possibly used as both p- and n-type component[6b,13] in BHJ OPV devices.

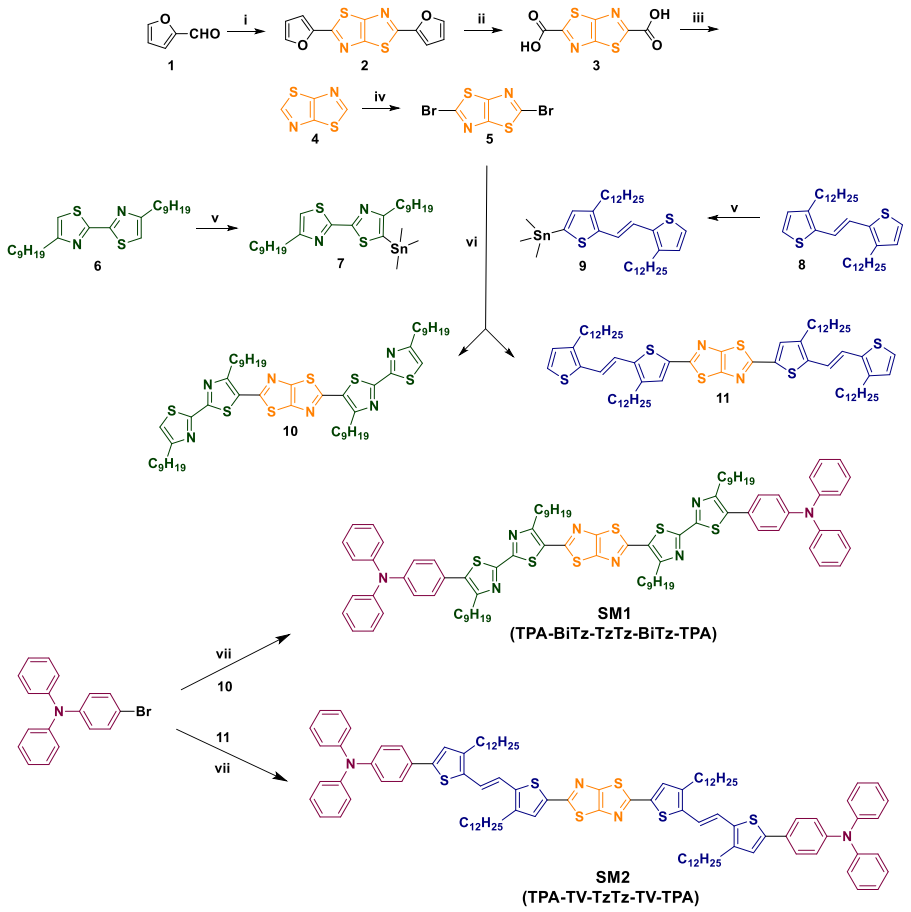

Scheme 1. Synthetic routes toward small molecules **SM1** and **SM2**: i. dithiooxamide, $PhNO_2$; ii. $KMnO_4$, pyridine; iii. Ethanol reflux; iv. Br_2, pyridine, CCl_4; v. a) *n*-BuLi, THF, 0 °C; b) Me_3SnCl; vi. $Pd(PPh_3)_4$, DMF/toluene, 90 °C, 15 h; vii. $Pd(OAc)_2$, PCy_3HBF_4, PivOH, K_2CO_3, toluene, 180 °C, 4 h (MW).

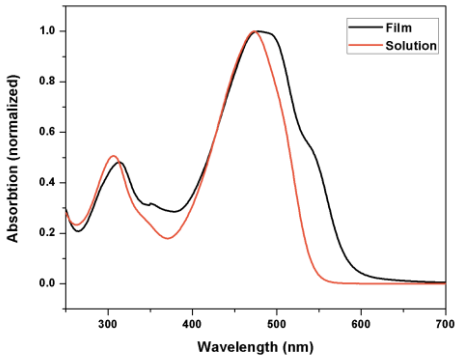

Fig. 1. Normalized UV-Vis absorption spectra of **SM1** in solution and thin film.

Table 1. Thermal, optical and electrochemical properties of **SM1**.

	T_m[a] (°C)	ΔH_m[a] (J/g)	λ_{max}[b] (nm) solution	λ_{max} (nm) film	E_g^{OPc} (eV)	HOMO[d] (eV)	LUMO[d] (eV)	E_g^{ECe} (eV)
SM1	219.4	56.0	478	489	2.28	-5.53	-3.40	2.13

[a] Determined by RHC. [b] In chloroform. [c] Optical bandgap, determined by the onset of the solid-state UV-Vis spectrum. [d] Determined by CV from the onset of oxidation/reduction. [e] Electrochemical bandgap.

In a following step, **SM1** was evaluated as a donor-type small molecule in BHJ organic solar cells in combination with $PC_{71}BM$. The blend solutions were prepared in a 1:1 ratio (wt/wt%) from either chloroform (CF) or chlorobenzene (CB) with total concentrations of 16 and 32 mg/mL, respectively. The photovoltaic devices were prepared by spin-coating the active layer blends on a PEDOT:PSS hole transport layer deposited on an ITO-covered transparent electrode followed by the vacuum deposition of Ca and Al as the top electrodes. As summarized in Table 2, without extensive optimization, a maximum PCE of 0.64% (Figure 2) was achieved for the CF based blend. The active layer deposited from the CB based solution had an enhanced tendency for aggregation, and therefore had to be spin-coated at an elevated temperature of 90 °C. Unfortunately, only a maximum PCE

of 0.37% could be obtained. These moderate efficiencies can mainly be attributed to low photocurrents and fill factors.

Table 2. Photovoltaic output parameters for the **SM1**:$PC_{71}BM$ (1:1) organic solar cells.[a]

	Processing solvent[b]	V_{OC} (V)	J_{SC} (mA cm^{-2})	FF	Average η (%)[c]	Best η (%)
SM1	CF	0.67	3.11	0.28	0.60	0.64
SM1	CB	0.68	1.75	0.27	0.32	0.37

[a] Device structure glass/ITO/PEDOT:PSS/**SM1**:$PC_{71}BM$/Ca/Al. [b] Total concentration of 16 mg mL^{-1} in chloroform (CF) and 32 mg mL^{-1} in chlorobenzene (CB). [c] Averages taken over 4 devices.

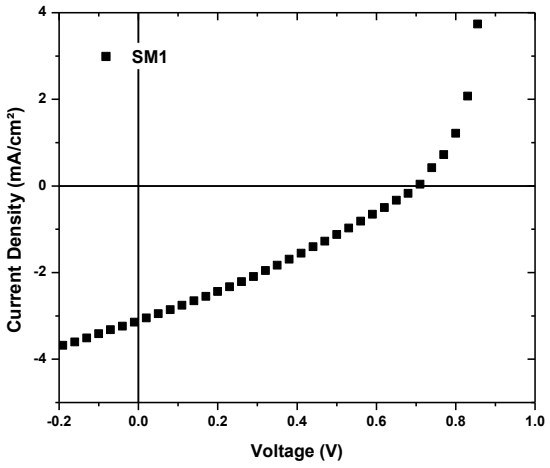

Fig. 2. *J-V* curve under illumination for the solar cell based on **SM1**:$PC_{71}BM$ with CF as the processing solvent.

5.3. CONCLUSIONS

In summary, two extended TzTz-based small molecules were prepared for organic solar cell applications. Whereas the first material was synthesized in a straightforward manner by successive Stille cross-coupling and direct hetarylation reactions, the second molecule was obtained as a complicated and inseparable product mixture due to the lack of C-H regioselectivity. Preliminary solar cell

measurements afforded a moderate power conversion efficiency (0.6%) based on the pure **SM1** material as a donor component. Current efforts are directed toward further solar cell optimization and the synthesis of **SM2** via traditional cross-coupling pathways.

5.4. EXPERIMENTAL SECTION

General experimental methods

Unless stated otherwise, all reagents and chemicals were obtained from commercial sources and used without further purification. Solvents were dried by a solvent purification system (MBraun, MB-SPS-800) equipped with alumina columns. Microwave reactions were carried out in a CEM Discovery microwave at the given temperature by varying the irradiation power and using a thick-walled pyrex reaction vessel (10 mL) with teflon septum. Preparative size exclusion chromatography (prep-SEC) was performed on JAIGEL 1*H* and 2*H* columns attached to an LC system equipped with a UV detector (path 0.5 mm) and a switch for recycling and collecting the eluent ($CHCl_3$: flow rate 3.5 mL min^{-1}, injection volume 2.5 mL).

NMR chemical shifts (δ, in ppm) were determined relative to the residual $CHCl_3$ (7.26 ppm) or CH_2Cl_2 (5.32 ppm) absorption or the ^{13}C resonance shift of $CDCl_3$ (77.16 ppm) or CD_2Cl_2 (54.00 ppm). MALDI-TOF mass spectra were recorded on a Bruker Daltonics Ultraflex II Tof/Tof. 1 µL of the matrix solution (16 mg mL^{-1} DTCB (*trans*-2-[3-(4-*tert*-butylphenyl)-2-methyl-2-propenylidene]malononitrile) in $CHCl_3$) was spotted onto an MTP Anchorchip 600/384 MALDI plate. The spot was allowed to dry and 1 µL of the analyte solution (0.5 mg mL^{-1} in $CHCl_3$) was spotted on top of the matrix. Rapid heat-cool calorimetry experiments were performed on a prototype RHC of TA Instruments, equipped with liquid nitrogen cooling and specifically designed for operation at high scanning rates.[14] RHC measurements were performed at 500 K min^{-1} in aluminum crucibles, using helium (6 mL min^{-1}) as a purge gas. UV-Vis absorption spectra were recorded with an Agilent Cary 500 Scan UV-Vis-NIR spectrometer in a continuous run from 200 to

800 nm at a scan rate of 600 nm min^{-1}. The thin film for the solid-state UV-Vis measurement was prepared by drop casting a dichloromethane solution of **SM1**. To estimate the optical HOMO-LUMO gap, the wavelength at the intersection of the tangent line drawn at the low energy side of the solid-state absorption spectrum with the x-axis was used (E_g (eV) = 1240/(wavelength in nm)). Electrochemical measurements were performed with an Eco Chemie Autolab PGSTAT 30 potentiostat/galvanostat using a three-electrode microcell equipped with a Pt wire working electrode, a Pt wire counter electrode and a $Ag/AgNO_3$ reference electrode (Ag wire dipped in a solution of 0.01 M $AgNO_3$ and 0.1 M NBu_4PF_6 in anhydrous MeCN). The **SM1** sample was prepared in anhydrous CH_2Cl_2 containing 0.1 M NBu_4PF_6 and ferrocene was used as an internal standard. **SM1** was dissolved in the electrolyte solution, degassed with Ar. To prevent air from entering the system, the experiments were carried out under a curtain of Ar. Cyclic voltammograms were recorded at a scan rate of 50 mV s^{-1}. The HOMO-LUMO energy levels were determined using the CV data. For the conversion of V to eV, the onset potentials of the first oxidation/reduction peaks were used and referenced to ferrocene/ferrocenium, which has an ionization potential of −4.98 eV *vs.* vacuum. This correction factor is based on a value of 0.31 eV for Fc/Fc^+ *vs.* SCE[15a] and a value of 4.68 eV for SCE *vs.* vacuum[15b]: $E_{HOMO/LUMO}$ (eV) = −4.98 − $E_{onset\ ox/red}^{Ag/AgNO3}$ (V) + $E_{onset\ Fc/Fc+}^{\ Ag/AgNO3}$ (V). The accuracy of measuring redox potentials by CV is about 0.01−0.02 V. Reproducibility can be less because the potentials do depend on concentration and temperature.

4,4'-Dinonyl-5-(trimethylstannyl)-2,2'-bithiazole (7). To an ice cold solution of 4,4'-dinonyl-2,2'-bithiazole (2.09 g, 4.75 mmol) in dry THF (10 mL), *n*-BuLi (2.5 M in *n*-hexane; 4.75 mL, 5.23 mmol) was added under a N_2 atmosphere. The mixture was stirred for 30 min at 0 °C and Me_3SnCl (1 M in THF;

5.7 mL) was added. The solution was allowed to warm gently to room temperature (overnight) and water was added. After extraction with ethyl acetate, the organic phase was washed with brine, dried over $MgSO_4$, filtered and evaporated to dryness. The crude product was used for Stille coupling without further purification.

4-Dodecyl-5-(2-(3-dodecylthiophen-2-yl)vinylthiophen-2-yl)trimethyl-stannane (9). To an ice cold solution of 1,2-bis(3-dodecylthiophen-2-yl)ethene (1.20 g, 4.75 mmol) in dry THF (10 mL), *n*-BuLi (2.5 M in *n*-hexane; 2.26 mL, 2.49 mmol) was added under a N_2 atmosphere. The mixture was stirred for 30 min at 0 °C and Me_3SnCl (1 M in THF; 2.26 mL) was added. The solution was allowed to warm gently to room temperature (overnight) and water was added. After extraction with ethyl acetate, the organic phase was washed with brine, dried over $MgSO_4$, filtered and evaporated to dryness. The crude product was used for Stille coupling without further purification.

2,5-Bis(4,4'-dinonyl-[2,2'-bithiazol]-5-yl)thiazolo[5,4-*d*]thiazole (10). 4,4'-Dinonyl-5-(trimethylstannyl)-2,2'-bithiazole (400 mg, 0.685 mmol) and 2,5-dibromothiazolo[5,4-*d*]thiazole (0.103 g, 0.343 mmol) were dissolved in dry DMF (10 mL) and dry toluene (10 mL) under N_2 atmosphere. $Pd(PPh_3)_4$ (0.008 g, 0.0068 mmol) was added and the mixture was stirred for 15 h at 90 °C. The solution was allowed to cool down to room temperature and water was added. After extraction with diethyl ether, the organic layer was washed with brine, dried over $MgSO_4$, filtered and the solvent was removed under vacuum. Purification by column chromatography (silica, petroleum ether:chloroform, 5:3) yielded the pure product as an orange solid (254 mg, 76%). ^{1}H NMR (300 MHz, $CDCl_3$): δ = 7.03 (s, 2H), 3.24–3.06 (m, 4H), 2.83 (t, J = 7.7 Hz, 4H), 1.95–1.81 (m, 4H), 1.82–1.67 (m, 4H), 1.58–1.43 (m, 4H), 1.43–1.58 (m, 44H), 0.96–0.82 (m,

12H); ^{13}C NMR (75 MHz, $CDCl_3$): δ = 161.0, 160.0, 159.9, 159.6, 157.9, 151.2, 128.6, 116.0, 32.1, 31.7, 31.6, 29.75, 29.7, 29.6, 29.5, 29.4, 29.3, 29.0, 22.8, 14.3.

2,5-Bis(4-dodecyl-5-((*E*)-2-(3-dodecylthiophen-2-yl)vinyl)thiophen-2-yl)thiazolo[5,4-*d*]thiazole (11). 4-Dodecyl-5-(2-(3-dodecylthiophen-2-yl)-vinylthiophen-2-yl)trimethylstannane (230 mg, 0.332 mmol) and 2,5-dibromothiazolo[5,4-*d*]thiazole (0.050 g, 0.166 mmol) were dissolved in dry DMF (10 mL) and dry toluene (10 mL) under N_2 atmosphere. $Pd(PPh_3)_4$ (0.004 g, 0.003 mmol) was added and the mixture was stirred for 15 h at 90 °C. The solution was allowed to cool down to room temperature and water was added. After extraction with diethyl ether, the organic layer was washed with brine, dried over $MgSO_4$, filtered and the solvent was removed under vacuum. Purification by column chromatography (silica, petroleum ether:chloroform, 5:3) yielded the pure product as an orange solid (140 mg, 70%). ^{1}H NMR (300 MHz, CD_2Cl_2): δ = 7.34 (s, 2H), 7.19–7.11 (m, 4H), 6.98 (d, *J* = 15.7 Hz, 2H), 6.89 (d, *J* = 5.1 Hz, 2H), 2.76–2.55 (m, 8H), 1.70–1.55 (m, 8H), 1.47–1.18 (m, 36H), 0.92–0.80 (m, 12H); ^{13}C NMR (100 MHz, CD_2Cl_2): δ = 162.5, 150.6, 142.8, 140.6, 136.3, 134.1, 130.6, 124.2, 121.8, 118.7, 32.5, 31.6, 31.3, 30.2, 29.9, 28.9, 23.3, 14.5.

3-{5'-[5-(5'-(4-(Diphenylamino)phenyl)-4,4'-dinonyl-[2,2'-bithiazol]-5-yl)thiazolo[5,4-*d*]thiazol-2-yl]-4,4'-dinonyl-[2,2'-bithiazol]-5-yl}-*N*,*N*-diphenylaniline (SM1). 4-Bromo-*N*,*N*-diphenylaniline (83 mg, 0.25 mmol, 2.1 equiv), K_2CO_3 (50.8 mg, 0.36 mmol, 3 equiv), $Pd(OAc)_2$ (1 mg, 4.9 µmol, 4 mol%), PCy_3HBF_4 (3.6 mg, 9.8 µmol, 8 mol%), pivalic acid (7.5 mg, 0.073 mmol, 60 mol%) and 2,5-bis(4,4'-dinonyl-[2,2'-bithiazol]-5-yl)thiazolo[5,4-*d*]thiazole (120 mg, 0.12 mmol, 1 equiv) were weighed in air and placed in a microwave vial (10 mL) equipped with a magnetic stirring bar. The vial was purged with Ar and

dry toluene (2 mL) was added. The reaction mixture was vigorously stirred under microwave irradiation at 180 °C for 4 h. The solution was then cooled down to room temperature and diluted with $CHCl_3$ and H_2O. The aqueous phase was extracted with $CHCl_3$. The organic fractions were combined and dried over $MgSO_4$, filtered, and evaporated under reduced pressure. The crude material was precipitated from ethyl acetate. The almost pure product was then further purified by column chromatography on silica gel using a mixture of $CHCl_3$ and petroleum ether (2:1) as an eluent, affording **SM1** as a pure orange solid (165 mg, 92%). ^{1}H NMR (400 MHz, $CDCl_3$): δ = 7.34–7.26 (m, 12H), 7.19–7.13 (m, 8H), 7.12–7.05 (m, 8H), 3.23–3.10 (m, 4H), 2.89–2.79 (m, 4H), 1.94–1.74 (m, 8H), 1.56–1.45 (m, 4H), 1.45–1.33 (m, 8H), 0.93–0.85 (m, 12H); ^{13}C NMR (75 MHz, $CDCl_3$): δ = 161.3, 159.6, 157.9, 156.8, 154.2, 151.1, 148.1, 147.4, 135.8, 130.1, 129.6, 128.4, 125.2, 124.8, 123.8, 122.6, 32.1, 31.8, 29.7, 29.6, 29.5, 29.1, 22.9, 14.3; MS (MALDI-TOF): calcd. for $C_{88}H_{104}N_8S_6$ *m/z* = 1465.7 ($[M]^+$), found *m/z* = 1465.6; UV-Vis ($CHCl_3$): λ_{max} (log ε) = 478 (4.94).

Photovoltaic device fabrication and characterization

Bulk heterojunction organic solar cells were fabricated for **SM1** using the traditional device architecture glass/ITO/PEDOT:PSS/photoactive layer/Ca/Al. Prior to processing, the pre-patterned indium tin oxide (ITO, Kintec, 100 nm, 20 Ohm/sq) coated glass substrates were thoroughly cleaned using soap, demineralized water, acetone, isopropanol and a UV/O_3 treatment. PEDOT:PSS [poly(3,4-ethylenedioxythiophene):poly(styrenesulfonic acid), Heraeus Clevios] was deposited by spin-coating, aiming at a layer thickness of ~30 nm. Afterwards, processing was continued under nitrogen atmosphere in a glove box (<1 ppm O_2/H_2O), starting off with an annealing step at 130 °C for 15 min to remove any residual water. Subsequently, the active layer **SM1**:$PC_{71}BM$ (1:1) ([6,6]-phenyl-

C_{71}-butyric acid methyl ester; Solenne) blend was spin-coated from either chloroform (CF) or chlorobenzene (CB) as the processing solvent. The total concentrations were taken to be 16 and 32 mg/mL for the CF and CB based solutions, respectively. In a final step, devices with an active device area of 3 mm² were obtained by evaporation of Ca and Al as top electrodes with thicknesses of 30 and 80 nm, respectively. The *I*-*V* characteristics of the resulting photovoltaic devices were evaluated under AM1.5G solar illumination (100 mW cm^{-2}) using a Newport class A solar simulator (model 91195A), calibrated with a silicon solar cell.

5.5. REFERENCES

1. (*a*) Service, R. F. *Science* **2011**, *332*, 293; (*b*) Walker, B.; Kim, C.; Nguyen, T. Q. *Chem. Mater.* **2011**, *23*, 470; (*c*) Mishra, A.; P. Bäuerle, P. *Angew. Chem. Int. Ed.* **2012**, *51*, 2020; (*d*) Lin, Y.; Li, Y.; Zhan, X. *Chem. Soc. Rev.* **2012**, *41*, 4245; (*e*) Chen, Y.; Wan, X.; Long, G. *Acc. Chem. Res.* **2013**, *46*, 2645; (*f*) Roncali, J.; Leriche, P.; Blanchard, P. *Adv. Mater.* **2014**, *26*, 3821.

2. (*a*) Sun, Y.; Welch, G. C.; Leong, W. L.; Takacs, C. J.; Bazan, G. C.; Heeger, A. J. *Nat. Mater.* **2011**, *11*, 44; (*b*) Zhou, J.; Wan, X.; Liu, Y.; Zuo, Y.; Li, Z.; He, G.; Long, G.; Ni, W.; Li, W.; Su, X.; Chen, Y. *J. Am. Chem. Soc*. **2012**, *134*, 16345; (*c*) Kyaw, A. K. K.; Wang, D. H.; Wynands, D.; Zhang, J.; Nguyen, T.-Q.; Bazan, G. C.; Heeger, A. J. *Nano Lett.* **2013**, *13*, 3796; (*d*) Zhou, J.; Zuo, Y.; Wan, X.; Long, G.; Zhang, Q.; Ni, W.; Liu, W.; Li, Z.; He, G.; Li, C.; Kan, B.; Li, M.; Chen, Y. *J. Am. Chem. Soc*. **2013**, *135*, 8484; (*e*) Liu, Y.; Yang, Y.; Chen, C.-C.; Chen, Q.; Dou, L.; Hong, Z.; Li, G.; Yang, Y. *Adv. Mater.* **2013**, *25*, 4657; (*f*) Liu, D.; Xiao, M.; Du, Z.; Yan, Y.; Han, L.; Roy, V. A. L.; Sun, M.; Zhu, W.; Lee, C. S.; Yang, R. *J. Mater. Chem. C* **2014**, *2*, 7523; (*g*) Qin, H.; Li, L.; Guo, F.; Su, S.; Peng, J.; Cao, Y.; Peng, X. *Energy Environ. Sci.* **2014**, *7*, 1397; (*h*) Kan, B.; Li, M.; Zhang, Q.; Liu, F.; Wan, X.; Wang, Y.; Ni, W.; Long, G.; Yang, X.; Feng, H.; Zuo, Y.; Zhang, M.; Huang, F.; Cao, Y.; Russell, T. P.; Chen, Y. *J. Am. Chem. Soc.* **2015**, *137*, 3886.

3. Bevk, D.; Marin, L.; Lutsen, L.; Vanderzande, D.; Maes, W. *RSC Adv.* **2013**, *3*, 11418.

4. TzTz-based donor polymers: (*a*) Osaka, I.; Saito, M.; Koganezawa, T.; Tamikiya, K. *Adv. Mater*. **2012**, *24*, 425; (*b*) Van Mierloo, S.; Kesters, J.; Hadipour, A.; Spijkman, M.-J.; Van den Brande, N.; D'Haen, J.; Van Assche, G.;

de Leeuw, D. M.; Aernouts, T.; Manca, J.; Lutsen, L.; Vanderzande, D.; Maes, W. *Chem. Mater.* **2012**, *24*, 587; (*c*) Shoaee, S.; Subramaniyan, S.; Xin, H.; Keiderling, C.; Tuladhar, P. S.; Jamieson, F.; Jenekhe, S. A.; Durrant, J. R. *Adv. Funct. Mater.* **2013**, *23*, 3286; (*d*) Osaka, I.; Saito, M.; Koganezawa, T.; Takimiya, K. *Adv. Mater.* **2014**, *26*, 331; (*e*) Subramaniyan, S.; Xin, H.; Sunjoo, F.; Murari, N. M.; Courtright, B. A. E.; Jenekhe, S. A. *Macromolecules* **2014**, *47*, 4199; (*f*) Helgesen, M.; Carlé, J. E.; dos Reis Benatto, G. A.; Søndergaard, R. R.; Jørgensen, M.; Bundgaard, E.; Krebs, F. C. *Adv. Energy Mater.* **2015**, 1401996.

5. TzTz-based small molecule donor compounds: (*a*) Shi, Q.; Cheng, P.; Li, Y.; Zhan, X. *Adv. Energy Mater*. **2012**, *2*, 63; (*b*) Dutta, P.; Park, H.; Lee, W-H.; Kang, I-N.; Lee, S-H. *Org. Electron.* **2012**, *13*, 3183; (*c*) Cheng, P., Shi, Q.; Lin, Y.; Li, Y.; Zhan, X. *Org. Electron.* **2013**, *14*, 599; (*d*) Dessi, A.; Consiglio, B. G.; Calamante, M.; Zani, L. *Eur. J. Org. Chem.* **2013**, *10*, 1916; (*e*) Chen, Y.; Du, Z.; Chen, W.; Wen, S.; Sun, L.; Liu, Q.; Sun, M.; Yang, R. *New J. Chem.* **2014**, *38*, 1559.

6. (*a*) Vasseur, K.; Van den Brande, N.; Boyukbayram, A. E.; Ruttens, B.; Rodriguez, S.; Botek, E.; Liégeois, V.; D'Haen, J.; Adriaensens, P. J.; Heremans, P.; Champagne, B.; Van Assche, G.; Lutsen, L.; Vanderzande, D. J.; Maes, W. *ChemPlusChem* **2012**, *77*, 923; (*b*) Nevil, N.; Ling, Y.; Van Mierloo, S.; Kesters, J.; Piersimoni, F.; Adriaensens, P.; Lutsen, L.; Vanderzande, D. J.; Maes, W. Manca, J.; Van Doorslaer, S.; Goovaerts, E. *Phys. Chem. Chem. Phys.* **2012**, *14*, 15774; (*c*) Kesters, J.; Ghoos, T.; Penxten, H.; Drijkoningen, J.; Vangerven, T.; Lyons, D. M.; Verreet, B.; Aernouts, T.; Lutsen, L.; Vanderzande, D.; Manca, J.; Maes, W. *Adv. Energy Mater.* **2013**, *3*, 1180.

7. Kudrjasova, J.; Herckens, R.; Penxten, H.; Adriaensens, P.; Lutsen, L.; Vanderzande, D.; Maes, W. *Org. Biomol. Chem.* **2014**, *12*, 4663.

8. (*a*) Goldoni, F.; Janssen, R. A. J.; Meijer, E. W. *J. Polym. Sci., Part A: Polym. Chem.* **1999**, *37*, 4629; (b) Roncali, J. *Macromol. Rapid Commun.* **2007**, *28*, 1761; (*c*) Jeeva, S.; Lukoyanova, O.; Karas, A.; Davand, A.; Rosei, F.; Perepichka, D. F. *Adv. Funct. Mater.* **2010**, *20*, 1661.

9. (*a*) Guo, X.; Quinn, J.; Chen, Z.; Usta, H.; Zheng, Y.; Xia, Y.; Hennek, J. W.; Ortiz, R. P.; Marks, T. J.; Facchetti, A. *J. Am. Chem. Soc.* **2013**, *135*, 1986; (*b*) Liu, Y.; Dong, H.; Jiang, S.; Zhao, G.; Shi, Q.; Tan, J.; Jiang, L.; Hu, W.; Zhan, X. *Chem. Mater.* **2013**, *25*, 2649; (c) Nanos, J. I.; Kampf, J. W.; Curtis, M. D. *Chem. Mater.* **1995**, *7*, 2232.

10. Johnson, J. R.; Ketcham, R. *J. Am. Chem. Soc.* **1960**, *82*, 2719.

11. Wong, W.-Y.; Wang, X.-Z.; He, Z.; Chan, K.-K.; Djurišić, A. B.; Cheung, K.-Y.; Yip, C.-T.; Ng, A. M.-C.; Xi, Y.-Y.; Mak, C. S.-K.; Chan, W.-K. *J. Am. Chem. Soc.* **2007**, *129*, 14372.

12. Jang, S.-Y.; Lim, B.; Yu, B.-K.; Kim, J.; Baeg, K.-J.; Khim, K.-Y.; Kim, D.-Y. *J. Mater. Chem.* **2011**, *21*, 11822.

13. (*a*) Facchetti, A. *Mater Today* **2013**, *16*, 123; (*b*) Lin, Y.; Zhan, X. *Mater. Horiz.* **2014**, *1*, 470; (*c*) Eftaiha, A. F.; Sun, J.-P.; Hill, I. G.; Welch, G. C. *J. Mater. Chem. A* **2014**, *2*, 120.

14. (*a*) Danley, R. L.; Caulfield, P. A.; Aubuchon, S. R. *Am. Lab.* **2008**, *40*, 9; (*b*) Ghoos, T.; Van den Brande, N.; Defour, M.; Brassinne, J.; Fustin, C.-A.; Gohy, J.-F.; Hoeppener, S.; Schubert, U. S.; Vanormelingen, W.; Lutsen, L.; Vanderzande, D. J.; Van Mele, B.; Maes, W. *Eur. Polym. J.* **2014**, *53*, 206.

15. (*a*) Bard, J.; Faulkner, L. R. *Electrochemical methods: fundamentals and applications*, 2nd Ed., 2001, Wiley; (*b*) Trasatti, S. *Pure Appl. Chem.* **1986**, *58*, 95.

5.6. SUPPORTING INFORMATION

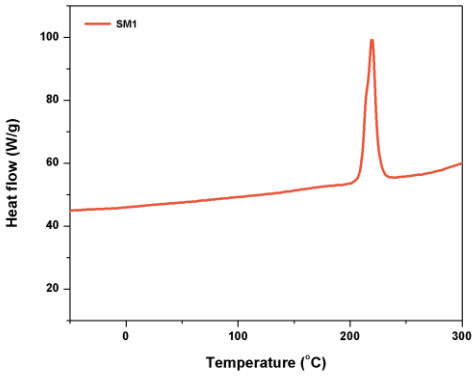

Fig. S1. RHC profile of **SM1** (second heating curve).

MALDI-TOF mass spectra

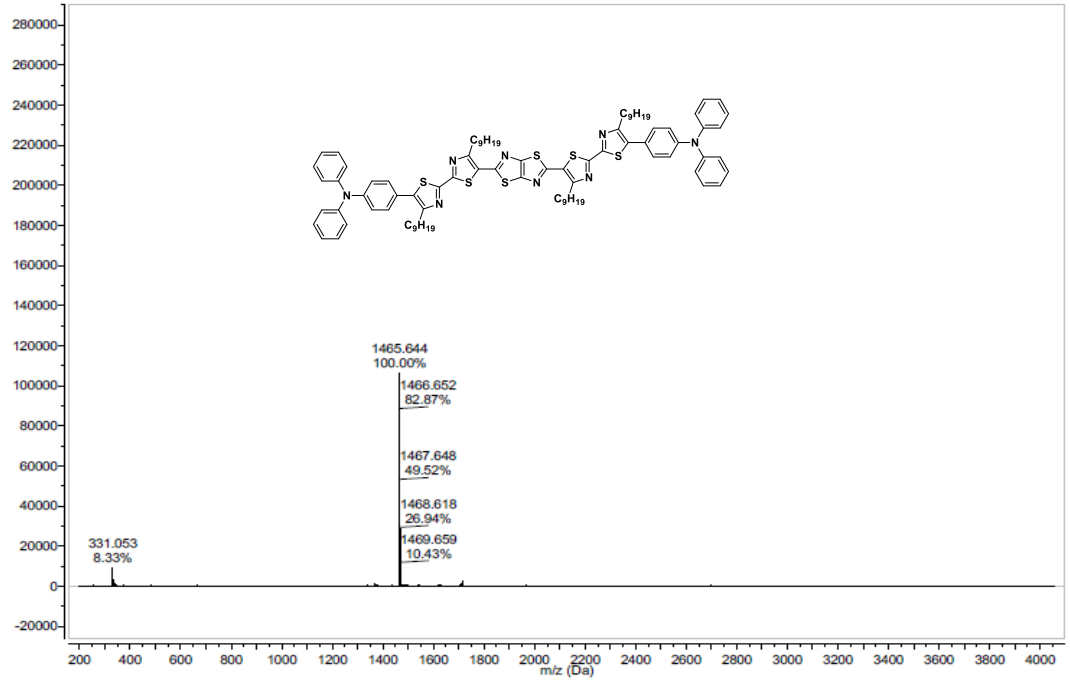

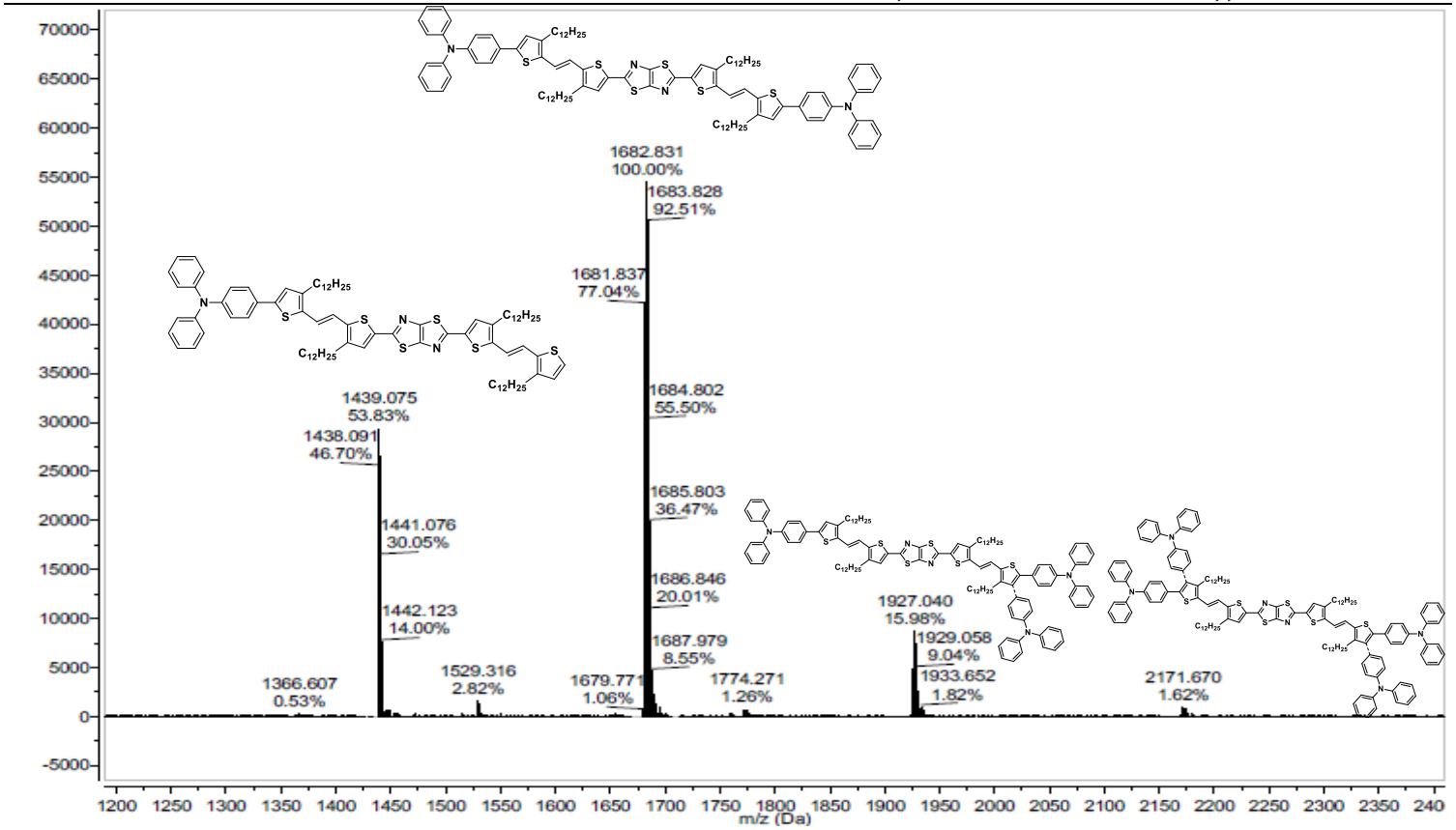
1682.831
100.00%
1683.828
92.51%
1681.837
77.04%
1684.802
55.50%
1439.075
53.83%
1438.091
46.70%
1685.803
36.47%
1441.076
30.05%
1686.846
20.01%
1442.123
14.00%
1687.979
8.55%
1927.040
15.98%
1929.058
9.04%
1933.652
1.82%
1366.607
0.53%
1529.316
2.82%
1679.771
1.06%
1774.271
1.26%
2171.670
1.62%
m/z (Da)

NMR spectra ($^{1}H/^{13}C$) of SM1

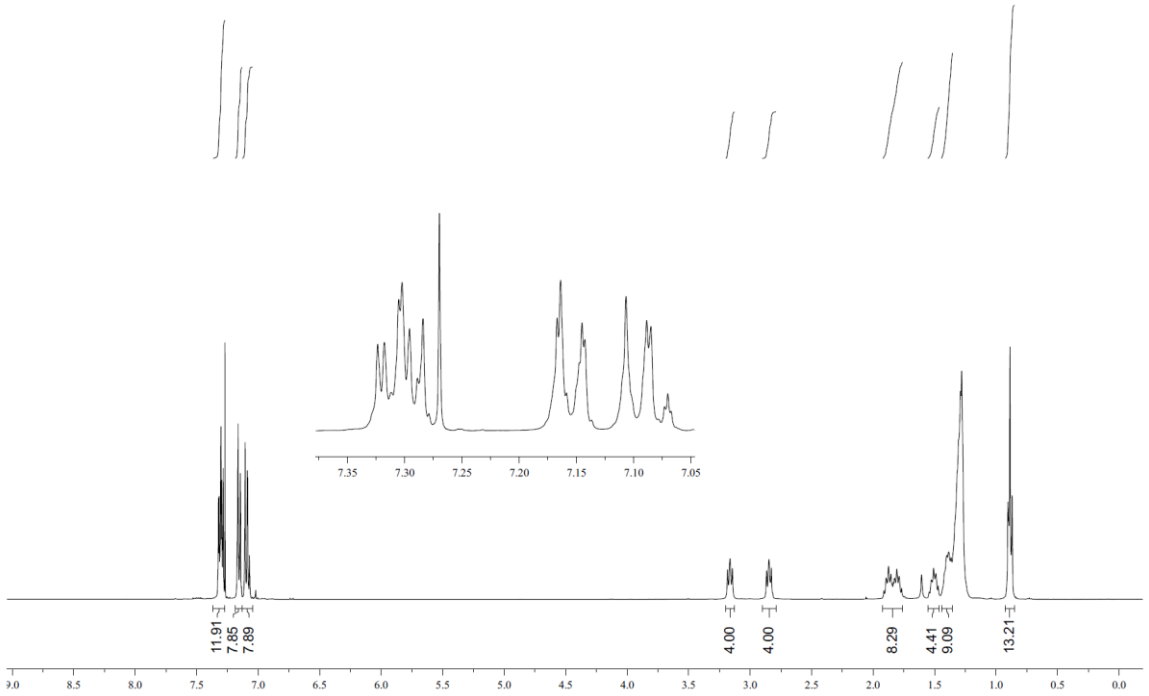

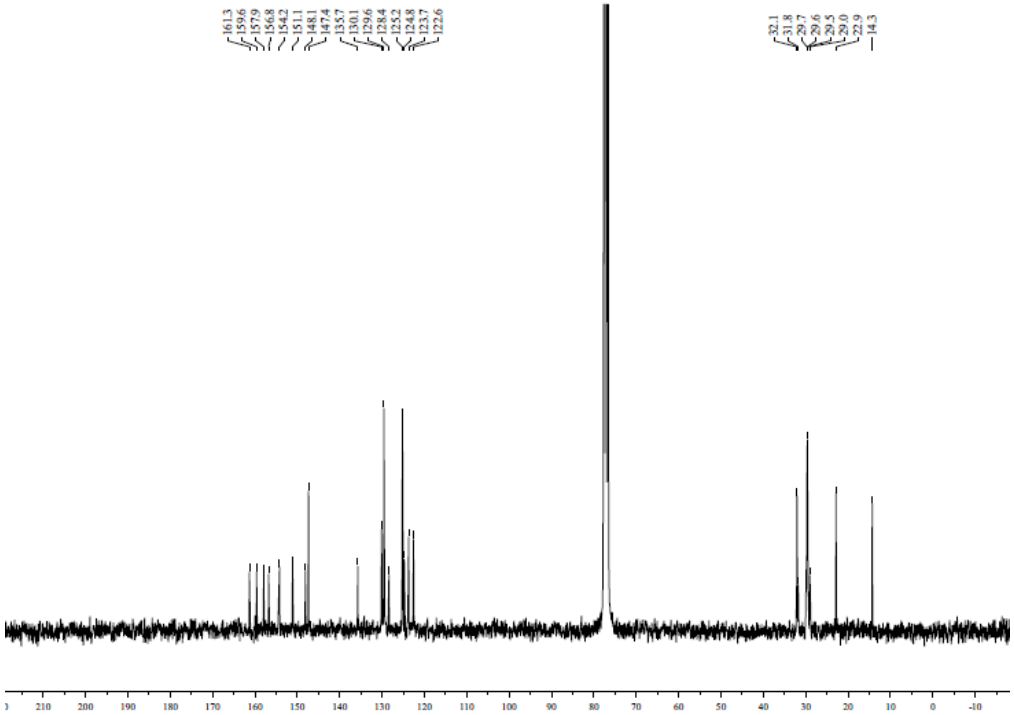
161.3
159.6
157.9
156.8
154.2
151.1
148.1
147.4
135.7
130.1
129.6
128.4
125.2
124.8
123.7
122.6
32.1
31.8
29.7
29.6
29.5
29.0
22.9
14.3
210
200
190
180
170
160
150
140
130
120
110
100
90
80
70
60
50
40
30
20
10
0
-10

Chapter 6

Quinoxaline-based cyclo(oligophenylenes)

Marin, L.; Kudrjasova, J.; Verstappen, P.; Penxten, H.; Robeyns, K.; Lutsen, L.; Vanderzande, D.; Maes, W., *J. Org. Chem.* **2015**, *80*, 2425–2430

(Article contribution: part of synthesis and chemical analysis, article writing and revision)

ABSTRACT

A series of fully conjugated quinoxaline-based oligophenylene macrocycles is synthesized by Ni^0-mediated Yamamoto-type diaryl homocoupling of (fluorinated) 2,3-bis(4'-bromophenyl)quinoxaline precursors. Cyclotrimers and cyclotetramers are obtained as the dominant reaction products. The cyclooligomers are fully characterized, including single-crystal X-ray structures, and their optoelectronic properties are analyzed toward possible applications in host-guest chemistry and organic electronics.

6.1. INTRODUCTION

Advanced 'shape-persistent' macrocyclic compounds built from rigid (aromatic) building blocks, interconnected in such a way that the final structure cannot collapse, have been widely explored in the last couple of years.[1] Among these, fully π-conjugated carbon nanorings composed of 1,4-connected phenyl units – known as [*n*]CPPs (cycloparaphenylenes), with *n* denoting the number of phenyl rings in the macrocycle – are of particular interest for optoelectronic applications and host-guest chemistry (e.g. fullerene binding).[2] Since their electro-optical and supramolecular (assembly) properties are strongly dependent on the size (of the cavity), continuous synthetic efforts have focused on variation and control over the diameter of the 'carbon nano-hoops'. [*n*]CPPs represent the shortest sidewall segment of armchair carbon nanotubes and can serve as a scaffold for the controlled growth of fully sp^2-hybridized carbon structures. For this reason, ways of expanding and interconnecting CPP units, for instance by arene bridges, are also actively pursued.[3] On the other hand, the introduction of other (hetero)aryl moieties can strongly influence the shape of the macrocycles, the π-π stacking properties, the HOMO-LUMO energy levels, and the molecular interactions.[4] Additionally, when some of the (hetero)aromatic rings are interconnected via the ortho positions, the cavity loses its circular shape and adopts a triangular conformation (releasing significant ring strain).[5] Most fully conjugated macrocyclic systems present a significant synthetic challenge. Synthesis protocols toward cyclic oligophenylenes are generally based on transition metal-mediated cross-coupling reactions, e.g. reaction of aryl Grignard/lithium reagents with $CuCl_2$ or homocoupling of aryl halides by electron transfer oxidation of Lipshutz cuprates,

producing cyclic products with a varying degree of selectivity (over other macrocycles and open-chain analogues).[1-5]

Quinoxaline heterocycles have been applied on multiple occasions as versatile building blocks for the development of various types of macrocyclic molecular receptors[6] as well as new semiconducting materials,[7,8] introducing electron deficient character (via the imine units within the fused biheterocycle) and allowing structural fine-tuning (e.g. extension of the chromophoric system and introduction of solubilizing side chains via the 2,3-positions). Push-pull copolymers incorporating quinoxalines as the acceptor parts have recently afforded high power conversion efficiencies in organic solar cells (combined with fullerenes in the photoactive layer of so-called bulk heterojunction devices).[7] On the other hand, a quinoxaline-based poly(arylene ethynylene) copolymer was applied as a chemosensor for explosive detection, with high fluorescence quenching sensitivity toward TNT.[8]

6.2. RESULTS AND DISCUSSION

In this letter, we report on the synthesis and characterization of a small family of quinoxaline-based ortho/para-linked nona- and dodecaphenylene macrocycles via Ni^0-mediated cyclooligomerization of 4'-bromophenyl-functionalized quinoxaline precursors. The quinoxaline heterocycles introduce π-acceptor character in the regular cyclic oligophenylene framework. The 'monomers' **Qx1**-**3** used in these transformations were prepared in high yields (79–94%) by acid-mediated condensation between 1,2-bis(4'-bromophenyl)ethane-1,2-dione (**1**) and the corresponding diamines (**A1**-**3**) (Scheme 1).[9] The introduction of fluorine atoms in positions 6 and/or 7 of the quinoxaline core is used as a (proof-of-concept) tool

for fine-tuning the energy levels[7e,10] and allows further elaboration of the final cyclooligomers by nucleophilic aromatic substitution (S_NAr) reactions.[11]

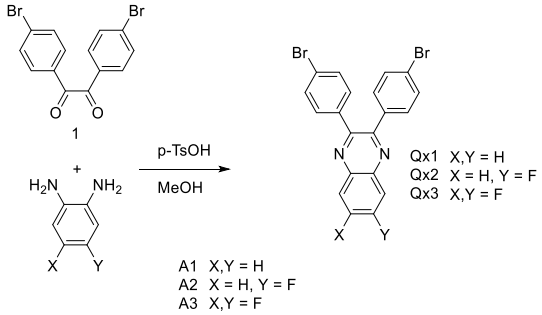

Scheme 1. Synthesis of quinoxaline monomers **Qx1-3**.

At the monomer stage, the presence of the bromine atoms in the para positions of the 2,3-phenyl groups allows to use these derivatives in Ni^0-mediated transformations (less toxic and less expensive than the Pd variants), resulting in the formation of new C-C bonds. Yamamoto homocoupling of quinoxaline monomers **Qx1-3** can give rise to cyclic structures and/or polymeric materials.[3c,5c,12] At first, **Qx1** was treated with $Ni(cod)_2$ (in the presence of 2,2'-bipyridine and 1,5-cyclooctadiene) in DMF/toluene and reacted for three days at 95 °C (slightly modified compared to the standard conditions used for Ni^0-mediated polymerizations[3c,5c,9,12]). The resulting crude material was purified by preparative size exclusion chromatography (prep-SEC). Cyclotrimer **CT3-1** (related to the regular *o*,*p*,*p*,*o*,*p*,*p*,*o*,*p*,*p*-nonaphenylene[5a,b]) was isolated as the major product in 35% yield, as analyzed by NMR and HRMS analysis (see SI), together with a smaller amount of the analogous cyclotetramer **CT4-1** in 13% yield, pointing to a bias for the reaction to produce the smallest achievable macrocycles (Scheme 2). The SEC profile of the crude reaction mixture showed that the formation of (cyclo)oligomers and/or polymers with molar masses

superior to 1000 Da was modest (Figure S1). Additionally, the monomer seemed to be completely consumed in the transformation. Initial confusion between cyclodimers and cyclotetramers (caused by the appearance of *m*/2 signals in the HRMS spectra, see SI) was countered by the prep-SEC results, the second products being 'larger' (in hydrodynamic volume) than the cyclotrimers (i.e. eluting first). Final confirmation was obtained by X-ray single-crystal analysis (*vide infra*).

The simple and concise synthetic protocol was then extended to fluorinated monomers **Qx2** and **Qx3**, affording similar results (Scheme 2). All macrocycles were obtained in pure form and showed reasonable to good solubility (e.g. in chlorinated organic solvents) allowing full structural characterization (see SI). In an effort to increase the macrocycle yield, a high dilution protocol favoring intramolecular cyclization was applied. The obtained results were, however, similar (slightly inferior) to the original approach (28 and 7% yield of **CT3-1** and **CT4-1**, respectively).

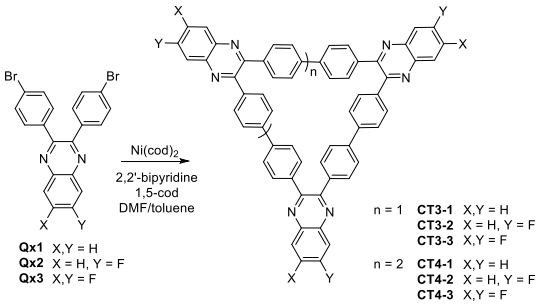

Scheme 2. Yamamoto cyclooligomerization protocol toward quinoxaline-based cyclic oligoarylenes.

Single crystals suitable for X-ray analysis were grown from $CHCl_3$ for **CT3-1** (Figure 1) and **CT4-3** (Figure 2), confirming the structures and illustrating the solid-state conformations.[13] The equilateral triangular structure of **CT3-1** has

sides of about 12.78 Å, as measured between the centroids of the pyrazine rings (Figure S8). The three quinoxaline moieties are situated in the same plane with a maximum deviation for C7 of 0.2027(26) Å from the plane calculated through all quinoxaline atoms (see Figure S7 for labeling scheme). The bridging phenyl rings are inclined and the angles between the quinoxaline plane and the phenyl rings are of the same order of magnitude for both phenyl rings attached to the same quinoxaline moiety (Q1-A: 51.57(7), Q1-B: 50.69(7); Q2-C: 88.36(8), Q2-D: 71.22(7); Q3-E: 43.57(8), Q3-F: 41.98(7)), showing that the rotation of one phenyl ring will have a cascade effect on the other. This is a direct result of steric hindrance and is less pronounced when the phenyl rings are nearly perpendicular as around Q2 (Figure 1). The angles between the phenyl rings belonging to the same diphenyl linker are 33.16(8)° (A-F) and 30.91(14)° (B-C), which is close to the average value of 31.5° found in the CSD for twisted non-conjugated diphenyls. The third diphenyl (D-E) residue has an internal angle of 12.24(13)°. The latter 'parallel' arrangement is a result of the crystal packing, as the D-E side of the triangle is in close contact (shortest distance 3.387 Å) with a neighboring D-E side through an inversion centre. This is accompanied by significant ring-overlap (offset stacking) for the flanking quinoxalines (Q1/Q3) with neighboring moieties (Figure S10).

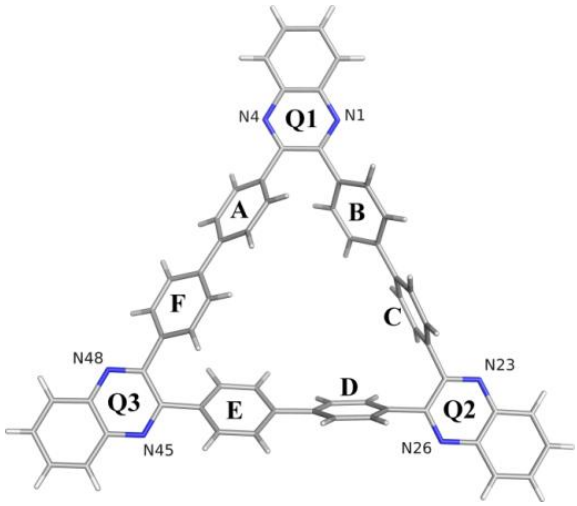

Figure 1. Stick representation of the X-ray structure of **CT3-1**, with labeling scheme for the quinoxaline (Q) and phenyl rings.

The **CT4-3** structure is not at all planar but shows a butterfly arrangement (Figure 2). As in the trigonal structure, the centroids of the pyrazine rings are separated by approximately the same distance, here on average 12.71 Å (Figure S9), which is to be expected with the linear diphenyl linker. Looking at the inclination of the phenyl rings with respect to the quinoxaline moieties one can see that – contrary to the triangular structure, where angles of the same order of magnitude were observed around the quinoxaline unit – similar inclinations are observed between two adjacent quinoxaline rings Q1-B: 51.67(24), Q2-C: 51.35(25); Q2-D: 38.88(32), Q3-E: 41.85(33); Q3-F: 52.03(25), Q4-G: 44.55(32); Q4-H: 42.44(26), Q1-A: 31.24(42). All internal diphenyl angles are similar (46.04(29)° (B-C), 40.43(24)° (D-E), 44.30(38)° (F-G) and 39,83(44)° (H-A)). The crystal packing shows that the residues are found around a two-fold screw axis, where the tetramers cradle 180° rotated residues that are stacked upon each other (Figure S11). One might consider π-stacking interactions between Q1 and Q3

within a stack, but the ring overlap is not as pronounced as seen in the triangular structure.

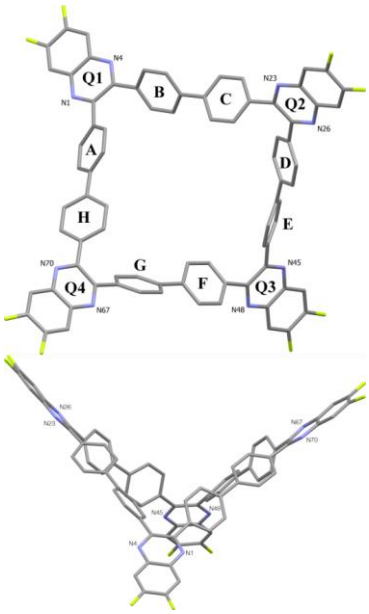

Figure 2. Stick representation of the X-ray structure of **CT4-3**, with labeling scheme for the quinoxaline (Q) and phenyl rings.

To judge their appropriateness for applications in organic electronics (notably photovoltaics and light-emitting diodes), the optical and electrochemical properties of the macrocycles were analyzed (Table 1).

Table 1. Optical and electrochemical properties of the synthesized cyclooligomers.

Cpd.	$\lambda_{max,abs}$ (nm)	log ε (x 10^3)	$\lambda_{max,PL}$ (nm)	ΔE_{opt}[a]	τ (ns)[b]	Φ_F	E^{ox}_{onset} (eV)	E_{HOMO} (eV)	E^{red}_{onset} (eV)	E_{LUMO} (eV)	ΔE_{ec} (eV)[c]	$E_{LUMO,calcd}$ (eV)[d]
CT3-1	281/366	4.757/4.639	424	2.98	0.53	0.44	1.53	-6.50	-1.96	-3.00	3.49	-3.52
CT3-2	280/369	4.923/4.822	427	2.97	0.62	0.52	1.55	-6.52	-1.85	-3.12	3.39	-3.55
CT3-3	280/369	4.936/4.866	428	2.99	0.67	0.61	1.59	-6.55	-1.84	-3.13	3.42	-3.56
CT4-1	297/366	4.985/4.939	420	2.97	0.31	0.22	1.39	-6.36	-1.87	-3.10	3.26	-3.39
CT4-2	298/375	4.949/4.966	424	2.97	0.49	0.41	1.47	-6.43	-1.83	-3.13	3.30	-3.46
CT4-3	285/370	5.134/5.162	425	2.99	0.60	0.44	1.48	-6.44	-1.78	-3.18	3.26	-3.45

[a] Optical HOMO-LUMO gap (film). [b] Fluorescence lifetime. [c] Electrochemical HOMO-LUMO gap. [d] $E_{LUMO,calcd} = E_{HOMO} + \Delta E_{opt}$.

The absorption features (Figure 3) are barely different within both cyclooligomer series (similar λ_{max} values and an evident increase in molar absorptivity for the cyclotetramers). The emission maxima (blue emission centered at ~ 425 nm, red-shifted with respect to the regular cyclic nona- and dodecaphenylenes[5b]), are also quite similar (Figure 3), but there is a noticeable increase in fluorescence quantum yield (and concomitant excited state lifetime) upon fluorination, up to an appreciable value of Φ_F = 0.61 for **CT3-3**. Fluorescence quantum yields are somewhat lower for the cyclotetramers. Compared to regular cyclic oligophenylenes, the quinoxaline-based macrocycles have more π-acceptor character, as can be seen from the HOMO/LUMO values (based on the oxidation/reduction onset potentials as determined by cyclic voltammetry). The presence of the fluorine atoms has a small influence on the frontier orbital energy levels, lowering both the HOMO and LUMO energies.[7e,10] The cyclotetramers are oxidized somewhat easier,[2,5b] leading to slightly reduced electrochemical bandgaps.

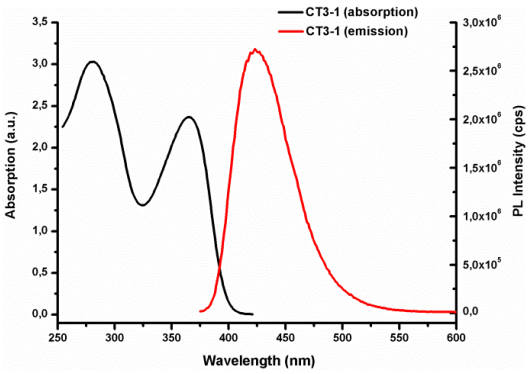

Figure 3. Absorption and emission spectra (in $CHCl_3$) of **CT3-1**.

6.3. CONCLUSIONS

In summary, triangular and butterfly-shaped fully π-conjugated cyclic oligophenylenes were readily prepared by a straightforward Ni-mediated biaryl coupling protocol employing suitably functionalized quinoxaline precursor molecules. These derivatives – after proper extension of the conjugated system and/or variation of the substitution pattern – can be regarded as attractive (complexity-building) molecular platforms toward sophisticated organic architectures applicable in materials science, e.g. organic electronics, self-assembly and nanostructure formation, size-selective supramolecular chemistry (fullerene complexation[2g,5d,14] or explosive detection[5b,8]), surface patterning[15] and conjugated organic frameworks[16].

6.4. ACKNOWLEDGMENTS

The authors thank Hasselt University for continuous financial support and BELSPO for supporting the IAP 7/05 network. The reported activity is also supported by the INTERREG project ORGANEXT (EMR. INT4-1.2.-2009-04/054, Euregio Maas-Rijn). We further acknowledge Hercules for providing the funding for the LTQ Orbitrap Velos Pro mass spectrometer.

6.5. REFERENCES

(1) (a) Zhang, W.; Moore, J. S. *Angew. Chem. Int. Ed.* **2006**, *45*, 4416. (b) Höger, S. *Pure Appl. Chem.* **2010**, *82*, 821. (c) Iyoda, M.; Yamakawa, J.; Rahman, M. J. *Angew. Chem. Int. Ed.* **2011**, *50*, 10522.

(2) (a) Jasti, R.; Bhattacharjee, J.; Neaton, J. B.; Bertozzi, C. R. *J. Am. Chem. Soc.* **2008**, *130*, 17646. (b) Yamago, S.; Watanabe, Y.; Iwamoto, T. *Angew. Chem. Int. Ed.* **2010**, *49*, 757. (c) Segawa, Y.; Miyamoto, S.; Omachi, H.; Matsuura, S.; Šenel, P.; Sasamori, T.; Tokitoh, N.; Itami, K. *Angew. Chem. Int. Ed.* **2011**, *50*, 3244. (d) Sisto, T. J.; Golder, M. R.; Hirst, E. S.; Jasti, R. *J. Am. Chem. Soc.* **2011**, *133*, 15800. (e) Kayahara, E.; Sakamoto, Y.; Suzuki, T.; Yamago, S. *Org. Lett.* **2012**, *14*, 3284. (f) Xia, J.; Jasti, R. *Angew. Chem. Int. Ed.* **2012**, *51*, 2474. (g) Hirst, E. S.; Jasti, R. *J. Org. Chem.* **2012**, *77*, 10374.

(3) (a) Xia, J.; Golder, M. R.; Foster, M. E.; Wong, B. M.; Jasti, R. *J. Am. Chem. Soc.* **2012**, *134*, 19709. (b) Sisto, T. J.; Tian, X.; Jasti, R. *J. Org. Chem.* **2012**, *77*, 5857. (c) Nishiuchi, T.; Feng, X.; Enkelmann, V.; Wagner, M.; Müllen, K. *Chem. Eur. J.* **2012**, *18*, 16621.

(4) (a) Iyoda, M.; Kondo, T.; Nakao, K.; Hara, K.; Kuwatani, Y.; Yoshida, M.; Matsuyama, H. *Org. Lett.* **2000**, *2*, 2081. (b) Maier, S. K.; Jester, S.-S.; Müller, U.; Müller, W. M.; Höger, S. *Chem. Commun.* **2011**, *47*, 11023. (c) Matsui, K.; Segawa, Y.; Itami, K. *Org. Lett.* **2012**, *14*, 1888. (d) Yang, F.; Wang, Z.; Song, F.; Liu, X.; Lan, J.; You, J. *Chem. Commun.* **2013**, *49*, 5975.

(5) (a) Meyer, H.; Staab, H. A. *Liebigs Ann. Chem.* **1969**, *724*, 30. (b) Rahman, M. J.; Yamakawa, J.; Matsumoto, A.; Enozawa, H.; Nishinaga, T.; Kamada, K.; Iyoda, M. *J. Org. Chem.* **2008**, *73*, 5542. (c) Schwab, M. G.; Qin, T.; Pisula, W.; Mavrinskiy, A.; Feng, X.; Baumgarten, M.; Kim, H.; Laquai, F.; Schuh, S.; Trattnig, R.; List, E. J. W.; Müllen, K. *Chem. Asian J.* **2011**, *6*, 3001. (d) Rahman, M. J.; Shimizu, H.; Araki, Y.; Ikeda, H.; Iyoda, M. *Chem. Commun.* **2013**, *49*, 9251.

(6) (a) Sessler, J. L.; Maeda, H.; Mizuno, T.; Lynch, V. M.; Furuta, H. *J. Am. Chem. Soc.* **2002**, *124*, 13474. (b) Azov, V. A.; Beeby, A.; Cacciarini, M.; Cheetham, A. G.; Diederich, F.; Frei, M.; Gimzewski, J. K.; Gramlich, V.; Hecht, B.; Jaun, B.; Latychevskaia, T.; Lieb, A.; Lill, Y.; Marotti, F.; Schlegel, A.; Schlittler, R. R.; Skinner, P. J.; Seiler, P.; Yamakoshi, Y. *Adv. Funct. Mater.* **2006**, *16*, 147.

(7) (a) Champion, R. D.; Cheng, K.-F.; Pai, C.-L.; Chen, W.-C.; Jenekhe, S. A. *Macromol. Rapid Commun.* **2005**, *26*, 1835. (b) Wang, E.; Hou, L.; Wang, Z.; Hellström, S.; Zhang, F.; Inganäs, O.; Andersson, M. R. *Adv. Mater.* **2010**, *22*, 5240. (c) Chang, D. W.; Lee, H. J.; Kim, J. H.; Park, S. Y.; Park, S.-M.; Dai, L.; Baek, J.-B. *Org. Lett.* **2011**, *13*, 3880. (d) Zhang, X.; Shim, J. W.; Tiwari, S. P.; Zhang, Q.; Norton, J. E.; Wu, P.-T.; Barlow, S.; Jenekhe, S. A.; Kippelen, B.; Brédas, J.-L.; Marder, S. R. *J. Mater. Chem.* **2011**, *21*, 4971. (e) Zhuang, W.; Zhen, H.; Kroon, R.; Tang, Z.; Hellström, S.; Hou, L.; Wang, E.; Gedefaw, D.; Inganäs, O.; Zhang, F.; Andersson, M. R. *J. Mater. Chem. A* **2013**, *1*, 13422. (f) Wang, K.; Zhang, Z.-G.; Fu, Q.; Li, Y. *Macromol. Chem. Phys.* **2014**, *215*, 597.

(8) Chen, S.; Zhang, Q.; Zhang, J.; Gu, J.; Zhang, L. *Sens. Actuators B* **2010**, *149*, 155.

(9) Marin, L.; Lutsen, L.; Vanderzande, D.; Maes, W. *Org. Biomol. Chem.* **2013**, *11*, 5866.

(10) (a) Albrecht, S.; Janietz, S.; Schindler, W.; Frisch, J.; Kurpiers, J.; Kniepert, J.; Inal, S.; Pingel, P.; Fostiropoulos, K.; Koch, N.; Neher, D. *J. Am. Chem. Soc.* **2012**, *134*, 14932. (b) Liu, P.; Zhang, K.; Liu, F.; Jin, Y.; Liu, S.; Russell, T. P.; Yip, H.-L.; Huang, F.; Cao, Y. *Chem. Mater.* **2014**, *26*, 3009.

(11) (a) Charushin, V. N.; Mokrushina, G. A.; Tkachev, A. V. *J. Fluor. Chem.* **2001**, *107*, 71. (b) Zhang, L.; Qiu, B.; Li, X.; Wang, X.; Li, J.; Zhang, Y.; Liu, J.; Li, J.; Shen, J. *Molecules* **2006**, *11*, 988.

(12) (a) Yamamoto, T.; Morita, A.; Miyazaki, Y.; Maruyama, T.; Wakayama, H.; Zhou, Z. H.; Nakamura, Y.; Kanbara, T.; Sasaki, S.; Kubota, K. *Macromolecules* **1992**, *25*, 1214. (b) Yamamoto, T.; Sugiyama, K.; Kushida, T.; Inoue, T.; Kanbara, T. *J. Am. Chem. Soc.* **1996**, *118*, 3930. (c) Zoombelt, A. P.; Fonrodona, M.; Wienk, M. M.; Sieval, A. B.; Hummelen, J. C.; Janssen, R. A. J. *Org. Lett.* **2009**, *11*, 903.

(13) Crystallographic data (excluding structure factors) have been deposited with the Cambridge Crystallographic Data Centre; deposition no. CCDC-1018570-1018571. These data can be obtained free of charge from the Cambridge Crystallographic Data Centre, 12 Union Rd., Cambridge CB2 1EZ, UK, by fax: +44(0)-1223-336033, or by e-mail: deposit@ccdc.cam.ac.uk.

(14) Van Rossom, W.; Kundrát, O.; Ngo, T. H.; Lhoták, P.; Dehaen, W.; Maes, W. *Tetrahedron Lett.* **2010**, *51*, 2423.

(15) Mössinger, D.; Chaudhuri, D.; Kudernac, T.; Lei, S.; De Feyter, S.; Lupton, J. M.; Höger, S. *J. Am. Chem. Soc.* **2010**, *132*, 1410.

(16) Guo, J.; Xu, Y.; Jin, S.; Chen, L.; Kaji, T.; Honsho, Y.; Addicoat, M. A.; Kim, J.; Saeki, A.; Ihee, H.; Seki, S.; Irle, S.; Hiramoto, M.; Gao, J.; Jiang, D. *Nat. Commun.* **2013**, *4*, 2736.

6.6. SUPPORTING INFORMATION

6.6.1. General experimental methods

Preparative size exclusion chromatography (prep-SEC) was performed on JAIGEL *1H* and *2H* columns attached to an LC system equipped with a UV detector (path 0.5 mm) and a switch for recycling and collecting the eluent ($CHCl_3$; flow rate 3.5 mL min^{-1}, injection volume 3 mL). NMR chemical shifts (δ, in ppm) were determined relative to the residual $CHCl_3$ absorption (7.26 ppm) or the ^{13}C resonance shift of $CDCl_3$ (77.16 ppm). ^{13}C signals split up by *J*-coupling with ^{19}F are indicated by their chemical shifts (with the observed signals between brackets). For the ^{19}F NMR spectra, the chemical shift scale was calibrated relative to trifluorotoluene (-63.72 ppm). Both proton coupled and decoupled ^{19}F NMR spectra were recorded. 2D short- and long-range HETeronuclear chemical-shift CORrelation experiments were performed to elucidate directly-bonded proton-carbon and two- and three-bonds proton-carbon connectivities, respectively. High resolution ESI-MS (electrospray ionization - mass spectrometry) was performed using a mass spectrometer equipped with an atmospheric pressure ionization source operating in the nebulizer assisted electrospray mode. The instrument was calibrated in the *m/z* range 220−2000 using a standard solution containing caffeine, MRFA and Ultramark 1621. MALDI-TOF mass spectra were obtained using DTCB (*trans*-2-[3-(4-*tert*-butylphenyl)-2-methyl-2-propenylidene]-malononitrile) as a matrix (matrix and analyte solutions in $CHCl_3$). Solid-state FTIR spectra were recorded in transmission mode. Background-corrected UV-vis absorption spectra were recorded using a band width of 1 and 2 nm for solution and film measurements, respectively. The molar absorption coefficients were estimated by linear regression of the absorbances as a function of concentration

of at least 5 solutions of different concentrations. Lamp corrected steady-state emission spectra for quantum yield determination were recorded on a fluorimeter using a band pass of 1 nm for the excitation monochromator and a scanning speed of 1 nm/s. Spectra were collected at rt at an excitation wavelength of 363 nm for all samples (without deoxygenation). The quantum yields were estimated from the absorbance and emission spectra of at least 5 solutions in chloroform with absorbance values lower than 0.1 at the absorption maximum. 9,10-Diphenylanthracene in cyclohexane was used as a quantum yield standard (Φ_F = 0.90).[1] The quantum yield values were corrected for refractive index variation between the solvents used for the sample and standard solutions. Fluorescence lifetime measurements in the frequency domain were performed versus a Ludox (colloidal silica) scattering solution in water. Modulation frequencies ranged between 10 and 250 Hz. For cyclic voltammetry, a three-electrode microcell setup was used with Ag/Ag^+ as a reference electrode (Ag wire dipped in a solution containing 0.01 M $AgNO_3$ in 0.1 M NBu_4PF_6 prepared in anhydrous acetonitrile), a Pt wire working electrode and a Pt wire counter electrode. The reference electrode was calibrated against the ferrocene/ferrocenium (Fc/Fc^+) redox couple. A solution containing 0.1 M NBu_4PF_6 in anhydrous acetonitrile (anhydrous CH_2Cl_2 for the solution measurements) was used as supporting electrolyte. To remove oxygen, the electrolyte solution was purged with Ar for at least 2 min prior to the experiments. The experiments were carried out under a curtain of Ar to prevent atmospheric gases from dissolving back into the solution during the measurements. For the film measurements, the products to be analyzed were deposited onto the working electrode from chloroform solutions. Cyclic voltammograms were recorded at a scan rate of 100 mV s^{-1}. The HOMO and LUMO energy levels of the products were determined using the CV data. For the

conversion of V to eV, the onset potentials of the first oxidation/reduction peaks were used and referenced to ferrocene/ferrocenium, which has an ionization potential of -4.98 eV *vs.* vacuum. This correction factor is based on a value of 0.31 eV for Fc/Fc^+ *vs.* SCE[2] and a value of 4.68 eV for SCE *vs.* vacuum[3]: $E_{HOMO/LUMO}$ (eV) = $-4.98 - E_{onset\ ox/red}^{Ag/AgNO3}$ (V) + $E_{onset\ Fc/Fc+}^{\ Ag/AgNO3}$ (V). Alternatively, the LUMO energy levels were calculated as the difference between the HOMO values and the optical HOMO-LUMO gaps. To estimate the optical HOMO-LUMO gaps, the wavelength at the intersection of the tangent line drawn at the low energy side of the UV-vis solid-state absorption spectrum with the x-axis was used (in the formula E_g (eV) = 1240/wavelength (nm)).

6.6.2. SEC profiles and ESI/MALDI-TOF mass spectra for the crude cyclooligomerization reaction mixtures

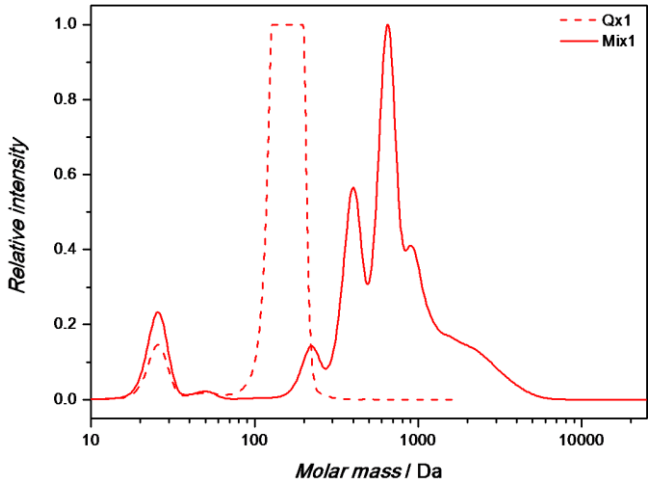

Figure S1. SEC profiles of monomer **Qx1** and the corresponding crude cyclooligomerization mixture.

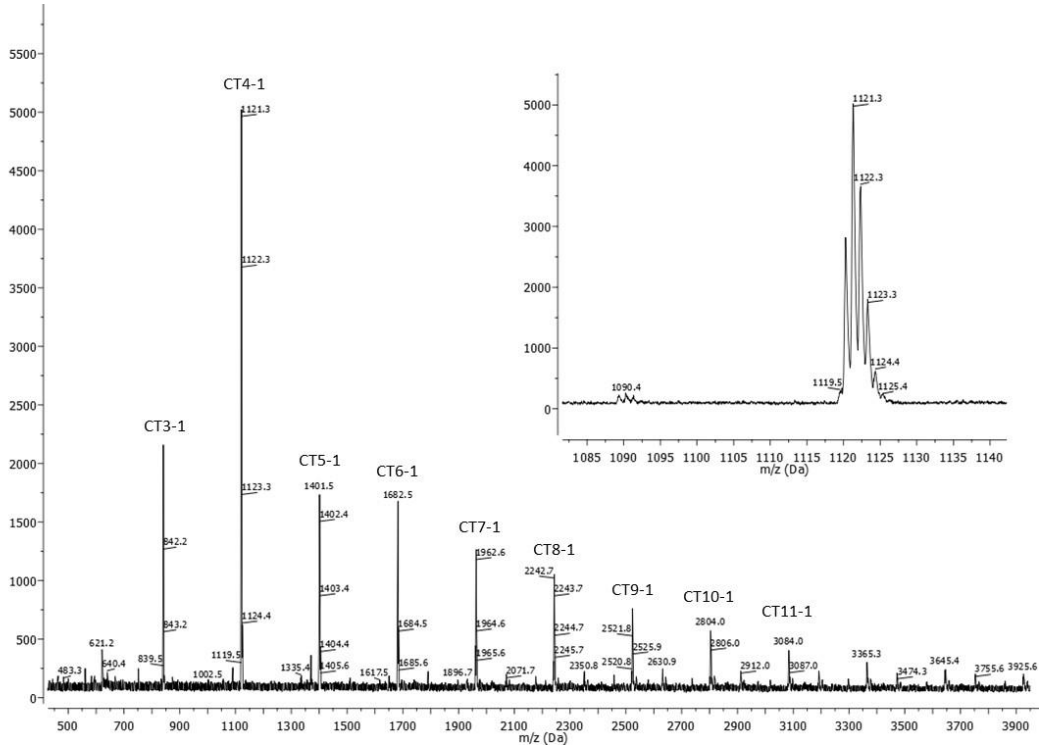

Figure S2. MALDI-TOF mass spectrum of the crude reaction mixture starting from **Qx1** (with the cyclotetramer in the inset).

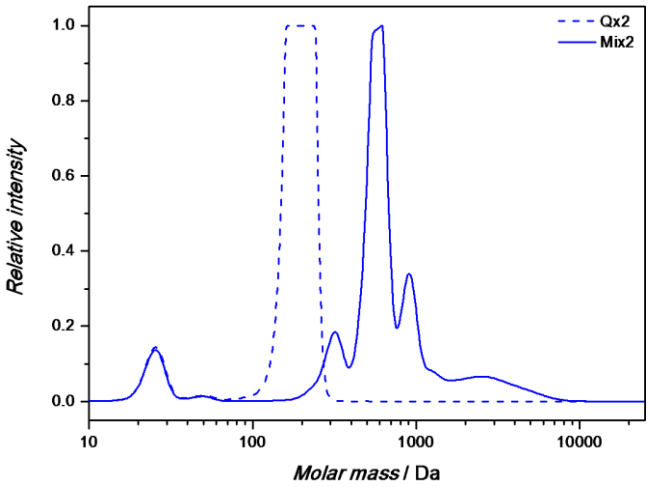

Figure S3. SEC profiles of monomer **Qx2** and the corresponding crude cyclooligomerization mixture.

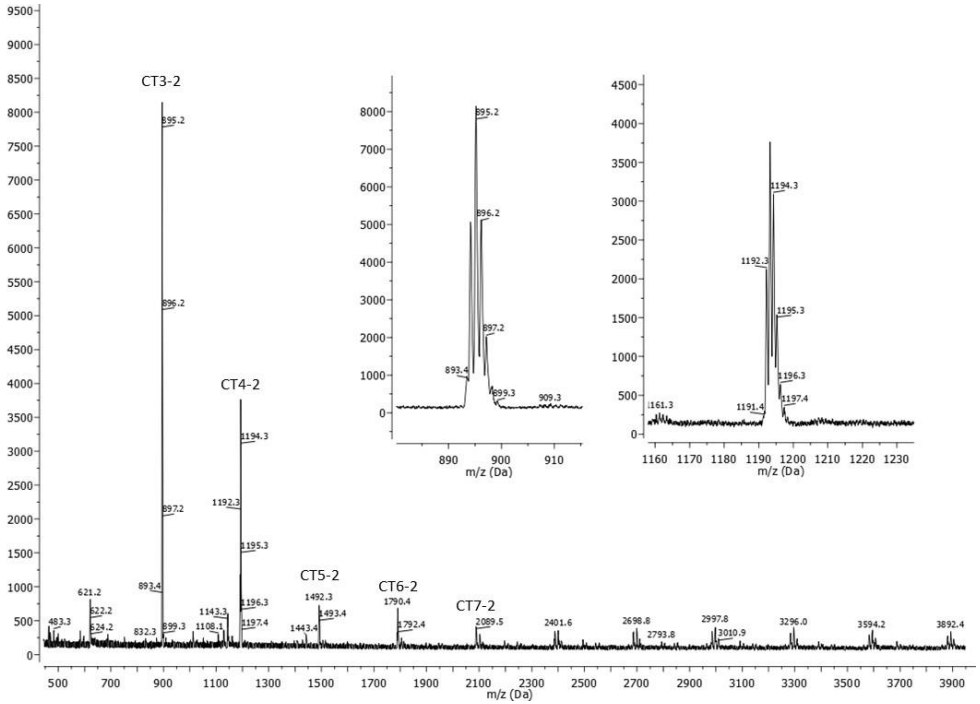

Figure S4. MALDI-TOF mass spectrum of the crude reaction mixture starting from **Qx2** (with the cyclotrimer and cyclotetramer in the inset).

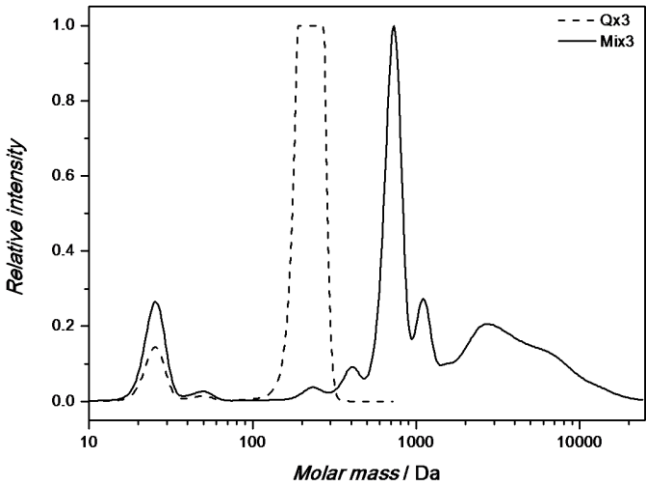

Figure S5. SEC profiles of monomer **Qx3** and the corresponding crude cyclooligomerization mixture.

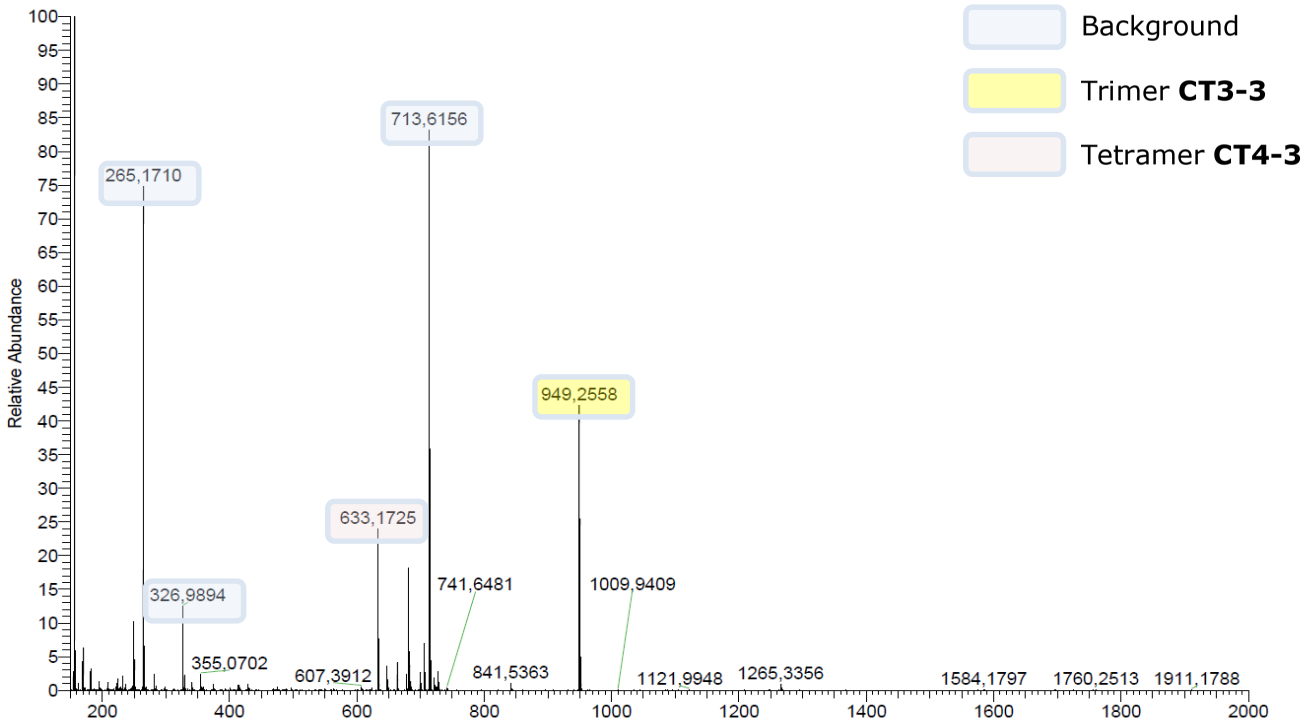

Figure S6. ESI-MS spectrum of the crude reaction mixture starting from **Qx3**.

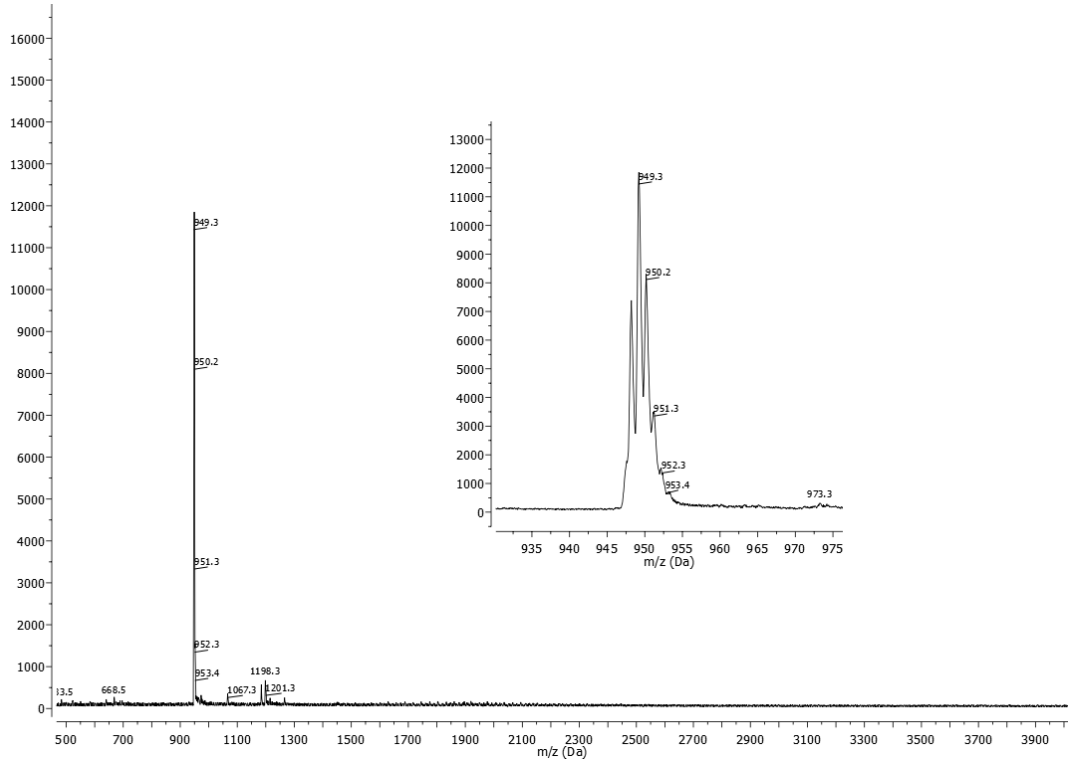

Figure S7. MALDI-TOF mass spectrum of **CT3-3**.

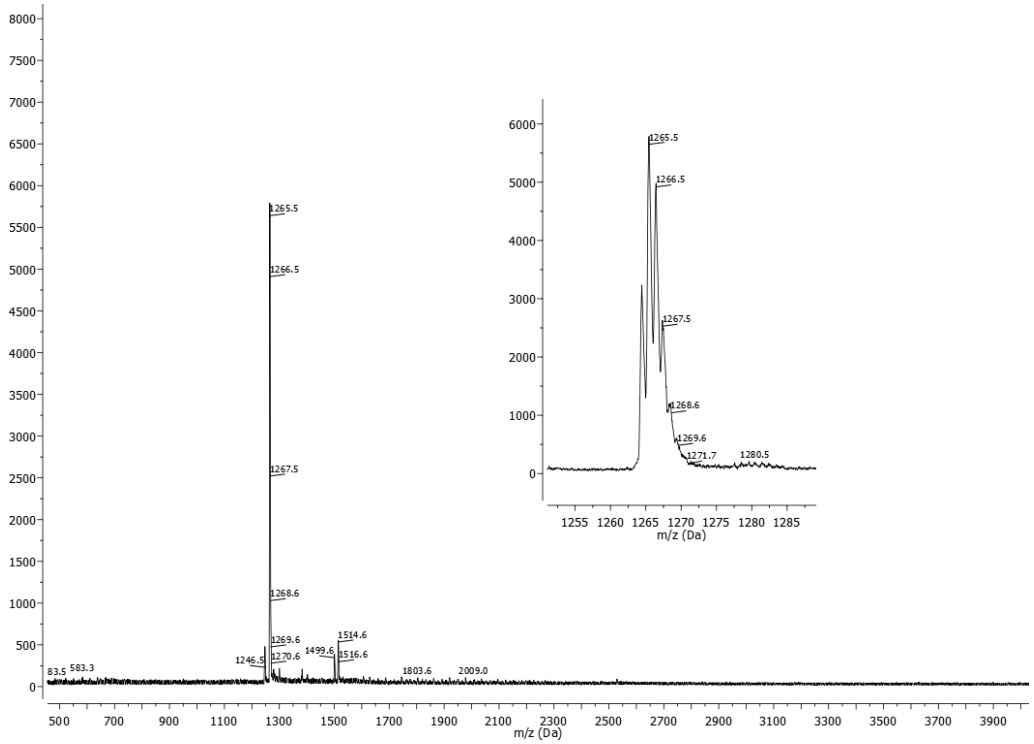

Figure S8. MALDI-TOF mass spectrum of **CT4-3**.

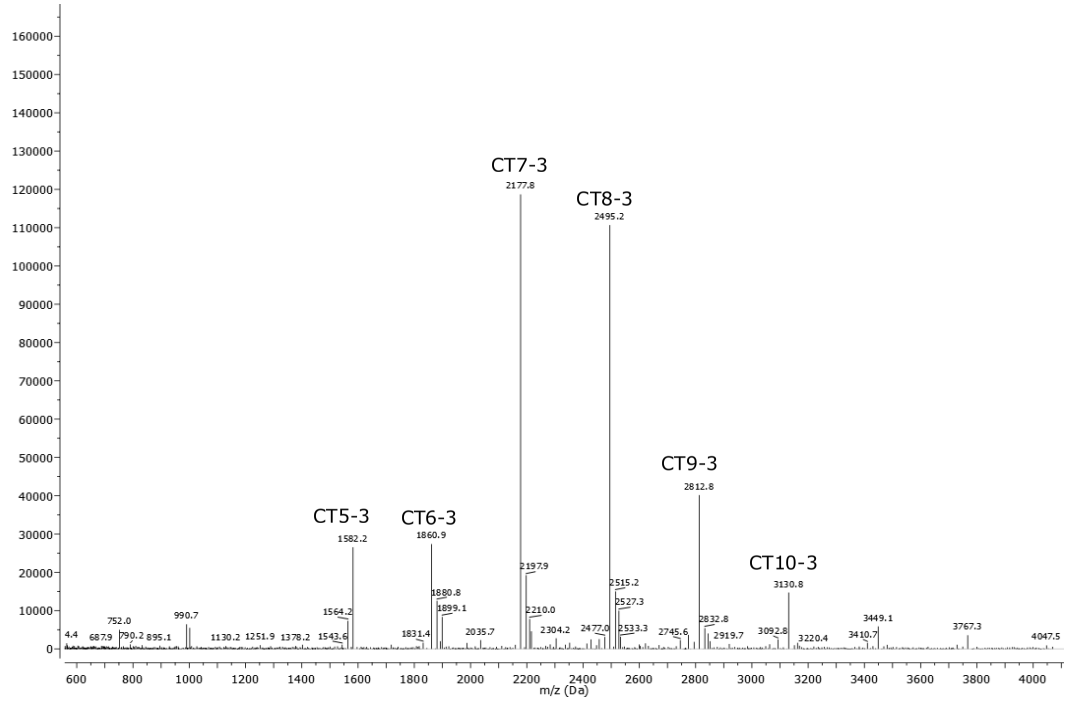

Figure S9. MALDI-TOF mass spectrum of the higher cyclooligomer fraction after purification of the crude reaction mixture starting from **Qx3**.

6.6.3. Cyclic voltammograms for the cyclotrimers/tetramers

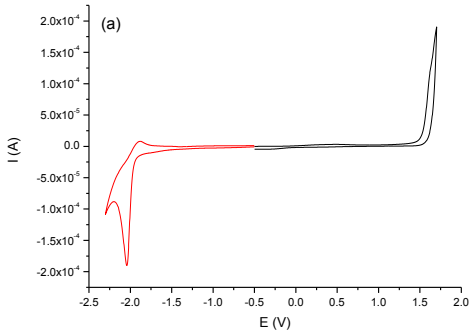

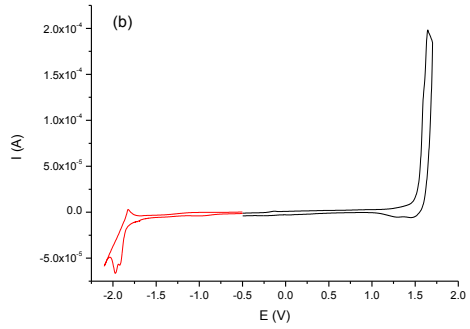

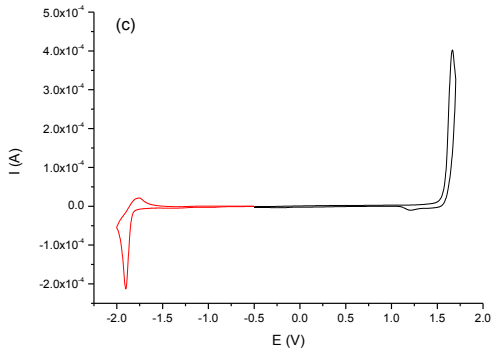

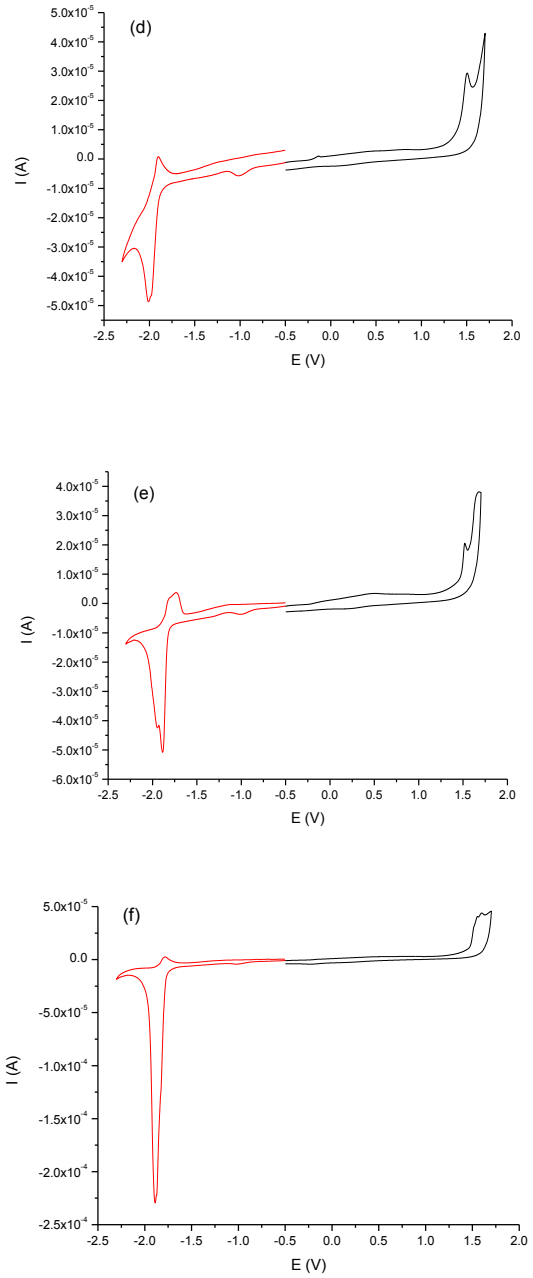

Figure S10. Cyclic voltammograms showing the oxidation and reduction of thin films of (a) **CT3-1**, (b) **CT3-2**, (c) **CT3-3**, (d) **CT4-1**, (e) **CT4-2** and (f) **CT4-3** (scan rate 100 mV sec^{-1}).

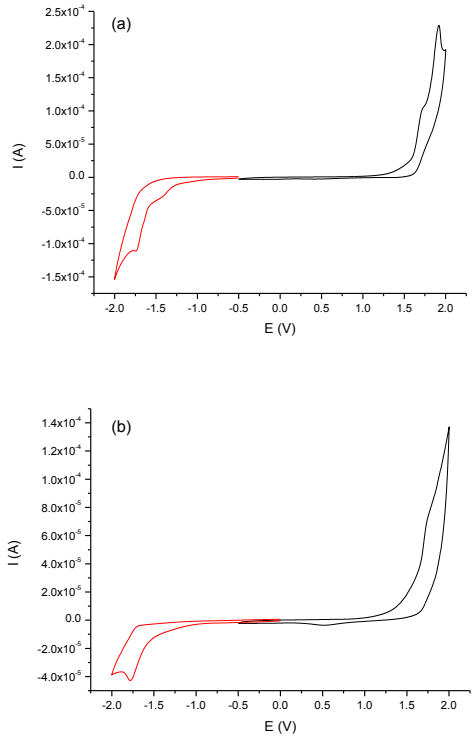

Figure S11. Cyclic voltammograms showing the oxidation and reduction of (a) **CT3-3** and (b) **CT4-3** in dichloromethane solution (scan rate 100 mV sec^{-1}).

Table S1. Electrochemical properties of **CT3-3** and **CT4-3** in solution (CH_2Cl_2).

Compd	ΔE_{opt}[a]	E^{ox}_{onset} (eV)	E_{HOMO} (eV)	E^{red}_{onset} (eV)	E_{LUMO} (eV)	ΔE_{ec} (eV)[b]	$E_{LUMO,calcd}$ (eV)[c]
CT3-3	3.08	1.58	-6.42	-1.65	-3.20	3.22	-3.34
CT4-3	3.10	1.57	-6.41	-1.67	-3.17	3.24	-3.31

[a] Optical HOMO-LUMO gap (in solution). [b] Electrochemical HOMO-LUMO gap. [c] $E_{LUMO,calcd} = E_{HOMO} + \Delta E_{opt}$.

6.6.4. Additional X-ray data and figures

Single crystals of **CT3-1** (CCDC-1018570) and **CT4-3** (CCDC-1018571) were obtained by slow evaporation of chloroform solutions of the macrocycles. A suitable crystal was selected and mounted on a loop using a little grease. The crystal was flash-frozen at 150 K prior to the diffraction experiment. Data collection was done on a MAR345 image plate using Mo Kα radiation (Rigaku Ultra X18S rotating anode, Xenocs fox3d mirror).

Both structures were solved by direct methods (SHELXS97) and refined by full-matrix least squares on $|F^2|$ (SHELXL97).[4] Non-hydrogen atoms were anisotropically refined and the hydrogen atoms were placed on calculated positions with temperature factors fixed at 1.2 times Ueq of the parent atoms.

For cyclotrimer **CT3-1** a total of two datasets (phi-scan) were recorded on the same crystal at two different orientations (the second dataset was only measured to increase the overall completeness of the data; final completeness 95.2% to 0.83 Å). The datasets were integrated by the Crysalis software[5] and a multiscan absorption correction was performed using the integrated scale3 abspack procedure on each separate dataset (R_{int} dataset 1: 0.086, R_{int} dataset 2: 0.055). Both were scaled not merged using xprep (R_{int}: 0.0704). The crystallographic data are listed in Table S2.

Crystals of cyclotetramer **CT4-3** showed limited diffraction and a data cut-off was imposed at 1.3 Å during the integration step in Crysalis. During the refinement, the phenyl rings of the linkers were constrained as ideal hexagons and rigid bond restraints were applied to all carbon atoms. For the $CHCl_3$ solvent molecules, rigid bond restraints on all atoms within one molecule were applied in combination with isotropic restraints on the Cl atoms, as they showed tendency for rotational disorder (two of the three $CHCl_3$ molecules were refined in two parts with for both

a refined occupancy of 57 and 43%). It should be noted that only global features of the structure are accurate (i.e. connectivity, angles between rings, …), and finer details, such as individual bond lengths or angles, should not be compared due the lower data quality. The crystallographic data for **CT4-3** are also listed in Table S2.

Figure S12 shows ORTEP representations of both structures.

Table S2. Crystallographic data for **CT3-1** and **CT4-3**.

	Cyclotrimer **CT3-1**	Cyclotetramer **CT4-3**
Formula	$C_{60}H_{36}N_6$, 3($CHCl_3$)	$C_{80}H_{40}F_8N_8$, 3($CHCl_3$)
M (g mol^{-1})	1199.05	1623.30
crystal dimensions (mm^3)	0.30x0.18x0.12	0.15x0.12x0.08
crystal system	Triclinic	Monoclinic
space group	P -1	P 2_1/n
a (Å)	13.7108(19)	19.293(3)
b (Å)	13.7888(13)	10.8085(10)
c (Å)	17.7891(15)	36.754(7)
a (deg)	89.424(7)	90
β (deg)	70.125(10)	104.829(19)
g (deg)	62.429(12)	90
V (Å^3)	2759.5(5)	7409.2(19)
Z	2	4
ρ_{calc} (g cm^{-3})	1.443	1.455
$2\theta_{max}$ (deg)	50.48	31.84
λ (Å)	0.71073 MoKa	0.71073 MoKa
F(000)	1224	
T (K)	150(2)	150(2)
measured reflections	40034	9539
unique reflections	9622	3437
observed reflections ($I_o > 2\sigma(I_o)$)	7634	2263
parameters/restraints	703/0	422/903
R_1	0.0586	0.0893
ωR_2	0.1489	0.2268
R_1 (all data)	0.0748	0.1320
ωR_2 (all data)	0.1599	0.2592
GOOF	1.015	1.041
μ (mm^{-1})	0.505	0.413

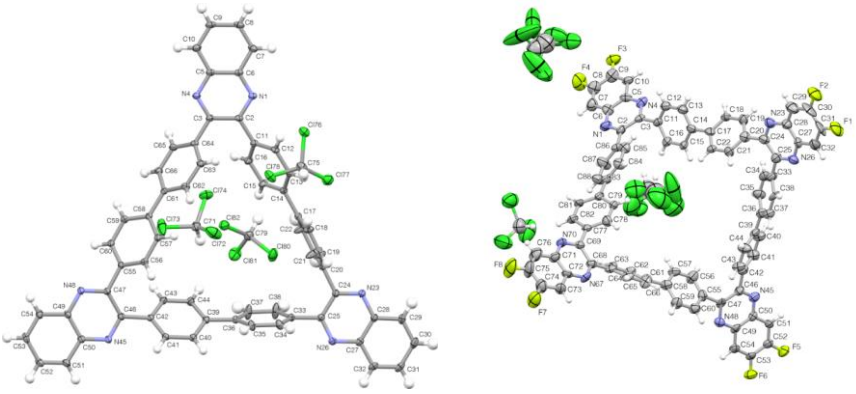

Figure S12. (top) Ortep representation of the X-ray structure of cyclotrimer **CT3-1**, with displacement ellipsoids drawn at the 50% probability level. The C79 chloroform molecule is situated above the plane of the triangle, whereas the C71 chloroform molecule is situated below. (bottom) Ortep representation of the X-ray structure of cyclotetramer **CT4-3**, with displacement ellipsoids drawn at the 50% probability level (labels for the solvent molecules are omitted for clarity).[6]

Figure S13 gives an indication of the size of the **CT3-1** molecular triangle, as well as an idea about the enclosed cavity, which is available for solvent molecules. The surface of the cyclotrimer is about 70.75 Å^2 (as measured between the centroids of the pyrazine rings). The enclosed cavity accessible for solvent molecules forms an equilateral triangle with average lengths of 8.624 Å, and is about 32.2 Å^2. These values are only approximate and do not completely take into account the Vanderwaals radii and/or the rotation of the phenyl rings.

Figure S14 gives a similar idea of the enclosed cavity for cyclotetramer **CT4-3**. Quinoxaline moieties Q2 and Q4 point upwards, Q1 and Q3 downwards, creating a butterfly-type conformation.

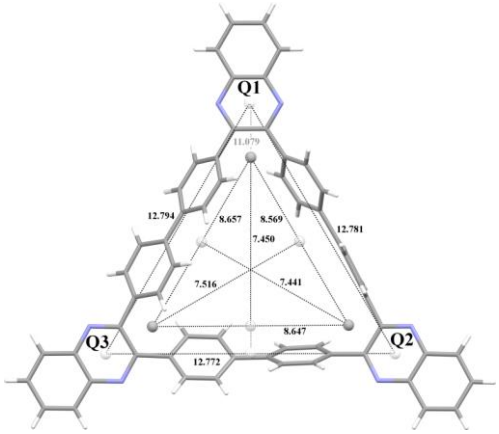

Figure S13. Stick representation of the X-ray structure of cyclotrimer **CT3-1**, with distance measurements (in Å) of the enclosed cavity.

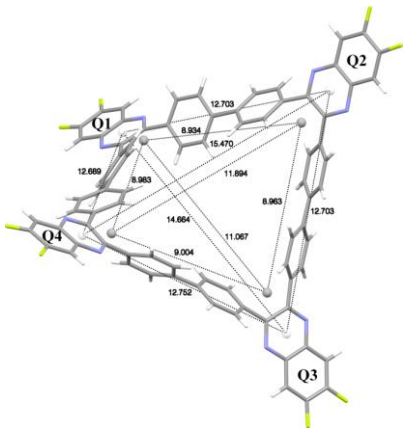

Figure S14. Stick representation of the X-ray structure of cyclotetramer **CT4-3**, with distance measurements (in Å) of the enclosed cavity.

The crystal packing for cyclotrimer **CT3-1** shows the presence of a $CHCl_3$ molecule on both sides of the triangle (see Figure S12). Furthermore, there is significant ring overlap between neighboring Q1 and Q3 quinoxaline moieties (Figure S15).

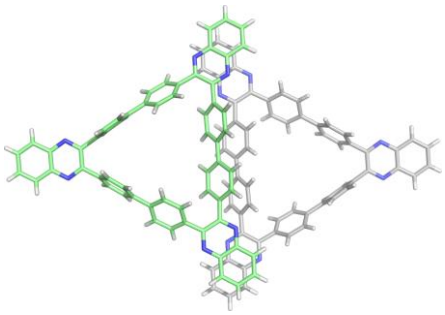

Figure S15. (top) Stick representation of two **CT3-1** cyclotrimers connected by an inversion center. Quinoxaline Q1 overlaps with Q3 and *vice versa* in an offset stacking arrangement. (bottom) Rotation around the vertical axis, with indication of the short contacts (the inversion center is shown as a red sphere).[7]

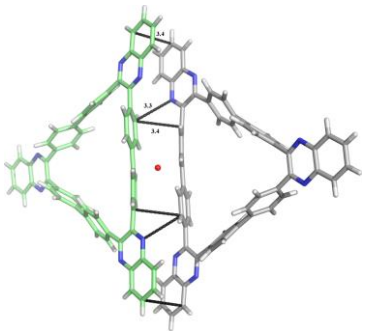

Figure S16 shows 3 adjacent **CT4-3** molecules within a stack. Some stabilizing π-stacking interactions might be observed between the Q1 and Q3 quinoxaline moieties, facing toward the reader.

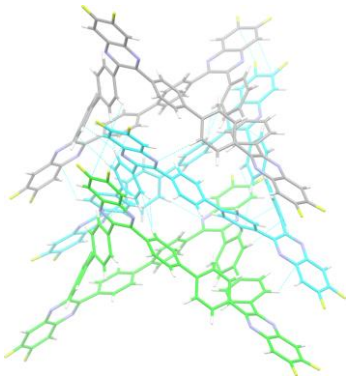

Figure S16. Stick representation of 3 adjacent **CT4-3** molecules within a stack, with custom carbon colors to be able to discriminate the different molecules. Short contacts are drawn as dashed bonds.

6.6.5. References

1. Hamai, S.; Hirayama, F. *J. Phys. Chem*. **1983**, *87*, 83.
2. Bard, J.; Faulkner, L. R. *Electrochemical methods: fundamentals and applications*, 2nd Ed., **2001**, Wiley.
3. Trasatti, S. *Pure Appl. Chem.* **1986**, *58*, 955.
4. Sheldrick, G. M. *Acta Crystallogr.* **2008**, *A64*, 112.
5. Agilent Technologies XRD (2010), Agilent Technologies, Xcalibur CCD system, CrysAlisPro Software system, Version 1.171.36.21.
6. Molecular figures created with Mercury: Macrae, C. F.; Bruno, I. J.; Chisholm, J. A.; Edgington, P. R.; McCabe, P.; Pidcock, E.; Rodriguez-Monge, L.; Taylor, R.; van de Streek, J.; Wood, P. A. *J. Appl. Cryst.* **2008**, *41*, 466.
7. Molecular figures created with PyMOL: The PyMOL Molecular Graphics System, Version 1.4.1 Schrödinger, LLC.

Chapter 7

Summary and outlook

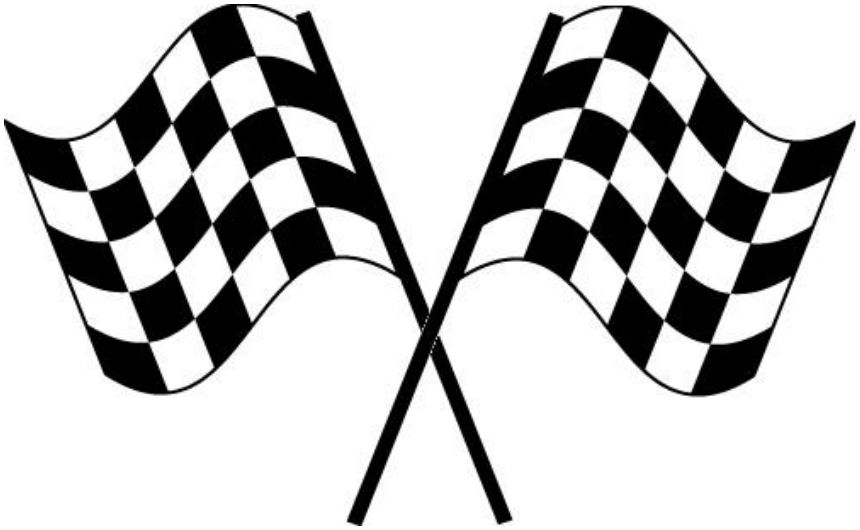

7.1. SUMMARY

Organic photovoltaics (OPV) are a promising technology for renewable energy production. Besides its esthetical and mechanical advantages compared to traditional solar cell technologies, the potential for low-cost high-throughput large area roll-to-roll manufacturing is of particular appeal. To foster further progress in the field, a predictive understanding of the relation between the chemical structure and physical properties of the applied organic semiconductors and the final device/module parameters is of critical importance and continuous research efforts in this direction are required. The development of new materials with advanced properties through modern and innovative synthetic routes (e.g. increasing the functional group tolerance) can certainly help to increase the probability that an economically viable technology and products can be realized. One such synthetic tool that could have a significant impact on organic semiconductor development is direct arylation (carbon−hydrogen bond activation and subsequent carbon−carbon bond formation). Direct functionalization of C–H bonds has emerged as an attractive alternative to the conventional cross-coupling methods due to its more sustainable character. In this PhD thesis, (hetero)arylation procedures have been developed for the synthesis of novel thiazolo[5,4-*d*]thiazole-based semiconducting materials to be applied as p or n-type small molecules in bulk heterojunction organic solar cells.

At the start, as outlined in **Chapter 2**, we have focused on the optimization of a microwave-assisted direct (hetero)arylation procedure of 2,5-dithienylthiazolo[5,4-*d*]thiazoles with different types of (hetero)aryl bromides. Once optimal conditions were found, new chromophores were easily prepared in high yields. Employing just one equivalent of the (hetero)arylbromide afforded

smooth access to monoarylated products as well, of which some were used for the consequent preparation of asymmetrical push-pull derivatives. The developed protocol allowed to obtain extended chromophores with tailor-made energy levels and absorption patterns depending on the introduced (hetero)aryl moieties and molecular (a)symmetry. In general, the diarylated molecules showed a broader absorption range and higher molar extinction coefficients. A selection of these materials was hence applied (as described in **Chapter 3**) as solution-processable photon-harvesting materials for bulk heterojunction organic photovoltaics, either as small molecule electron donor or acceptor constituents. For the donor-type compounds, high-bandgap OPV devices with high open-circuit voltages were realized, with a maximum power conversion efficiency of 2.7%. On the other hand, the most electron-poor TzTz was used as an alternative to the commonly applied fullerene acceptors. In combination with P3HT as an electron donor copolymer, a power conversion efficiency of 0.4% was achieved, mainly limited by the low short-circuit current.

Encouraged by these initial results, we then designed (see **Chapter 4**) a small series of extended TzTz-based 'second generation' molecular chromophores via a two-fold C-H arylation protocol. Employing a common mono-arylated TPA-T-TzTz-T precursor, three novel D'A'DADA'D'-type structures with different central acceptor units - a bithiazole (BiTz), diphenylquinoxaline (Qx) or isoindigo (II) derivative - were synthesized to be applied as small molecule electron donor components in bulk heterojunction organic solar cells. Unfortunately, rather modest yields (~30%) were obtained, resulting from the formation of (multiple) side products, clearly indicating the regioselectivity issues that can occur during C–H heteroarylation reactions. Best results were achieved for the TPA-T-TzTz-T-

Qx-T-TzTz-T-TPA material, providing a power conversion efficiency of 4.86% when blended with $PC_{71}BM$ in the photoactive layer.

Finally (**Chapter 5**), we also synthesized two novel D–π-A-π–D-type molecules with TzTz as an acceptor unit, triphenylamine (TPA) as the donor end group and two different π-bridging entities, bithiazole (BiTz) and thienylenevinylene (TV). Whereas the material containing the BiTz core was synthesized in a straightforward manner by successive Stille cross-coupling and direct heteroarylation reactions, the TV-containing small molecule could not be obtained in pure form (yet) due to the lack of C-H selectivity. Although a highly crystalline character was observed for the BiTz-based electron donor material, important to have a good charge carrier mobility, preliminary solar cell measurements afforded a moderate power conversion efficiency of 0.6%.

The final chapter (**Chapter 6**) stands a bit apart from the main thesis work since it is based on another electron-deficient heterocyclic system, quinoxaline, that is applied toward the synthesis of triangular and butterfly-shaped fully π-conjugated cyclic oligophenylenes through a straightforward Ni-mediated biaryl coupling protocol. Cyclotrimers and cyclotetramers were obtained as the dominant reaction products and they were fully characterized, including single-crystal X-ray structures. The optoelectronic properties were analyzed as well toward possible applications in host-guest chemistry and organic electronics.

7.2. OUTLOOK

In this PhD thesis we have focused on the design and synthesis of novel TzTz-based semiconducting materials via both traditional cross-coupling and novel direct coupling methods. Despite the satisfying results obtained, there are obviously a few items that deserve to be investigated to a further extent.

In **Chapter 3**, it has been demontrated that the synthesized small molecule semiconductors can be successfully applied as p-type materials in bulk heterojunction organic solar cells. However, n-type materials remain challenging and the efficiencies obtained so far were very low. Since the performance seems mainly limited by the short-circuit current, it would be worthwhile to investigate the charge transfer (state) and polaron formation to a further extent. Current efforts in collaboration with the group of Prof. E. Goovaerts (Universiteit Antwerpen) are oriented toward deepened understanding of the loss factors in our small molecule acceptor devices. Furthermore, synthesis of new n-type materials with deeper LUMO levels and broadened absorption profiles could also be beneficial.

The small molecules in **Chapter 4** were synthesized in moderate yields due to the formation of multiple side products. In this respect, dedicated optimization of the two-fold direct arylation conditions (catalyst, ligand and solvent) could be the easiest way to increase reaction yields and simplify purification. The power conversion efficiencies obtained are satisfactory, but further solar cell optimization studies are still required. Exploration of the thermal and photostability of the developed small molecules in OPV devices looks certainly worthwhile as well. Additionally, it would be of interest to test the small molecule with the lowest

LUMO value (**SM3**) as an acceptor material, also in combination with novel low bandgap copolymers.

In **Chapter 5**, preliminary solar cell results were demonstrated for **SM1** as a donor component. However, more elaborate solar cell optimization is still required. Additionally, small molecule **SM1** could probably also be used as an acceptor material. Due to the lack of regioselectivity, direct arylation turned out to be not very suitable for the synthesis of **SM2**. Therefore, an alternative (Stille cross-coupling) method should be developed.

7.3. NEDERLANDSE SAMENVATTING

Organic photovoltaics (OPV) vormen een interessante technologie voor de productie van hernieuwbare energie. Naast de esthetische en mechanische voordelen geassocieerd aan OPV is zeker ook het potentieel voor productie op grote schaal en grote oppervlakken via allerlei (*roll-to-roll*) printtechnieken erg aantrekkelijk. Om verdere vooruitgang in het domein te stimuleren is een (voorspellend) begrip van de relatie tussen de chemische structuur en fysicochemische eigenschappen van de gebruikte organische halfgeleiders van groot belang. Verder fundamenteel onderzoek in deze richting is dus zeker nog vereist. De ontwikkeling van nieuwe materialen met geavanceerde eigenschappen via moderne en innovatieve syntheseprotocols (bv. ter verhoging van de functionele groep tolerantie) kan zeker helpen om de doelstellingen – een verhoging van de kans op een economisch rendabele OPV-technologie en producten – te realiseren. Een synthetische *tool* die een voorname impact kan hebben op de ontwikkeling van organische halfgeleiders is de zogenaamde 'directe arylering' (activering van een koolstof−waterstof binding en daaropvolgende vorming van een koolstof−koolstof binding). Directe functionalisatie van (geactiveerde) C–H bindingen vormt een aantrekkelijk alternatief voor de conventionele *cross-coupling* methoden omwille van het meer economisch en milieuvriendelijk karakter. In deze doctoraatsthesis zijn synthetische (hetero)aryleringsprocedures ontwikkeld voor de aanmaak van nieuwe thiazool[5,4-*d*]thiazool-gebaseerde organische halfgeleiders met het oog op hun toepassing als p of n-type ´kleine´ moleculen in bulk heterojunctie organische zonnecellen.

Bij de start, zoals besproken in **Hoofdstuk 2**, hebben we ons toegelegd op de optimalisatie van een directe (hetero)aryleringsprocedure van 2,5-dithiënylthiazool[5,4-*d*]thiazolen (TzTz's) met verschillende (hetero)arylbromides. Op basis van de geoptimaliseerde reactie-omstandigheden werden dan een aantal nieuwe chromoforen bereid in hoge opbrengsten. Bij het gebruik van één enkel equivalent van het (hetero)arylbromide konden op eenvoudige wijze eveneens monogearyleerde producten verkregen worden, waarvan er enkele verder gebruikt werden voor de aanmaak van asymmetrische *push-pull* moleculen. Het ontwikkelde protocol laat toe uitgebreide TzTz-chromoforen met afgestemde energieniveaus en absorptiepatronen te bereiden, afhankelijk van de ingevoerde (hetero)aryleenheden en de moleculaire (a)symmetrie. Over het algemeen vertoonden de digesubstitueerde producten een bredere absorptie en hogere extinctiecoëfficiënten. Een selectie van deze verbindingen werd dan ook toegepast (zoals beschreven in **Hoofdstuk 3**) als lichtabsorberende materialen voor bulk heterojunctie organische zonnecellen (printbaar vanuit oplossing), ofwel als elektron-donor of elektron-acceptor component. Voor de TzTz-donorverbindingen werden *high-bandgap OPV devices* met hoge *open-circuit voltages* bekomen, met een maximale efficiëntie van 2.7%. Anderzijds resulteerde het meest elektronenarme TzTz in een zonnecel met een efficiëntie van 0.4% (vnl. begrensd door de lage *short-circuit current*) in combinatie met P3HT als elektron-donor.

Gesterkt door deze initiële resultaten hebben we dan (zie **Hoofdstuk 4**) een kleine familie van uitgebreide TzTz-gebaseerde 'tweede generatie' moleculaire chromoforen gesynthetiseerd via een twee-staps C-H aryleringsprotocol. Gebruik makend van éénzelfde mono-gearyleerde TPA-T-TzTz-T precursor werden drie nieuwe D'A'DADA'D'-type structuren bereid met verschillende acceptorkernen -

een bithiazool (BiTz), een difenylquinoxaline (Qx) en een isoindigo (II) derivaat – met het oog op hun toepassing als elektron-donor moleculen in bulk heterojunctie organische zonnecellen. Jammer genoeg waren de reactie-opbrengsten vrij laag (~30%) als gevolg van het gebrek aan selectiviteit van de aanwezige C–H eenheden, resulterend in productmengsels. De beste resultaten werden behaald voor de TPA-T-TzTz-T-Qx-T-TzTz-T-TPA verbinding, met een zonnecelefficiëntie van 4.86% (in combinatie met $PC_{71}BM$).

Finaal hebben we dan ook nog twee nieuwe D–π-A-π–D-type moleculen gesynthetiseerd met een centrale TzTz-eenheid, eindstandige trifenylamine (TPA) donorgroepen en twee verschillende π-bruggen, nl. een bithiazool (BiTz) en een thiënyleenvinyleen (TV) (**Hoofdstuk 5**). Hoewel het materiaal op basis van de BiTz kern eenvoudig bekomen werd in een hoge opbrengst via achtereenvolgende Stille *cross-coupling* en directe heteroaryleringsreacties, kon de tweede verbinding (op basis van TV) (nog) niet in zuivere toestand verkregen worden door het gebrek aan C–H selectiviteit. Ondanks het hoog-kristallijne karakter van het BiTz-gebaseerde elektron-donor materiaal, belangrijk om een goede ladingsmobiliteit te kunnen garanderen, leidden preliminaire zonnecelresultaten slechts tot een erg matige efficiëntie van 0.6%.

Het finale hoofdstuk (**Hoofdstuk 6**) staat een beetje apart van de rest van de thesis, in die zin dat een alternatieve elektronenarme bouwsteen, nl. quinoxaline, gebruikt werd voor de synthese van driehoekige en vlinderachtige volledig π-geconjugeerde cyclische oligofenylenen via een Ni-gemedieerde biaryl-koppelingsreactie. Cyclotrimeren and cyclotetrameren werden afgezonderd als de dominante reactieproducten en ze werden volledig gekarakteriseerd, inclusief X-stralen structuren. De opto-elektronische eigenschappen werden eveneens

geanalyseerd met het oog op mogelijke toepassingen in *host-guest* chemie en organische elektronica.

PUBLICATION LIST

JOURNAL PUBLICATIONS

* "Quinoxaline-based cyclo(oligophenylenes)": Marin, L.; Kudrjasova, J.; Verstappen, P.; Penxten, H.; Robeyns, K.; Lutsen, L.; Vanderzande, D.; Maes, W., *J. Org. Chem.* **2015**, *80*, 2425–2430 (IF_{2013} 4.638).

* "Direct arylation as a versatile tool towards thiazolo[5,4-*d*]thiazole-based semiconducting materials": Kudrjasova, J.; Herckens, R.; Penxten, H.; Adriaensens, P.; Lutsen, L.; Vanderzande, D.; Maes, W. *Org. Biomol. Chem.* **2014**, *12*, 4663–4672 (IF_{2013} 3.487).

* "Enhanced open-circuit voltage in polymer solar cells by dithieno[3,2-*b*:2',3'-*d*]pyrrole N-acylation": Vanormelingen, W.; Kesters, J.; Verstappen, P.; Drijkoningen, J.; Kudrjasova, J.; Koudjina, S.; Liégeois, V.; Champagne, B.; Manca, J.; Lutsen, L.; Vanderzande, D.; Maes, W., *J. Mater. Chem. A* **2014**, *2*, 7535–7545 (IF_{2012} 6.108).

* "Combined experimental-theoretical NMR study on 2,5-bis(5-aryl-3-hexylthiophen-2-yl)thiazolo[5,4-*d*]thiazole derivatives for printable electronics": Van Mierloo, S.; Liégeois, V.; Kudrjasova, J.; Botek, E.; Lutsen, L.; Champagne, B.; Vanderzande, D.; Adriaensens, P.; Maes, W. *Magn. Reson. Chem.* **2012**, *50*, 379–387 (IF_{2012} 1.528).

POSTER PRESENTATIONS

* "Synthesis of 2,5-bis(5-aryl-3-hexylthiophene-2-yl)thiazolo[5,4-*d*]thiazole derivatives for printable electronics": Kudrjasova, J.; Bevk, D.; Van Mierloo, S.; Lutsen, L.; Vanderzande, D.; Maes, W. 15th Sigma-Aldrich Organic Synthesis Meeting, December 2011, Spa, Belgium.

* ''Synthesis of 2,5-bis(5-aryl-3-hexylthiophene-2-yl)thiazolo[5,4-*d*]thiazole derivatives for printable electronics": Kudrjasova, J.; Bevk, D.; Van Mierloo, S.; Lutsen, L.; Vanderzande, D.; Maes, W., 16th Sigma-Aldrich Organic Synthesis Meeting, December 2012, Spa, Belgium.

* ''Organic solar cells based on symmetrical and asymmetrical extended dithienylthiazolo[5,4-*d*]thiazole donor and acceptor small molecules'': Kudrjasova, J.; Kesters, J.; Lutsen, L.; Vanderzande, D.; Maes, W., Annual meeting of Belgian polymer group, May 2013, Blankenberge, Belgium.

* ''Direct arylation as a versatile tool toward thiazolo[5,4-*d*]thiazole-based semiconducting materials'': Kudrjasova, J.; Kesters, J.; Lutsen, L.; Vanderzande, D.; Maes, W., Next-generation organic photovoltaics, June 2013, Groningen, The Netherlands.

* ''Thiazolo[5,4-*d*]thiazoles – promising building blocks for OPV small molecule and polymer materials'': Kudrjasova, J.; Kesters, J.; Lutsen, L.; Vanderzande, D.; Maes, W., Annual IAP Network Meeting, September 2013, Ghent, Belgium.

ACKNOWLEDGEMENTS

Four years ago, I started on this journey of being a PhD student, not knowing what laid before me. New country, people and new chemistry (not at last). But I am lucky now to acknowledge that all was for good. I will remember this time with great pleasure.

The completion of this thesis would not have been possible without the support and encouragement of several special people. Hence, I would like to take this opportunity to show my gratitude to those who have assisted me in a myriad of ways.

I would first like to express my heartfelt thanks to my promoter, Prof. Dr. Wouter Maes. A more supportive and considerate supervisor I could not wish for. Thank you that you always had time to listen to my troubles and always made me feel that my work really mattered. I have never felt abundant and lost in my research. At once, you said ''I will solve all your problems'' and you really did your best to do so. Thank you for this and for so much more.

I would also like to thank my co-promoter Laurence Lutsen for taking care of the financial part of my thesis, making sure that we always had our chemicals ordered for the synthesis and in general for your solid support. Of course I am also grateful to my second co-promoter Dirk Vanderzande for sharing over the years gathered knowledge. Thank you for giving your professional opinion on my published papers (and the ones in progress).

I would like to thank Prof. Dr. Jean Manca, Prof. Dr. Wim Dehaen, Prof. Dr. Etienne Goovaerts and Prof. Dr. Peter Adriaensens for accepting to be a part of my PhD jury and as well for their time and valuable feedback.

I would like to express my gratitude to Gunter and Koen, who always took care of the good functioning of the - crucial for organic chemists - NMR equipment, and as well for recording ∞ amount of NMR spectra.

Huguette, thank you so much for your top top CV and UV-VIS measurements.

Jurgen, your fabricated solar cells eventually made my thesis much better looking. I have to confess that in my mind I imagined how I am sufficating you after you were saying me ''I need more material''. ☺ But of course you were right. Thanks!

Pieter …, you have one problem, you never say NO. ☺ You are the most helpful and responsive person around. Even if you are already overcrowded with your own tasks and responsibilities, you always find time for those who ask it from you. You helped me so many times and thank you for this!

Kayte it was really great to have you around these years. Thanks for our elaborate girly talks and always sharing my passion for sweets. Thank you for the friendship.

Veronique, I will certainly miss you. I can just hope that in future I will have colleagues like you. I wish you all the best in your future from all perspectives.

First thing what comes into my mind when I think of you, Geert, is that it would be nice to have a nice pair of black sun glasses and ''neutralizer'', which I could test on you ☺. Thanks for being an excellent lab buddy and a friend. Sorry for the failed chocolate cake.

Thank you Wouter for fruitful discusions and your true interest in what I do. I hope you and Inge will have more exciting journeys to some super exotic places.

Matthias, I find you a very interesting and determined person. There were countless times when I was asking for your advice or practical info and in no time I got answers. Thank you also for accommodating Ella at your place. I wish to you and your beautiful family a healthy, happy and no-worry life.

Benjamin, I truly enjoyed to discuss our monthly orthodonthic experiences. Good luck further to you and Sarah.

Lidia, we had a great time together at different conferences. It was a great pleasure to know you.

Sarah, thank you for all the encouragement and optimism you gave me at the beginning of my way.

Rafael, you were always so truthfully interested about my chemistry. You are such a passionate chemist. You were my wonderful shoulder to cry on. Thank you!!!

Gael, thank you for your solar cell measurements, you did a great job. I have to say I was rather surprised in your interest in Russian classisists as Прокофьев.

Neomy, Joke, Evelien, Sanne, Yasmine, Yami, Joris, Matthias, Joachim and Jeroen, it was a great pleasure to be your colleague. My best wishes to all of you in your career and personal life.

Tim, Jeroen and Ilaria, thank you for all the physical measurements.

Roald, thank you for being such a thoughtful and patient student. Sorry for the number of columns you had to do.

I also want to thank all external colleagues with whom I have worked, especially Prof. dr. Bruno Van Mele, Niko and Maxime from the Vrije Universiteit Brussel for all thermal analyses.

The best outcome from these past four years is finding my best friend, soul-mate, boyfriend and chemist ☺ at the end - Giedrius. I feel that we both strengthened our commitment and determination to each other and to live life to the fullest. Thank you for being you and being with me! All the rest is more than words.

The last word of acknowledgment I have saved to my parents. I am deeply thankful to my mother for her love, support and sacrifices, and to my father and

grandmother, who are not with me anymore. I know you both would be very proud. Without all of you, this thesis would never have been written.